

**Geothermal Measurements  
and  
Subsurface Temperature Modelling  
in Denmark**

**by**

**Niels Balling, Jan I. Kristiansen, Niels Breiner**

**Kurt D. Poulsen, Rasmus Rasmussen and Svend Saxov**

**Department of Geology**

**Aarhus University**

GEOTHERMAL MEASUREMENTS  
AND  
SUBSURFACE TEMPERATURE MODELLING  
IN DENMARK

by

Niels Balling\*, Jan I. Kristiansen\*, Niels Breiner\*  
Kurt D. Poulsen\*\*, Rasmus Rasmussen\*\*\*, and Svend Saxov\*

Department of Geology  
Aarhus University

- \* Laboratory of Geophysics, Finlandsgade 6-8, DK-8200 Aarhus N, Denmark
- \*\* present address: Geological Survey of Denmark, Thoravej 31,  
DK-2400 Copenhagen NV, Denmark
- \*\*\* present address: GECO, P.O.Box 2508, Ullandhaug, N-4001 Stavanger,  
Norway.

<u>CONTENTS</u>	Page
Abstract	1
1. INTRODUCTION	2
2. GEOTHERMAL MEASUREMENTS	4
2.1 Temperatures	4
2.1.1 BHT values	4
2.1.2 New measurements	14
2.2 Thermal conductivity	23
2.3 Heat production	41
2.4 Heat flow	44
2.4.1 Prediction of perturbations	46
2.4.2 On observations in lakes	64
2.4.3 Shallow observation boreholes	70
2.4.4 Interpretation	77
3. TEMPERATURE MODELLING	89
3.1 The heat equation	89
3.2 Model parameters	90
3.2.1 Thermal conductivity	90
3.2.2 Heat flow	92
3.2.3 Heat production	93
3.2.4 Surface temperature	93
3.3 Calculated model temperatures	93
3.4 Temperatures of potential geothermal reservoirs	98
4. CONCLUSIONS	115
Acknowledgements	117
References	119
APPENDIX A: Geothermal Equipment	124
A1: Temperature logging equipment	125
A2: Divided bar apparatus	135
A3: Needle probe instruments	138
A4: Construction principles of needle probes	146
A5: Data acquisition system	152
APPENDIX B: Bottom Hole Temperatures	153
APPENDIX C: Thermal Conductivity and Porosity	160
APPENDIX D: Radioactive Heat Production	170

### Abstract

The first order subsurface temperature pattern of Cenozoic and Mesozoic sedimentary strata in Denmark is established. Depths to 7000 m are considered, with the greatest emphasis on depths above the 3000 m level. Reported Bottom Hole Temperatures are used in combination with new accurate temperature logs and calculated model temperatures to interpolate and extrapolate measured temperature and temperature gradient relations. The regional model temperatures are calculated from analytical solutions of the heat equation and constrained by measured and estimated parameters of thermal conductivity, heat flow, and heat production. Regional alternative isothermal models are presented for the potential geothermal reservoirs. At depths of 2000-3000 m temperatures are generally within 60-100°C. New geothermal equipment has been developed and is described, including prototype quartz temperature logging equipment and needle probe thermal conductivity instruments. Porosity and lithology are experimentally demonstrated to be important factors of the rock thermal conductivity variations and thus temperature gradient variations. Main regional temperature variations are interpreted to be caused by variations of thermal conductivity. Significant local temperature and heat flow anomalies associated with salt structures are demonstrated. The possibilities of measuring heat flow in shallow lakes are theoretically analysed using the iterative least squares inversion method. Our first theoretical and experimental studies on the variations of heat flow with depth indicate a significant regional palaeoclimatic effect at shallow depth and local major anomalies caused by ground water movements. At shallow depth Danish Tertiary formations are found to be favourable for the accurate measurements of the conductive heat flow depth record to be used in the forward-inverse studies of the palaeoclimatic-terrestrial heat flow problem. More accurate observations of vertical and lateral variations of heat flow, temperature gradients and conductivity are needed for the detailed interpretation of results, and will further enable the mapping and understanding of local Danish geothermal anomalies superimposed on the regional trends.

## 1. INTRODUCTION

The purpose of this study is to increase knowledge of the Danish subsurface temperature pattern and to provide the basis for a better understanding of the physical nature of main geothermal trends.

The area forms part of the stable continental crust with no indication of recent geothermal activity (Balling, 1976a, 1979), thus the temperature field variations are closely associated with the variation of terrestrial heat flow, the thermal conductivity stratigraphy and the distribution of radioactive heat sources. Measurements and knowledge of these basal geothermal parameters constrain the subsurface temperatures predicted by the extrapolation and interpolation of borehole measurements of temperatures and temperature gradients.

The Danish area constitutes the northeastern part of the Northwest European Sedimentary Basin (Fig. 1). Here thick sequences of Paleozoic, Mesozoic, and Cenozoic sediments are observed in deep drillings and by seismic studies. The reflection seismic interpretations indicate thicknesses of up to about 10 km in the Danish Subbasin. A comprehensive synthesis on the Tectonics, basin development, and sediments of North Western Europe is given by Ziegler (1978). Further specific information from the Danish area is found in e.g. Sorgenfrei and Buch (1964), Michelsen (1978), Rasmussen (1978), and Bertelsen (1980).

The Danish sedimentary sequence contains several permeable formations of supposed great geothermal energy potential (Handelsministeriet, 1977; Balling and Saxov, 1978; Michelsen et al., 1981). The most promising reservoirs seem to be found in the Jurassic and Triassic of the Danish Subbasin and the North German Basin. Emphasis is placed on the modelling of temperatures of the potential geothermal reservoirs.

In the present paper we describe and discuss results obtained during the period 1978-80 on the development of geothermal equipment, techniques and results of observations, the theoretical modelling and interpretations. The most recent observations included originate from December 1980.

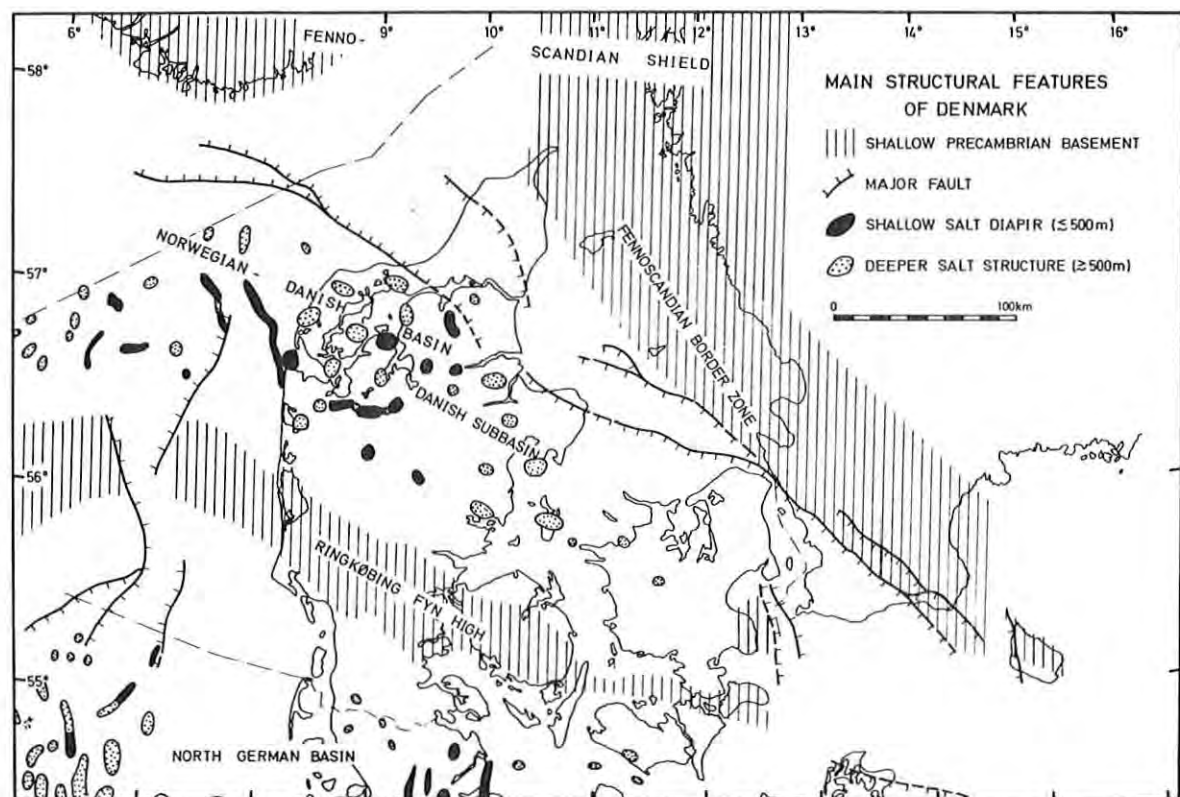


Fig. 1. Main structural geological features of Denmark  
(compiled from various sources).

## 2. GEOTHERMAL MEASUREMENTS

### 2.1 Temperatures

#### 2.1.1 BHT values

In the first phase of the EC geothermal energy programme, all temperatures reported from Danish land boreholes drilled to depths greater than 500 m were compiled (Ballings and Madsen in Saxov, 1979). From 50 holes a total of 194 measurements were available, almost exclusively bottom hole temperatures (BHT) from the oil and gas exploration drillings. The measured, non-equilibrium values were corrected by theoretical and empirical functions, where possible, to yield the approximate equilibrium temperatures. Data are here summarized in Appendix B.

Due to inhomogeneity of data, groups of BHT were considered. Based on distances between boreholes and geological environments 9 groups (A to I, Fig. 2) were formed. Disregarding some data estimated to be greatly inaccurate or from holes drilled into salt structure of anomalous temperatures, the BHT values were plotted as a function of depth, and the estimated and generalized  $T(z)$  functions were drawn (Figs. 3, 4, and 5) based especially on the corrected and most accurate and representative values. Temperatures were read from these curves at depth intervals of 500 m within the range 500 to 3000 m and used to construct generalized isothermal maps. These maps were used in the compilation of subsurface temperatures in the West European region (Haenel et al. 1979), from which parts of the isothermal maps of 1000, 2000, 3000, and 5000 m depths are shown in Figs. 6, 7, 8, and 9 to illustrate Danish isotherms in relation to those of the adjacent area. Due to the construction principles and the accuracy of data, the Danish temperature pattern does not show the shorter wavelength trends and anomalies.

All temperatures are plotted in Fig. 10, which also shows the relation to simple one-dimensional theoretical temperature-depth functions. The thermal parameters are chosen with a view to obtaining the general minimum and maximum  $T(z)$  relations. At depths of 2000 m and 3000 m, models I and II differ by  $16^{\circ}\text{C}$

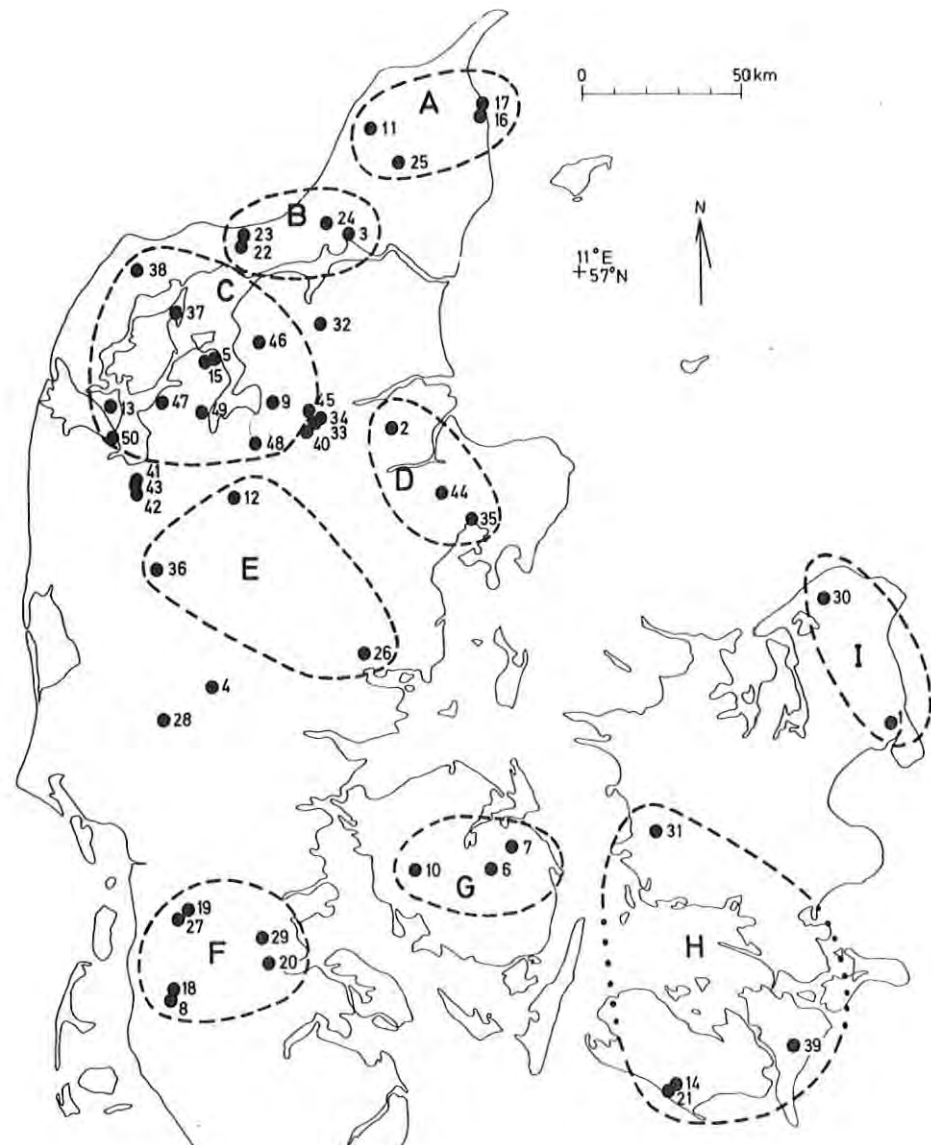


Fig. 2. Groups of boreholes (A to I) for which the generalized temperature-depth relations were constructed (Figs. 3, 4, and 5) based upon the reported BHT values (Appendix B). Holes drilled into salt structures and those of the estimated least accurate data are not considered.

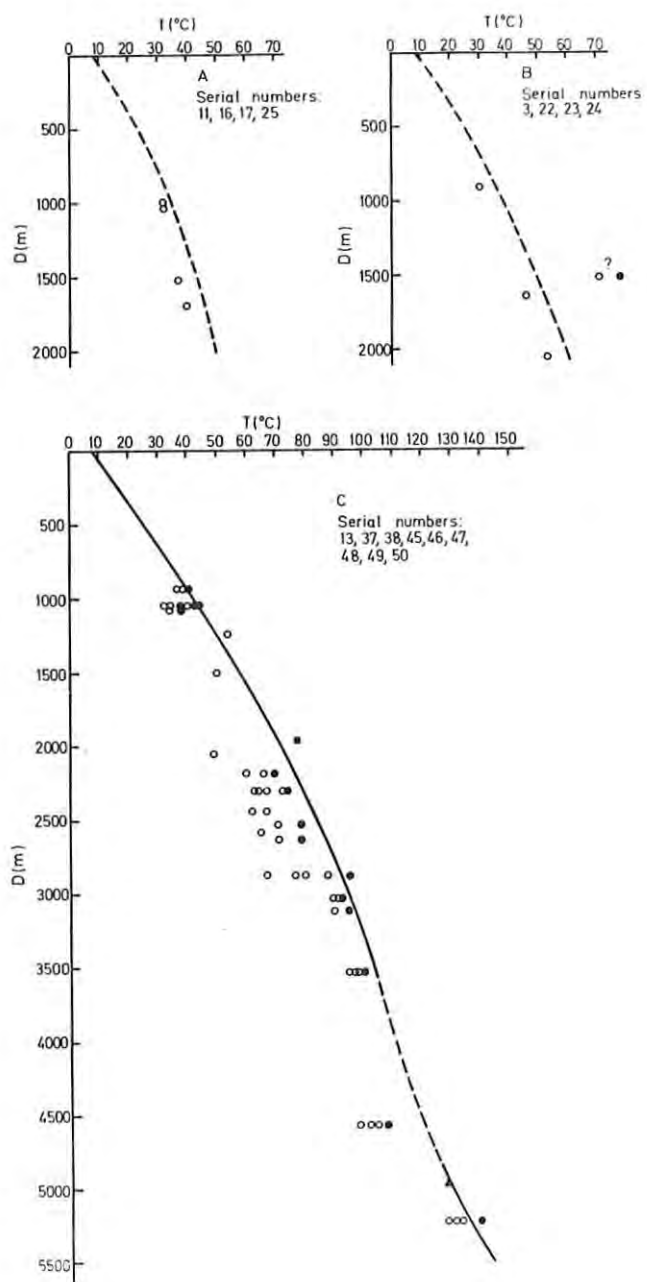


Fig. 3. BHT observations and the estimated generalized equilibrium temperature-depth relations of borehole groups A, B, and C (Fig. 2). Circles indicate uncorrected BHT values; dots corrected values; the square indicates a value measured during drill stem testing; and the triangle an estimated equilibrium value

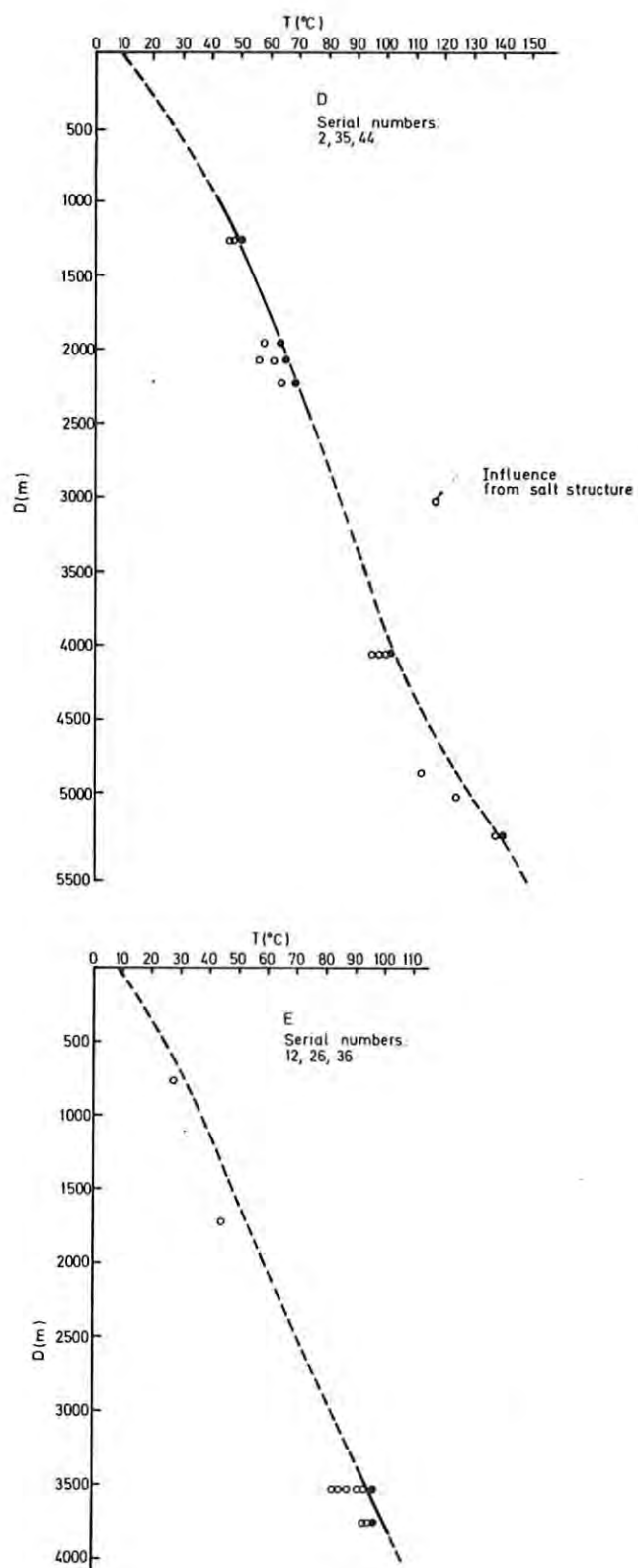


Fig. 4. BHT observations and the estimated generalized equilibrium temperature-depth relations of borehole groups D and E (Fig. 2). See also text to Fig. 3.

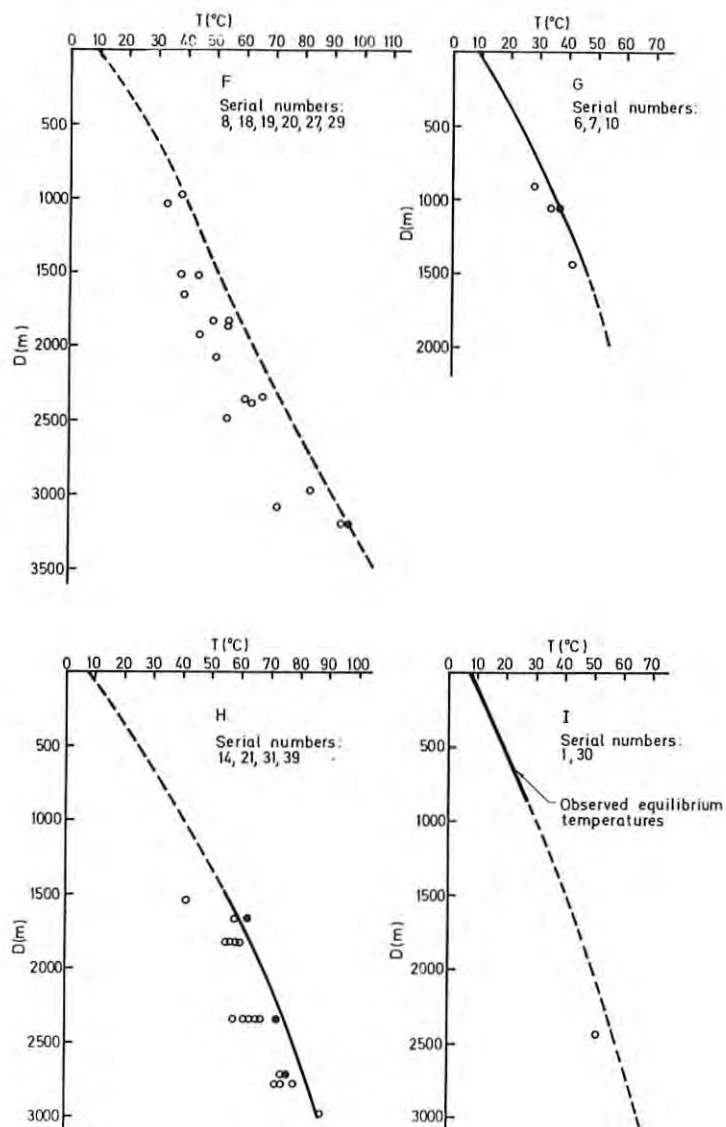


Fig. 5. BHT observations and the estimated generalized equilibrium temperature-depth relations of borehole groups F, G, H, and I (Fig. 2). See also text to Fig. 3.

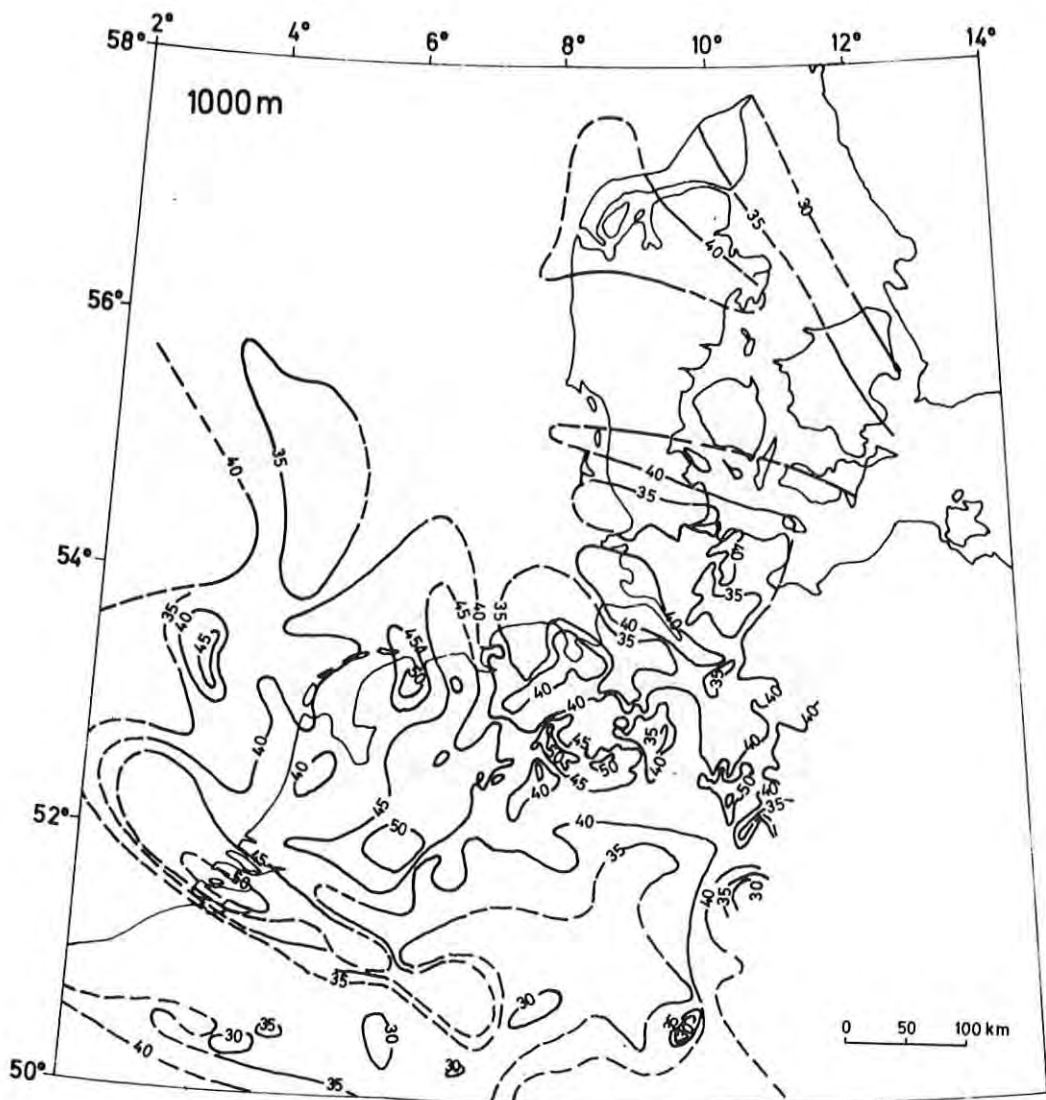
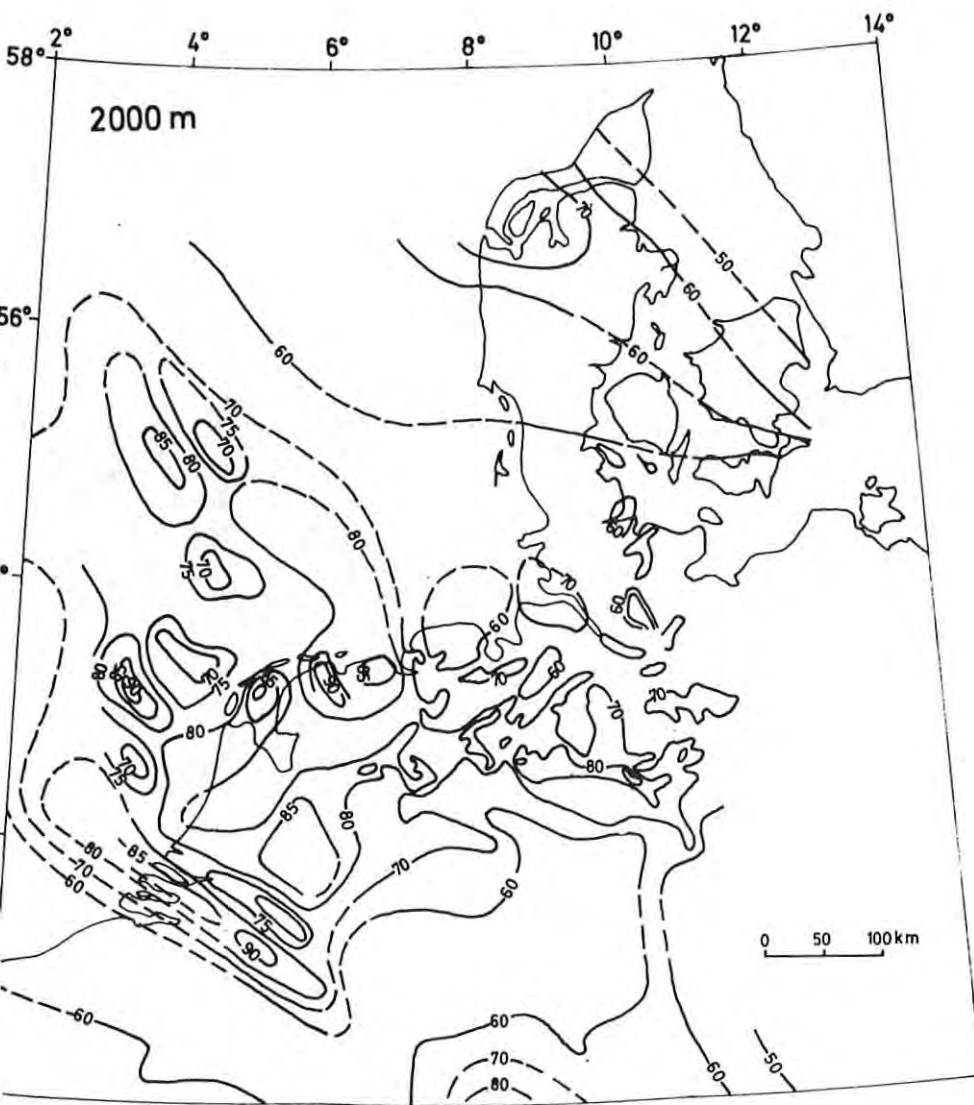


Fig. 6. Isothermal map for a depth of 1000 m for Denmark and the adjacent part of NW Europe (from Haenel et al., 1979). The Danish isotherms are constructed from the generalized graphs of Figs. 3, 4, and 5.



7. Isothermal map for a depth of 2000 m. See text to Fig. 6.

Fig. 8

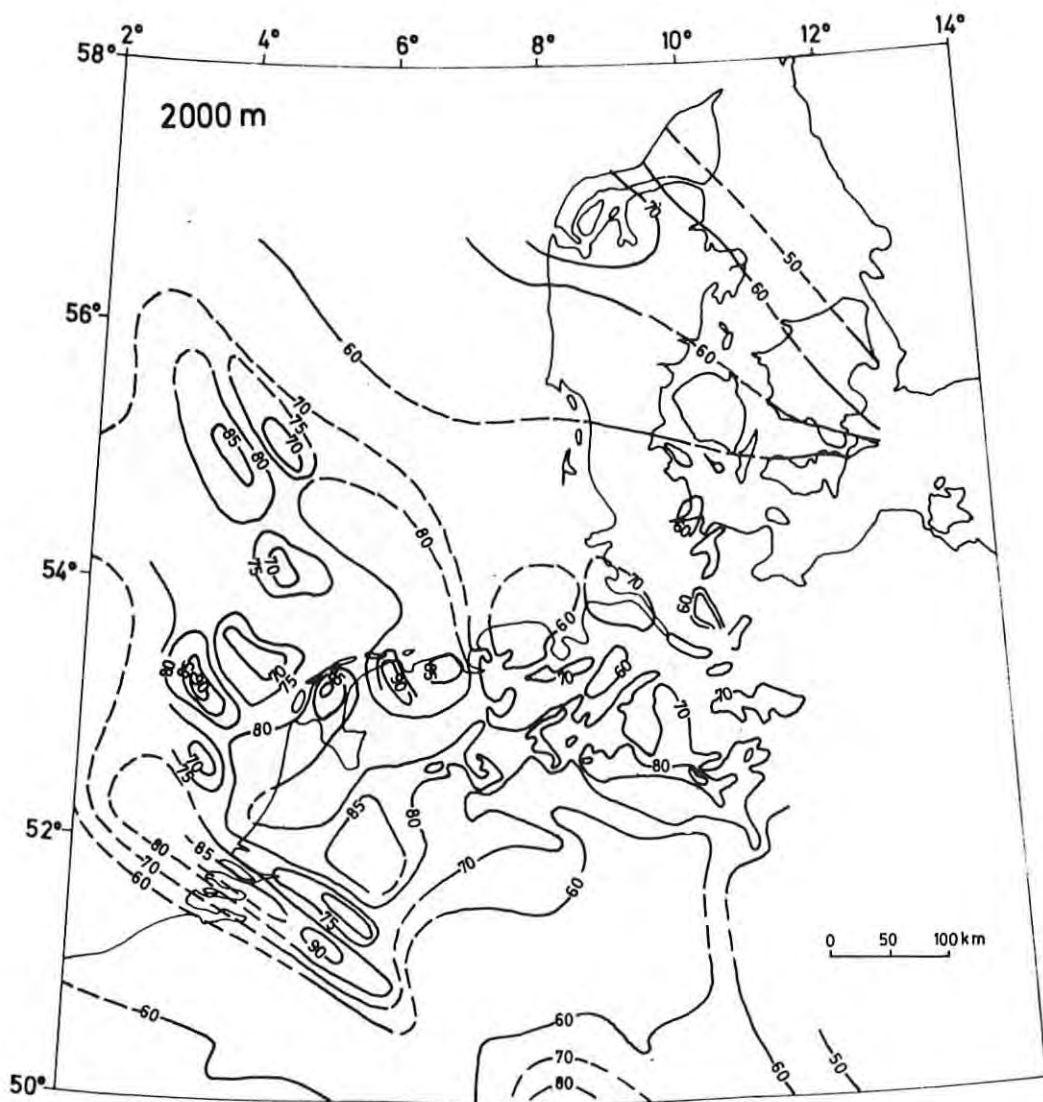


Fig. 7. Isothermal map for a depth of 2000 m. See text to Fig. 6.

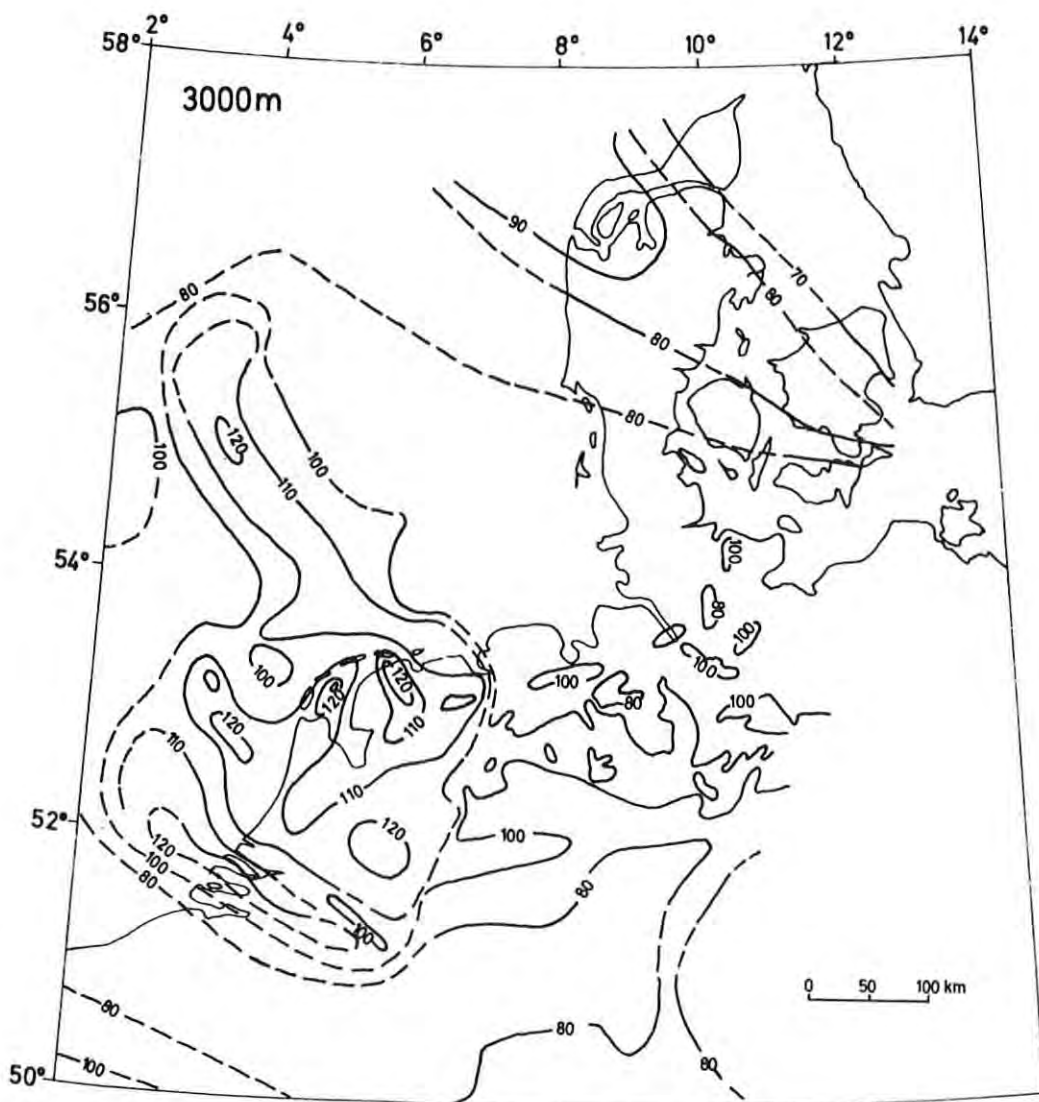


Fig. 8. Isothermal map for a depth of 3000 m. See text to Fig 6.

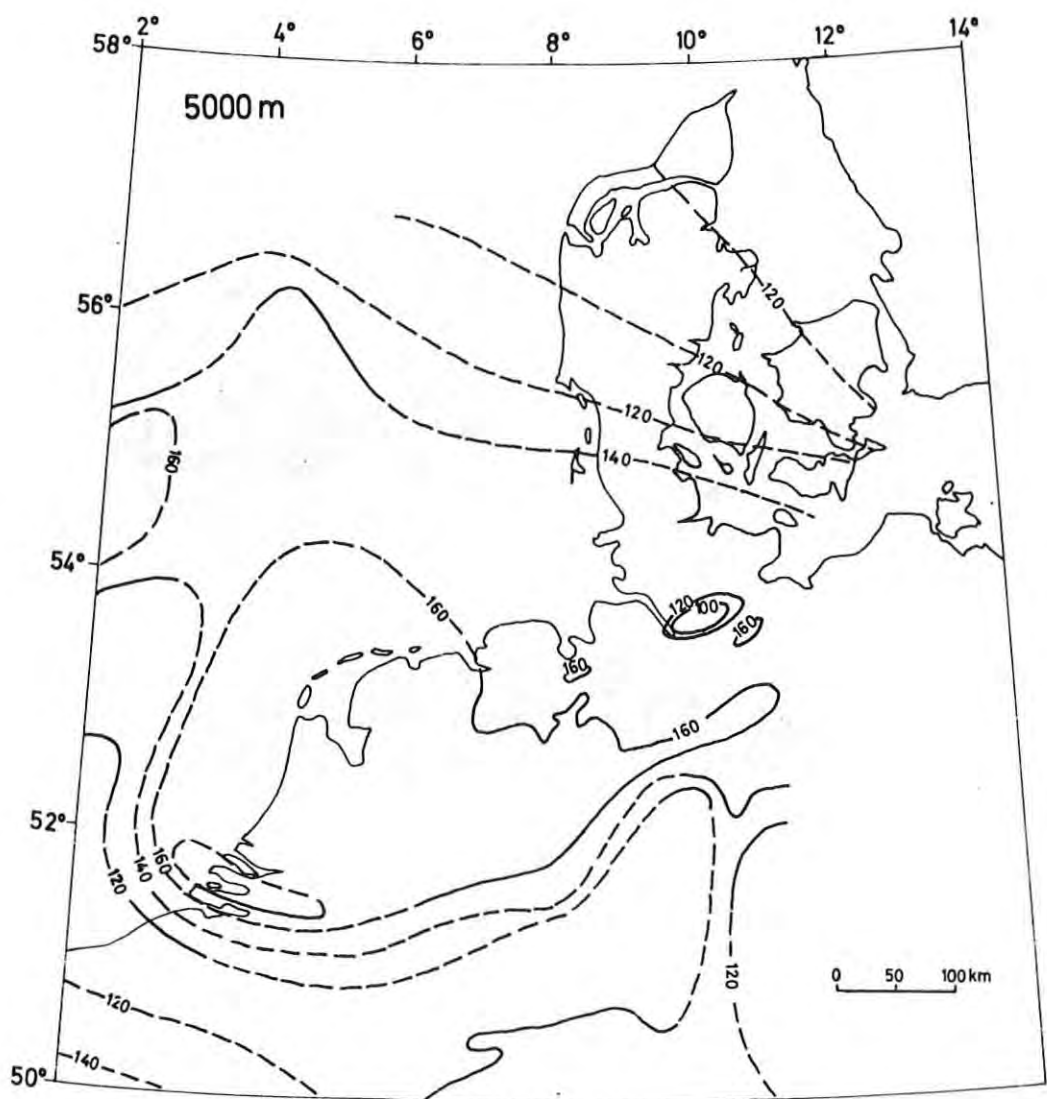


Fig. 9. Isothermal map for a depth of 5000 m. See text to Fig. 6.

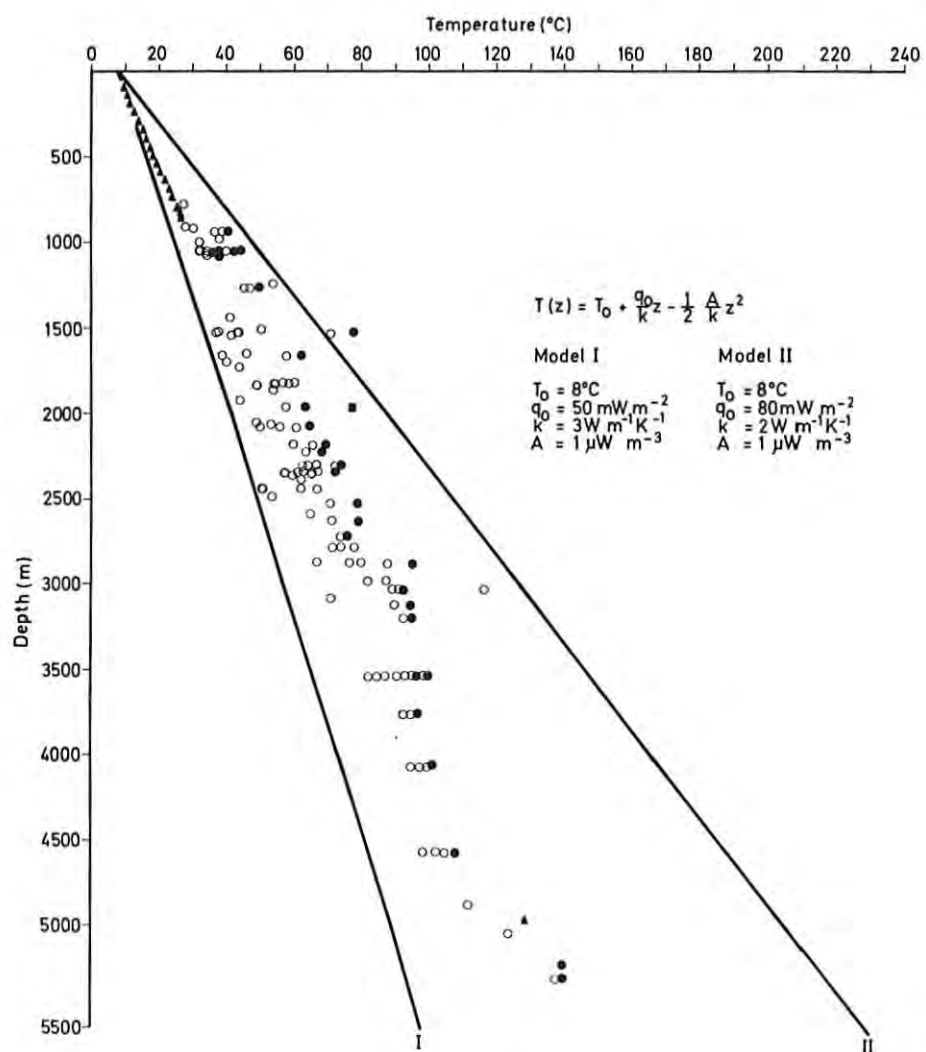


Fig. 10. Temperatures reported from all Danish land borings drilled before 1977 to depths greater than 500 m. Symbols as in Figs. 3, 4, and 5. The one-dimensional functions  $T(z)$  are calculated with thermal parameters as indicated;  $T_0$ : surface temperature,  $q_0$ : surface heat flow,  $k$ : thermal conductivity, and  $A$ : heat production. The more detailed models are considered in section 3.

and 39°C, respectively. These simple models clearly illustrate the significance of heat flow and thermal conductivity variations. In section 4 we consider temperature models based on new thermal conductivity measurements and a thermal conductivity layering of the sediments in questions.

#### 2.1.2 New measurements

Temperatures were measured in 2 boreholes drilled by other agencies for their own purposes, and in 4 holes of our own drilled as heat flux research holes (section 2.4). The object of the measurements is to provide new accurate temperatures and temperature gradients to be applied in temperature and heat flow mapping and general geothermal studies.

#### Temperature logging equipment

In shallow holes (depth < 500 m) temperatures were measured by traditional thermistor probes connected by 3-conductor cable to a recording unit of the Wheatstone bridge principle (Fig. A-1, p. 125).

New equipment was built for the temperature measurements in deep boreholes. A quartz crystal frequency thermometer suitable for measurements to great depth was developed in prototype and used in combination with the traditional Mueller bridge and a four-point resistance method. The basic principles of the transmission, recording and probe-sensor systems are described in Appendix A1. This equipment was successfully tested to a depth of 3260 m in the deep geothermal test borehole Aars 1A (Fig. 11) by use of a professional logging firm's wrench and cable units. A 7-conductor cable allowed simultaneous measurement of four-point resistance or Mueller bridge resistance temperatures (4-leads), quartz frequency temperatures (1 lead and the armor), and a collar electromagnetic signal used as depth reference control (2 leads). The preliminary results obtained by the quartz thermometer prototype showed very precise and stable readings ( $\pm \sim 1-2$  mK). Compared with the electrical resistance methods the quartz frequency method is free from potential errors associated with contact resistance variations and electrical



Fig. 11. Map of borehole (circles) and lake (crosses) localities where new temperature observations or new and previous heat flow observations were made.

noise. Further, it should be emphasized that this quartz principle can be used applying only 2-conductor or 1-conductor plus armor light-weight cables. The four-point and quartz temperatures are available on digital display and on magnetic or punched tape. Before and after measurements, probes were calibrated against a laboratory quartz thermometer. Measurements of associated temperatures and scale units are taken over the actual temperature intervals by use of an extremely stable ( $\pm 2 \text{ mK}$ ) thermal bath, in which temperatures can be changed continuously or in steps of 1 K. A (normally fifth degree) least squares Chebyshev polynomial was fitted to the data points and defined the calibration function. An example is given in Table 1.

Table 1

Mueller bridge temperature calibration example.  
The reference temperature is measured by a laboratory quartz thermometer and the calibration function, is defined by a least squares Chebyshev polynomium.

Data nr.	Resistance (ohm)	Measured reference temperature $T_1$ ( $^{\circ}\text{C}$ )	Theoretical calibration temperature $T_2$ ( $^{\circ}\text{C}$ )	Temperature difference $T_1 - T_2$ ( $^{\circ}\text{C}$ )
1	2611.26	61.614	61.614	.000
2	2799.40	59.534	59.535	-.001
3	2981.38	57.673	57.672	.001
4	3197.53	55.623	55.623	.000
5	3433.63	53.559	53.559	.000
6	3688.21	51.508	51.508	.000
7	3966.98	49.441	49.441	.000
8	4183.02	47.952	47.951	.001
9	4501.74	45.907	45.907	.000
10	4851.58	43.844	43.844	.000

### Results of observations

The deep borehole Aars 1A was logged so far by two series of measurements, the first one 19 days (Sept. 1979) and the second one 100 days (Dec. 1979) after the last drilling operations and bore fluid circulation. The hole was drilled to a depth of 3400 m during the period October 1978 to September 1979. In the first log temperatures were measured at discrete intervals (generally every 200 m) and in the second log readings with the quartz and four-point thermometers were taken continuously. The probe was lowered into the borehole at constant rate; in the upper 1600 m at 0.25 metres per second, and in deeper levels at  $0.083 \text{ m s}^{-1}$  (1600-2000 m) or  $0.167 \text{ m s}^{-1}$  ( $> 2000 \text{ m}$ ). The four-point resistance values and the quartz frequencies were recorded digitally with a sampling rate of 2 and 0.2 per second, respectively. Data and corresponding depth values were processed by computer to yield temperatures and temperature gradients. The whole procedure is generally of the same type as that described by Costain (1970), Conaway (1977), and Conaway and Bech (1977). The data are deconvolved to compensate for the effects of the probe time constant and a convolution operator produces the temperature gradients versus depth.

Examples of observations are given in Figs. 12 and 13. The smoothing part of the gradient filter is gaussian, and we used an interval of 15 sample points, which associate depth intervals of 18.8 m (Fig. 13a) and 6.3 m (Fig. 13b). The December 1979 measurements taken within the depth interval 400-3260 m (upper part air filled, and deeper penetration through drilling mud at bottom was not possible) showed a temperature increase relative to the September reading at depth below  $\sim 2300 \text{ m}$  and a decrease above this level; temperature gradients are also observed to change (Fig. 14). However, averaged over large intervals, e.g. 200 m, gradients are much closer to the equilibrium values as compared to the local values representing variations over few metres (Fig. 13). The average interval gradients are fairly constant at  $20-25 \text{ mK m}^{-1}$  in the upper part of the hole ( $< 1400 \text{ m}$ ) and increase generally with depth reaching about  $45 \text{ mK m}^{-1}$  at the deepest levels. This increase of gradient is interpreted to

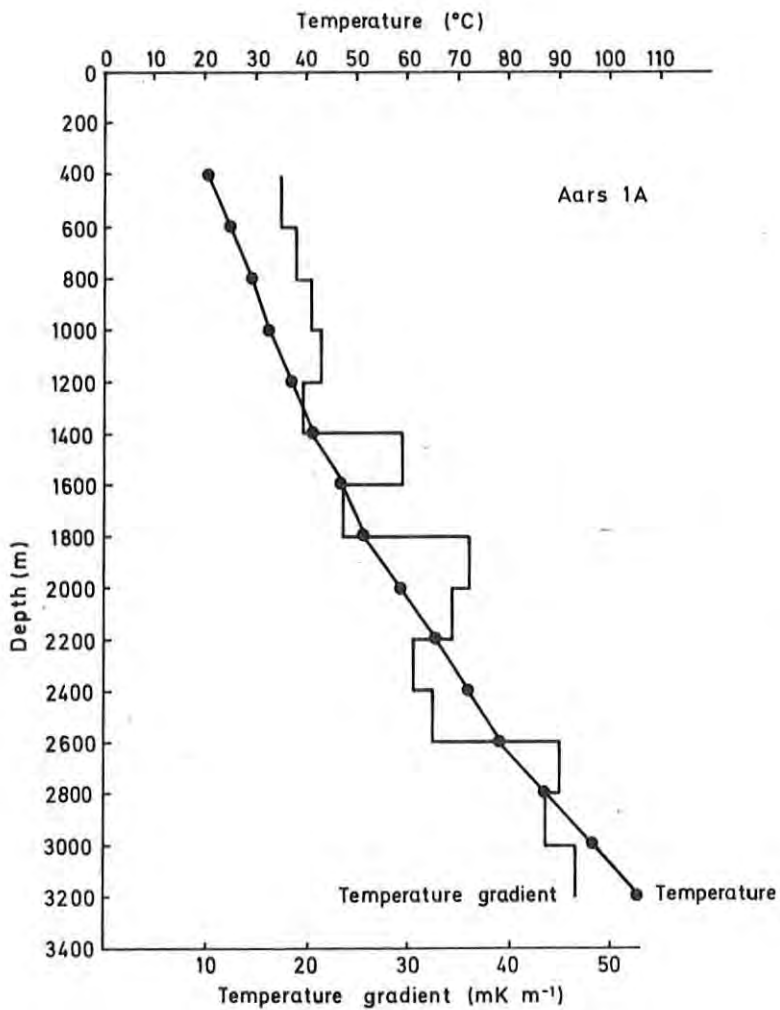


Fig. 12. Temperatures and temperature gradients (200 m interval mean values) measured Dec. 1979 in borehole Aars 1A, 100 days after last drilling activities.

be associated with decreasing thermal conductivity. The highly variable pattern of gradients over the 1400-2000 m interval (Fig. 13b) including large negative values are interpreted to be associated with formations of variable thermal properties. Strongly disturbed gradients are easily produced when temperatures are disturbed by drilling and return to equilibrium over intervals of significant variations of rock thermal diffusivity. Some 200 thermal conductivities were measured on cores, mostly from the depth interval 1900-3300 m, with a view to obtaining heat flow values if equilibrium temperature gradients may be measured. New temperature loggings are planned for 1981. The

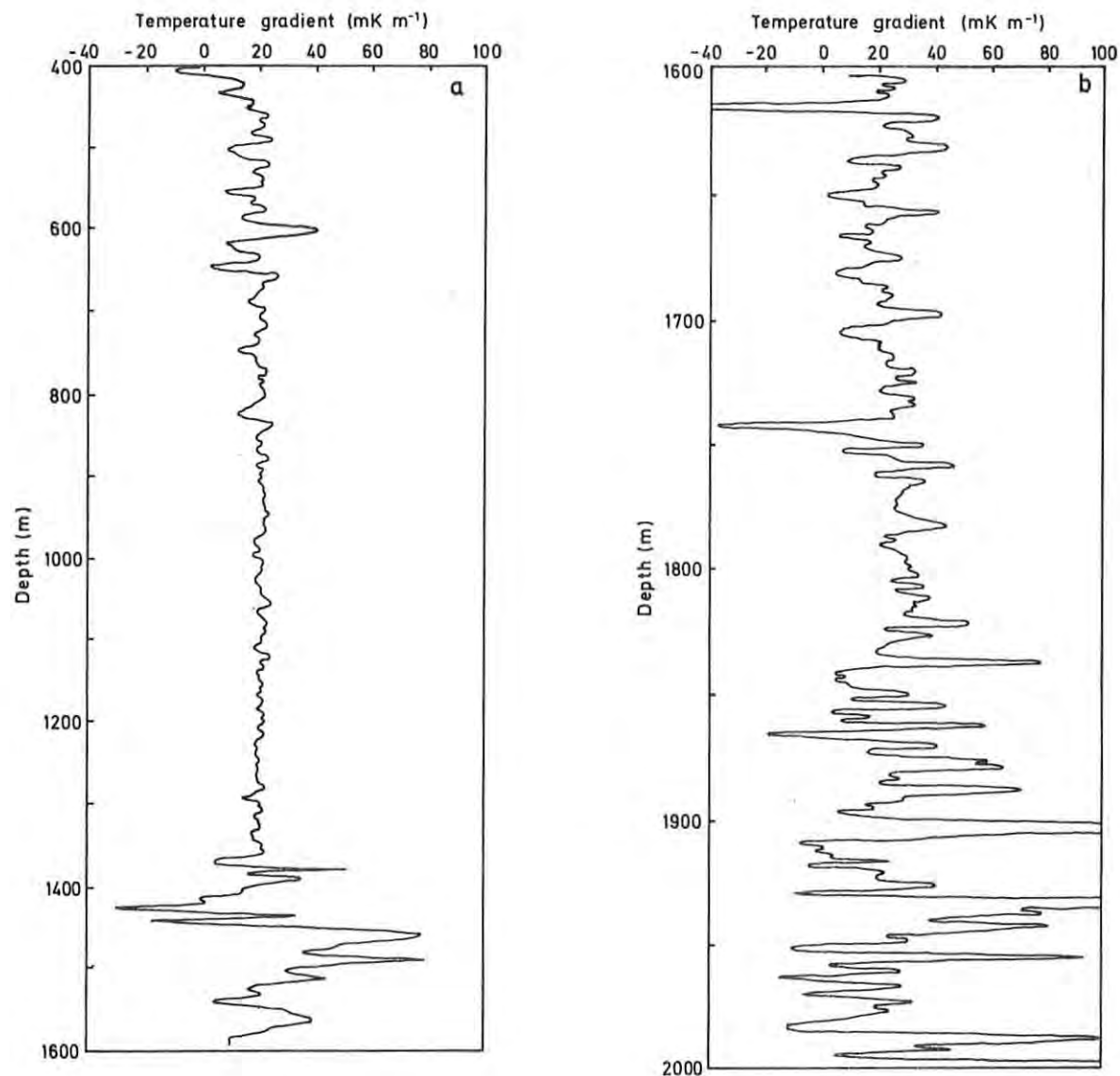


Fig. 13. Examples of continuous temperature gradient logs obtained from the quartz frequency thermometer measurements in borehole Aars 1A. The logs are from Dec. 1979 (cf. Fig. 12). Especially within the interval 1350-2000 m gradients have not reached thermal equilibrium.

continuous logging of temperature gradients is useful for the observations of the return to equilibrium and the selection of intervals suitable for heat flow observations. The gradient variations can also be used for stratigraphic correlation.

The upper 315 m of the deep oil exploration borehole Oddesund 1 (Fig. 11), drilled in 1976, was measured. Deeper parts are not available for observations due to cement plugging. Here some BHT-values were measured by companies during drilling, and a geo-

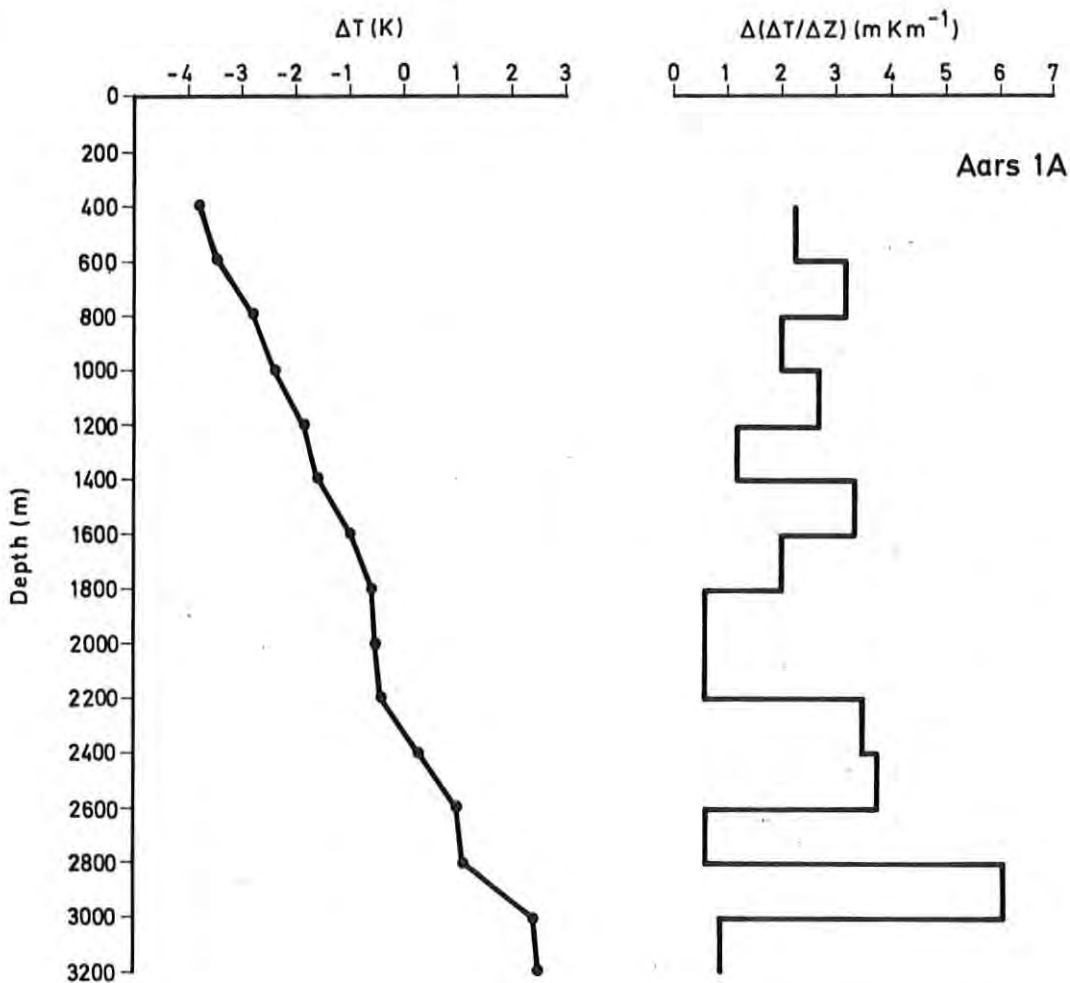


Fig. 14. Temperature and temperature gradient variations measured in borehole Aars 1A (Fig. 11). Graphs show differences between log 2 (measured December 1979) and log 1 (measured September 1979), 100 and 19 days, respectively, after the final borefluid circulation. A temperature of  $107.4^{\circ}\text{C}$  was measured in log 2 at the maximum depth of 3260 m. See also Fig. 12.

thermal drill stem test temperature was measured at depth 1949-61 m (Balling, 1976b). Our temperatures measured in December 1980 were compared to other observations made since 1976 and show equilibrium values and normal temperatures and temperature gradients (Fig. 15 and Table 2). A high BHT-value of  $40^{\circ}\text{C}$  reported from 615 m is most likely  $10-15^{\circ}\text{C}$  too high. The BHT-data are of low quality and do not allow calculation of accurate equilibrium values. Based on the measured shallow temperatures, the DST-value, and guided by the uncorrected BHT, the generalized equilibrium  $T(z)$  given in Fig. 16 most probably shows tempera-

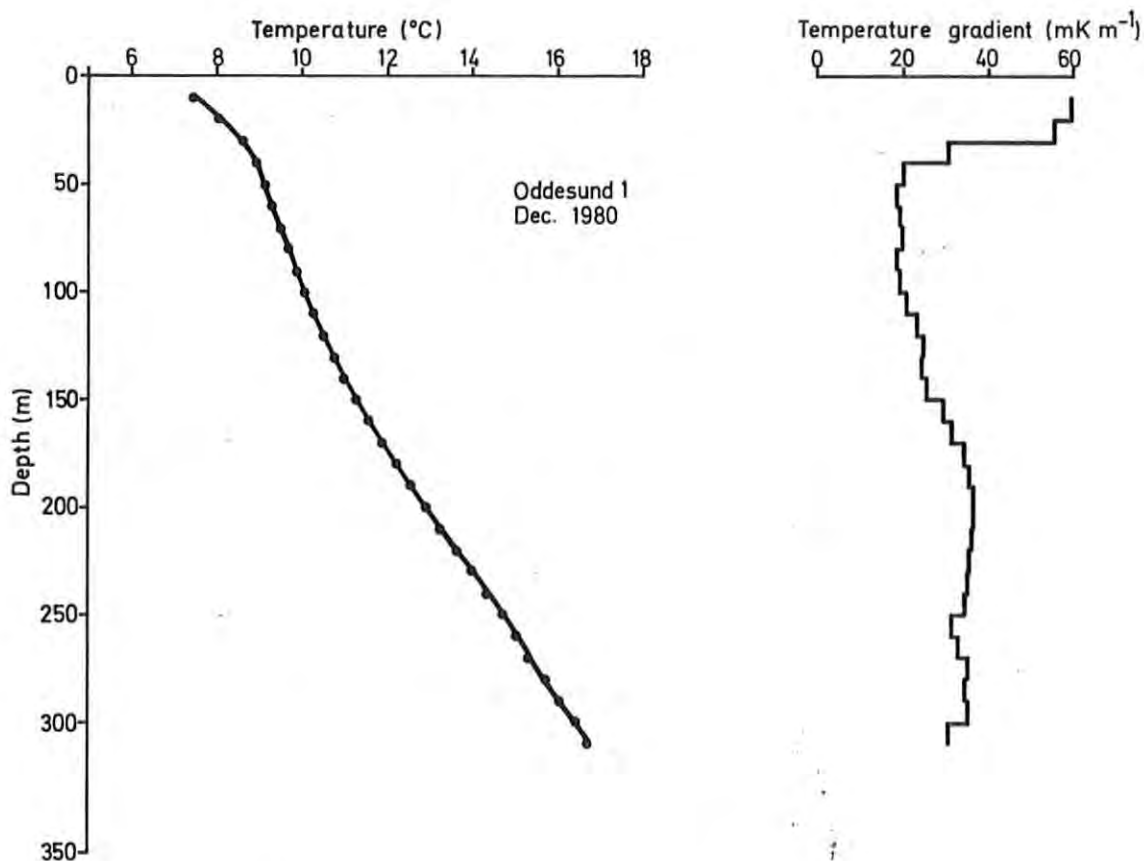


Fig. 15. Equilibrium temperatures and temperature gradients measured in the available upper 315 m of the deep Oddesund 1 borehole (Fig. 11 and Table 3). Temperatures were measured December 1980, four years after drilling activities. No anomalies are observed.

Table 2

Temperatures at selected depths measured December 1980 in borehole Oddesund 1 (cf. Figs. 13)

<u>Depth (m)</u>	<u>Temperature (<math>^{\circ}\text{C}</math>)</u>
10	7.4
50	9.1
100	10.0
150	11.2
200	12.9
250	14.7
300	16.4

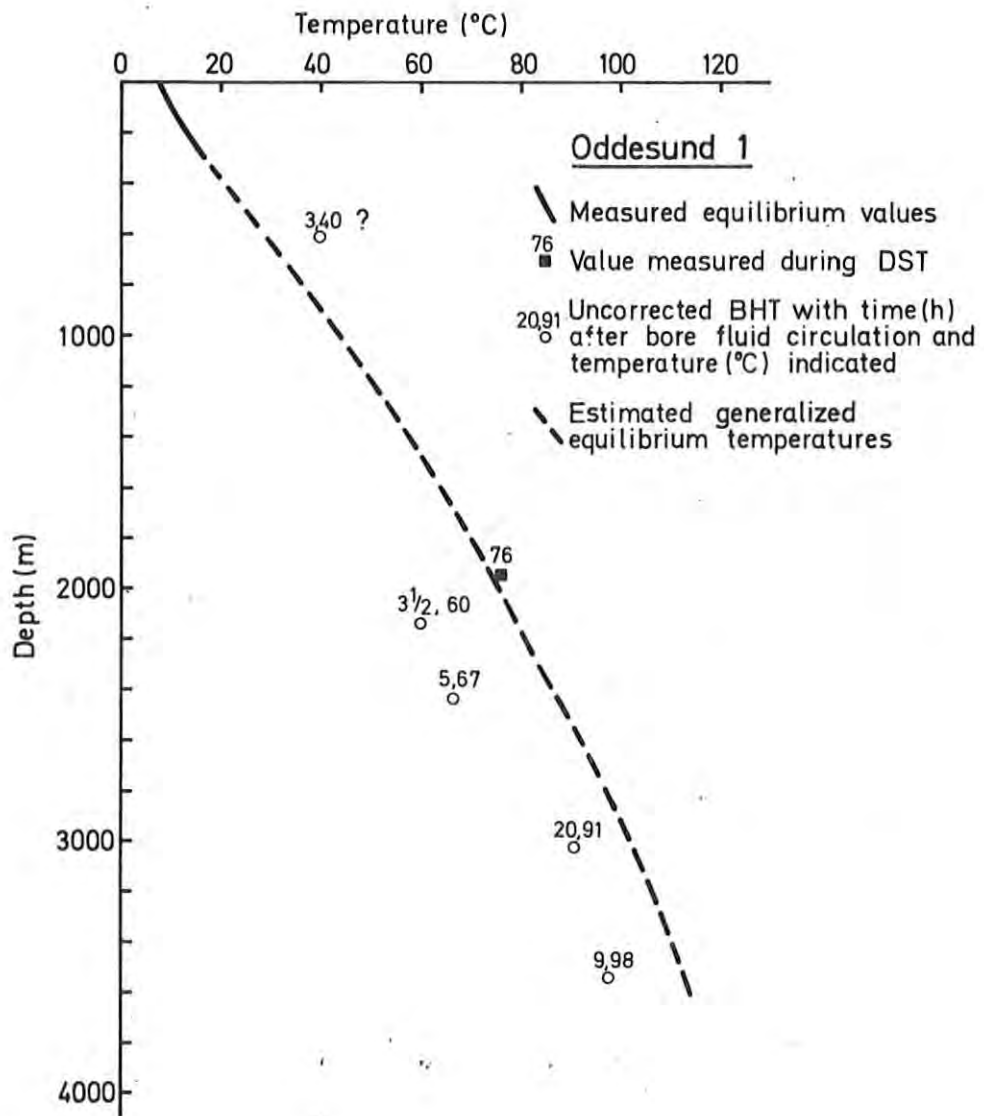


Fig. 16. Compilation of all temperature information available from the borehole Oddesund 1, and the estimated generalized equilibrium temperature-depth relation.

tures accurate within  $\pm 5-10^{\circ}\text{C}$ . At 1000, 2000, and 3000 m the approximate temperatures are 45, 75, and  $100^{\circ}\text{C}$ , respectively. At the 3540 m level, where the deepest BHT-value was measured, the equilibrium temperature is estimated to be around  $115^{\circ}\text{C}$ . These values are about normal for the area in question. At 2000 m temperatures may be slightly higher than normal.

## 2.2 Thermal conductivity

Thermal conductivity is the important rock thermal parameter to be used in the temperature modelling in section 3.

Conductivity of rocks is defined by the mineral composition, their structure, orientation, and porosity, and the extent to which pores and cracks are occupied by fluids or gas. Thermal conductivity is also a function of temperature and pressure (Bridgeman, 1924; Birch and Clark, 1940; Woodside and Messmer, 1961; Horai, 1971). The conductivity to be used in studies like this is that of the water-saturated rocks.

A series of thermal conductivities have been measured on samples of core materials from the Danish sedimentary sequence. The cores originate from the exploration boreholes drilled on land area and have been made available for the present investigations by the Danish Geological Survey. The samples are selected with representation of the main Cenozoic and Mesozoic formations in mind, but with constraints as to cores available and their quality.

The conductivities were measured by the transient needle probe technique (Von Herzen and Maxwell, 1959). The needle temperature response was basically interpreted in accordance with the continuous line source large times solution (Carslaw and Jaeger, 1959) by least squares determination of the slope of the linear part of the temperature rise-log time curve and compared to results obtained by an iterative least squares inversion technique. In the latter method we apply the exact integral solution of the transient cylindrical probe problem. The measured and calculated probe responses were found to agree within the measuring accuracies of 2-3 mK. Divided bar measurements were carried out on selected samples for comparison of methods and for evaluation of the influence of pressure upon conductivity. The needle probes were standardized against lexan (polycarbonate) with a reference conductivity (at 20°C) of  $0.220 \text{ W m}^{-1} \text{ K}^{-1}$  (Balling, 1979). The same type of lexan was used as divided bar reference material, together with pyrex glass and fused quartz (Ratcliffe, 1959). Most needle probes applied have lengths of about 85 mm,

but a few have a length of about 50 mm so as to fit the dimensions of small core samples. The basic principles of the needle probe measuring equipment are described in Appendix A3, and the needle probe construction principles are described in detail in Appendix A4. The divided bar apparatus is of conventional design (cf. Appendix A2). Probe thermistors were calibrated against a laboratory quartz thermometer (Table 3) with the same procedure as applied to the temperature logging equipment (section 2.1). Before and during the period of measurements all needle probes employed were systematically tested by measurements in the standard reference material.

Table 3

Needle probe temperature calibration example.  
(See text of Table 1).

Data nr.	Resistance (scale units)	Measured reference temperature $T_1$ ( $^{\circ}$ C)	Theoretical calibration temperature $T_2$ ( $^{\circ}$ C)	Temperature difference $T_1 - T_2$ ( $^{\circ}$ C)
1	-104.00	26.862	26.862	.000
2	- 82.64	25.847	25.847	.000
3	- 60.89	24.822	24.822	.000
4	- 39.09	23.805	23.804	.001
5	- 17.12	22.786	22.786	.000
6	4.72	21.780	21.781	-.001
7	26.84	20.769	20.768	.001
8	49.59	19.732	19.732	.000
9	71.11	18.757	18.757	.000
10	93.65	17.740	17.740	.000
11	115.90	16.739	16.739	.000

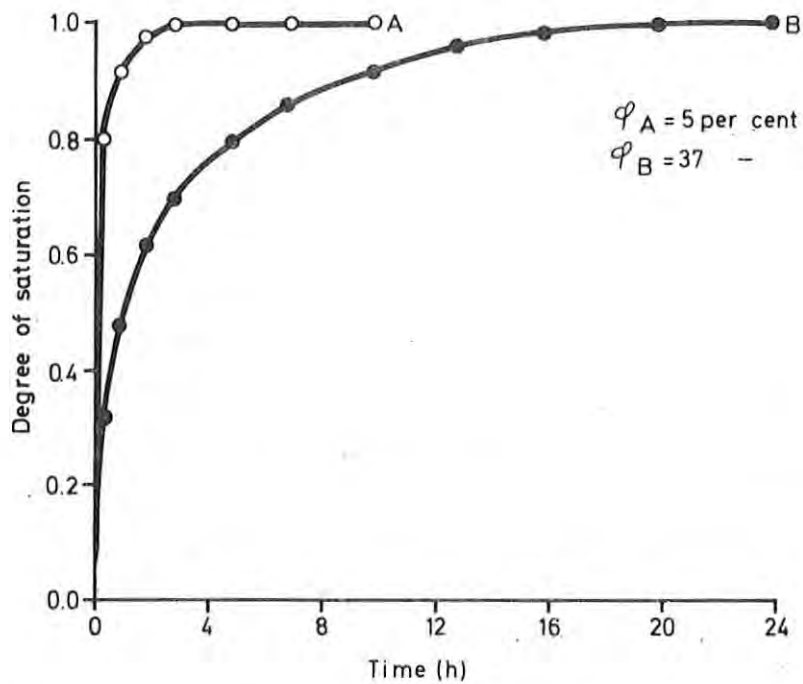


Fig. 17. Time necessary to reach water saturation, illustrated as the degree of saturation as a function of the time for which samples were under water and vacuum. Results from two limestone samples of high (B) and low (A) porosity as indicated.

As most of the samples consist of consolidated sediments, small holes were drilled with high speed drills for the insertion of the probes. All samples of limestone and sandstone and some other lithologies were saturated with water under vacuum for at least 24 hours before measurement (Fig. 17). Since clay minerals often disintegrate when water is added, we applied ethanol to most of the clay-rich samples, such as claystone. The equivalent conductivity of water-saturated material was calculated by the geometric mean formula (e.g. Woodside and Messmer, 1961) which for a two-component material reads  $k = k_f^\phi \cdot k_m^{(1-\phi)}$ , where  $k$  is the sample bulk conductivity,  $k_f$  the fluid conductivity,  $k_m$  the matrix conductivity, and  $\phi$  the porosity. Porosity was measured on all samples by the conventional technique of measuring saturated sample weight, sample volume, and sample weight of dried ( $110^\circ$  over 48 hours) material. Given porosity, fluid conductivity at room temperature ( $0.60 \text{ W m}^{-1} \text{ K}^{-1}$  for water, and 0.167 for

ethanol (Handbook of Chemistry and Physics, 1978-79)), the sample water-saturated conductivity is calculated from known parameters. This procedure gave satisfactory results in cases like this where no individual values of maximum accuracy are to be used, but a statistical averaging of values is made before application. Due to the varying quality of the sample material, the accuracy of results obtained varies, but is generally better than 5 per cent.

Results of conductivity and porosity measurements are listed in Appendix C, together with information on rock types, stratigraphy, depth, and locality. The stratigraphic classification of the Jurassic and Triassic formation is based upon Michelsen (1978) and Berthelsen (1980). The classification of rock types follows the Danish Geological Survey core description catalogue. Conductivities range from 1.1 (porous claystone) to  $6.4 \text{ W m}^{-1} \text{ K}^{-1}$  (dolomite and anhydrite), the mean value of all 178 samples measured being  $2.49 \text{ W m}^{-1} \text{ K}^{-1}$  with a standard error of 0.08 (Fig. 18). 87 per cent of the value lie between 1.1 and  $3.5 \text{ W m}^{-1} \text{ K}^{-1}$ , and 68 per cent between 1.5 and  $3.0 \text{ W m}^{-1} \text{ K}^{-1}$ . Conductivity histograms from main lithologies, estimated to cover about 95 per cent of Danish post-Permean sediments, are shown in Fig. 19. Apart from clays of low conductivity and the saline rocks with high values (where only few samples were measured), the mean conductivity of the dominant rock types ranges from about  $2.0 \text{ W m}^{-1} \text{ K}^{-1}$  for limestone (incl. chalk) and claystone (incl. shale) to  $3.1 \text{ W m}^{-1} \text{ K}^{-1}$  for sandstone, while the fine-grained and "mixed" rock types have an intermediate mean value of  $2.6 \text{ W m}^{-1} \text{ K}^{-1}$ .

Subdivision according to stratigraphic age and lithology and plotting conductivity as a function of depth (Figs. 20 to 24) shows that a) the depth interval from surface to about 2 km is well covered by observations; b) the conductivity of the Danian and Upper Cretaceous limestone increases with depth from abt.  $1.5 \text{ W m}^{-1} \text{ K}^{-1}$  at surface level to abt.  $2.5 \text{ W m}^{-1} \text{ K}^{-1}$  below 1 km; and c) the mean values for samples of strata from the Lower Cretaceous to the base Triassic are almost constant at 2.5. As will be discussed in section 3.2, a greater degree

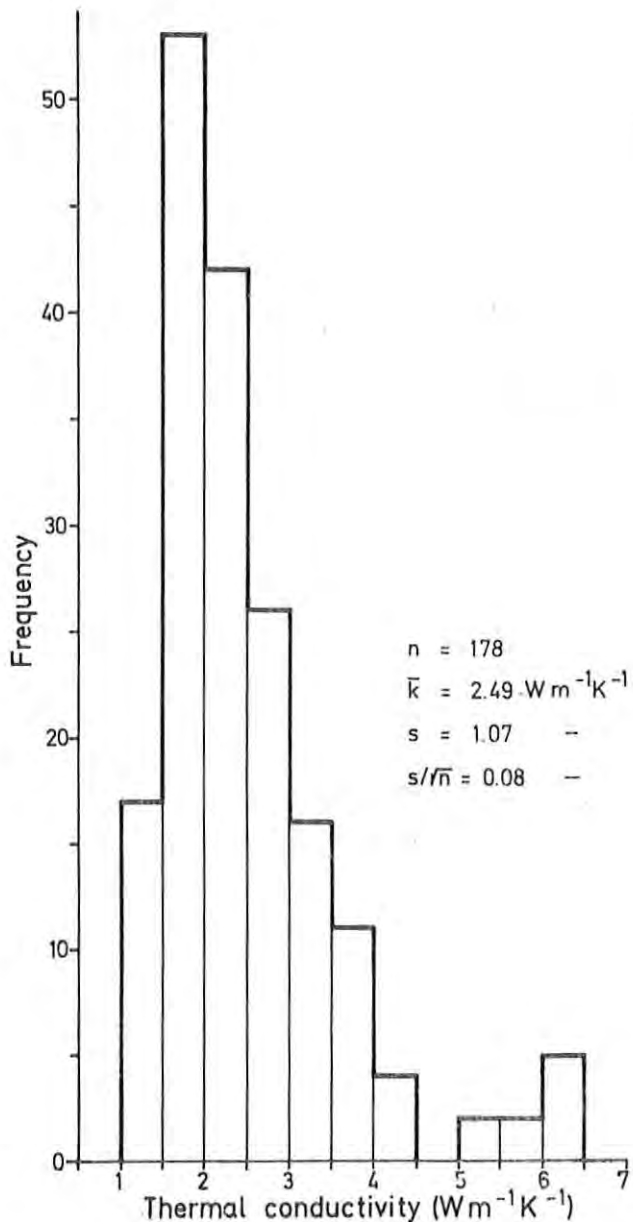


Fig. 18. Thermal conductivity histogram. Results of measurements on Danish core (water saturated) samples of sediments as listed in Appendix C.  
n: number of measurements, k: mean conductivity, s: standard deviation, and  $s/\sqrt{n}$ : standard error of the mean.

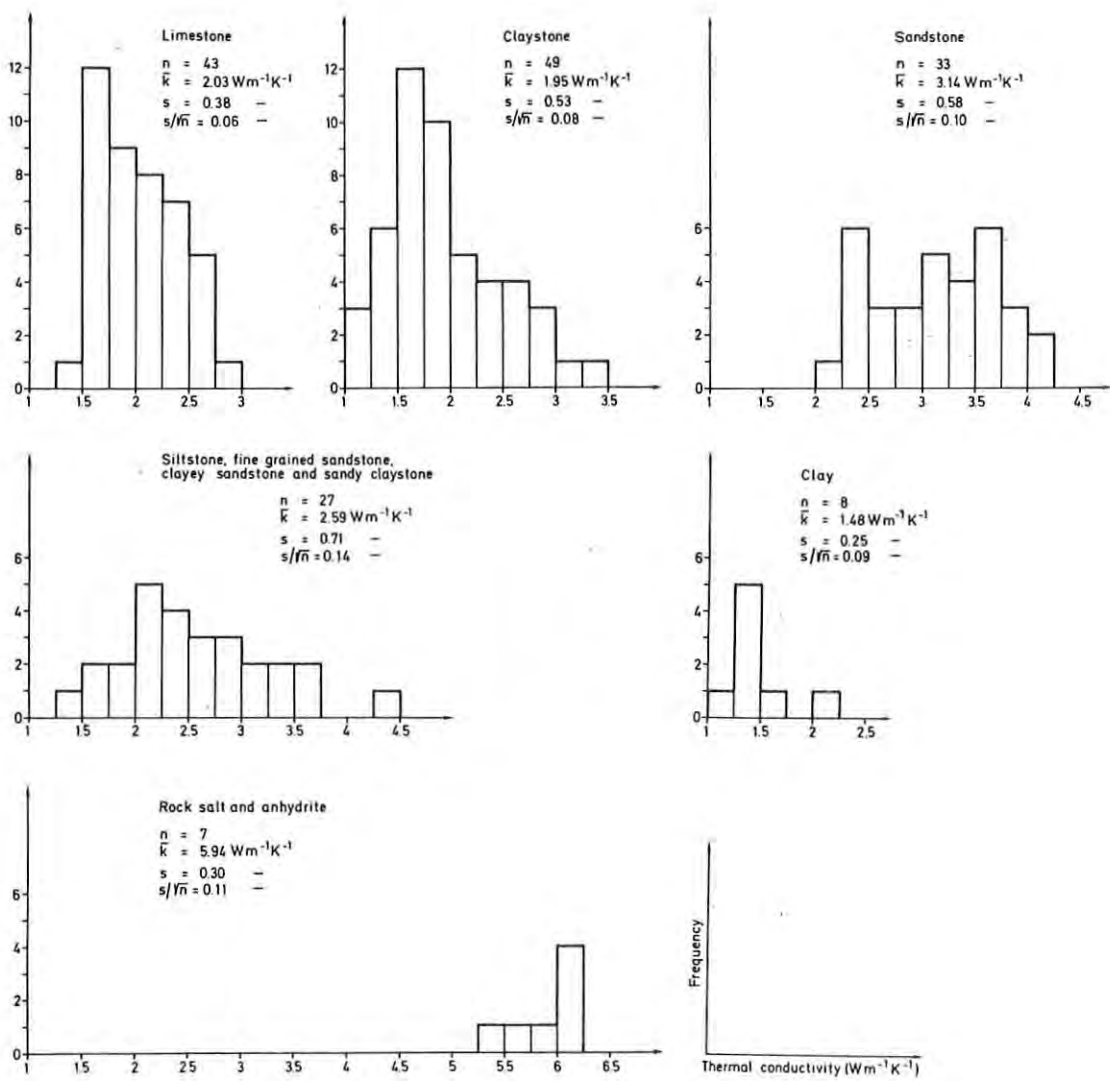


Fig. 19. Thermal conductivity histograms of groups of lithologies. See also text to Fig. 18. Statistical data on porosities are given in Table 4.

Table 4

Statistical data on porosity for the six groups of rocks for which conductivities are given in Fig. 19. n: number of samples,  $\bar{\phi}$ : mean porosity, s: standard deviation, and  $s/\sqrt{n}$ : standard error of the mean. Values in per cent.

	n	$\bar{\phi}$	s	$s/\sqrt{n}$
1. Limestone	43	26	11	2
2. Claystone	49	30	14	2
3. Sandstone	33	25	10	2
4. Siltstone etc.	27	27	14	3
5. Clay	8	46	10	3
6. Rock salt and anhydrite	7	3	1	0.3

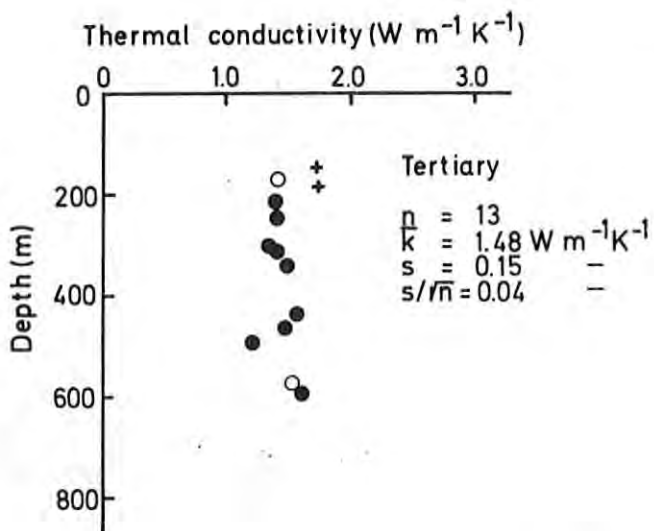


Fig. 20. Thermal conductivity of Tertiary samples plotted as a function of the depth from which cores were taken.

Symbols here and for Figs. 21-24:

□: limestone (incl. chalk), +: sand and sandstone, ●: clay and claystone (incl. shale), ○: siltstone, fine-grained sandstone, clayey sandstone, and sandy claystone, ×: dolomite and anhydrite, and Δ: clay ironstone ( $n$ ,  $k$ ,  $s$ , and  $s/\sqrt{n}$  as in Fig. 18).

of variation is expected for the Jurassic and Triassic formations than indicated by the data given here.

For rock types chiefly composed of two-component materials, such as the porous limestones and sandstones, the conductivity is found to be strongly associated with the porosity, and in general the porosity is observed to play an important role (Figs. 25 and 26). Thus if the porosity and lithology are known from logs, important constraints are given to the mean conductivities. Considering the mean conductivities of Fig. 19, the associated mean porosities are of great importance. Mean values, standard deviation and standard error of the mean are given in Table 4. Few samples originate from depths below 2.5 km, where porosities are likely to be lower and generally decreasing with depth. The conductivities of main lithologies summarized in Fig. 19 are thus considered to be most representative for the upper 2-2.5 km of the sedimentary sequence.

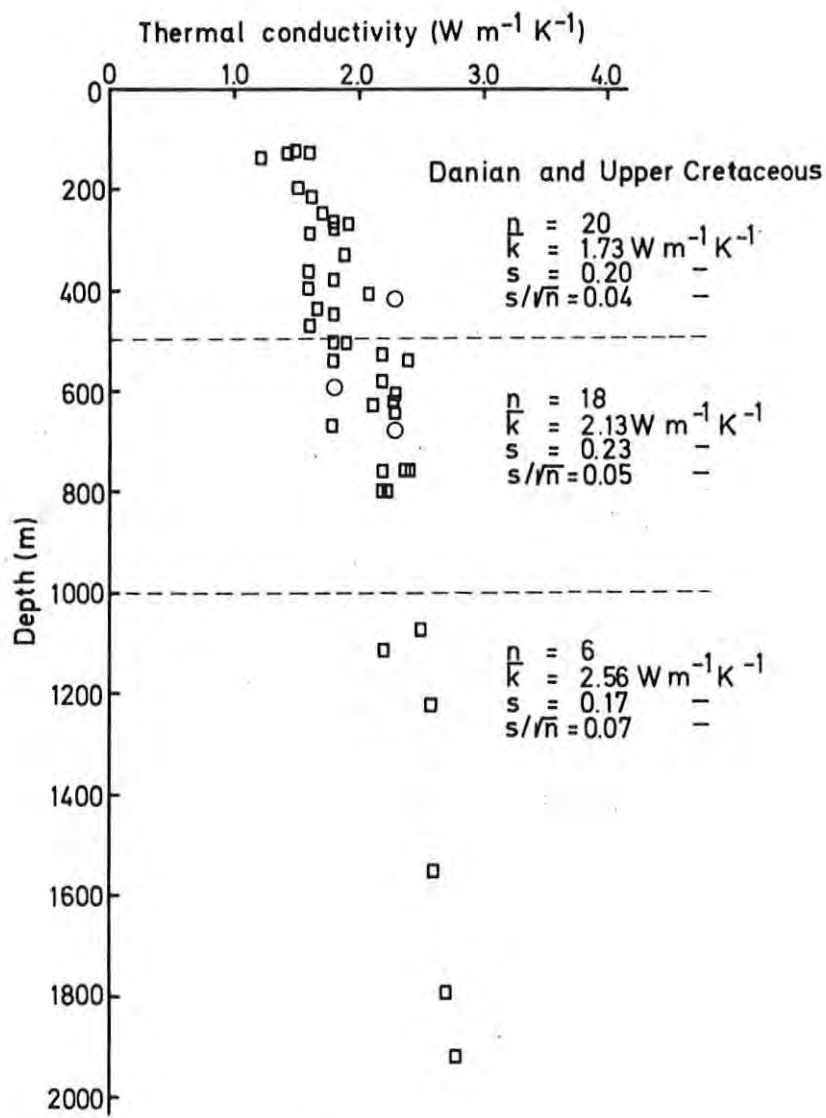


Fig. 21. Thermal conductivity of Danian and Upper Cretaceous samples plotted as a function of depth. See also text to Fig. 20 for symbols.

The limestone conductivity-porosity analysis was extended to include recent results obtained from measurements on Danish outcrop samples of high porosity and Swedish outcrop samples of generally low porosity measured by Poulsen et al. 1981. A few limestone samples from Appendix C with significant elements of clay minerals were excluded. Results are summarized in Fig. 27, and a distinct conductivity-porosity correlation is demonstrated and well described by the geometric mean relation  $k(\phi) = 0.58^\phi \cdot 3.26^{(1-\phi)}$  defined from 58 sample values. Parameters are determined by the

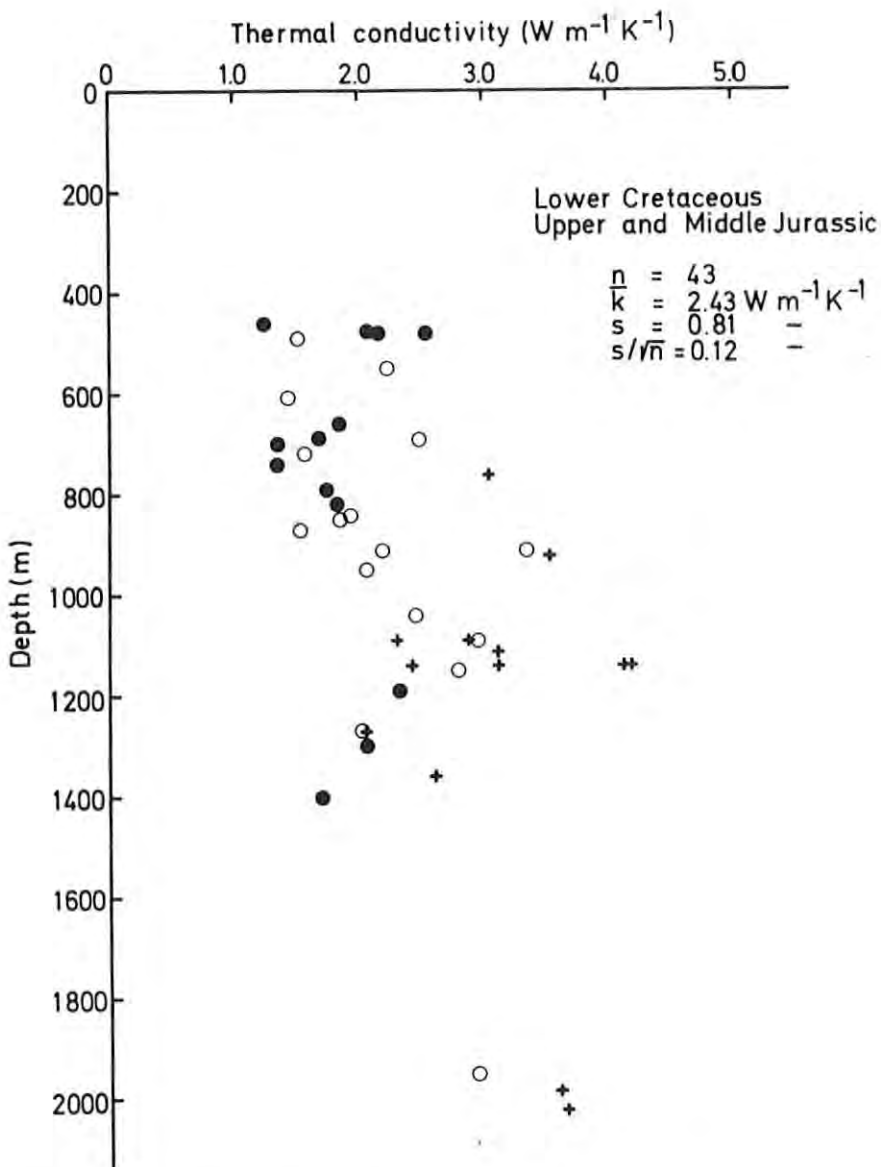


Fig. 22. Thermal conductivity of Lower Cretaceous, Upper and Middle Jurassic samples plotted as a function of depth. See text to Fig. 20 for symbols.

method of least squares and are in close agreement with those of water (at room temperature) and pure non-porous calcite (Birch and Clark, 1940).

The increase of conductivity of limestones with depth (Fig. 21) is thus closely related to the decrease in porosity (Fig. 28).

Most claystones, and especially laminated shale, show thermal conductivity anisotropy with a low conductivity perpendicular to bedding-planes and higher parallel-components. Values reported

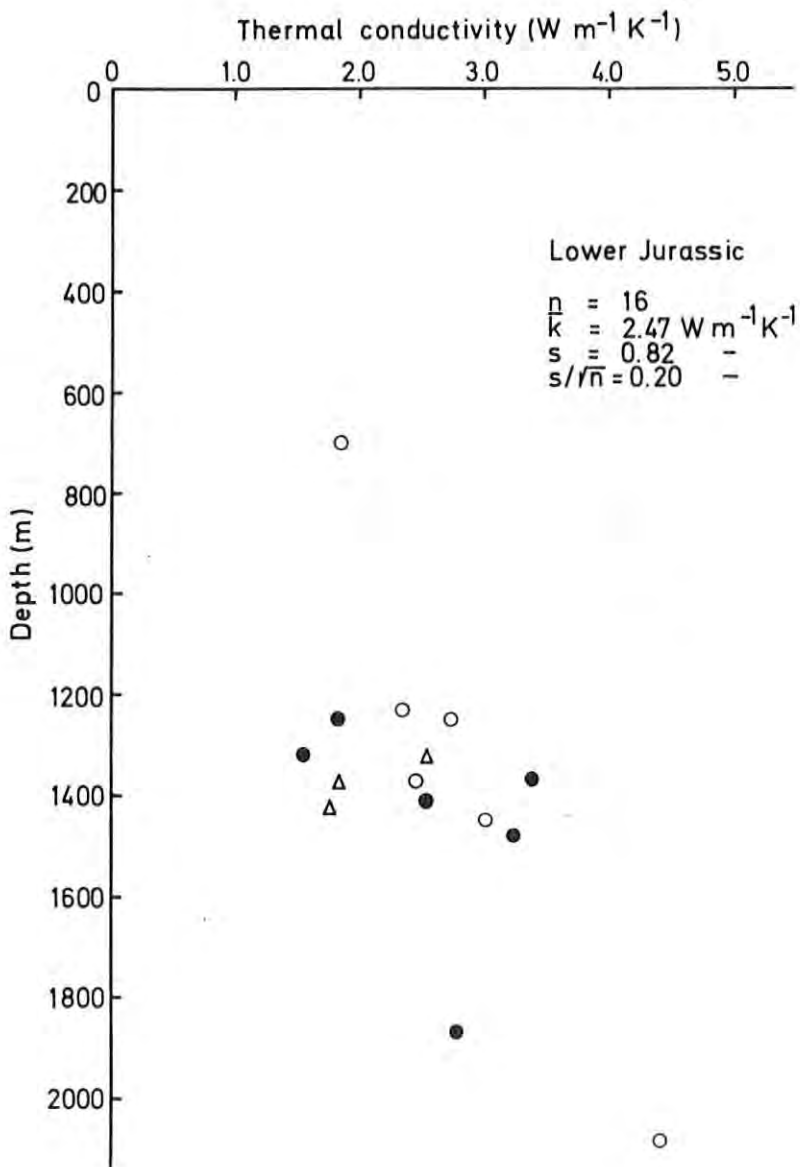


Fig. 23. Thermal conductivity of Lower Jurassic samples plotted as a function of depth. See text to Fig. 20 for symbols.

here include measurements with needles placed perpendicular to bedding, providing the parallel-component of conductivity, and needles placed parallel to bedding, providing a weighted mean of components. Bedding planes are observed to be generally almost horizontal, and our conductivities thus represent the maximum values of the vertical component, which is the component to be used in subsurface temperature extrapolation. Due to the poor quality of most laminated core material, no systematic anisotropy analysis was performed. The limestones and most

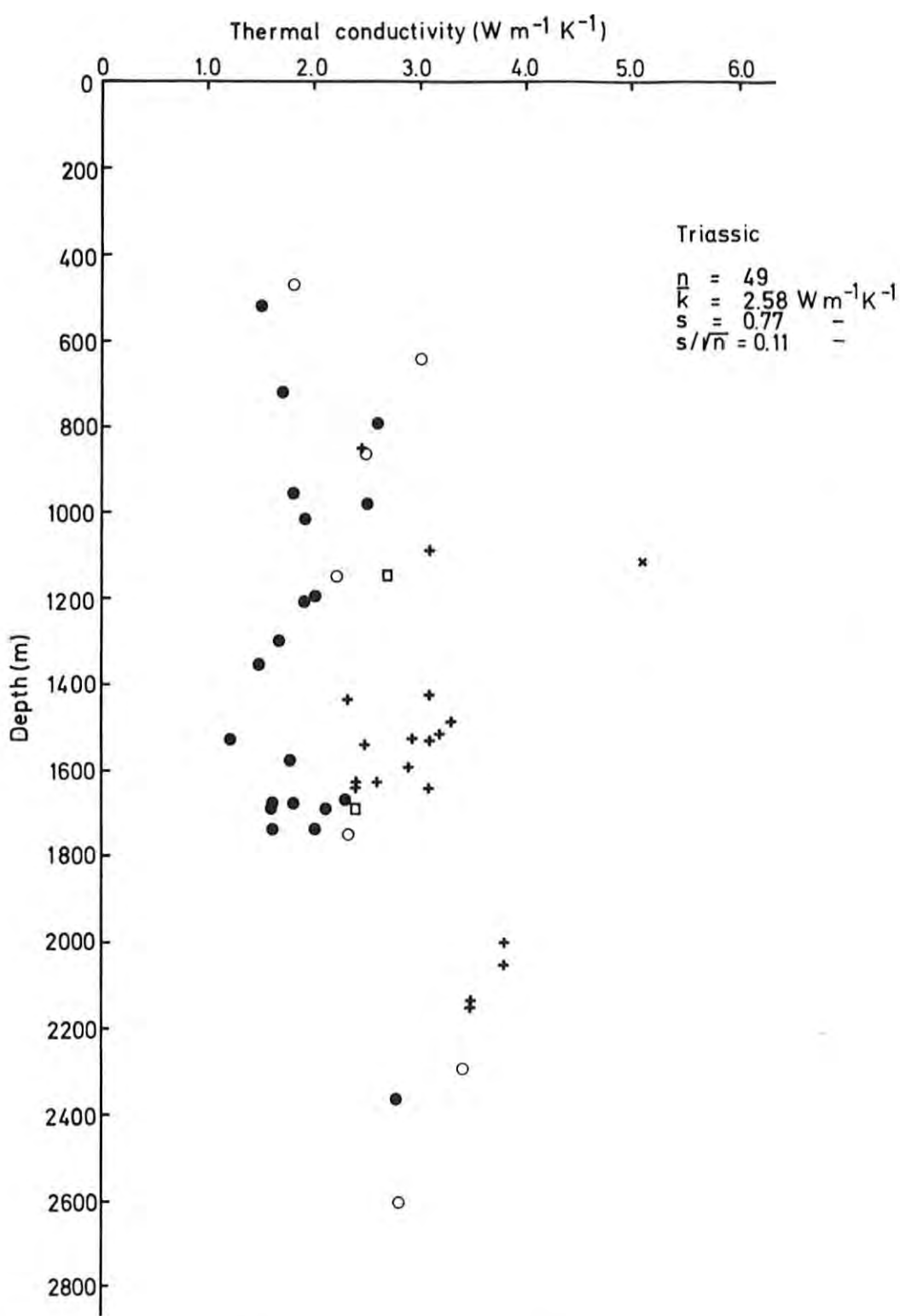
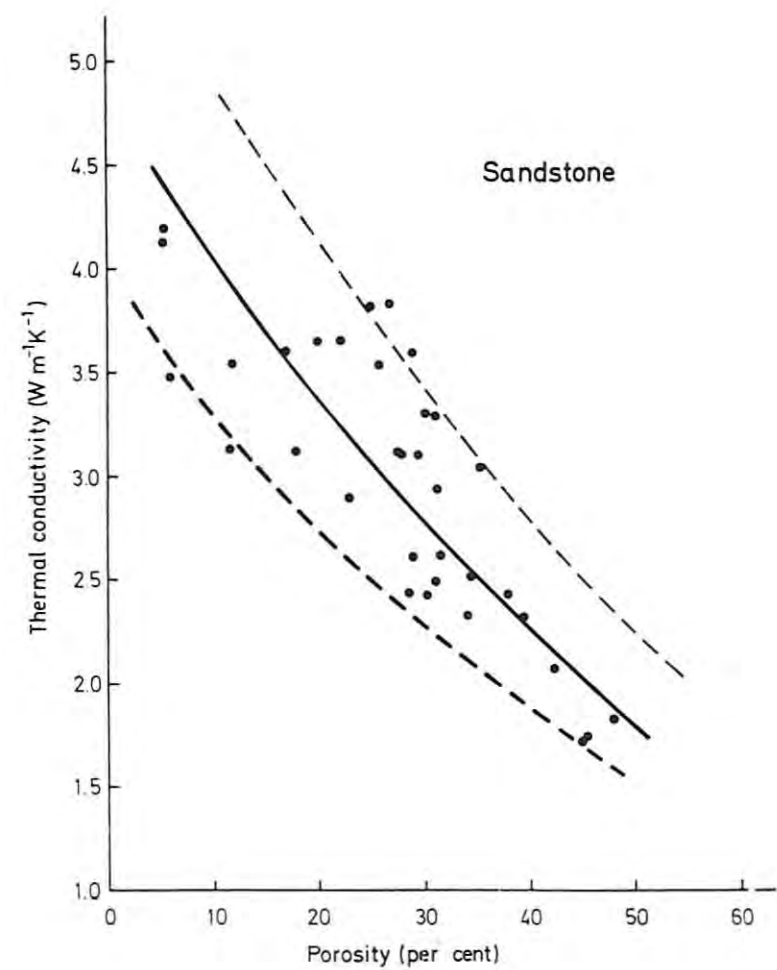
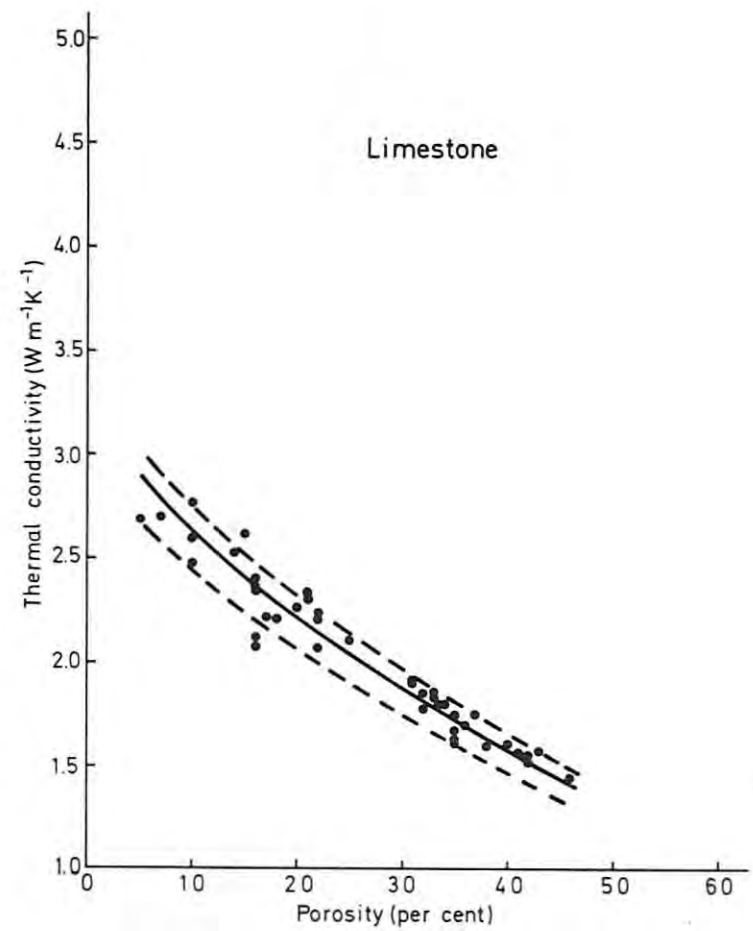


Fig. 24. Thermal conductivity of Triassic samples plotted as a function of depth. See text to Fig. 20 for symbols.



Sandstone



Limestone

Fig. 25. Thermal conductivity of sandstone and limestone (incl. chalk) as a function of porosity. The estimated general mean, maximum, and minimum relations are drawn.

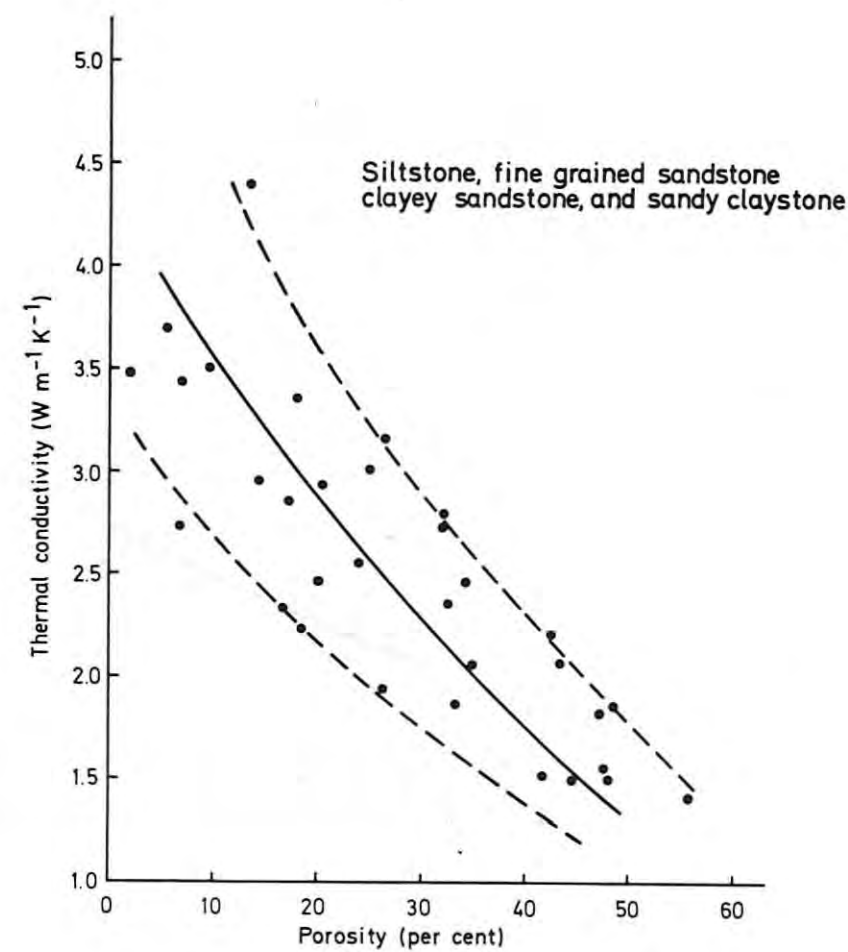
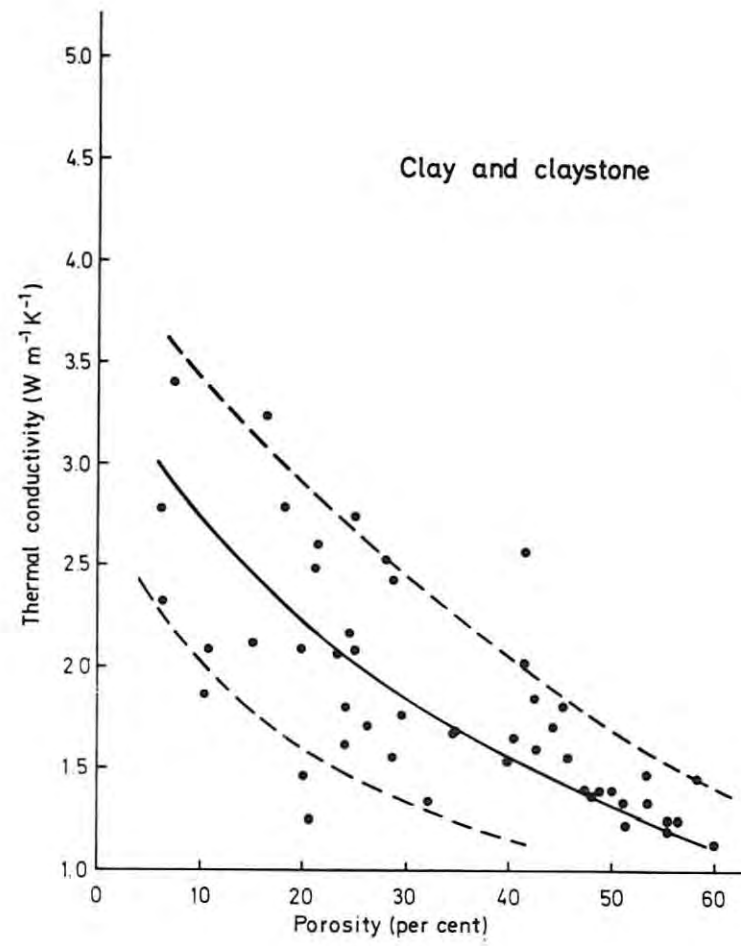


Fig. 26. Thermal conductivity of clay, claystone (incl. shale) and siltstone etc. as a function of porosity. The estimated general mean, maximum and minimum relations are drawn.

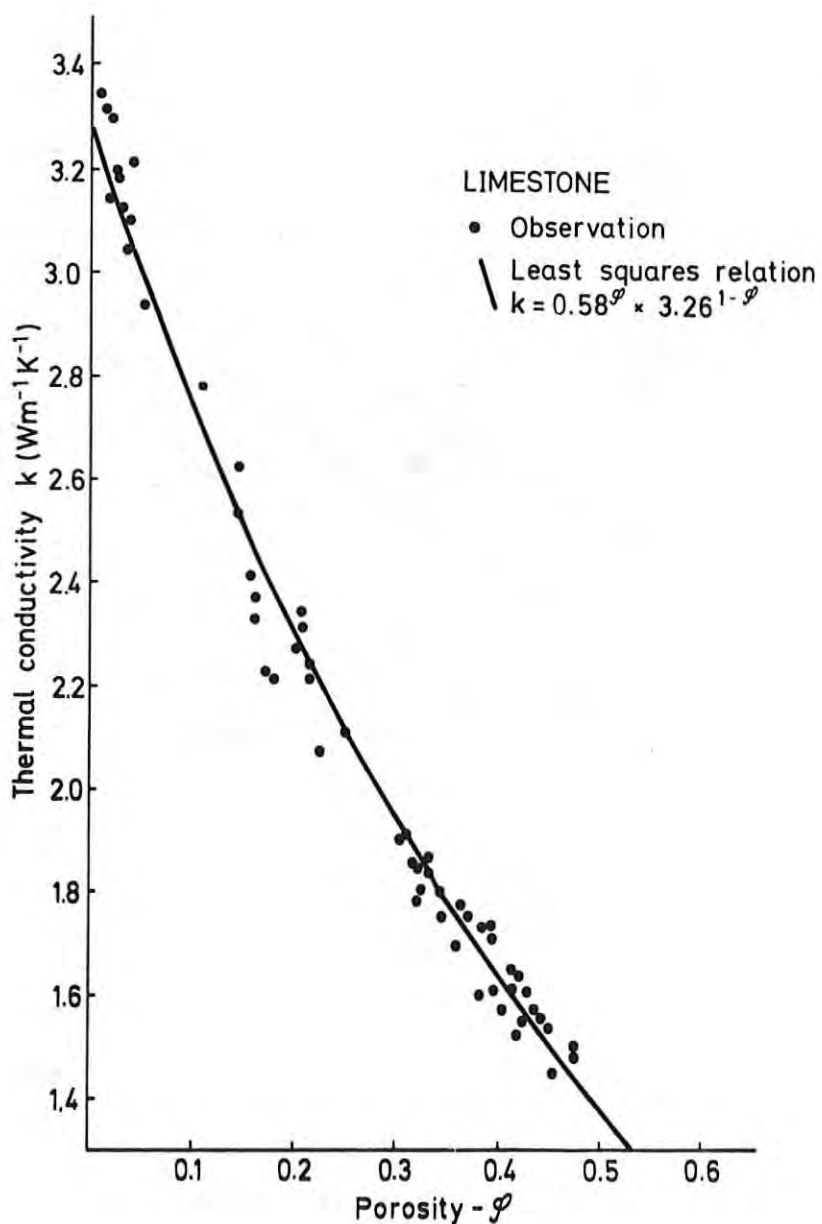


Fig. 27. Thermal conductivity (water-saturated) of limestones as a function of porosity, and the least squares geometric mean function. Results of measurements from 58 Danish and Swedish samples.

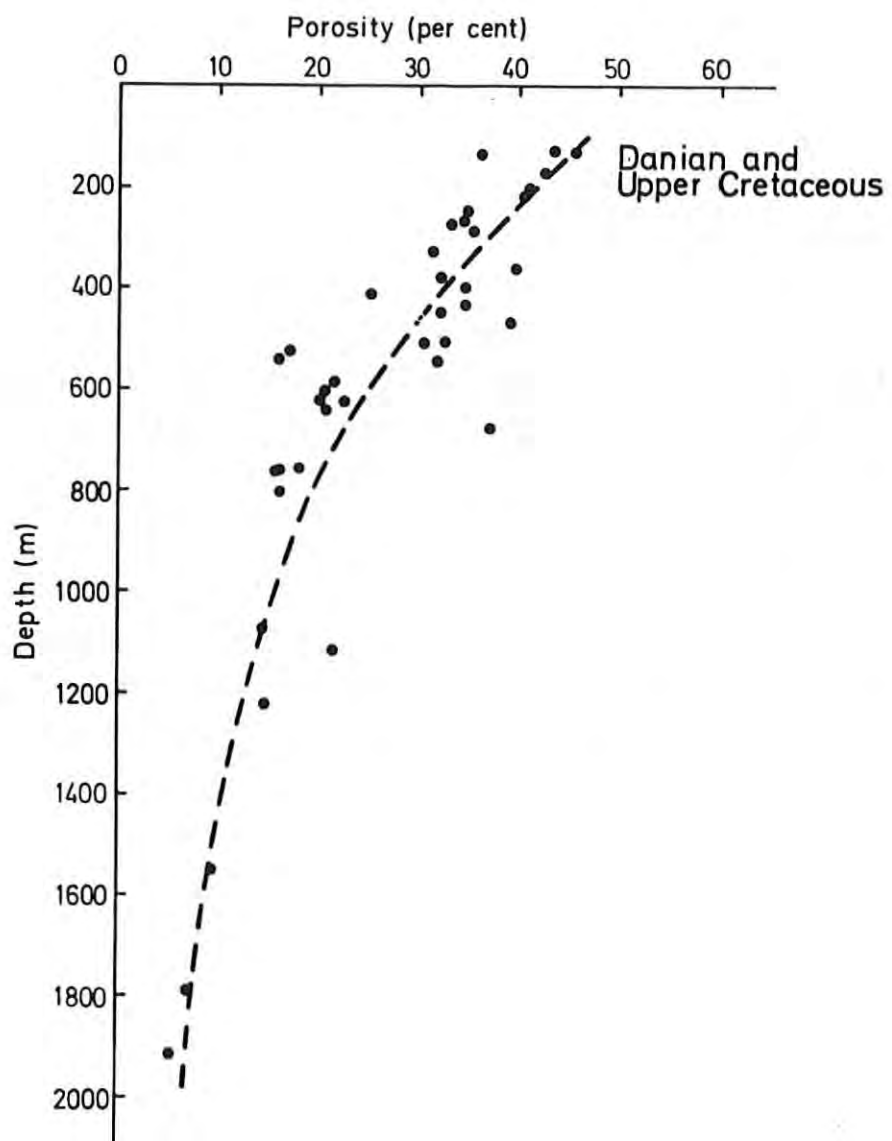


Fig. 28. Porosity of Danian and Upper Cretaceous limestone samples plotted as a function of depth. The estimated general trend of porosity decrease with depth is indicated.

sandstones showed no significant conductivity anisotropy.

Some preliminary investigations have been carried out to measure the conductivity as a function of temperature and pressure. The conductivity temperature dependence was measured by the needle probes on water-saturated samples where the samples were thermally isolated in a water bath of constant but variable temperatures between 10 and 70°C. The divided bar apparatus was used to measure the conductivity pressure dependence. Pressure was increased hydraulically and uniaxially up to about 100 bar without destroying the samples. All samples measured (porous limestone and claystone) showed an almost linear decrease in conductivity with temperatures of about 5 per cent within the actual temperature range (Fig. 29).

Both dry and water-saturated samples were measured as a function of pressure. The examples given in Fig. 30 seem to be typical of the rock types in question, showing an increase in conductivity of about 10 per cent for the dry sample and about 5 per cent for the water-saturated sample, with most effect observed at low pressures ( $\leq 50$  bar). Within the uppermost few km of the sedimentary sequence, a decrease of conductivity with temperature may to some degree be compensated by an increase with increasing pressure, and with a generally small total effect.

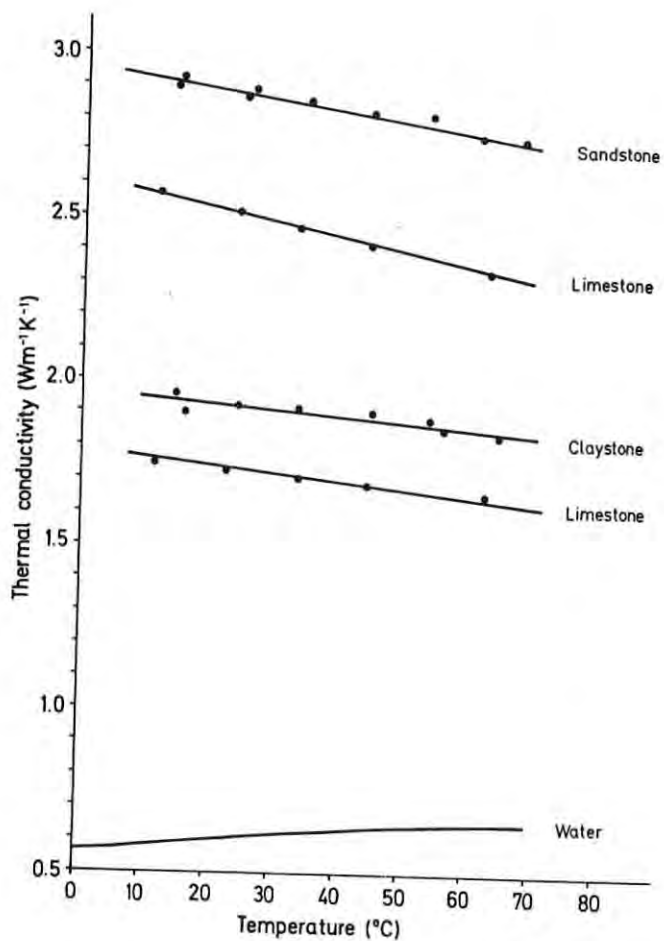


Fig. 29. Examples of thermal conductivity measured by needle probes as a function of temperature. The two limestone samples are of different porosity. Since water conductivity increases with temperature (also shown in the figure) the water-saturated samples of high porosity generally show the least conductivity decrease.

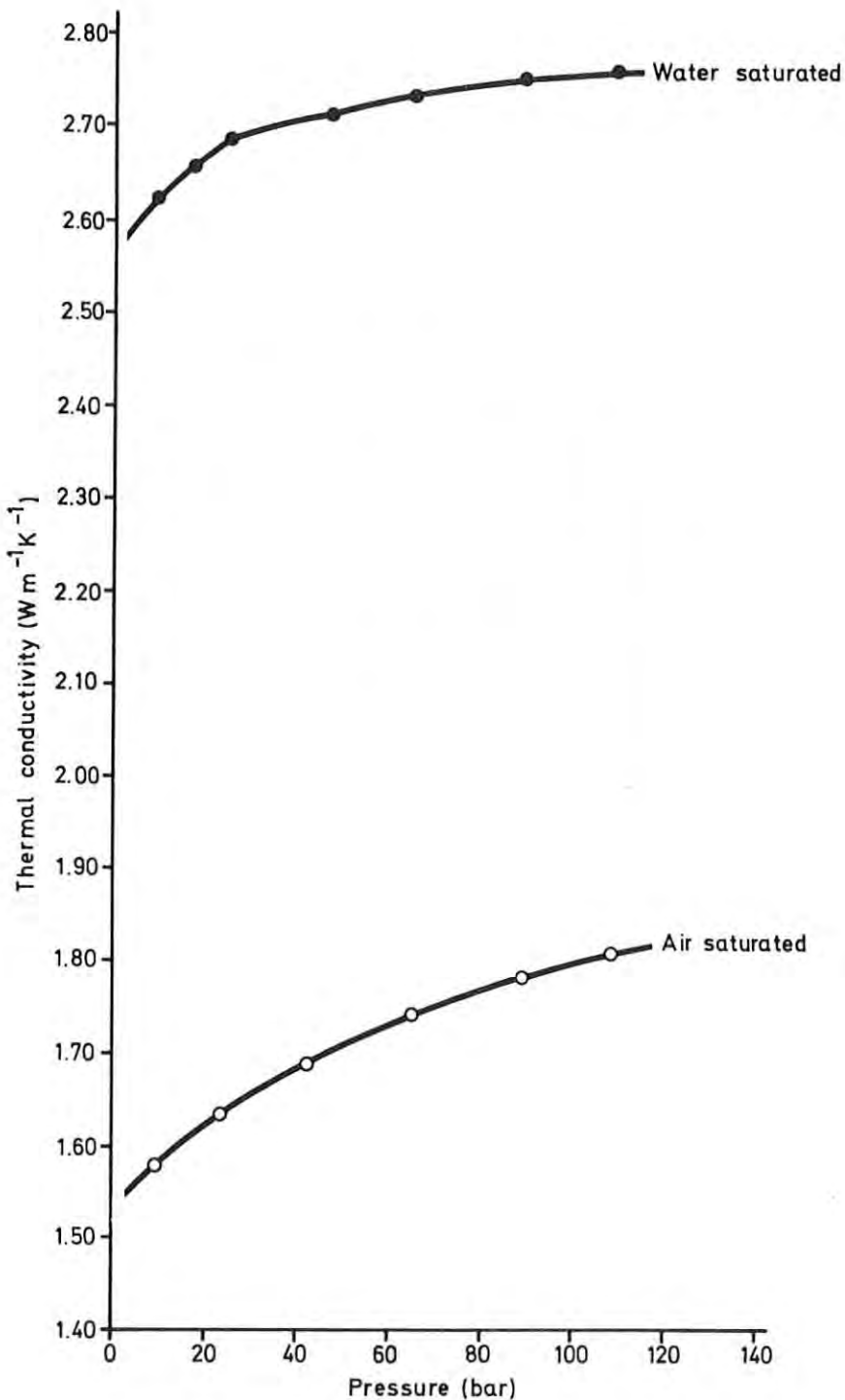


Fig. 30. Examples of thermal conductivity measured as a function of uniaxial pressure. The divided bar apparatus was applied. Results are from the same specimen of limestone (porosity 0.15) and illustrate the significant differences in values and degree of variation for dry and water-saturated samples.

### 2.3 Heat production

Heat is generated by the natural decay of radioactive nuclei of rocks, but only the long-lived decay series of  $U^{238}$ ,  $U^{235}$ ,  $Th^{232}$  and  $K^{40}$  are significant (Birch, 1954). The heat production constants of Birch (Table 5) are normally used to convert concentrations of elements to generated heat per unit time. Within the Danish geological environment we have observed no indications of other processes of significant heat release such as chemical reactions and crystallization. The radioactive heat production of typical sediments is normally low (e.g. Kappel-meyer and Haenel, 1974) and has little influence on temperatures to depths of a few kilometres as considered here. The number of samples was thus limited. 28 samples were selected from the main lithologies and analysed by gamma ray spectrometry at the Risø National Laboratory. This method enables the simultaneous determination of concentrations of uranium, thorium and potassium and involves a simple sample preparation. The Risø laboratory spectrometer houses a 5 x 5 inch NaI(Tl) scintillation detector contained within an 11 cm thick lead shield. A 3 inch thick cylinder of non-activated NaI between the detector crystal and the photomultiplier serves to attenuate  $K^{40}$  background radiation. The sample canisters typically take some 250 g of finely crushed material. Our samples were measured for 5000 s (83.3 min.).

Table 5

Heat generation constants (Birch 1954)

<u>Element</u>	<u>Heat generation</u>	
	$cal\ g^{-1}\ y^{-1}$	$W\ kg^{-1}$
U (natural)	0.73	$9.7 \cdot 10^{-5}$
$Th^{232}$	0.20	$2.7 \cdot 10^{-5}$
K (natural)	$2.7 \cdot 10^{-5}$	$3.6 \cdot 10^{-9}$

With the heat generation constants of Table 5, measured concentrations of natural U( $c_U$ ),  $\text{Th}^{232}$ ( $c_{\text{Th}}$ ), natural K( $c_K$ ), and measured (dry) density ( $\rho$ ), the heat generation per unit volume is calculated from

$$A[\mu\text{W m}^{-3}] = \rho[\text{kg m}^{-3}] (9.7 c_U[\text{ppm}] + 2.7 c_{\text{Th}}[\text{ppm}] + 3.6 c_K[\text{per cent}]) \cdot 10^{-5}$$

Results of measurements and the calculated sample heat generation are listed in Appendix D and summarized in Fig. 31.

(Error of calculation in preliminary results reported by Balling et al. 1980, which resulted in too low heat production values, has here been corrected).

The experimental standard deviations of values are typically 0.03% K, 0.15 ppm U and 0.3 ppm Th equivilating about 0.05  $\mu\text{W m}^{-3}$  ( $\rho = 2 \cdot 10^3 \text{ kg m}^{-3}$ ). Considering maximum uncertainty of density of about  $0.1 \cdot 10^3 \text{ kg m}^{-3}$ , the associated heat production standard deviation is about  $0.1 \mu\text{W m}^{-3}$ . The mean value obtained ( $1.13 \mu\text{W m}^{-3}$ ) and distribution of values are typical for the rock types in question (Rybáček, 1973; Kappelmeyer and Haenel, 1974). Claystone shows the highest concentrations of all elements and consequently the highest heat production. The lowest values are observed for saline rocks, sandstone, and limestone.

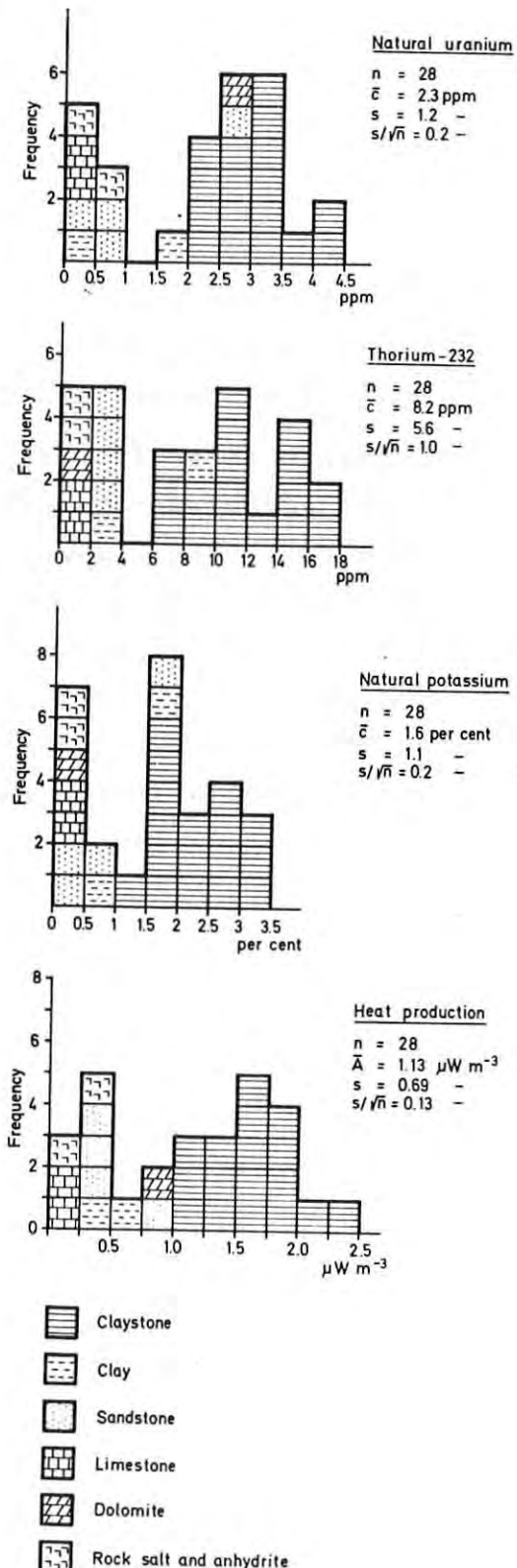


Fig. 31. Histograms on measured concentrations of natural uranium, thorium-232, natural potassium, and the associated calculated heat production of 28 samples of various lithologies. Values are listed in Appendix D.

## 2.4 Heat flow

The outflow of heat from the Earth, the terrestrial heat flow or geothermal flux, combined with surface temperature defines the physical surface boundary constraint on subsurface temperatures. In land areas heat flow values are obtained from observations in a) deep boreholes (almost always drilled for other than geothermal purposes) b) shallow or intermediate deep holes (which may be drilled for geothermal purposes) c) suitable lakes and d) mines and tunnels (Lee, 1965).

Compared with measurements at shallow depth measurements in deep boreholes have the advantage that they are not (or only very slightly) influenced by the environmental variations at or near the Earth's surface, such as temperature variations associated with palaeoclimate and ground water movements. However, the number of deep borings available for heat flow observations is usually limited. Such holes may be unevenly distributed and may not be available for measurements for economic and practical reasons. Expensive coring is essential if accurate and representative thermal conductivities are to be measured, and boring should be left undisturbed and available for temperature logging for months or even years after the termination of drilling activities before the equilibrium temperatures (Bullard, 1947) or temperature gradients are measured. In some cases, especially if thick sequences of thermally uniform strata are penetrated, valuable heat flow values may be obtained from a combination of measured and estimated thermal conductivities, and equilibrium temperatures found from extrapolation of non-equilibrium values, such as bottom hole temperatures measured during drilling (Lachenbruch and Brewer, 1959; Oxburgh et al., 1972).

Six such estimated heat flow values have been published from the Danish area (Balling, 1979). In Fig. 32 values are given without palaeoclimatic corrections, the effect of which is evaluated separately later in this section.

It would be a great improvement if the number of accurate and representative terrestrial heat flow values could be increased



Fig. 32. Heat flow estimates from deep boreholes; depths ~1000 m (Balling, 1979). Values are here given without palaeoclimatic corrections. See also Tables 11 and 12.

by more observations at shallow depths in boreholes, lakes and shallow waters. This is a general problem and applies especially to the Danish area.

The question is whether we can find methods and geological formations suitable for accurate conductive heat flow measurements at near surface level. This also involves the problems of corrections of observations. In the following some calculations on the possible perturbations of heat flow from surface or near surface effects are made, with the main emphasis on the palaeoclimatic influence in shallow holes and the annual temperature variations in lake bottom sediments. These studies are essential for the planning and placing of observation sites and for the interpretation of results. The first results of measurements are then presented.

#### 2.4.1 Prediction of perturbations

In subsurface temperature modelling and most other applications of terrestrial heat flow values, we devote our main interest to the values unaffected by or corrected for the influence of surface or near-surface phenomena such as climatic and annual temperature variations, contrasts in mean annual soil temperature, topography, sedimentation, erosion, uplift, subsidence, ground water movements, and local contrasts in thermal conductivity. The basic physical-mathematical problems encountered in most of the perturbations or reductions associated with these phenomena are reviewed by Jaeger (1965).

Within the Danish geological environment only few reductions are expected to be significant. A number of analytical and numerical calculations have shown typical near surface heat flow perturbations of  $\pm 1-2 \text{ mW m}^{-2}$  or less, associated with topographic and microclimatic variations, sedimentation, erosion, uplift, and subsidence. Perturbations from palaeoclimatic temperature variations and annual temperature variations (e.g. in lake bottom sediments) may be an order of magnitude higher and therefore be significant. In the following we consider some calculations and models on these problems.

### Effect of palaeoclimatic temperature variations

It has long been recognized that variations of temperature at the Earth's surface may significantly affect subsurface temperature gradients and heat flow (Anderson, 1934; Benfield, 1939; Birch, 1948; Jessop, 1971; and Beck, 1977) and several authors have corrected measurements with a view to obtaining heat flow values unaffected by the variation of palaeoclimate. However, various palaeoclimatic models are in use even for the same areas and regions, resulting in different corrections. Čermák (1971) attempted to resolve past climate from measured temperature gradients. This inverse procedure requires ideal environments and data of very high accuracy.

A very large data material proving the variability of ancient and recent climates has been compiled and discussed by Lamb (1972 and 1977). During recent years the literature on studies of climatic variations has been considerably increased. Berger (1979) and Frakes (1979) survey the topic and the potential causes of climatic variations recorded since the origin of the Earth, including the most recent variations. It is generally accepted that for the last 2 million years at least, climatic variations have been characterized by the alternation of glacial and interglacial episodes, marked by falling and rising temperatures. There may have been more than thirty Late Cenozoic glaciations spaced at intervals of about 100 000 years. Warm intervals similar to that of to-day, may have existed for only 5 per cent of Quaternary time. Cycles of 100 000, 41 000, 23 000, and 19 000 years which may have dominated through the Quaternary, are all related to the Earth's orbital elements (Berger op.cit.). In terrestrial heat flow studies only temperature variations through the very Late Quaternary (last 100-200 000 years) seem to influence observations significantly. From that period of time, evidence on temperature changes is produced from a variety of sources (e.g. Lamb, 1977, Fig. 15.10, p. 333) including the oxygen isotope records from ice cores from the Greenland ice sheet (Dansgaard et al., 1971, 1973; Johnson et al., 1972).

In the following we calculate geothermal effects of three basic temperature models (A, B, and C) approximating the surface

Table 6

Models of surface temperature history used for the calculation of subsurface geothermal perturbations. Model C is the model of Bech (1977) for latitudes  $40^{\circ}$ - $60^{\circ}$ . Time (t) in years before present and temperature change ( $\Delta T$ ) in K.

MODELS A and A1		MODELS B, B1, B2, and B3		MODEL C	
t	$\Delta T$	t	$\Delta T$	t	$\Delta T$
A	70,000 -10			190,000 -10	65,000 9
A1	10,000 10			130,000 10	35,000 -3
				70,000 -10	10,000 12
B				10,000 10	7,000 1.5
				8,000 2	2,000 -1.5
B1				5,000 -1	1,000 0.75
				1,600 -1	700-500 -3 *)
				1,300 0.5	150-100 2.5*)
				1,000 1	
B2				700-350 -2*)	
				350- 0 1*)	
B3					

\*) linear change

temperature history, and submodels (A1, B1, B2, and B3) as shown in Table 6.

Our physical model consists of a thermally homogeneous, isotropic half space, and the boundary temperature variations are mathematically defined as step and linear changes. For that model the half space (subsurface) disturbances on temperatures are easily calculated by the analytical solutions (Carslaw and Jaeger, 1959, p. 63) to the heat equation  $\frac{\partial^2 T}{\partial z^2} = \frac{1}{\kappa} \frac{\partial T}{\partial t}$ . For a step change of temperature  $\Delta T$  at time  $t'$ , the disturbance at depth  $z$  and time  $t$  is

$$\Delta T(z, t) = \Delta T \operatorname{erfc} \frac{z}{(4\kappa(t-t'))^{\frac{1}{2}}} \quad (1)$$

where  $\kappa$  is the half space thermal diffusivity. For a linear change of temperature at the surface

$$\Delta T(t) = \begin{cases} 0 & t \leq 0 \\ kt & t > 0 \end{cases}$$

The solution is given by

$$\Delta T(z, t) = kt \left[ \left(1 + \frac{z^2}{2kt}\right) \operatorname{erfc} \frac{z}{2(kt)^{\frac{1}{2}}} - \frac{z}{(\pi kt)^{\frac{1}{2}}} \exp\left(-\frac{z^2}{4kt}\right) \right] \quad (2)$$

After differentiation with respect to  $z$ , we obtain the disturbance to temperature gradients; for the step change

$$\Delta G(z, t) = - \frac{\Delta T}{(\pi k(t-t'))^{\frac{1}{2}}} \exp\left(-\frac{z^2}{4k(t-t')}\right) \quad (3)$$

and for the linear change

$$\Delta G(z, t) = kt \left( \frac{z}{kt} \operatorname{erfc} \frac{z}{2(kt)^{\frac{1}{2}}} - \frac{2}{(\pi kt)^{\frac{1}{2}}} \exp\left(\frac{-z^2}{4kt}\right) \right) \quad (4)$$

The effects of a sequence of temperature events are obtained by summation. Since heat flow ( $\bar{q}$ ) is related to gradient by Fourier's law  $\bar{q} = -k \operatorname{grad} T$ , where  $k$  is the thermal conductivity, disturbances to heat flow are readily calculated if conductivity is known.

Model A of Table 6 is the most simple one, containing only two events but including the most significant temperature variations during about the past 100,000 years, viz. the cold period of the last (Weichselian) ice age. Model B goes as far back as about 200,000 years and includes the two last ice ages and the Eemian interglacial and also events of  $\pm 0.5-2$  K from the past 10,000 years. This model is mostly based on data compiled and discussed by Lamb (1977) and Berger (1979), and has been derived to attempt to cover the region of NW Europe including the Danish area. Most major events seem to be global, but with some variations especially in amplitude but also in time. Model C is the global model for latitudes  $40-60^\circ$  used by Beck (1977) in his detailed treatment of the influence from palaeoclimate on regional and continental climates.

nental heat flow. We emphasize that the complex nature of climatic temperature changes are approximated in this study by a limited number of events, which is justified by the present application. No general agreement exists among climatic workers on the amplitudes of the basic variations and their exact placing in space and time. We model disturbances with a double amplitude of 10 K for the long wavelength variations associated with the two last ice ages, but do not exclude other possibilities. In Berger (1979, Table V, p. 381) a double amplitude of 8 K is given, and as seen from Table 5 Beck applies 9 and 12 K. By using climatic models for the last glacial maximum about 18,000 B.P., Gates (1976) found air surface temperatures south of the North American and the North European ice sheets to be 5-15 K colder than at present, and global air mean temperatures about 5 K less than at present. If the deep cooling at that time only lasted for a short period, it will have little influence on present subsurface temperature gradients. We emphasize the approximate nature of values and their accuracy by using 10 K. Since, by Equation (3), temperature and gradient perturbations are directly proportional to  $\Delta T$ , the evaluation of the effects of variations of  $\Delta T$  is straightforward. The model temperature step of -10 K at 70,000 B.P. approximates a temperature history which is much more complex, containing interglacials and perhaps an overall more gradual decrease of temperature associated with the last ice age cooling period, which may have started in Europe at about 110-115,000 B.P. It is generally accepted that the first major deglacial warming following the last glaciation occurred about 13,000 B.P. and culminated at 12,000 - 11,000 B.P. Both cooling and warming episodes followed, which we include in the +10 K step at 10,000 B.P.

We believe that our model B is in better agreement with literature data for our region than the model used by Beck (op.cit.), especially for the time and temperature variation of the Little Ice Age (e.g. Lamb, 1977, Table 16.2, p. 407).

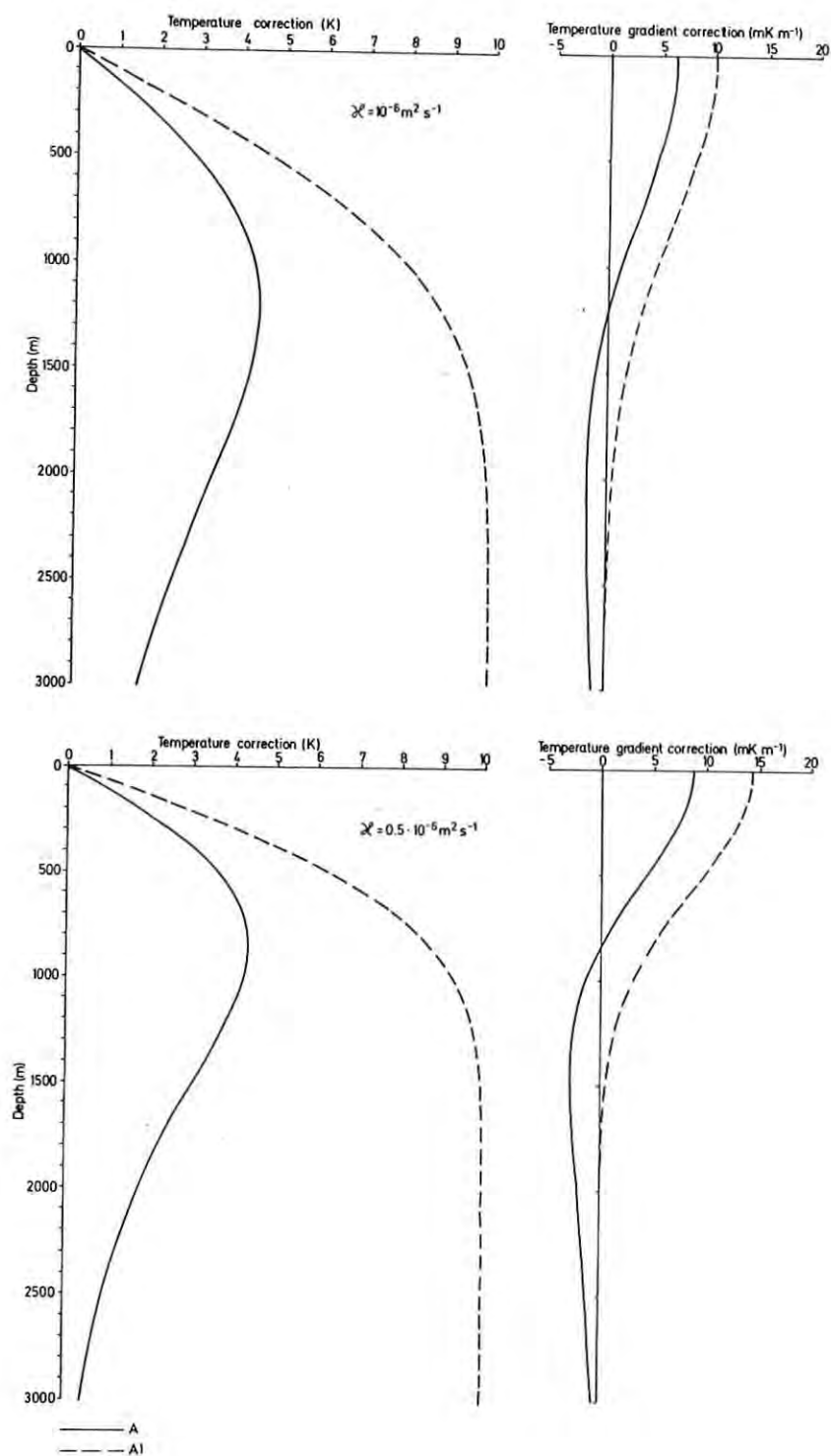


Fig. 33. Temperature and temperature gradient corrections associated with surface temperature models A and A1 (Table 6). Curves for two different thermal diffusivities ( $10^{-6}$  and  $0.5 \cdot 10^{-6} \text{ m}^2 \text{ s}^{-1}$ ) are shown. The corrections are those to be added to observations. Values are listed in Tables 7 and 8.

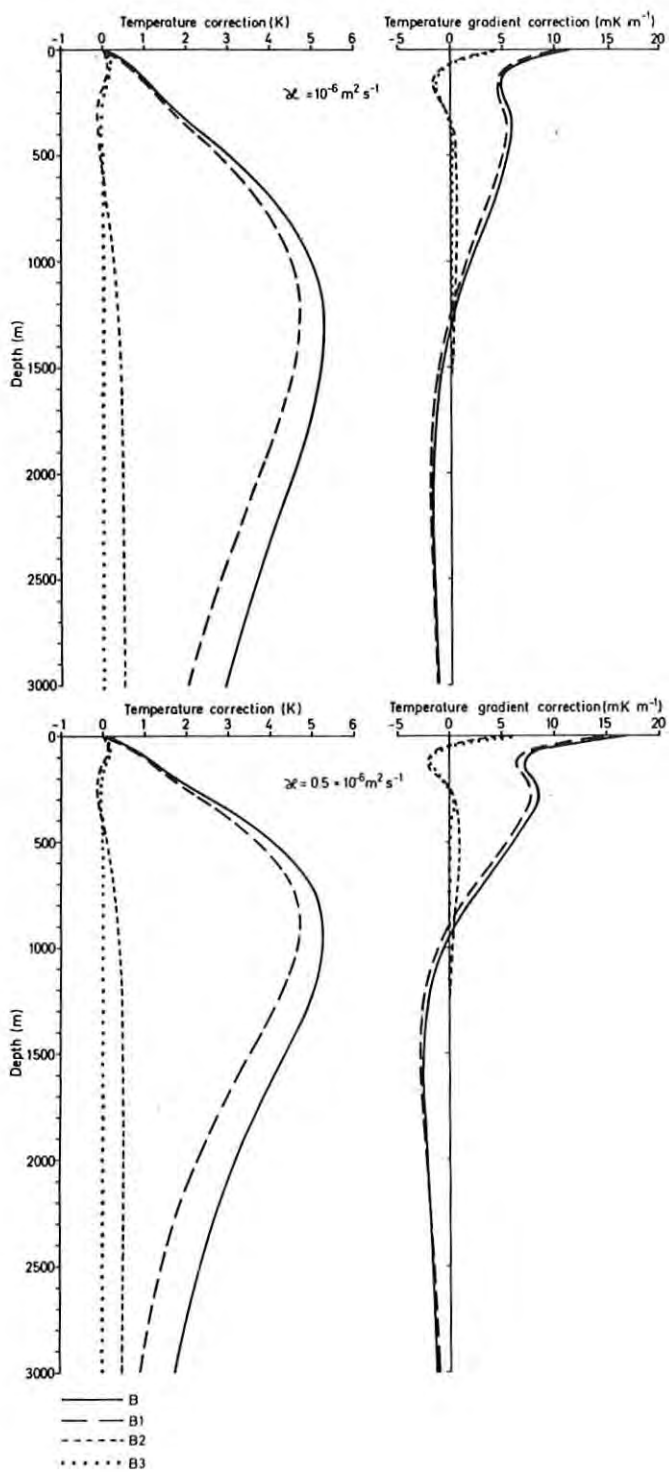


Fig. 34. Temperature and temperature gradient corrections associated with the surface temperature model B and submodels B1, B2, and B3 (Table 6). Calculations equivalent to those of Fig. 33.

Table 7

Calculated geothermal gradient corrections (values to be added to observations) for the 7 models of surface temperature history (Table 6) and a half space of thermal diffusivity  $0.5 \cdot 10^{-6} \text{ m}^2 \text{ s}^{-1}$ .

Graphs appear in Figs. 33, 34, and 35.

Depth (m)	MODELS						
	A	A <sub>1</sub>	B	B <sub>1</sub>	B <sub>2</sub>	B <sub>3</sub>	C
0	8.8	14.2	16.2	15.5	6.7	7.1	25.4
50	8.8	14.2	9.6	8.9	0.1	0.5	17.6
100	8.6	14.0	7.2	6.5	-2.1	-1.8	6.0
150	8.4	13.7	7.1	6.5	-1.9	-1.7	2.3
200	8.0	13.3	7.9	7.2	-0.8	-0.8	3.6
250	7.6	12.9	8.4	7.7	0.1	-0.1	5.5
300	7.1	12.3	8.4	7.7	0.6	0.3	6.6
350	6.5	11.7	8.0	7.3	0.8	0.3	6.9
400	5.8	11.0	7.4	6.7	0.9	0.2	6.7
450	5.2	10.3	6.7	6.1	0.9	0.1	6.2
500	4.5	9.6	6.0	5.4	0.9	0.1	5.5
600	3.1	8.0	4.5	3.9	0.9	0.0	4.0
700	1.7	6.5	3.1	2.5	0.8	0.0	2.3
800	0.5	5.2	1.7	1.1	0.6	0.0	0.8
900	-0.5	3.9	0.5	-0.1	0.5	0.0	-0.6
1000	-1.4	2.9	-0.5	-1.0	0.4	0.0	-1.6
1500	-2.8	0.4	-2.5	-2.8	0.0	0.0	-3.2
2000	-2.1	0.0	-2.1	-2.1	0.0	0.0	-2.2
2500	-1.3	0.0	-1.4	-1.3	0.0	0.0	-1.2
3000	-0.7	0.0	-0.9	-0.7	0.0	0.0	-0.6

#### Results of calculations

Temperature and temperature gradient corrections are calculated for models A, A<sub>1</sub>, B, B<sub>1</sub>, B<sub>2</sub>, and B<sub>3</sub> with thermal diffusivities of  $0.5$  and  $1.0 \cdot 10^{-6} \text{ m}^2 \text{ s}^{-1}$  (Figs. 33 and 34 and Tables 7 and 8). Results obtained by models A, B, and C are compared in Figs. 35, 36, and 37, where we also present results with a rather high diffusivity of  $1.5 \cdot 10^{-6} \text{ m}^2 \text{ s}^{-1}$  and associated heat flow corrections.

Table 8

Calculated geothermal gradient corrections for a half space of diffusivity  $10^{-6} \text{ m}^2 \text{ s}^{-1}$  (cf. Tables 6 and 7 and Figs. 33, 34, and 36).

Depth (m)	MODELS						
	A	A <sub>1</sub>	B	B <sub>1</sub>	B <sub>2</sub>	B <sub>3</sub>	C
0	6.2	10.0	11.5	11.0	4.7	5.0	17.9
50	6.2	10.0	7.8	7.3	1.1	1.4	14.9
100	6.2	10.0	5.8	5.3	-0.9	-0.6	8.6
150	6.1	9.9	5.0	4.5	-1.6	-1.4	3.6
200	6.0	9.7	5.0	4.5	-1.4	-1.3	1.7
250	5.8	9.6	5.3	4.8	-1.0	-0.9	1.9
300	5.6	9.4	5.7	5.2	-0.4	-0.4	2.9
350	5.4	9.1	5.9	5.4	0.1	-0.1	3.9
400	5.1	8.8	5.9	5.5	0.4	0.1	4.5
450	4.8	8.6	5.8	5.4	0.5	0.2	4.8
500	4.5	8.2	5.6	5.1	0.6	0.2	4.9
600	3.9	7.6	5.0	4.5	0.6	0.1	4.6
700	3.2	6.8	4.3	3.9	0.6	0.1	4.0
800	2.5	6.0	3.6	3.1	0.6	0.0	3.2
900	1.8	5.3	2.8	2.4	0.6	0.0	2.4
1000	1.2	4.5	2.1	1.7	0.5	0.0	1.5
1500	-1.3	1.7	-0.7	-1.1	0.2	0.0	-1.5
2000	-2.0	0.4	-1.7	-2.0	0.0	0.0	-2.3
2500	-1.8	0.1	-1.7	-1.8	0.0	0.0	-2.0
3000	-1.4	0.0	-1.3	-1.4	0.0	0.0	-1.4

These are calculated on the assumption that the product of density ( $\rho$ ) and specific heat ( $c$ ) of rocks are nearly constant (e.g. Beck, op.cit.). Normally, values of  $\rho c$  range between 2 and  $3 \cdot 10^6 \text{ J m}^{-3} \text{ K}^{-1}$ , and we applied the constant value of  $2.5 \cdot 10^6 \text{ J m}^{-3} \text{ K}^{-1}$ . The thermal conductivity is then directly calculated from  $k = \kappa \rho c$ . Low thermal diffusivities ( $\sim 0.5 \cdot 10^{-6} \text{ m}^2 \text{ s}^{-1}$ ) and low conductivities ( $\sim 1 \text{ W m}^{-1} \text{ K}^{-1}$ ) have been measured from shallow ( $\lesssim 300 \text{ m}$ ) Danish clay lithologies, and are thus of special interest.

for our shallow borehole observations. High diffusivities of  $\sim 1.5 \cdot 10^{-6} \text{ m}^2 \text{ s}^{-1}$  may be found primarily in crystalline areas, and apart from the island of Bornholm (Kristiansen et al., 1981) such high diffusivities will seldom occur in Denmark. Locally, the salt structures show very high conductivities of about  $5-6 \text{ W m}^{-1} \text{ K}^{-1}$  which are not dealt with in this connection.

From Fig. 33 and Tables 7 and 8 we find that if the single event of model A1 is considered, i.e. only including the increase of temperature at the beginning of the Holocene and disregarding the decrease at the beginning of the Weichselian glaciation, model gradient and heat flow corrections are generally too high by  $4-6 \text{ mK m}^{-1}$  and  $8-10 \text{ mW m}^{-2}$ , respectively.

Comparison of results obtained by model B and the submodels of B shows three main characteristics; firstly that the effect from the cooling period of the last but one glaciation (within the time interval approximately 100,000 - 200,000 B.P.) is very small and about  $0.5-1 \text{ mK m}^{-1}$  (difference between models B and B1 results); secondly that the minor temperature variations from the period  $\sim 1,000$  to  $\sim 10,000$  B.P. are of the same order of magnitude or less (difference between models B2 and B3); and thirdly that temperature variations in the past 500 - 1,000 years may significantly affect the uppermost  $\sim 300$  m. Furthermore, we observe that decrease of diffusivity generally amplifies the gradient perturbations.

Temperature, temperature gradient, and heat flow corrections predicted by models A, B, and C (Figs. 35, 36, and 37, and Table 9) show small differences for depths greater than 500 m (max.  $3-4 \text{ mW m}^{-2}$ ) but considerable differences and variations at shallow depth amounting to  $20-30 \text{ mW m}^{-2}$  or even more at near surface level in high conductivity areas. We observe that although gradient corrections and the degree of variations decrease with increasing diffusivity, the heat flow corrections increase due to the increase of thermal conductivity. On the assumption of a constant  $\rho c$  product the highest heat flow perturbations are expected in areas of higher diffusivity although these areas generally have the lowest temperature gradient perturbations. At depths shallower than 300-500 m, corrections vary considerably

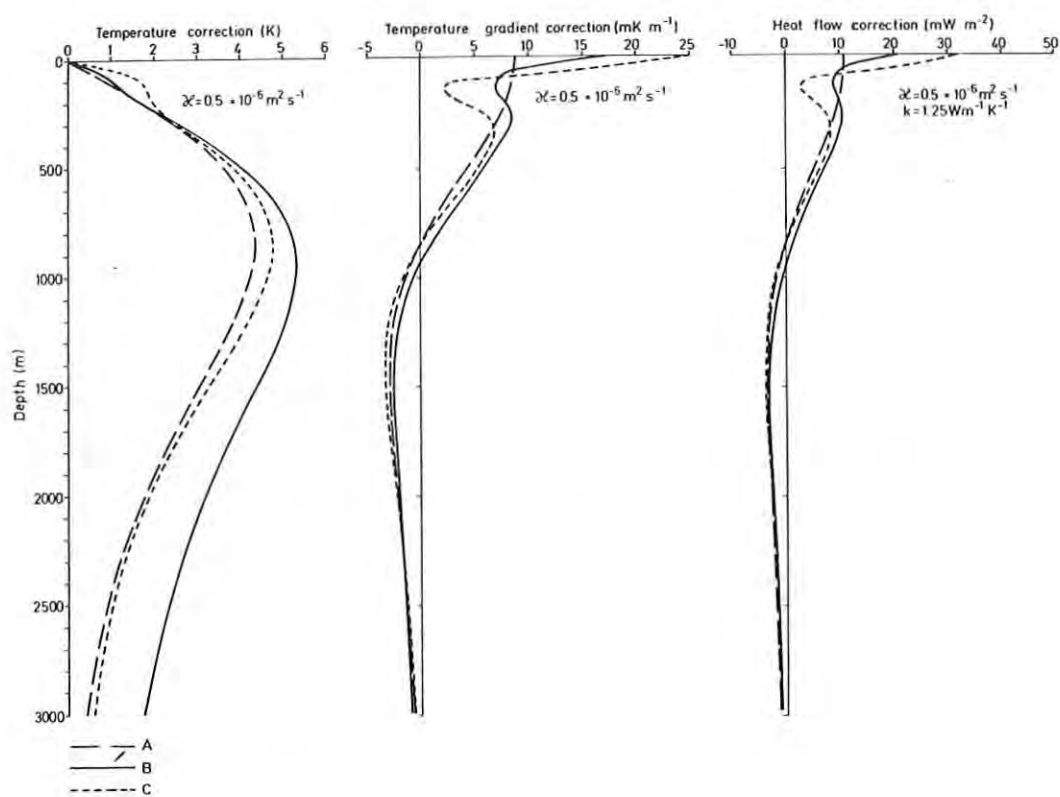


Fig. 35. Comparisons of temperature, temperature gradient and heat flow corrections associated with surface temperature models A, B, and C (Table 6). Temperature and gradient corrections are calculated with the thermal diffusivity of  $0.5 \cdot 10^{-6} \text{ m}^2 \text{ s}^{-1}$ , and the heat flow corrections are given for the thermal conductivity of  $1.25 \text{ W m}^{-1} \text{ K}^{-1}$  assuming a constant  $\rho c$  value of  $2.5 \cdot 10^6 \text{ J m}^{-3} \text{ K}^{-1}$ . Calculations with the diffusivities  $10^{-6}$  and  $1.5 \cdot 10^{-6} \text{ m}^2 \text{ s}^{-1}$  are shown in Figs. 36 and 37. Values of heat flow corrections are listed in Table 9.

with the temperature history model. Model differences of  $\pm 1-2 \text{ K}$  for the past 500-1000 years result in highly different gradient and heat flow corrections, as shown by the differences between model B and model C perturbations. Model A temperature events define the general trend and level of perturbations upon which the effects, especially associated with more recent climatic temperature changes, are superimposed. Thus, apart from the uppermost 50-100 m, model A produces first order corrections which differ very little from corrections using model B. If, instead of the  $\pm 10 \text{ K}$  steps used in model A,  $\pm 5 \text{ K}$  and  $\pm 15 \text{ K}$  are applied, we may obtain for the area in question the general minimum and

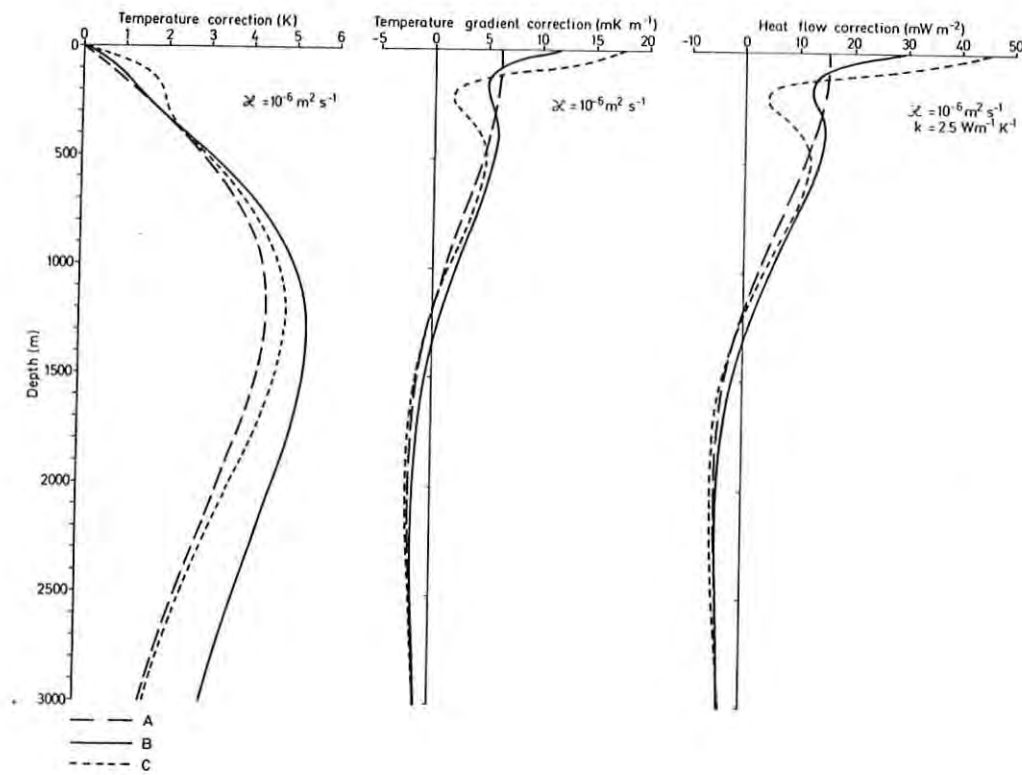


Fig. 36. Calculations equivalent to those in Fig. 35, but with a diffusivity of  $10^{-6} \text{ m}^2 \text{ s}^{-1}$ .

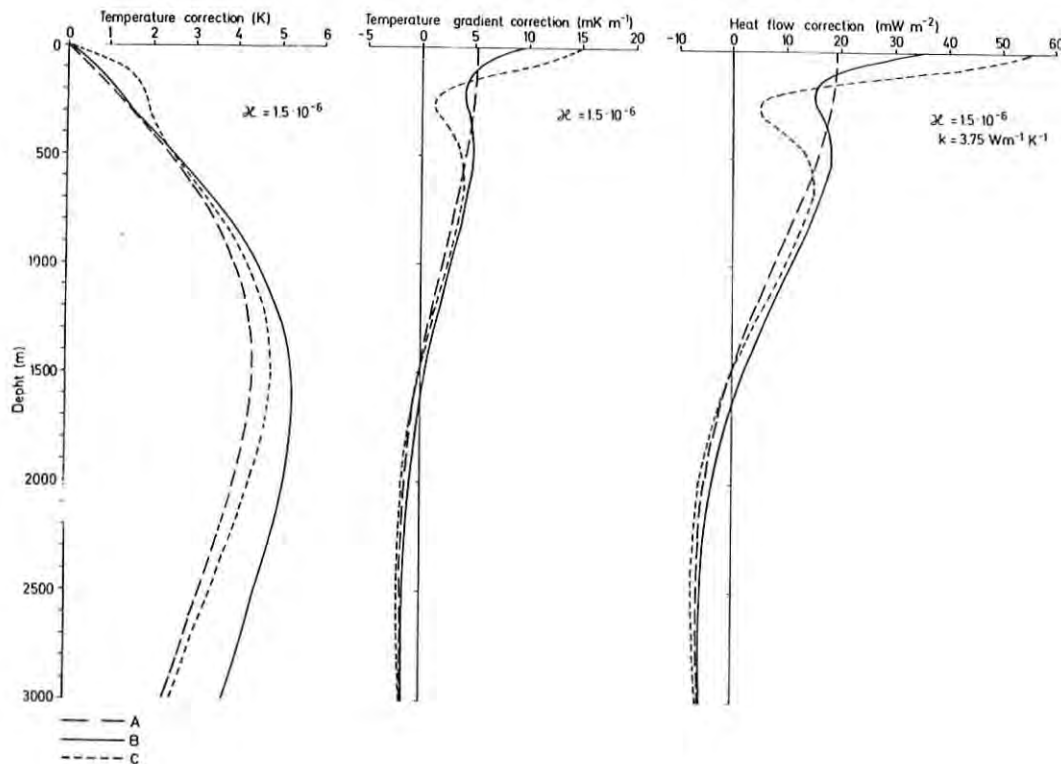


Fig. 37. Calculations equivalent to those in Fig. 35 and Fig. 36, but with a diffusivity of  $1.5 \cdot 10^{-6} \text{ m}^2 \text{ s}^{-1}$ .

Table 9

Calculated heat flow corrections (values to be added to observations) for the models A, B, and C (table 6). Three half spaces are considered with thermal diffusivity ( $\kappa$ ) and conductivity ( $k$ ) as indicated. Graphs appear in Figs. 35, 36, and 37.

$$\kappa = 0.5 \cdot 10^{-6} \text{ m}^2 \text{ s}^{-1}$$

$$k = 1.25 \text{ W m}^{-1} \text{ K}^{-1}$$

$$\kappa = 1.0 \cdot 10^{-6} \text{ m}^2 \text{ s}^{-1}$$

$$k = 2.5 \text{ W m}^{-1} \text{ K}^{-1}$$

$$\kappa = 1.5 \cdot 10^{-6} \text{ m}^2 \text{ s}^{-1}$$

$$k = 3.75 \text{ W m}^{-1} \text{ K}^{-1}$$

Depth (m)	Models			Models			Models		
	A	B	C	A	B	C	A	B	C
0	11.0	20.3	31.8	15.5	28.8	44.8	19.1	34.5	55.1
50	11.0	12.0	22.0	15.5	19.5	37.3	19.1	25.1	48.8
100	10.8	9.0	7.5	15.5	14.5	21.5	19.1	19.1	33.8
150	10.5	8.9	2.9	15.3	12.5	9.0	18.8	16.1	18.4
200	10.0	9.9	4.5	15.0	12.5	4.3	18.4	15.4	8.6
250	9.5	10.5	6.9	14.5	13.3	4.8	18.4	15.8	4.9
300	8.9	10.5	8.3	14.0	14.3	7.3	17.6	16.5	5.6
350	8.1	10.0	8.6	13.5	14.8	9.8	17.3	17.3	8.3
400	7.3	9.3	8.4	12.8	14.8	11.3	16.9	18.0	10.5
450	6.5	8.4	7.8	12.0	14.5	12.0	16.1	18.4	12.8
500	5.6	7.5	6.9	11.3	14.0	12.3	15.4	18.4	13.9
600	3.9	5.6	5.0	9.8	12.5	11.5	14.3	17.3	15.0
700	2.1	3.9	2.9	8.0	10.8	10.0	12.4	15.8	14.6
800	0.6	2.1	1.0	6.3	9.0	8.0	10.9	14.3	13.1
900	-0.6	0.6	-0.8	4.5	7.0	6.0	9.0	12.4	11.3
1000	-1.8	-0.6	-2.0	3.0	5.3	3.8	7.5	10.5	9.4
1500	-3.5	-3.1	-4.0	-3.3	-1.8	-3.8	-0.4	1.9	-0.4
2000	-2.6	-2.6	-2.8	-5.0	-4.3	-5.8	-4.9	-3.4	-6.0
2500	-1.6	-1.8	-1.5	-4.5	-4.3	-5.0	-6.0	-5.3	-7.1
3000	-0.9	-1.1	-0.8	-3.5	-3.3	-3.5	-5.6	-5.3	-6.0

maximum perturbations, respectively. For depths of 0-500 m steps of  $\pm 10$  K yield (Table 9) corrections of 6-11, 11-16, and 15-19  $\text{mW m}^{-2}$  for the low, medium and high conductivities, respectively. The equivalent (minimum) values for  $\pm 5$  K are 3-6, 6-8, and 8-10  $\text{mW m}^{-2}$ , and the (maximum) values for  $\pm 15$  K are 9-17, 17-24, and 23-29  $\text{mW m}^{-2}$ .

The model results predict that significant increase of heat flow with depth may be observed from near surface level to depths of

about 100 m (or somewhat deeper if model C is valid) and again from depths of 300-500 m to about 1500 m. Above the level of about 1000 m corrections are positive, and below about 1500 m they are negative. Between 1000 and 1500 m corrections may be positive or negative, depending on subsurface diffusivity. For normal diffusivities and conductivities, corrections below 1000 m are expected to be small ( $\lesssim 5 \text{ mW m}^{-2}$ ).

If model C is valid we should observe heat flow decreases with depth from the depth of 50 m to 150 m, 200 m, and 250 m of 19, 33, and  $44 \text{ mW m}^{-2}$ , respectively, for the model diffusivities and conductivities of  $(0.5 \cdot 10^{-6}, 1.25)$ ,  $(10^{-6}, 2.5)$ , and  $(1.5 \cdot 10^{-6}, 3.75)$ , respectively. Much smaller variations of  $3\text{-}10 \text{ mW m}^{-2}$  are predicted by model B. For the application of heat flow values measured at shallow depth, e.g. as boundary constraints in subsurface temperature modelling and generally in scientific applications, differences of that size are very important. Our calculations clearly demonstrate the variability of corrections depending on surface temperature history, subsurface thermal properties, and depth. Inversely, the significant differences between models imply that observations of accurate heat flow values measured as a function of depth will enable us to constrain the surface temperature variations. The temperature variations which can be resolved are closely related to the accuracy of measurements and to the potential disturbances from other sources than those related to climatic temperature variations. The inverse method briefly described in the following section and applied to the problems of measuring heat flow in lake bottom sediments, may be used for the more systematic analysis of this forward-inverse, climatic temperature-terrestrial heat flow relationship. A computer program has been developed, and some preliminary calculations were performed. From our forward calculations presented here we observe that significant climatic temperature variations over the past 500-1000 years may be measured at depths from near surface to about 300 m. If information on the last ice age temperature amplitudes is to be resolved, heat flow measurements from greater depths ( $\lesssim 1000 \text{ m}$ ) must be combined with measurements from shallow to intermediate depths.

### Effects from other sources of disturbances

Danish topographic variations are generally of the order of tens of metres, and only over long distances and very seldom do they exceed 100 m. The topographic effect on the geothermal gradients is thus very small and normally less than 5% even at near-surface level. For example at locality Harre (see later in this section) calculations by the method of Jeffreys (1940) and Bullard (1940) applied to a distance of 50 km yield a negative effect of 3% at a depth of 25 m, 2% at 50 m, and 1% at 200 m. Half the disturbance originates from topography within 1 km from the hole. At Harre the gradient is about  $34 \text{ mK m}^{-1}$ , the uncorrected heat flow about  $33 \text{ mW m}^2$ , and the topographic reductions are thus about  $1 \text{ mW m}^{-2}$  or less. This is a typical example of localities selected with a view of minimizing the topographic effect.

Below a thin cover of Quaternary sediments, normally a few tens of metres thick, we observe Tertiary and Upper Cretaceous sediments in almost all areas. During the Quaternary ice ages, glaciers and melt water caused erosion and sedimentation of material, which, for a time, influenced subsurface thermal environments. Apart from local anomalies, these changes of surface conditions, estimated to involve thicknesses of material of the order of  $\pm 50$  m or less, have little influence on present geothermal gradients.

A sudden removal of 50 m of surface material with typical near-surface geothermal gradients of  $20-30 \text{ mK m}^{-1}$  corresponds to a temperature decrease of 1 to 1.5 K. A temperature decrease of 1 K at 10,000 B.P. causes at present and at depths less than 500 m a gradient decrease of up to about 1 to  $1.5 \text{ mK m}^{-1}$  calculated with thermal diffusivities of  $0.5$  to  $1.0 \cdot 10^{-6} \text{ m}^2 \text{ s}^{-1}$ . Late glacial and Postglacial sedimentation may, in some cases, e.g. in lake bottoms, cause greater disturbances. If, say, up to 20 m is sedimented over 10,000 years, the present surface gradients are decreased by about 5-10%, depending on subsurface thermal diffusivity. A postglacial sedimentation of 10-15 m may be typical for Danish lakes. Assuming a thermal diffusivity of  $0.2 \cdot 10^{-6} \text{ m}^2 \text{ s}^{-1}$  and a continuous and constant rate of sedimentation over the past

10,000 years, calculations by Jaeger's (1965) equation 38, yield positive corrections of 5% for 10 m and 7% for 15 m. If the lake bottom heat flow is, say,  $50 \text{ mW m}^{-2}$ , corrections may thus be  $3-4 \text{ mW m}^{-2}$ . Calculations on the topographic effect in lakes have been carried out by the method described by Carslaw and Jaeger (1959, pp. 424-25) and may in several cases be significant and around  $10-15 \text{ mW m}^{-2}$ . The problems associated with the annual temperature wave at lake bottom environment is treated separately later in this section.

In shallow holes, the effect of Late- and Postglacial sedimentation depends on the sedimentation history and may be difficult to calculate exactly, but since the thickness of the material involved is normally very small, the associated reductions are generally quite insignificant.

Most geothermal measurements resulting in heat flow observations have been obtained from the Tertiary and Cretaceous sedimentary sequence. The thickness of Tertiary sediments of Post Danian age is less than ca. 500 m and typically 100-200 m, while the thickness of Tertiary, Danian, and Upper Cretaceous deposits may be up to about 2500 m centrally in the Danish Subbasin (Michelsen et al. 1981). Sedimentation of 500 m over the past ca. 70 mill. years results in a surface gradient decrease of ca. 1% (thermal diffusivity  $10^{-6} \text{ m}^2 \text{ s}^{-1}$ ) and a sedimentation of 2500 m over the past ca. 135 mill. years yields a decrease of ca. 4%. Since perturbations decrease with depth, and the above figures are maximum values, the effects of Tertiary and Cretaceous sedimentation is of the order of 1%.

During the last major ice age, Denmark was situated in the border area of the NW European ice sheet. The Postglacial isostatic and eustatic land/sea variations are of the order of  $\pm 10-50 \text{ m}$  (Mertz, 1924), and with a present submergence rate of maximum ca.  $1.5 \text{ mm year}^{-1}$  in the southern part of the country. Only the northernmost part is slightly emerging (Andersen et al., 1974; Balling, 1980). The temperature variations associated with such changes in surface level are very small when compared with the palaeoclimatic variations. Relative altitude variations of up to  $\pm 50 \text{ m}$  at Late glacial and Early Postglacial times may be associated with temperature variations of up to  $\pm 0.5$  to 1 K, assuming a decrease of temperature with altitudes of  $0.01 - 0.02 \text{ K m}^{-1}$ .

This is an order of magnitude lower than the climatic increase of temperature at the time of glacial melting, and well below the limits of uncertainty.

Refraction of heat by lateral contrasts in thermal conductivity may cause significant temperature and heat flow anomalies (Lachenbruch and Marshall, 1966; Lee, 1975) and local perturbations to heat flow (Jones and Oxburgh, 1979).

The dominating lateral thermal conductivity variations observed in Denmark are related to the salt structures with a thermal conductivity typically 2 to 3 times higher than that of the surrounding sediments. Such structures are known to produce a significant heat flow and temperature anomalies (e.g. Von Herzen et al., 1972; Balling, 1978).

To predict heat flow anomalies associated with salt structures of the size, shape and conductivity contrasts typical in Denmark we calculated finite difference and finite element numerical models. Two examples of the finite element modelling are shown in Fig. 38, a shallow salt diapir and a deeper salt pillow. The models are three-dimensional axial-symmetric. Our finite element solution of the heat equation with prescribed boundary conditions is based upon the variational principle (e.g. Zienkiewicz, 1971), and the resulting set of simultaneous linear equations is solved by Gaussian elimination. A triangular mesh was used with the smallest elements in areas of largest thermal variations. The subsurface temperature anomalies and surface heat flow anomalies were calculated assuming steady state heat conduction and temperature anomalies produced only by contrasts in thermal conductivity.

For the examples in Fig. 38 calculations were carried out for three subspaces of constant thermal conductivity: the sediments above the salt, the salt, and the rocks below salt, and with the ratios of 2:5:3. The undisturbed boundary vertical heat flow was taken at  $60 \text{ mW m}^{-2}$ , which, together with the realization of no horizontal transfer of heat at the axis of symmetry and at large distances from the structure ( $\gtrsim 20 \text{ km}$ ) and a constant surface temperature, defines the boundary conditions. Above shallow

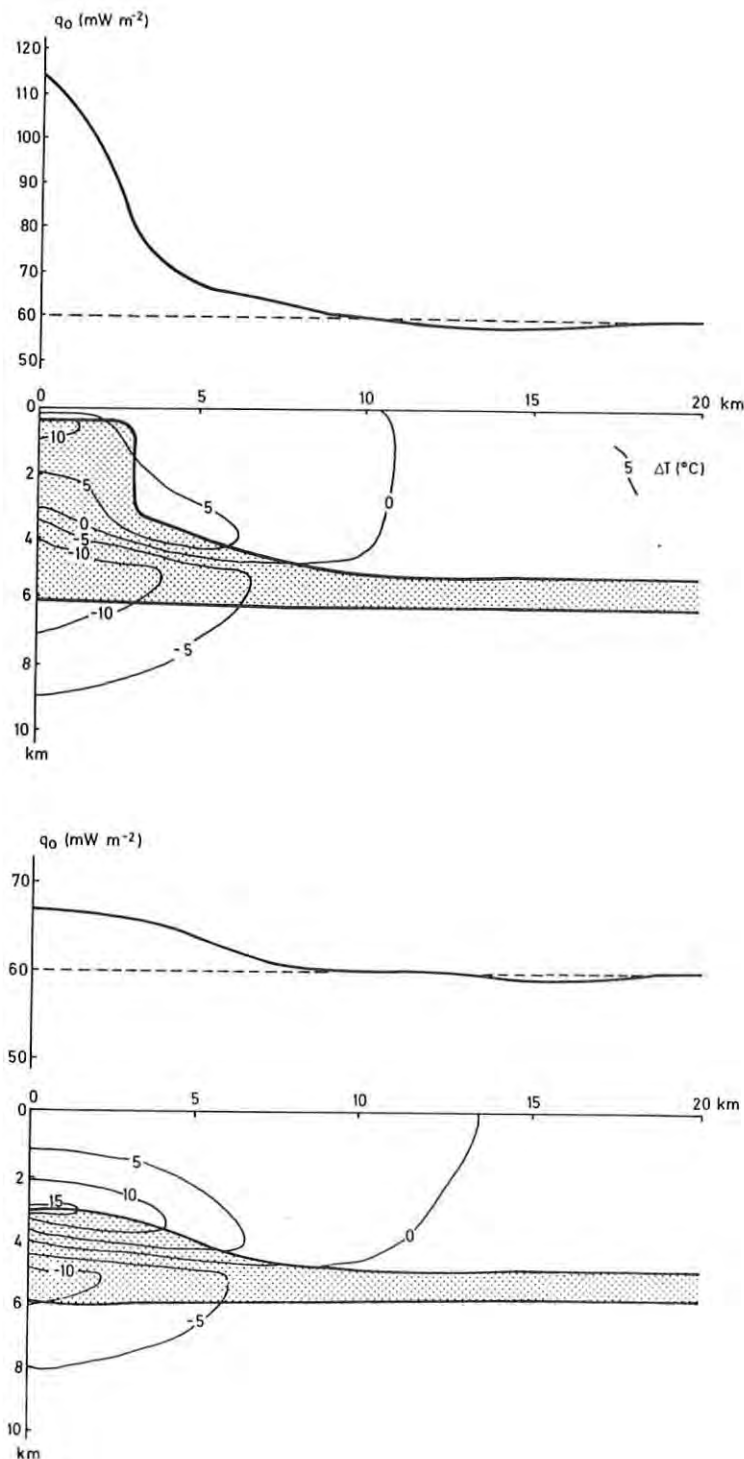


Fig. 38. Two examples of three-dimensional axi-symmetric finite element calculations of surface heat flow ( $q_0$ ) and subsurface temperature anomalies ( $\Delta T$ ) produced by salt structures (dotted area) of contrasting thermal conductivity. The model conductivity ratios for sediments above salt to salt and rocks below salt are 2:5:3, and the undisturbed vertical boundary heat flow 60 mW m<sup>-2</sup>. Depth to salt is 500 m for the diapir structure and 3000 m for the pillow structure.

diapirs we found positive heat flow anomalies of 50-100% varying with the structural size, shape and thermal parameters. The surrounding negative anomaly zone is much smaller, generally 5-10%. Above deeper structures we calculated temperature anomalies of up to 15-20°C. In Fig. 56 two-dimensional finite difference models are shown. The main characteristic difference between the two- and three-dimensional models is a wider distribution of the positive anomaly zone for the three-dimensional structures.

Heat flow variations caused by ground water movements may be serious, since small water velocities may cause significant anomalies. It is very difficult, if possible at all, to correct in detail for such movements, and if possible, strata with potential ground water movements should be avoided. The potential effects may be evaluated by observation of heat flow as a function of depth through strata of varying permeability.

#### 2.4.2 On observations in lakes

Annual bottom temperature variations measured during the past few years in the lakes of Glenstrup, Hald, Knud and Ravn (Fig. 11), which are the deepest lakes in Denmark with max. depths of about 30 m, have shown rather high amplitudes of 2-3 K. For example, the temperatures in lake Hald typically vary between 2.5 and 8°C (Fig. 39). Usually, the annual temperature variations do not exceed 1-2 K in lakes from which heat flow measurements have been reported (e.g. Haenel, 1968; Haenel et al., 1974; Von Herzen et al., 1974; Allis and Garland, 1976; Lee and Cohen, 1979). Prior to our experimental observations we found it essential to analyse theoretically the size of errors which may originate from these relatively high annual temperature disturbances.

The basic temperature change

$$T(z=0, t) = \begin{cases} 0 & t \leq 0 \\ kt & t > 0 \end{cases}$$

constitutes the basis of the annual temperature model. The lake bottom is defined as a homogeneous, isotropic half space of diff-

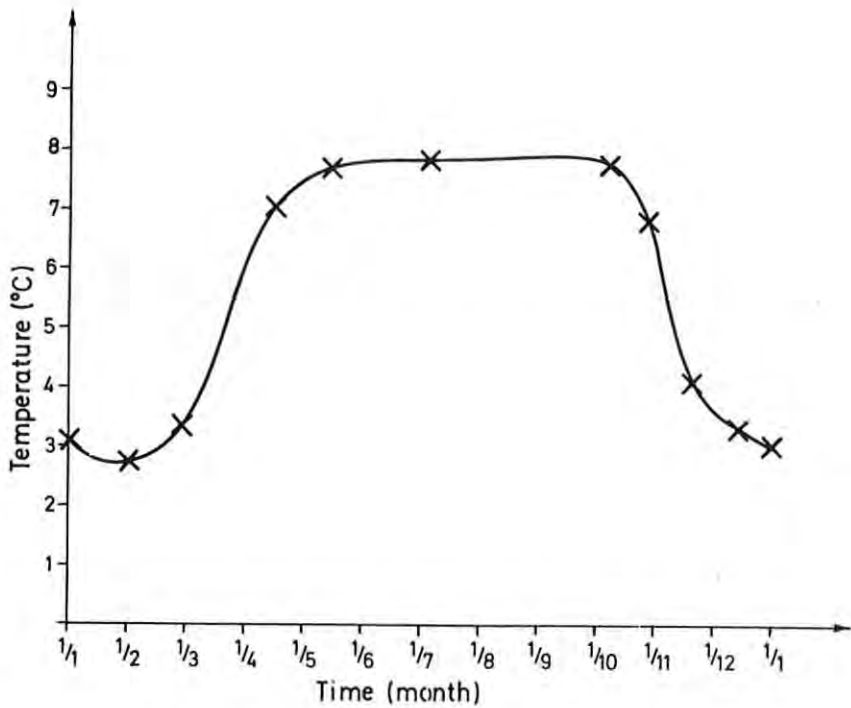


Fig. 39. Typical annual temperature variations measured at the bottom of lake Hald (Fig. 11) at its maximum depth of about 30 m. Crosses subdivide the curve into almost linear parts as used in the iterative least squares inversion analysis.

fusivity  $\kappa$ , and the forward solution is given by Equation (2) on page 49. By repeated superposition of the above linear temperature changes, an arbitrary stepwise linear surface temperature model is generated. Based on that model we apply the iterative least squares inversion method as described in detail by Jackson (1972) and based upon the Lanszos (1961) least squares matrix inversion. We include the possibilities of using constraints, as by Pedersen (1979), on the potential field problems. The basic unknown model parameters are the normal vertical temperature gradient ( $\frac{\partial T_n}{\partial z}$ ), which is the main unknown, the diffusivity ( $\kappa$ ) and a depth reference for probe penetration. Data points are the observed  $T(z_i)$  as measured by a lake heat flow probe with a

number of thermistors placed along it.

There are two main reasons for using the linear model instead of an alternative harmonic model. Rather rapid temperature variations are easily represented, and the model is easily constructed in terms of the applied method of inversion, while we noted some problems of non-linearity in the harmonic model.

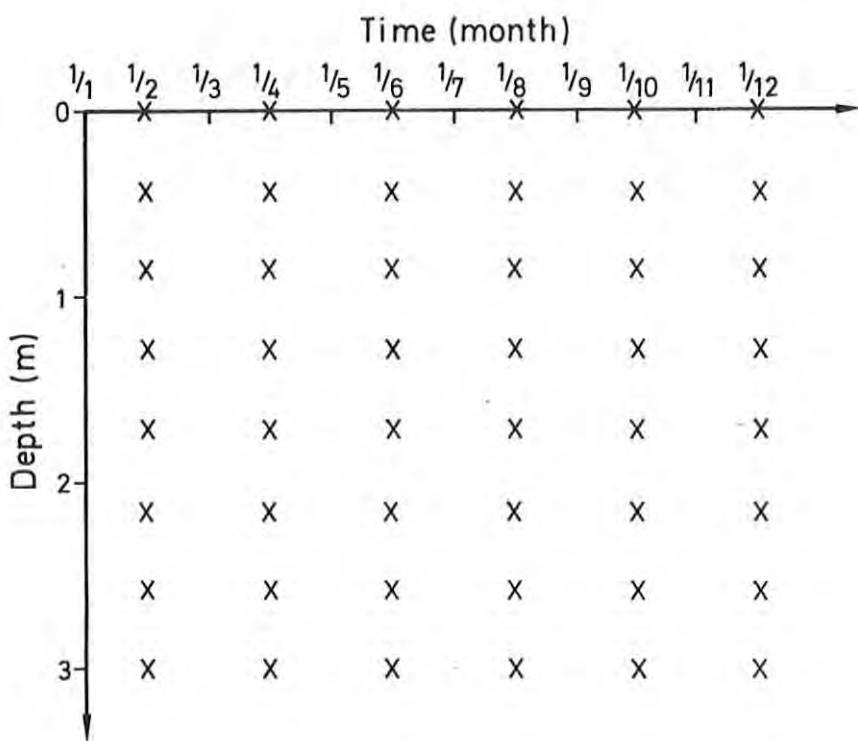


Fig. 40. Example illustrating a possible distribution of temperature measurements  $T(z_i)$  in lake bottom sediments.  $T(z_i)$  are measured equispaced 6 times through the year with a probe of 7 equispaced thermistors. Temperatures are also measured at the water-sediment interface.

An example of measuring configuration is illustrated in Fig. 40 with six equally spaced temperature soundings during the year measured by a 3 m long probe containing 7 equally spaced thermistors. (An instrument with these specifications is under construction). Some theoretical examples with this configuration, and a surface temperature variation as in Fig. 39, were calculated. Assuming a standard deviation of the  $T(z_i)$  of 0.04 K,

$\frac{\partial T_n}{\partial z} = 70 \text{ mK m}^{-1}$ , and  $\kappa = 0.2 \cdot 10^{-6} \text{ m}^2 \text{ s}^{-1}$ , we calculated a standard deviation for the normal temperature gradient,  $s(\frac{\partial T_n}{\partial z}) = 8.7 \text{ mK m}^{-1}$  and for the diffusivity  $s(\kappa) = 0.007 \cdot 10^{-6} \text{ m}^2 \text{ s}^{-1}$ .

A typical thermal conductivity of lake sediments may be around  $0.7 \text{ W m}^{-1} \text{ K}^{-1}$  and the associated heat flow and standard deviation are  $49.0$  and  $6.1 \text{ mW m}^{-2}$ , respectively. Under the given assumptions this procedure seems to result in values of an acceptable accuracy.

To obtain a general idea of the influence on resolution of the temperature gradient by varying a) the number of measurements during the year, b) the number of thermistors and c) the depth penetration of the probe, we applied the single harmonic temperature model ( $T(z=0,t) = T_o \sin(\omega t + \phi_o)$ ). The calculations were carried out with the numerical data:  $T_o = 3 \text{ K}$ ,  $\frac{\partial T_n}{\partial z} = 60 \text{ mK m}^{-1}$ ,  $\kappa = 0.2 \cdot 10^{-6} \text{ m}^2 \text{ s}^{-1}$ , and  $s(T(z_i)) = 0.04 \text{ K}$ .

The observations were equispaced throughout the year. Results of this theoretical analysis as to standard deviations of temperature gradients are summarized in Fig. 41. The calculations also yield the statistical accuracies of diffusivity (Fig. 42). With this measuring method we found that the standard deviations of gradient and diffusivity were almost unaffected by displacements in time of measuring point, if at least 3-5 measurements were taken during the year. We clearly observe the increase of accuracy with increasing number of measurements, depth of probe penetration, and number of thermistors. To obtain results with a reasonable standard deviation (<10-15%) from shallow depth, we shall expect at least about 6 measurements during the year with a depth penetration of at least about 3 m and with the number of thermistors around our maximum of 7.

The topographic and sedimentation corrections were discussed previously. Overall there is a number of significant corrections, all of which have to be minimized if accurate values of heat flow are to be measured in Danish lakes. Another problem which may arise is disturbance due to water movements in the sediments. Such potential effects can only be evaluated when appropriate experimental observations have been carried out.

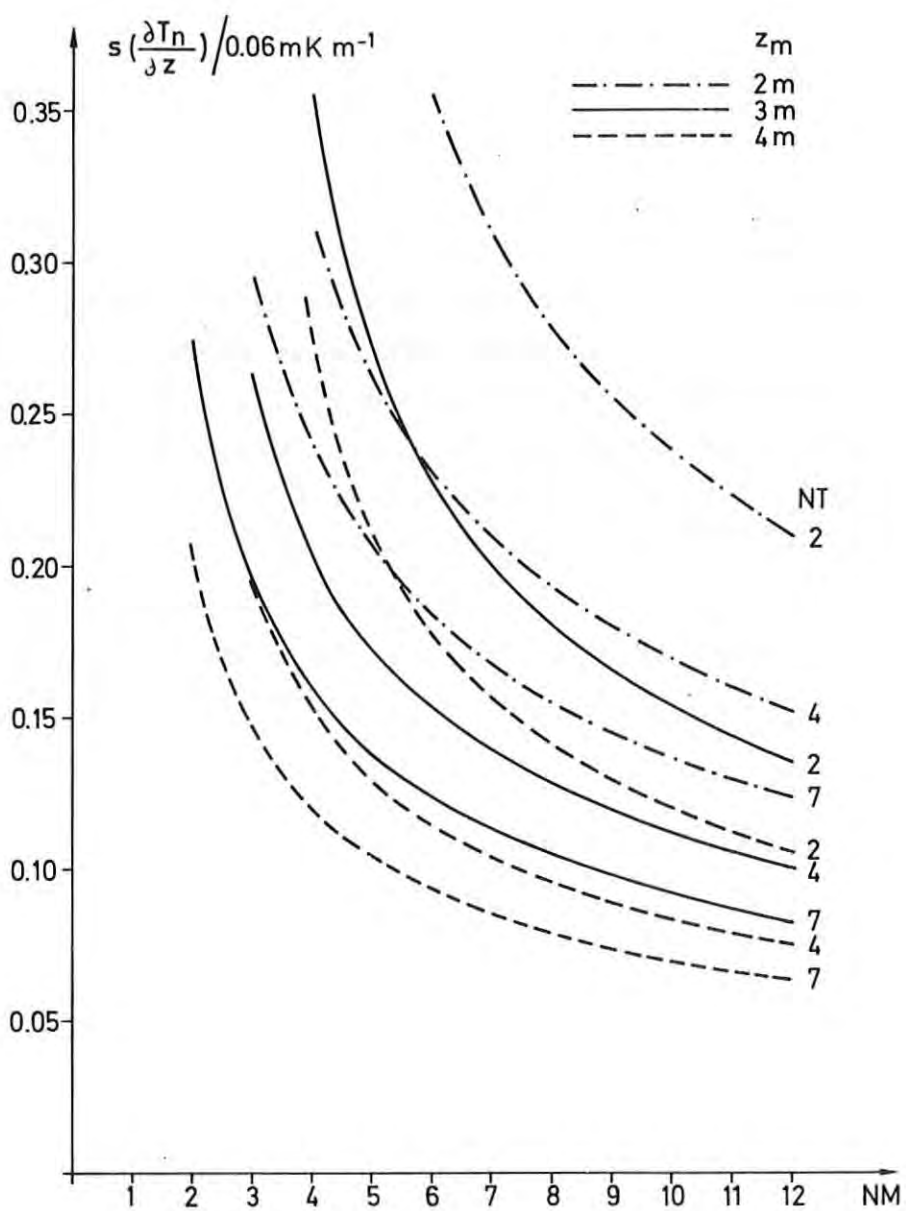


Fig. 41. Normalized temperature gradient standard deviations calculated as described in the text.  $z_m$ : maximum depth penetration of probe, NT: number of equispaced thermistors along the probe, and NM: number of yearly equispaced  $T(z_i)$  measurements.

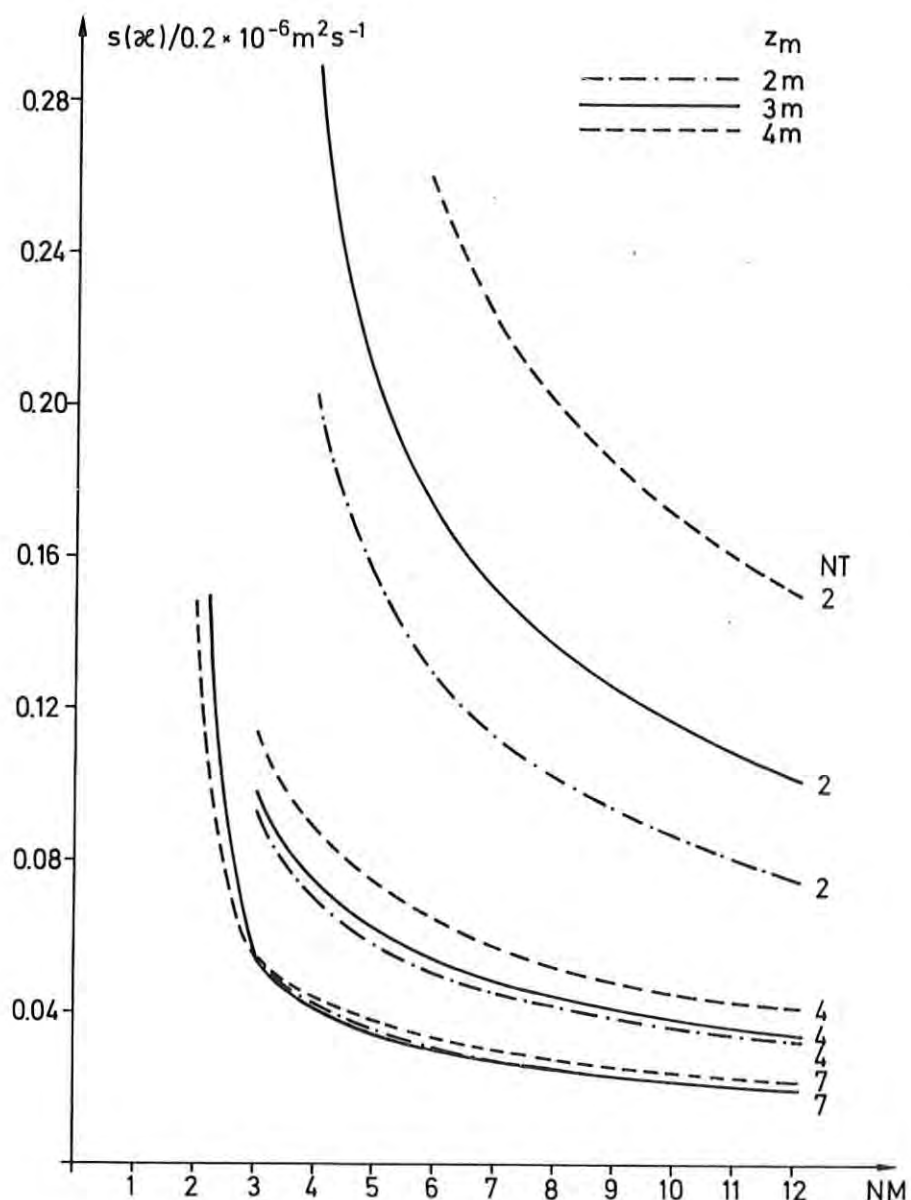


Fig. 42. Normalized thermal diffusivity standard deviations. Calculation as for temperature gradient in Fig. 41.

Table 10

Some drilling data from the shallow observation holes.

Name	Maximum drilling depth (m)	Interval available for tempe- rature logging (m)	Period of drilling activities
Jebjerg 1	176	0 - 150	18.01.79 - 26.02.79
Selde 1	251	0 - 250	30.07.79 - 19.10.79
Års 2	203	0 - 203	16.11.79 - 23.01.80
Harre 1	284	0 - 280	25.02.80 - 25.05.80

#### 2.4.3 Shallow observation boreholes

Four heat flow boreholes (Jebjerg 1, Selde 1, Åars 2, and Harre 1, Fig. 11) were drilled to shallow depth. The holes were drilled in the mentioned order in the period January 1979 to May 1980 (Table 10). The maximum drilling depth was 200-300 m but varied locally according to geology and budget.

#### Criteria of site selection

The localities were selected according to local geological conditions and in an area where we already have or may expect to obtain good possibilities of correlating heat flow observed at shallow depth with that obtained from intermediate and great depth. When heat flow-depth relations are established we will, for the first time, be able to evaluate the degree to which the heat flow obtained from near-surface level represents that of the "undisturbed" deeper flow of heat, and how the observations from shallow holes may be used in subsurface temperature prediction. It is essential to make observations from different lithologies with varying potential sources of disturbances, especially as to the thermal conductivity measurements and from ground water movements. Furthermore, in the selected area it was easy to find a suitable

site (Selde) for the observations on the anomalous heat flow from salt structures.

The Jebjerg and Harre sites were chosen within a large area of known, relatively thick, impermeable, and rather homogeneous, Tertiary formations characterized by clays and extending from near-surface level (generally 10-30 m) to depths of about 200-300 m. Prior to drilling we had good indications from outcrops, and especially from the commercial totally negative ground water wells in the area, that these sequences had a minimum permeability with no indication of ground water movements. Furthermore, the formations might be suitable for routine, accurate and representative needle probe thermal conductivity measurements. For the actual sites numerical calculations have predicted negligible disturbances of heat flow from salt structures.

The Selde locality is situated centrally over a major salt diapir (Batum) with a position and surface geometry well known from boreholes (Rasmussen, 1960) and gravity measurements (Fig. 43). Here, close to the observation sites of Harre and Jebjerg, the purpose was to obtain experimental information on the theoretically predicted positive heat flow anomaly. Moreover, highly varying lithologies (permeable chalk/limestone, caprock, and rock salt) could be penetrated within the limits of drilling depth.

The shallow Aars 2 hole was drilled at a distance of 500 m from the deep geothermal test observation hole Aars 1A which is available for intermediate and deep observations of temperatures and heat flow (section 2.1). The possibility of also being able to measure heat flow from shallow depth at that locality was given high priority, and the shallow hole was drilled, even though the local near-surface lithologies (sand, gravel, clay, and chalk with chert) were known to potentially cause difficulties in drilling, which actually happened.

At Jebjerg the permeable Quaternary deposits (sand and gravel) appeared to be locally anomalously thick (96 m). Impermeable Tertiary formations were reached, as expected, below these. This situation was not ideal, but since we had here the possibility of measuring and estimating heat flow from various lithologies with different potential sources of disturbances, we main-

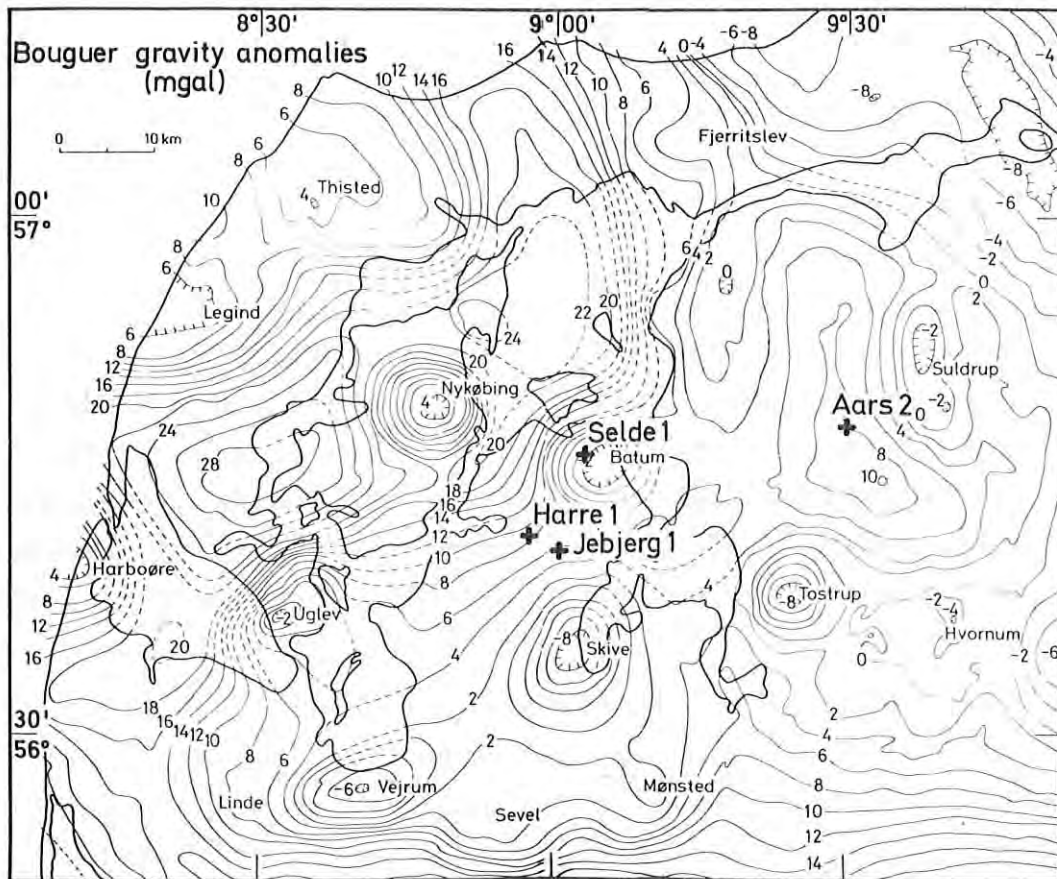


Fig. 43. Sites of the shallow heat flow boreholes shown on the Bouguer gravity map of NW Jylland. Anomalies known to be associated with salt structures are indicated by the names of structures (Saxov, 1956, 1976, and Balling 1978).

tain this hole as one of the main heat flow observation holes.

Before drilling at Harre, geoelectrical soundings, a shallow preliminary well, and a detailed geological analysis of available data from previous shallow wells in the adjacent areas, together with our information from Jebjerg available at that time, indicated that we might obtain, within the maximum drilling depth, an optimal sequence of impermeable Tertiary formations (generally clay dominated), suitable for the accurate measurements of heat flow as a function of depth. Furthermore, at this locality the topographic, sedimentation, refraction, and local convection effects were predicted to be at a minimum. The results so far obtained from Harre indicate that these predictions were correct.

### Methods of observations

The four holes were drilled by a Danish drilling company (Poul Christiansen A/S), specialized in shallow boreholes.

We aimed at a continuous coring of formations suitable for accurate thermal conductivity measurements. The first hole at Jebjerg was drilled by means of the hammer technique which gave cores of a length of 1 m and a diameter of 50 mm. This technique proved to be less suitable for the more lithified formations, and for the subsequent holes a rotary technique was applied. Here cores were taken in lengths of 1.5 m and with a diameter of 100 mm, in a tight PVC tube core barrel which minimized the physical disturbances and the drying of cores. Apart from loose sand and gravel, and the very hard limestones with chert, about 95% core recovery of excellent quality was generally obtained.

The holes at Jebjerg, Selde, and Harre were lined with sealed casing of 2 inch iron pipe cemented to the formation wall. This technique preserves the holes for equilibrium temperature observations to be measured months or years after drilling, and prevents potential movements of ground water along the hole (Roy et al., 1968; Oxburgh et al., 1977). Thus the purpose is to recreate, as far as possible, the natural temperature depth profile which existed before drilling activities. The hole at Aars was neither lined nor cemented but iron cased (8.6 inches) to the top of the limestone. Below this the hole was left open to allow deepening of possible additional coring at a later date.

Temperatures and temperature gradients were measured in the water-filled pipe by traditional high precision thermistor probes (section 3.1) at 5 m intervals. Thermal conductivities were measured on the cores by the needle probe technique (section 2.2 and appendix A3), generally every half metre or less. By measuring with the needles placed in different directional positions, any conductivity anisotropy could be measured. For horizontally bedded media the vertical conductivity is determined by two needle probe measurements: One with the needle placed perpendicular to the bedding yielding the horizontal component ( $k_h$ ), and the other placed parallel to the bedding yielding a weighted mean of values

$k_m = (k_h k_v)^{\frac{1}{2}}$ , where  $k_v$  is the vertical component to be applied in the calculation of heat flow.

Divided bar test measurements were carried out for comparison of the methods, but since the needle probe technique was generally both much faster and more accurate, our results are based on these measurements.

In lithified samples (limestone, caprock, rock salt, and some clay lithologies) small holes were drilled for the insertion of needles. Most measurements were carried out in the laboratory within 24 to 48 hours after coring, and to correct for any change in conductivity some measurements were also taken at the drill sites immediately after core appearance. A few samples (e.g. porous limestones) were re-water-saturated in the laboratory.

Generally, core tubes were put into plastic covered, water-filled vessels leaving free space for the insertion of needle probes, and ensuring that water was not in direct contact with samples due to the risk of disintegration, which is especially important for the clay lithologies. This procedure minimized drying (and the associated thermal conductivity variation) and the influence of ambient temperature variations which might otherwise be superimposed on the needle temperature rise and thus introduce some systematic error of conductivity. In general, and for cores of normal quality, the differences between field and laboratory conductivity measurements did not exceed 5 %, and in most cases no measurable differences were observed.

At the drilling site all cores were marked with "depth" and "up/down". Depths were defined relative to local surface level and checked by measurements during drilling. The conductivities are thus easily defined as to depths and with a maximum error of 1.5 m in cases of minimum recovery. Cores were lithologically classified, and the holes were, before and after cementing, gamma ray logged to control the quality of cementing and to improve the basis of the lithostratigraphical classifications.

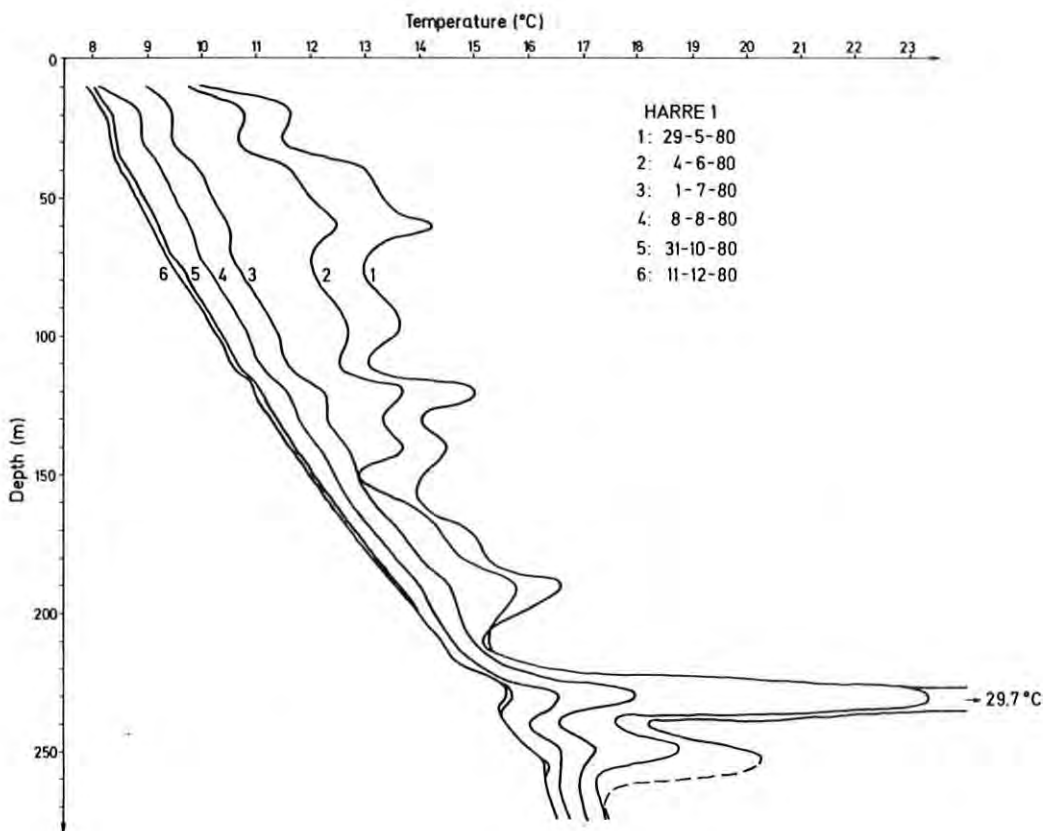


Fig. 44. Temperature logs from Harre 1 measured at different dates. The hole was drilled, lined and cemented in the period 25.02.80 to 25.05.80.

#### Observational results

Temperatures were measured in all holes several times after completion of boring so as to observe variations and to ensure that the final measurements were equilibrium values. The most detailed record was measured at Harre (Fig. 44) showing the significant variations and the time necessary to retain thermal equilibrium. In our case the recovery time is about 1 year or more. Most of the major disturbances are due to the release of heat from the setting process of the cement.

Results obtained here are based on temperatures measured in December 1980. Parts of the Harre borehole have not reached temperature equilibrium, while the others are at, or at least very close to gradient equilibrium, but observations are still being made to observe any possible variations.

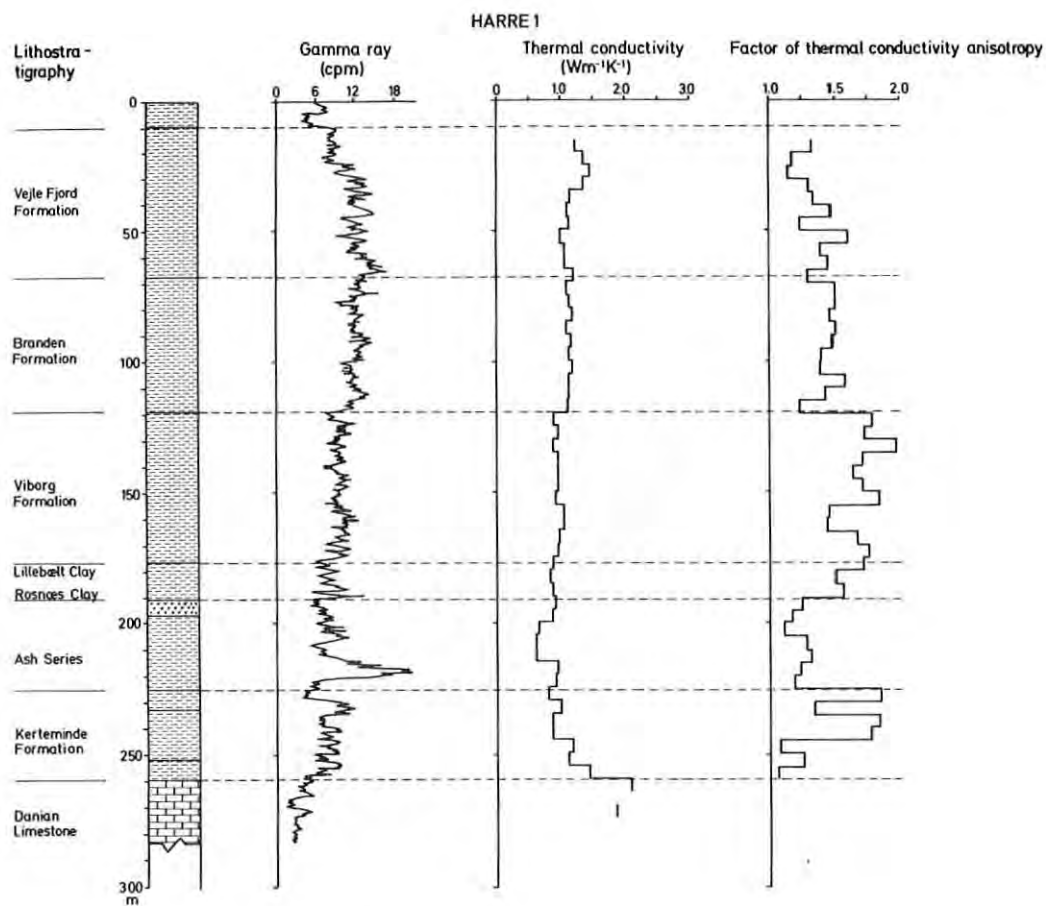


Fig. 45. Harre 1. Lithostratigraphic classification (see also Fig. 50), gamma ray log, thermal conductivity (vertical component) and conductivity anisotropy (ratio of horizontal to vertical component). Lithological classification by H. Friis and O. Bjørnslev Nielsen, Geological Institute, University of Aarhus.

Results from the lithostratigraphical classification of the Harre section appear in Fig. 45, which also gives the gamma ray and thermal conductivity stratigraphy. It is important to note the observed significant conductivity anisotropy and the variations between formations. The vertical component of conductivity shows only small variations.

Heat flow is calculated as the product of the measured 5 m interval, vertical temperature gradients and the associated mean vertical conductivity. Since conductivities were measured along the cores, almost equispaced and at distances of about 0.4 m, we calculated the 5 m interval mean conductivities as simple arithmetic means of observations. We define this product of gra-

dient and conductivity as the apparent conductive heat flow density ( $q_a$ ). If the temperature gradients are those of the conductive equilibrium values, and conductivity is accurately represented,  $q_a$  is to be interpreted as the true conductive heat flow density.

Results obtained so far on temperature gradients, conductivity, and heat flow are summarized in Figs. 46 to 50. Computer programs were developed for the processing of data, and results are available on plotted and printed output. (The above figures are directly reproduced from computer drawings).

The most complete and accurate records are observed at Selde and Harre. At Jebjerg and Aars the Quaternary sand/gravel lithologies, and also the very hard Danian limestone/chert unit at Aars, did not allow continuous coring, and only few, and in general non-representative, thermal conductivities were measured from these units. At Jebjerg core samples were supplemented by cuttings, but results from these were found to be less representative of formation conductivities although still indicative of larger variations (Fig. 47). The cores of rock salt from Selde generally show extensive horizontal cracking thought to be secondary and caused by the drilling processes. Measured conductivities here range from  $\sim 2$  to  $\sim 6 \text{ W m}^{-1} \text{ K}^{-1}$ , and the low values clearly reflect high thermal resistances across cracks. The constant value of  $5.7 \text{ W m}^{-1} \text{ K}^{-1}$  (dotted curves in Fig. 48) which obtained from the measurements of samples of best quality was used.

#### 2.4.4 Interpretation

The observations of the form presented, and especially the  $q_a(z)$  records, provide an effective tool for the evaluation of accuracies, effects from possible non-equilibrium temperatures, transient surface temperature variations, and potential convective transfer of heat by natural or man-made ground water movements.

The upper few tens of metres are influenced by the annual temperature variation. The observations at Harre and Selde indicate a detectable disturbance to depth of 30-40 m. A more detailed

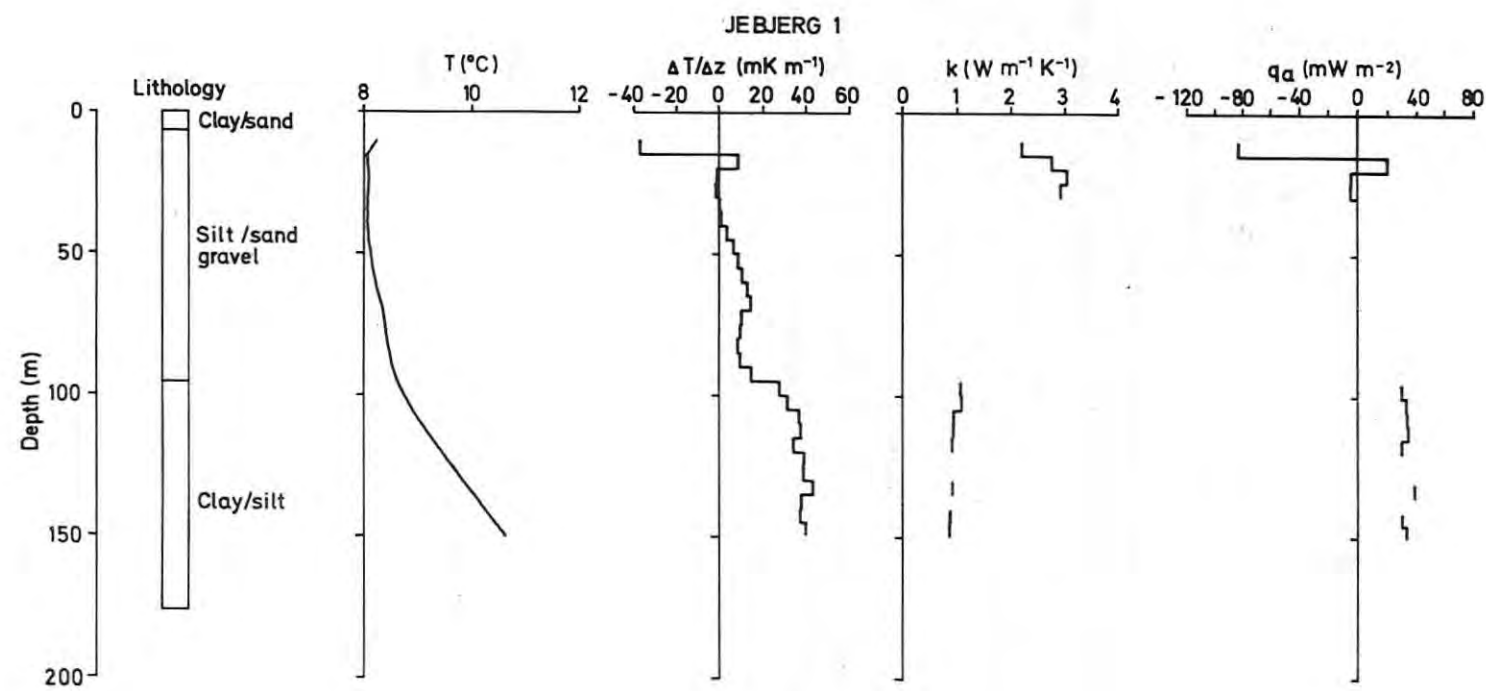


Fig. 46. Observational results: Lithology, temperature, temperature gradient, thermal conductivity (vertical component) and apparent heat flow, from the Jebjerg heat flow borehole. Graphs on temperature gradients, conductivity and heat flow represent the 5 m interval mean values. Conductivities are given for the cored sections and were all measured on cores (cf. Fig. 47).

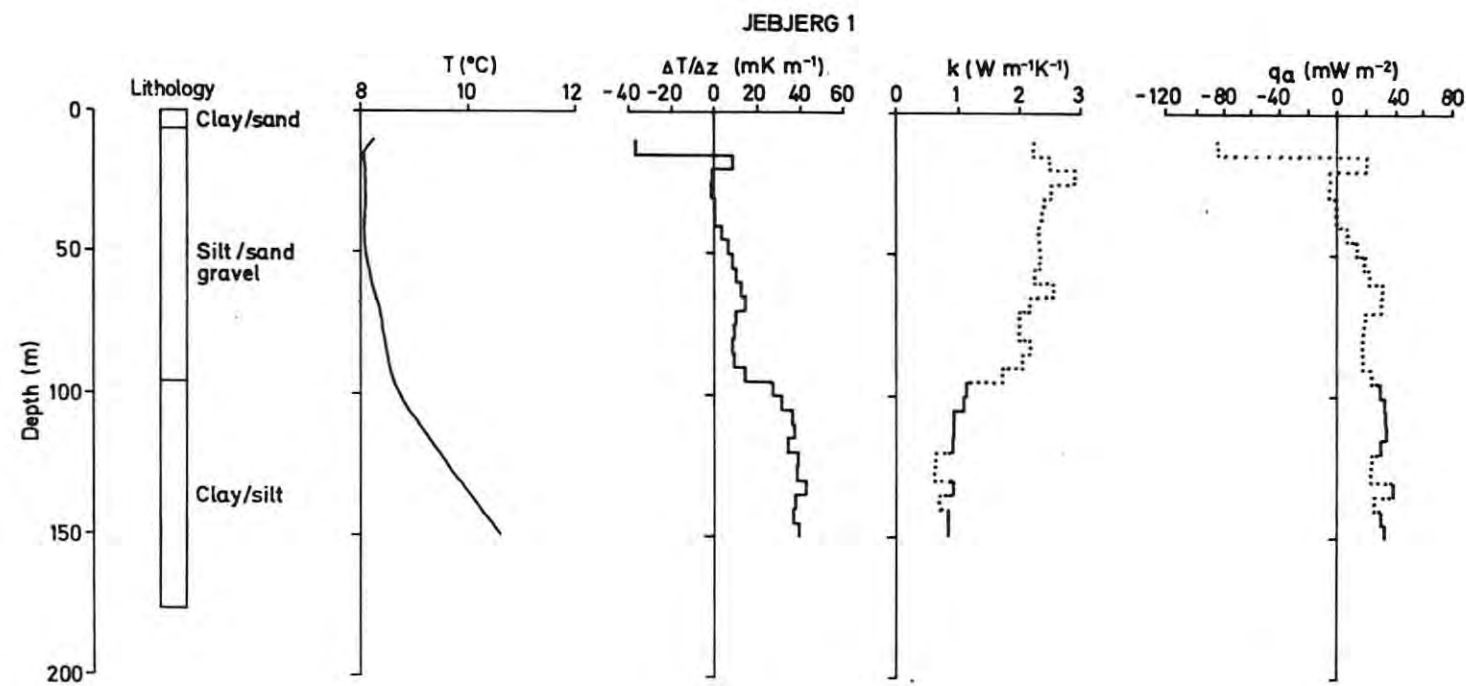


Fig. 47. Observational results from Jebjerg 1 with additional (less representative) conductivities measured on cuttings (dotted curve).

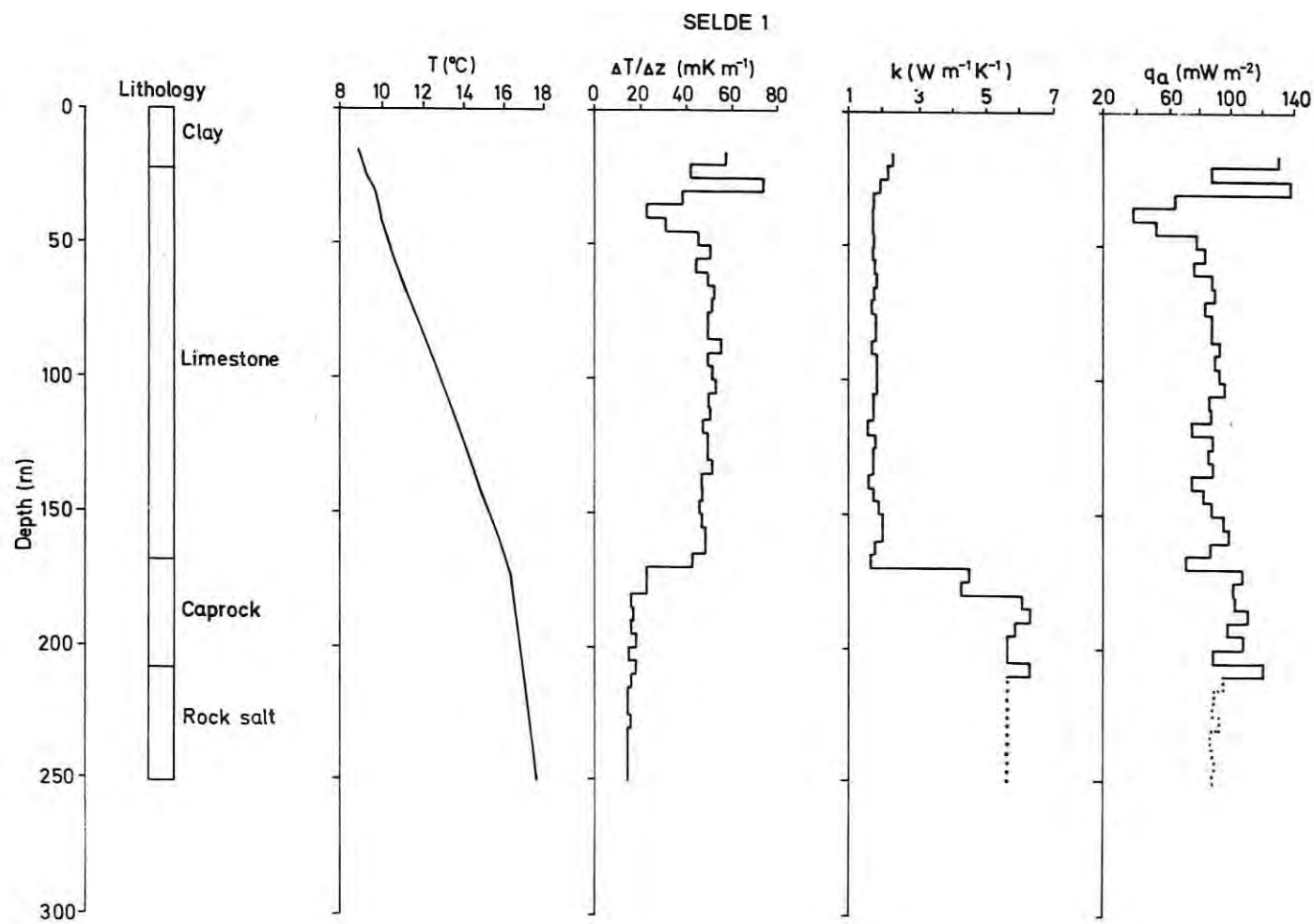


Fig. 48. Observational results from Selde 1. Results displayed equivalent to those in Fig. 46. Dotted curves indicate intervals where conductivity may be less representative.

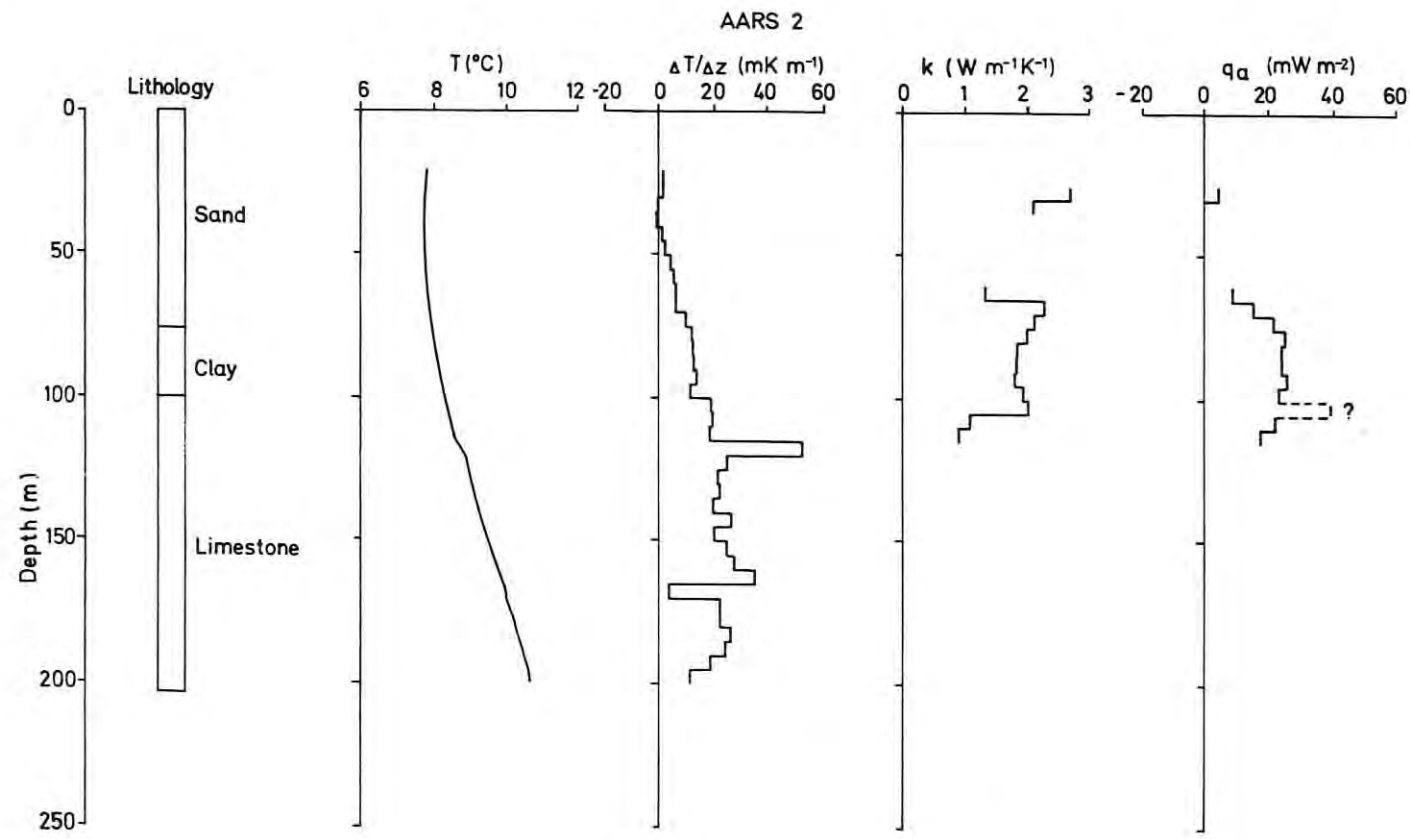


Fig. 49. Observational results from Aars 2. Results displayed equivalent to those in Fig. 46.

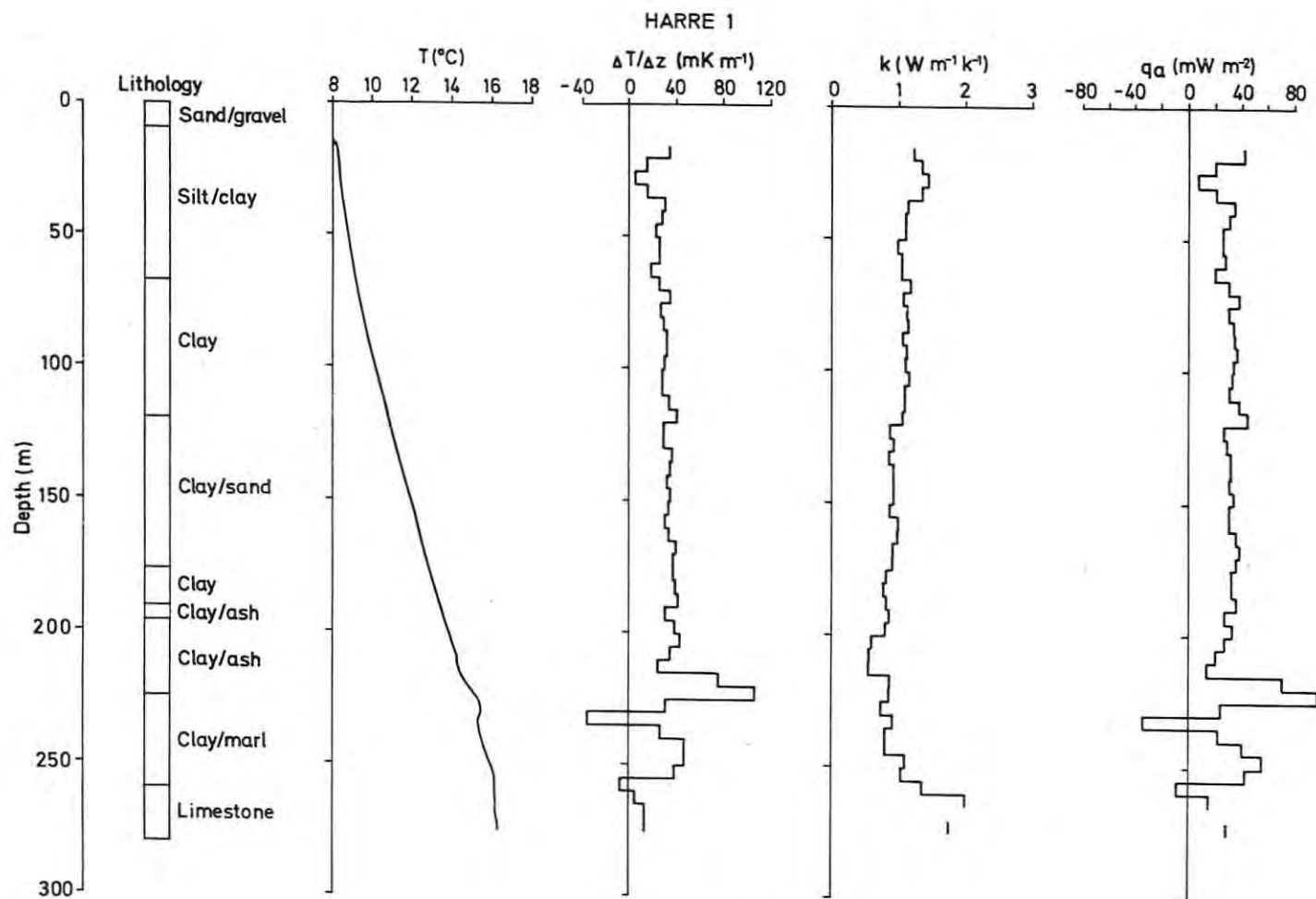


Fig. 50. Observational results from Harre 1. Results displayed equivalent to those in Fig. 46. Temperature, temperature gradients and consequently heat flow from the deeper parts of the hole do not represent the equilibrium values (see also Fig. 44).

experimental and theoretical analysis of the depth penetration and perturbations from this variation is in progress.

The lower part of the Harre borehole (Fig. 50) has definitely not reached temperature nor temperature gradient equilibrium (see also Fig. 44). It is important to note that here, 7 months after borehole completion, we locally (215-230 m) observe heat flow "in error" by up to  $\pm 60 \text{ mW m}^{-2}$ . Since no unusual thermal effects were introduced during drilling, the only explanation for this local anomaly is the heat release from the thickening of the cement to fill a large cavity created during drilling activities. The Jebjerg, Aars, and Selde heat flow results are found to represent the equilibrium values within measuring accuracies. However, temperatures are still being measured in all holes to detect any variations which may occur over long spans of time. At Jebjerg and Aars the  $q_a$ -values measured at depths to 50-75 m show significant variations with depth which cannot be explained by transient surface temperature variations. Since the formations here are highly permeable we interpret the variations as mostly being caused by ground water movements, producing a reduction of the apparent heat flow by up to about  $30 \text{ mW m}^{-2}$ . At Jebjerg we observe no significant  $q_a$  variations with depth in the impermeable Oligocene clay and silt formations below 96 m. The  $q_a$  from that lithology is interpreted as representing the conductive heat flow at this locality. At Aars we obtain the most representative and constant  $q_a$ -values from the clay/silt unit (76-100 m) and expect these observations to yield the local conductive flow of heat. At Selde a positive heat flow anomaly, produced by thermal refraction from the shallow Batum salt diapir (Fig. 43), is experimentally demonstrated. From Fig. 48 we observe no indication of significant convective transfer of heat within the permeable limestone above the saline rocks. A slightly higher ( $\sim 10 \text{ mW m}^{-2}$ ) apparent heat flow in the caprock, and the variability of values, may originate from less representative thermal conductivity measurements from that section of variable gypsum and anhydrite lithology. The mean value from the 50-200 m interval is about  $60 \text{ mW m}^{-2}$  higher than the equivalent values measured at Jebjerg and Harre, and may be interpreted as the (uncorrected) heat flow anomaly due to the thermal refraction from the salt diapir of

high thermal conductivity. This figure (cf. Fig. 38) and an observed general increase of heat flow with depth by  $10-20 \text{ mW m}^{-2}$  over the actual depth interval is in agreement with numerical model results. Any variations of heat flow with depth produced by palaeoclimatic temperature variations are thus here disturbed by the effect of refraction, and the  $q_a(z)$  record at Selde cannot be used for a detailed study of these relations.

During drilling through the main sequence (10-260 m) of the Harre borehole we observed no indications of aquifers (e.g. no lost circulation). Only below 260 m, within the Danian limestone, of which the upper 23 m were drilled, were there indications of some permeability. We shall here consider only the 50-200 m  $q_a$ -record, which, apart from local minor anomalies, is thought to be very close to equilibrium and probably within  $\pm 5 \text{ mW m}^{-2}$ . The uncorrected mean value of 30 interval (5 m) observations measured in December 1980 is  $33.4 \text{ mW m}^{-2}$  with a standard error of  $0.9 \text{ mW m}^{-2}$ . The 25 m interval means are given in Fig. 51, uncorrected and after palaeoclimatic corrections by models A, B, and C (cf. Table 6). The uncorrected ( $q_U$ ) 25 m observations range from 29 to  $36 \text{ mW m}^{-2}$  with standard errors between 1 and  $3 \text{ mW m}^{-2}$ . The actual lithologies, and the high number of thermal conductivities, thus provide very accurate observations. Within the accuracy of observation we do not so far observe significant uncorrected heat flow variations with depths between 50 and 200 m. Corrections by climatic models A and B do not change this apparently constant flow of heat, whereas model C introduces an overall decrease with depth of the corrected  $q_a$  by about  $10 \text{ mW m}^{-2}$ . From Fig. 52 the introduction of depth variations by model C is expected to appear more pronouncedly when the shorter interval (e.g. 5 m interval values) obtained after full equilibrium may be applied for a similar and more detailed analysis.

The calculated mean uncorrected heat flow values from the shallow holes, and from sections of supposed most accurate and representative conductive heat flow, are summarized in Tables 11. Results obtained previously from deeper Danish holes are also given for comparison. The uncorrected heat flow measured at shallow depth (50-200 m) at Jebjerg, Harre, and Aars is low (25-35

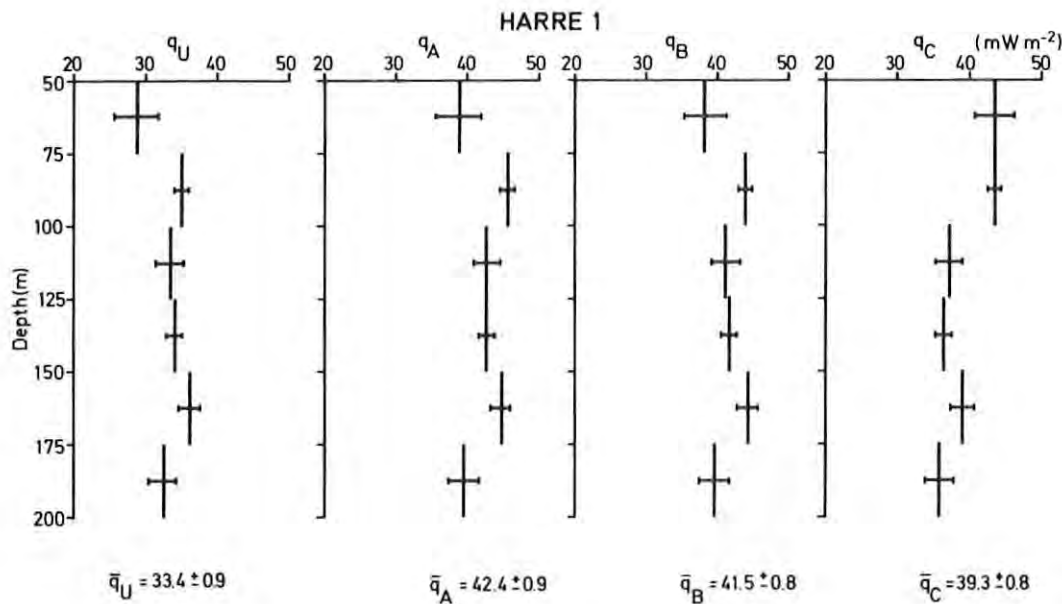


Fig. 51. The 25 m interval mean heat flow values at Harre calculated on the basis of temperatures measured in December 1980.  $\bar{q}_U$ : uncorrected,  $\bar{q}_A$ ,  $\bar{q}_B$ , and  $\bar{q}_C$  corrected by climatic models A, B, and C, respectively (Table 6). The 25 m mean values are calculated from the basal 5 m interval observations (Fig. 50) and with standard error indicated. The mean values (with standard error) for the whole 50-200 m interval are also shown.

$\text{mW m}^{-2}$ ) and represents only about 50% of the estimated flow from deeper ( $\leq 1 \text{ km}$ ) holes within the same area. The climatically (model A) corrected values (Table 12) still show significant differences. We emphasize the first order nature of corrections by using model A. Use of model B (or C) will not significantly change results. The model A corrected values show shallow heat flow at Jebjerg, Harre, and Aars, about  $20-30 \text{ mW m}^{-2}$  lower than the estimated deeper flow of heat. Potential effects from topography and sedimentation are an order of magnitude lower, as discussed previously in this section, and do not reduce differences. We are apparently left with the following possible explanations  
 a) generally too low palaeoclimatic corrections at shallow depth  
 b) too high estimates of heat flow from greater depth    c) removal of heat from shallow depth by water movements (e.g. within the upper part of the generally porous Danian and Upper Cretaceous limestone), and    d) real local lateral heat flow anomalies.

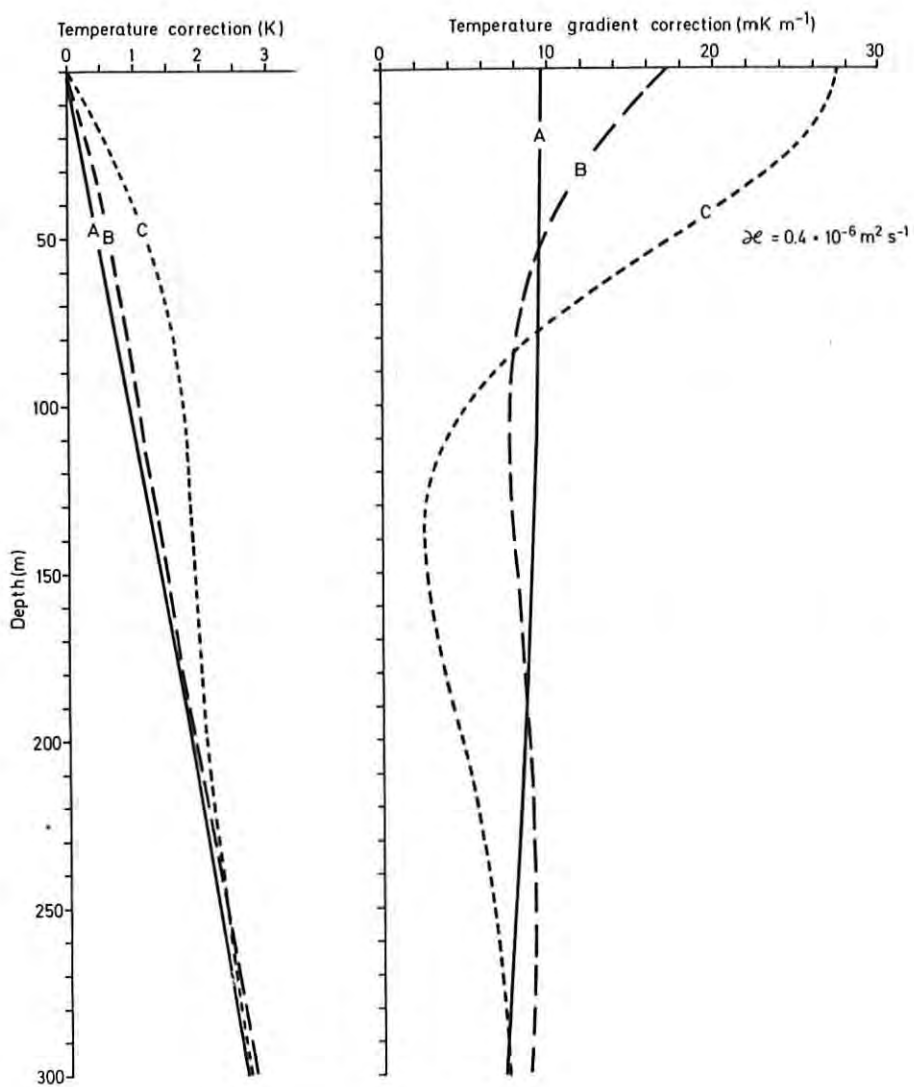


Fig. 52. Temperature and temperature gradient corrections associated with climatic models A, B, and C for a diffusivity of  $0.4 \cdot 10^{-6} m^2 s^{-1}$ . This value is obtained from the measured mean conductivity at Harre (pc constant at  $2.5 \cdot 10^6 J m^{-3} K^{-1}$ ), and the corrections (and associated perturbations) are supposed to yield trends relevant to that locality.

Table 11

Results of terrestrial heat flow observations. Values of deep holes (sites 1 to 6) are estimated based on measured BHT and estimated mean conductivity (Balling, 1979). New values from shallow holes (sites 7 to 10) are obtained from measured temperature gradients and conductivities as described in the text.

n: number of observations,  $\Delta T/\Delta z$ : mean vertical temperature gradient,  $\bar{k}$ : mean vertical conductivity,  $\bar{q}_1$ : uncorrected heat flow ( $K \times \Delta T/\Delta z$ ),  $\bar{q}_2$ : heat flow corrected for the influence of local deep salt structures, s.e.: standard error of mean values. Values from shallow holes are obtained from temperatures measured December 1980. Small variations towards full equilibrium especially at Harre may occur.

No.	Name	Lat.	Long.	Elevation (m)	Depth interval (m)	Temperature gradient (mK m <sup>-1</sup> )			Thermal conductivity (Wm <sup>-1</sup> K <sup>-1</sup> )			Heat flow			
						n	$\Delta T/\Delta z$	s.e.	n	$\bar{k}$	s.e.	n	$\bar{q}_1$	s.e.	$\bar{q}_2$
1	Grøndalseng	55°41.3'N	12°30.7'E	7	100-861	1	21.5			2.0		1	43		
2	Voldum 1	56°23.0'N	10°16.0'E	30	0-1272	1	33.0			2.12		1	70		63
3	Hyllebjerg 1	56°48.9'N	9°20.9'E	21	0-1055	1	28.4			2.05		1	58		
4	Rødding 1	56°38.8'N	8°48.3'E	25	0-1059	1	28.3			2.05		1	58		
5	Kvols 1	56°31.8'N	9°17.9'E	12	0-1048	1	34.4			2.05		1	71		66
6	Skive 1	56°37.6'N	9° 0.2'E	21	0-1054	1	33.3			2.05		1	68		65
7	Jebjerg 1	56°41.5'N	9° 0.4'E	34	95- 150	11	37.1	1.3	124	0.97	0.03	11	34.1	1.3	
8	Selde 1	56°46.0'N	9° 3.3'E	12	50- 200	30	43.9	2.3	276	2.50	0.29	30	91.4	1.8	
9	Års 2	56°47.8'N	9°30.0'E	42	75- 100	5	13.3	0.4	44	1.91	0.04	5	25.3	0.5	
10	Harre 1	56°41.5'N	8°57.5'E	32	50- 200	30	33.9	1.1	520	0.99	0.02	30	33.4	0.9	

Table 12

Heat flow corrected by climatic model A (table 6). The values from sites 2, 5 and 6 are also corrected for the influence of saltstructures (cf. Table 11). Mean values ( $\bar{q}_A$ ) and standard error of the mean(s.e.)

No.	Name	$\bar{q}_A$	Heat flow ( $\text{mW m}^{-2}$ )	s.e.
1	Grøndalseng	43	52	-
2	Voldum 1	79	70	-
3	Hyllebjerg 1	58	67	-
4	Rødding 1	58	66	-
5	Kvols 1	79	74	-
6	Skive 1	68	74	-
7	Jebjerg 1	36	41.8	1.2
8	Selde 1	37	109.4	3.6
9	Aars 2	25	39.4	0.4
10	Harre 1	33	42.4	0.9

Effects may be combined. Recently, for the area of the mainland of the United Kingdom, Richardson and Oxburgh (1979) and Oxburgh et al. (1980), based upon a relatively dense distribution of observations, demonstrated an interesting pattern of variable heat flow including zones of high and locally low values. A detailed discussion of the above elements for the Danish area will be hypothetical until more information is obtained on heat flow from great depth and a better statistical and geographical coverage of heat flow at shallow and intermediate depth, including accurate heat flow depth records, have been attained. However, we do not find indications of a normal regional deep conductive flow of heat within the central Danish Subbasin as low as about  $40 \text{ mW m}^{-2}$ . In the temperature modelling of section 3 we obtain good agreement between calculated deep temperatures and the measured values by using a boundary surface heat flow of about  $60 \text{ mW m}^{-2}$ . If that value is reduced to about  $40 \text{ mW m}^{-2}$  the model thermal conductivity is to be decreased from a typical mean value of about  $2 \text{ W m}^{-1} \text{ K}^{-1}$ ,

from surface to depth of 3 km, to about  $1.3 \text{ W m}^{-1} \text{ K}^{-1}$ , well below the results of observations (section 2.2). Heat flow measured at Jebjerg, Harre and Aars at depths down to 150-200 m is thus likely to be significantly lower than the actual deep flow of heat from that area.

### 3. TEMPERATURE MODELLING

The purpose of the present subsurface temperature modelling study was twofold, a) generation of a suitable physical model structure for the forward calculation of temperatures at any arbitrary depth point and group of points approximating three-dimensional surfaces, profiles of two dimensions, and the one-dimensional situation relevant to prediction and comparison of borehole temperatures, and b) production of geoisothermal maps for selected depths and stratigraphic horizons. Special emphasis was given to the prediction of temperatures of potential geo-thermal reservoirs.

#### 3.1 The heat equation

The transfer of heat in porous media may be described from the following generalized heat equation:

$$\operatorname{div}(k \operatorname{grad} T) - \operatorname{div}(\rho' c' \bar{v} T) + A = \frac{\partial}{\partial t} (\rho c T) \quad (5)$$

correlating temperature ( $T$ ) with time ( $t$ ), thermal conductivity ( $k$ ), density ( $\rho', \rho$ ), specific heat ( $c', c$ ), heat production ( $A$ ), and the filtration velocity of a saturating fluid phase ( $\bar{v}$ );  $\rho' c'$  is the heat capacity of the fluid and  $\rho c$  that of the solid matrix.

On a regional scale, and within the depth intervals to be considered here the following simplifying assumptions seem to be well founded (see section 4.3): a) steady state conditions ( $\frac{\partial}{\partial t} (\rho c T) = 0$ ), b) transfer of heat only by conduction ( $\bar{v} = 0$ ), no horizontal transfer of heat ( $k \frac{\partial T}{\partial x} = k \frac{\partial T}{\partial y} = 0$ ), and d) constant thermal conductivity and constant heat production of sub-spaces (layers). Then Equation (5) reduces to

$$\frac{\partial^2 T}{\partial z^2} = - \frac{A}{k} \quad (6)$$

where  $z$  (depth) is the only space variable. The subsurface is subdivided into intervals (layers) of constant thermal conductivity ( $k_i$ ) and constant heat production ( $A_i$ ), and the temperature ( $T_n$ ) at the base of the  $n^{th}$  layer is determined by the following easily derived analytical solution of Equation (6):

$$T_n = T_o + \sum_{i=1}^n \left[ \frac{(z_i - z_{i-1})}{k_i} (q_o - \sum_{j=1}^{i-1} A_j (z_j - z_{j-1})) - \frac{A_i (z_i - z_{i-1})^2}{2k_i} \right] \quad (7)$$

where  $T_o$  and  $q_o$  are the boundary ( $z=0$ ) conditions for temperature and heat flow, and the  $z$ 's are depths at basis of layers as indicated. With fixed model parameters ( $q_o$ ,  $T_o$ ,  $k_i$ , and  $A_i$ ), this solution is suitable for computer calculations of temperature at any depth point. Parameters may easily be varied within chosen limits, which may be defined from observations, to generate alternative model temperatures. If the above simplifying assumptions are locally not fulfilled within acceptable approximations, the temperatures calculated are superimposed by anomalies which may be found by additional numerical solutions of the heat equation. This is relevant to the local areas of salt structures (see section 3.3). In the following we define the physical model structure used. The thermal conductivity of layers and the boundary surface heat flow are by far the most important parameters.

### 3.2 Model parameters

#### 3.2.1 Thermal conductivity

As displayed by Tables 13 and 14, the sedimentary sequence from sea level ( $z=0$  m) to the base of Triassic ( $z \leq 7000$  m) is subdivided into 7 layers, each with constant and characteristic (vertical) thermal conductivity. Three models are given, A, B, and C, of which model A contains our preferred parameters, and models B and C contain values estimated to be close to the general maximum and minimum conductivity, respectively.

Table 13

Definition of layers estimated to be reasonably homogeneous as to mean characteristic thermal conductivity.

<u>Layer</u>	<u>Period (d: depth below sea level)</u>
1	Sea level to top Danian
2	Danian and Upper Cretaceous ; d < 500 m
3	Danian and Upper Cretaceous ; 500 m < d < 1000 m
4	Upper Cretaceous ; d > 1000 m
5	Lower Cretaceous, Upper and Middle Jurassic
6	Lower Jurassic
7	Triassic

Table 14

Model thermal conductivities of layers defined in Table 13 (Values in  $\text{W m}^{-1}\text{K}^{-1}$ ). See text for explanation.

<u>Layer</u>	<u>Model A</u>	<u>Model B</u>	<u>Model C</u>
1	2.0	2.5	1.5
2	1.7	1.8	1.6
3	2.1	2.3	2.0
4	2.7	2.9	2.5
5	2.0	2.4	1.8
6	1.5	1.8	1.3
7	3.0	3.5	2.5

Our present basis of observations (section 2.2) does not allow the introduction of horizontal variations in conductivity, and such variations, which are likely to occur, are considered by applying alternative regional models. For layers 1 to 4, parameters are in close agreement with the thermal conductivity measurements, whereas the values of deeper layers (5, 6, and 7) are defined by adjustments of measured mean values to produce a

better agreement between measured and calculated temperatures and temperature gradients. The experimental observations of section 2.2 are thus considered to be most representative of the upper layers for the area as a whole. By the adjustment procedure we also introduce the possibility of considering any significant change of conductivity by temperature and pressure. However, the chosen values are directly linked to surface model heat flow (see below) to produce the observed temperature gradients, and if actual heat flow differs from the model values applied, conductivity consequently differs also. Layer 6 (Lower Jurassic) is dominated by a relatively uniform series of marine claystone (mostly shale) with a varying silt content, resulting in a low thermal conductivity. The highest values are defined for the chalk and limestone of low porosity below the 1000 m level (layer 4), and for the generally sandy and/or silty series of Triassic age (layer 7). The models are based mostly on data from the central parts of the Danish Subbasin and are thus likely to be most representative for that part of the Danish area.

### 3.2.2 Heat flow

As described in section 2.4, only a few accurate heat flow values have so far been measured, and the problems of significant vertical and horizontal variations are still being studied. Based on the heat flow observations and knowledge of conductivity and temperature gradients we assume that the regional flow of heat, undisturbed by local thermal anomalies and transient surface temperature variations, is usually to be found within  $50-80 \text{ mW m}^{-2}$  (Fig. 32, Tables 11 and 12). By applying  $60 \text{ mW m}^{-2}$  and the thermal conductivities of model A, we generally found a good agreement between observed and calculated temperatures. By combining model B and model C conductivities with heat flow of  $50$  and  $80 \text{ mW m}^{-2}$ , respectively, the general minimum and maximum temperatures are calculated. Analogously with the conductivity models, data do not allow the introduction of horizontal variations in heat flow. Thus we apply the constant values of  $60 \text{ mW m}^{-2}$  in temperature model A,  $50 \text{ mW m}^{-2}$  in model B, and  $80 \text{ mW m}^{-2}$  in model C.

### 3.2.3 Heat production

The heat production of sediments is generally low, as are the results of measurements reported in section 2.3 (mean value of observations  $1.1 \mu\text{W m}^{-3}$ ). The associated decrease of heat flow and temperature gradients with depth is very small, and we found it most reasonable to use the constant model value of  $1 \mu\text{W m}^{-3}$  for all layers. The effect of varying the heat production parameter by  $\pm 1 \mu\text{W m}^{-3}$  is, with the thermal conductivity stratigraphy of Table 14, a model temperature variation of ca.  $\pm 2^\circ\text{C}$  at a depth of 3000 m, ca.  $\pm 5^\circ\text{C}$  at 5000 m, and ca.  $\pm 10^\circ\text{C}$  at the model maximum depth of about 7000 m.

### 3.2.4 Surface temperature

Meteorological observations of mean annual air temperatures in Denmark show  $7-8^\circ\text{C}$ , and our observations of mean annual soil temperatures at some 20 localities did not exceed  $9^\circ\text{C}$ . With Danish topography, temperatures increase by about  $1-3^\circ\text{C}$  from surface level to sea level, which forms the model reference level. Thus, by using a constant  $T_0$  value of  $10^\circ\text{C}$  in all models, only small and insignificant errors are introduced.

## 3.3 Calculated model temperatures

The theoretical model temperatures were tested against measured values, mostly the corrected BHT. Considering the Danish area as a whole, model A is found to yield good first order information for the regional interpolation and extrapolation (Fig. 53). As a regional physical model it combines simplicity with reasonable accuracy and takes into account present knowledge of temperature, thermal conductivity, and heat flow. The few temperature measurements from the areas of Sjælland and northernmost Jylland indicate that here model B may yield values in better agreement with observations than model A. We have only few measurements of temperatures as high as those of model C, but locally, as well as regionally (e.g. above zones of basement enriched in radioactive heat producing elements), these rather high temperatures may exist, and we found it reasonable to include this hypothetical model.

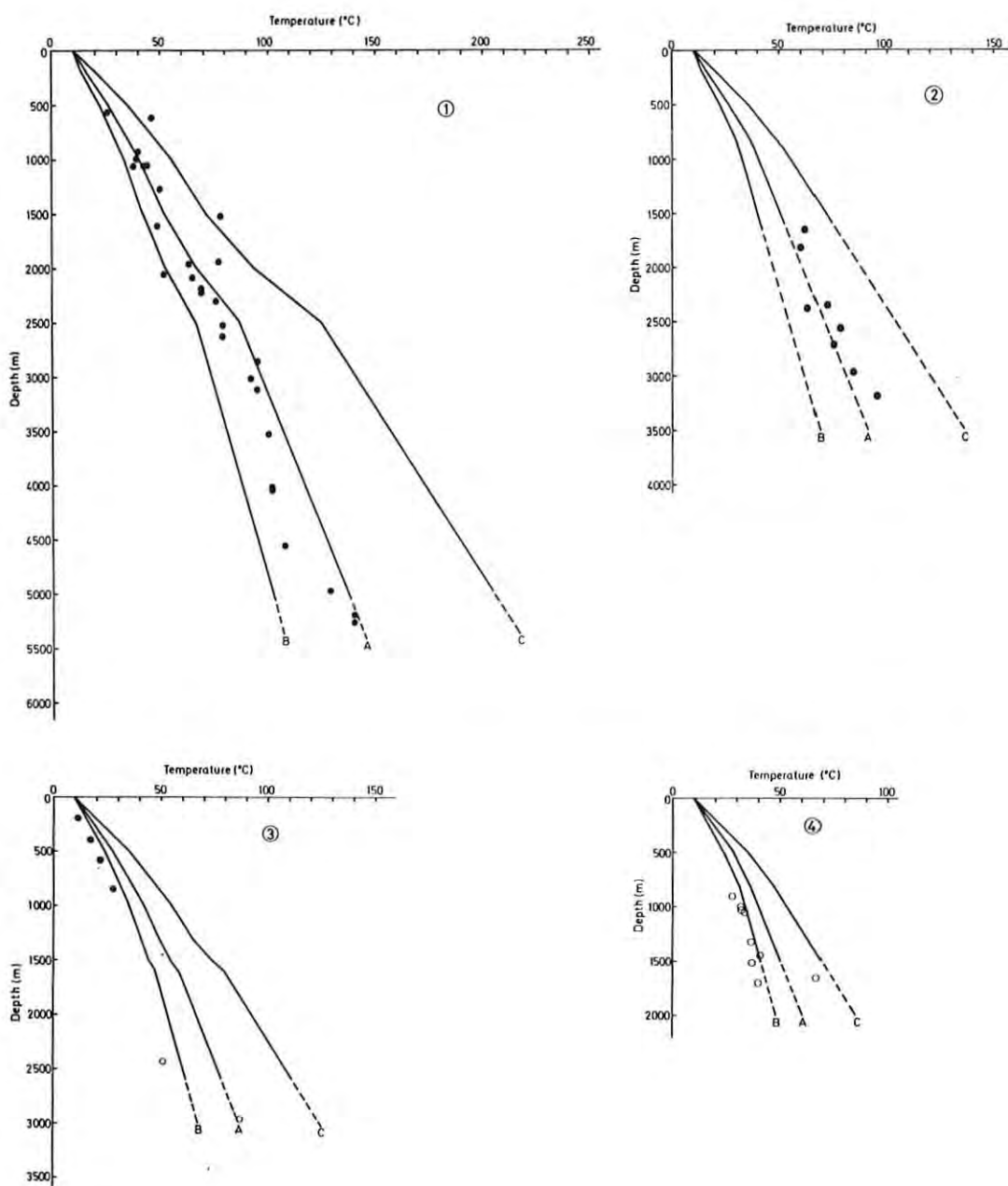


Fig. 53. Model temperatures calculated for typical layer thicknesses and shown in relation to the BHT values for 1) central parts of the Danish Subbasin, 2) Danish part of the North German Basin, 3) the island of Sjælland, and 4) areas above the Ringkøbing-Fyn High and the northernmost Jylland (areas of shallow Precambrian basement). Uncorrected BHT values (circles) are shown for areas of few or without corrected values (dots).

Table 15

Calculated model temperature gradients. Values obtained as  $q_o/k_i$ , where  $k_i$  is layer thermal conductivity as given in Table 14 and 60, 50 and 80  $\text{mW m}^{-2}$  are surface heat flow ( $q_o$ ) of models A, B, and C, respectively. Units of  $\text{mK m}^{-1}$  (or  $^{\circ}\text{C km}^{-1}$ )

Layer	Model A	Model B	Model C
1	30	20	53
2	35	28	50
3	29	23	40
4	22	17	32
5	30	21	44
6	40	28	62
7	20	14	32

Since the heat production is low, the model layer temperature gradients are almost constant (within  $1-2 \text{ mK m}^{-1}$ ) at  $(\Delta T/\Delta z)_i = q_o/k_i$ . Values are given in Table 15. The lowest temperature gradients are found for the layers with the highest conductivity (4 and 7), and layers 2 and 6 of low conductivity contain the highest gradients. If locally, normal to medium high heat flow is combined with low thermal conductivity, the gradients reach  $40-60 \text{ mK m}^{-1}$ , and a combination of low to normal heat flow and high conductivity yields low gradients of  $10-20 \text{ mK m}^{-1}$ . Temperature prediction by constant temperature gradient extrapolation may thus result in errors of several tens of degrees, even at depths of only 2000-3000 m.

All regional temperature isothermal models presented in this section were calculated from a grid pattern of points with mesh distances of 5' (east-west) and 3' (north-south) in the area north of  $56^{\circ}\text{N}$  and east of  $10^{\circ}\text{E}$ , where shorter wavelength variations as to layer depth and temperatures are to be approximated. For the rest of the country, which generally has longer wavelength variations, the double mesh distance of 10'x6' was applied (Fig. 54). At each grid point, depth to layer interfaces were read manually from stratigraphical maps produced by the

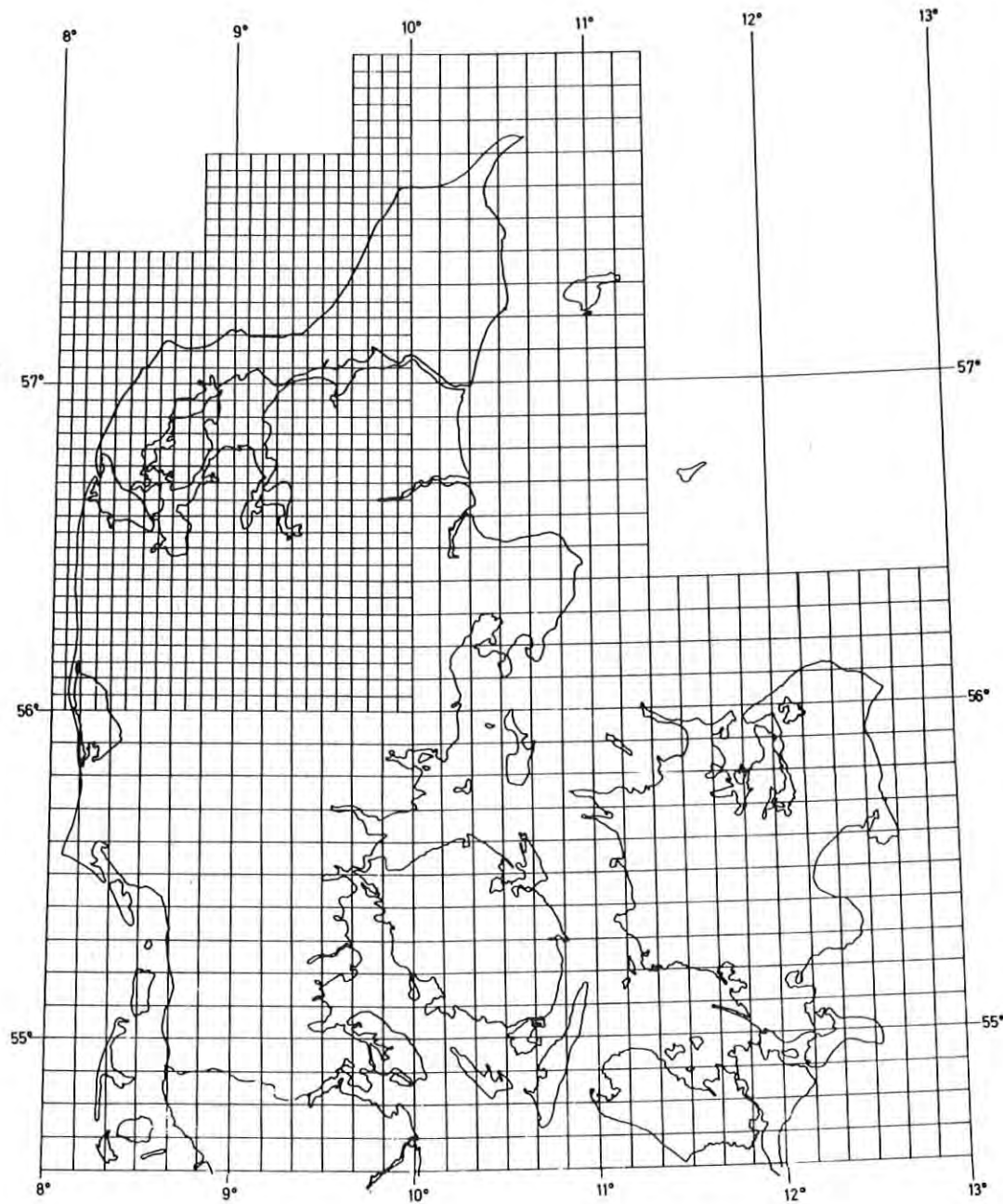


Fig. 54. Grid pattern applied in the subsurface temperature modelling. Temperatures are calculated at appropriate depths at each mesh point.

Geological Survey of Denmark. Reflection seismic data and wells formed the basis of interpretation. Generally, apart from local anomalies, and probably also the deepest part of the basins, the depths of actual stratigraphic horizons were defined with an accuracy of about  $\pm 200$  m. A north-south cross section through the strata is shown in Fig. 55 for illustration. For further details as to layer thicknesses and stratigraphy we refer to Michelsen et al. (1981).

Temperatures were calculated at each grid point at appropriate depths by a developed computer program based on Equation (7), and the model results thus determined were displayed as printed output and as plotted isothermal maps.

The maps presented here are hand contoured directly on the basis of the computer maps. This procedure enables us to introduce personal geological judgements as to the more accurate extension of actual stratigraphic horizons, and the position of local thermal anomalies not considered in the models, of which the salt structures are the most frequent. Contours were dotted in the areas of known salt structures (Fig. 1), and the temperature anomalies of the form shown in Figs. 38 and 56 are here to be superimposed on the calculated general model isotherms.

Model A isotherms are calculated for the constant depths of 2000 and 3000 m (Figs. 57 and 58). In local areas where the depth of layer 7 (the Triassic) is situated above the 2000 and 3000 m levels, temperatures were calculated by extrapolating layer 7 conductivity also to deeper layers. A comparison with the isothermal maps constructed on the basis of purely BHT information, as described in section 2.1 (Danish part of Figs. 7 and 8), generally shows agreement within  $\pm 10-15^{\circ}\text{C}$ , and both map types show the same main trend of temperature isolines, generally following the main structural trends (Fig. 1). We emphasize that the calculated horizontal model temperature variations are associated with horizontal thermal conductivity variations since the model heat flow is constant at  $60 \text{ mW m}^{-2}$ . In parts of North Jylland at 3000 m, model A temperatures are  $20-25^{\circ}\text{C}$  higher than those predicted by simple linear interpolation (and partly extrapolation) of BHT data. New accurate temperatures measured

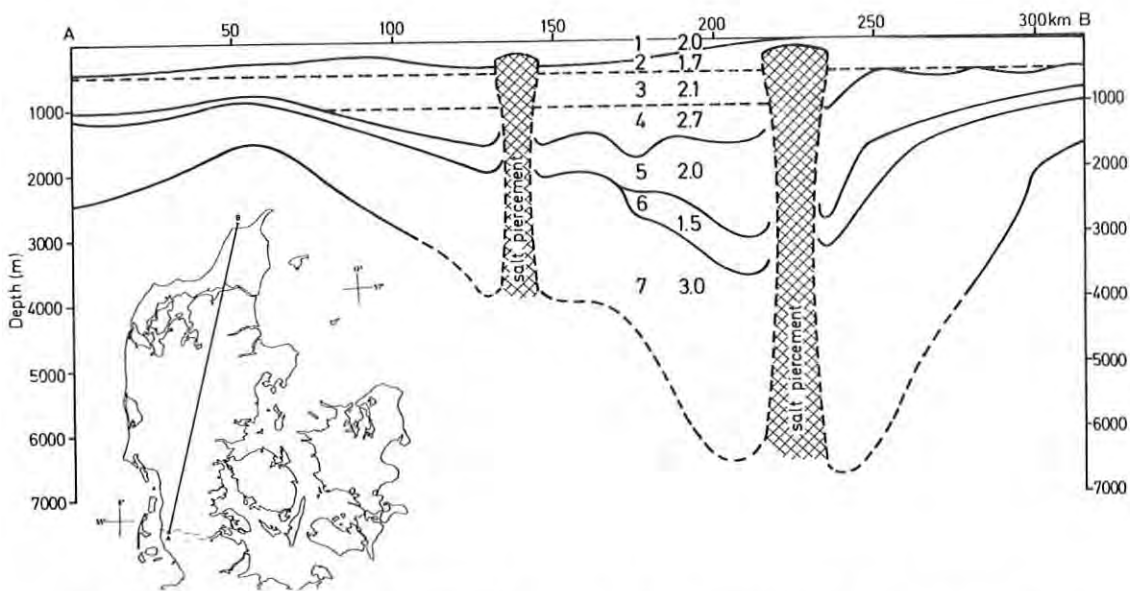


Fig. 55. N-S cross section through the Cenozoic and Mesozoic sedimentary sequence with layers (Table 13) and model A thermal conductivities (Table 14) indicated. Layer boundaries are slightly smoothed; faults are not shown.

at Aars in North Jylland (section 2.1) to a maximum depth of 3260 m show agreement with model A within  $\pm 5-10^{\circ}\text{C}$ . Where models differ and no observations exist, we generally prefer predictions by model A.

#### 3.4 Temperatures of potential geothermal reservoirs

Geothermal reservoirs, which may display economic exploration possibilities (Balling and Saxov, 1978; Dansk Olie og Naturgas, 1980; Michelsen et al., 1981) are observed within the Gassum Formation (Upper Triassic - Lower Triassic), Bunter Sandstone Formation (Lower Triassic) and the Haldager Formation (Middle Jurassic). Most information is available from the areas of North and Middle Jylland. Reservoirs of interest are found in the Frederikshavn member of the Bream Formation (Upper Jurassic) and within the Triassic Ørslev-Falster-Tønder-Skagerrak Formation sequence. Reservoirs of Pre-Triassic age, such as Zechstein limestone, Rothliegendes sandstone, Carboniferous limestone, and Cambrian quartzite/sandstone are as a rule only observed locally, and little is known as to their porosity and permeability.

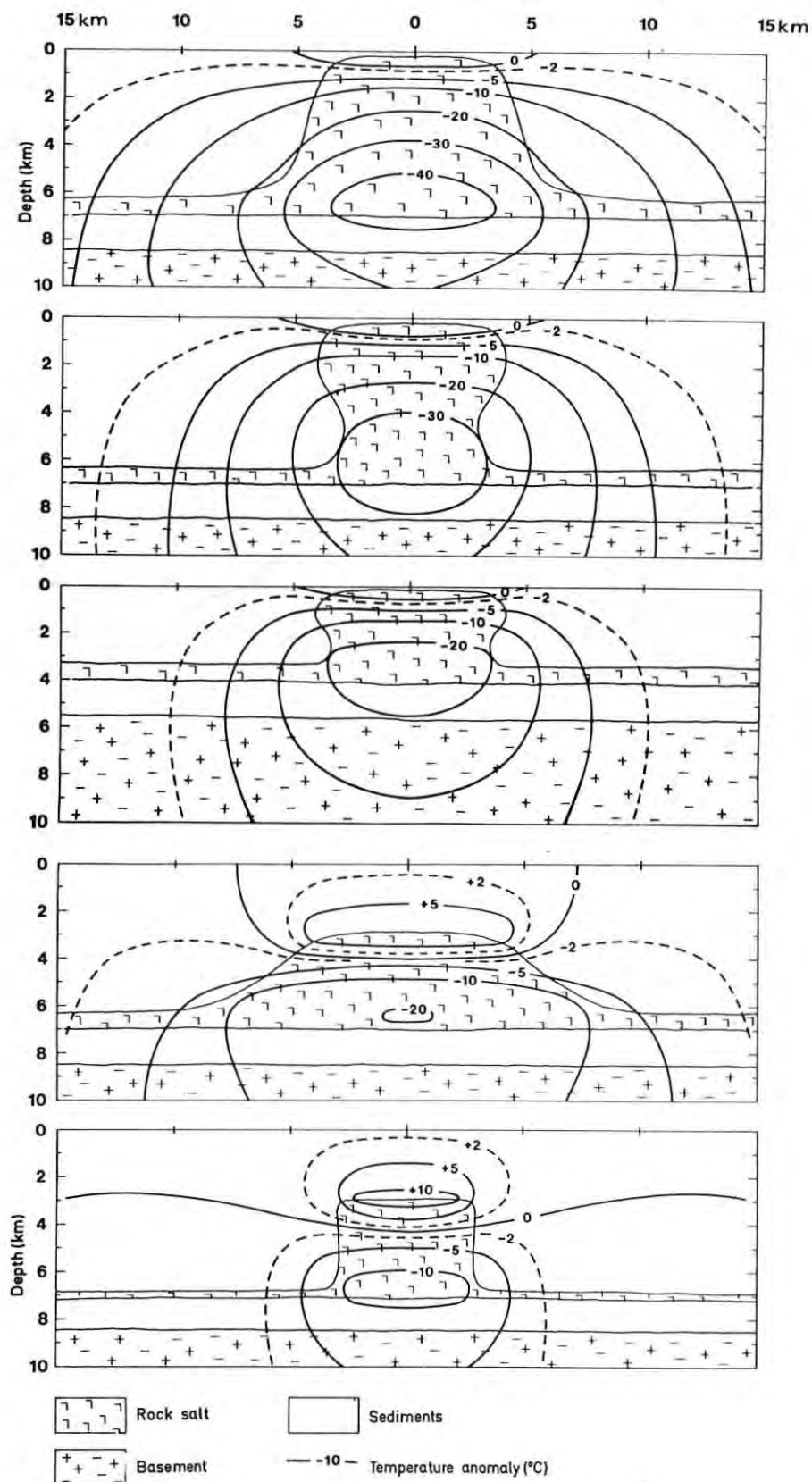


Fig. 56. Numerical two-dimensional finite difference temperature anomalies calculated for salt structures of various forms (Balling, 1978). The following thermal conductivity-temperature functions were applied: for the sediments  $2.2 \text{ W m}^{-1} \text{ K}^{-1}$  (constant), for the rock salt  $k(T) = 6.0/(1+0.0045T)$ , and for the basement rocks  $k(T) = 3.0/(1+0.001T)$ .

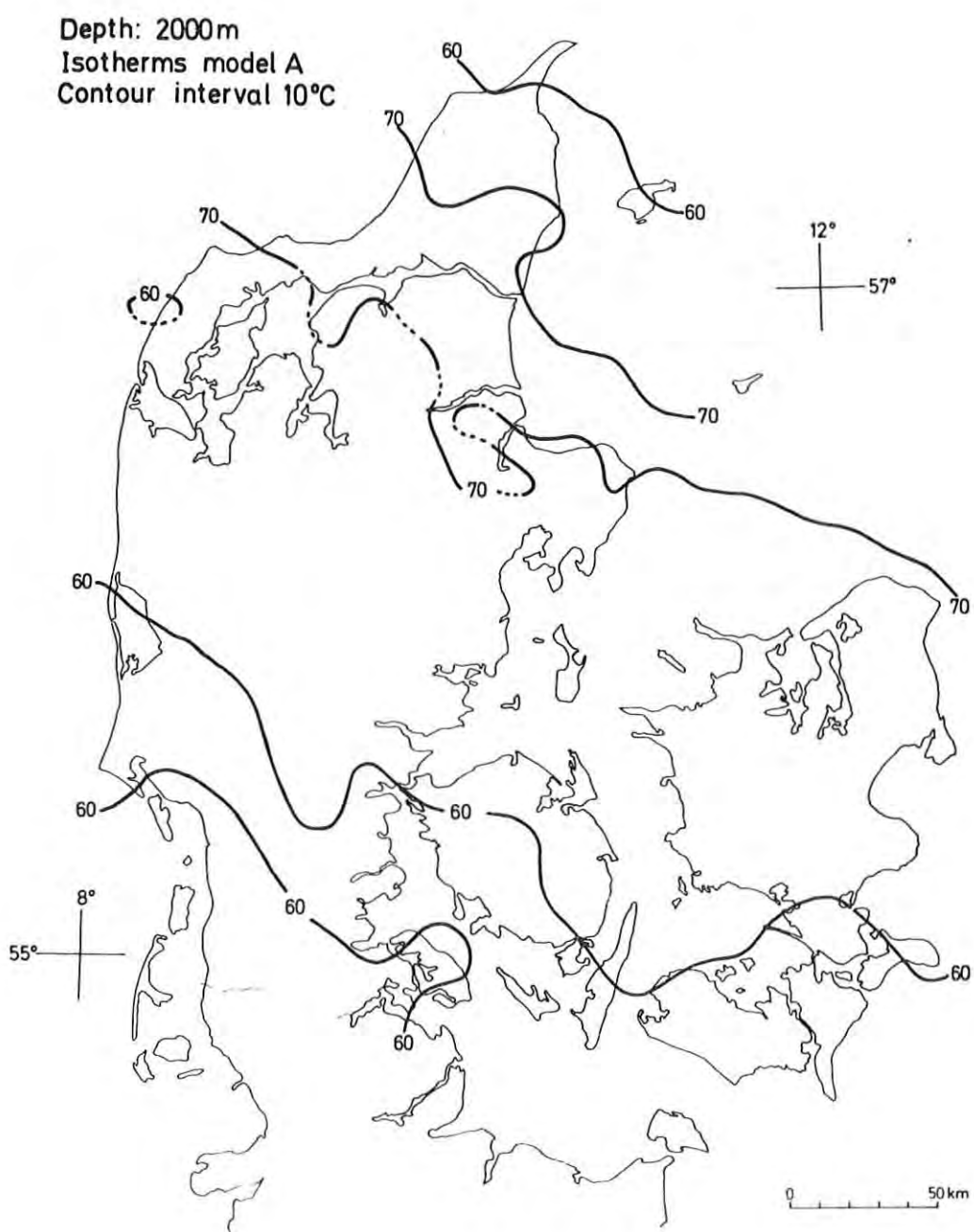


Fig. 57. Model A isothermal map for a depth of 2000 m.

Depth: 3000m  
Isotherms model A  
Contour interval 10°C

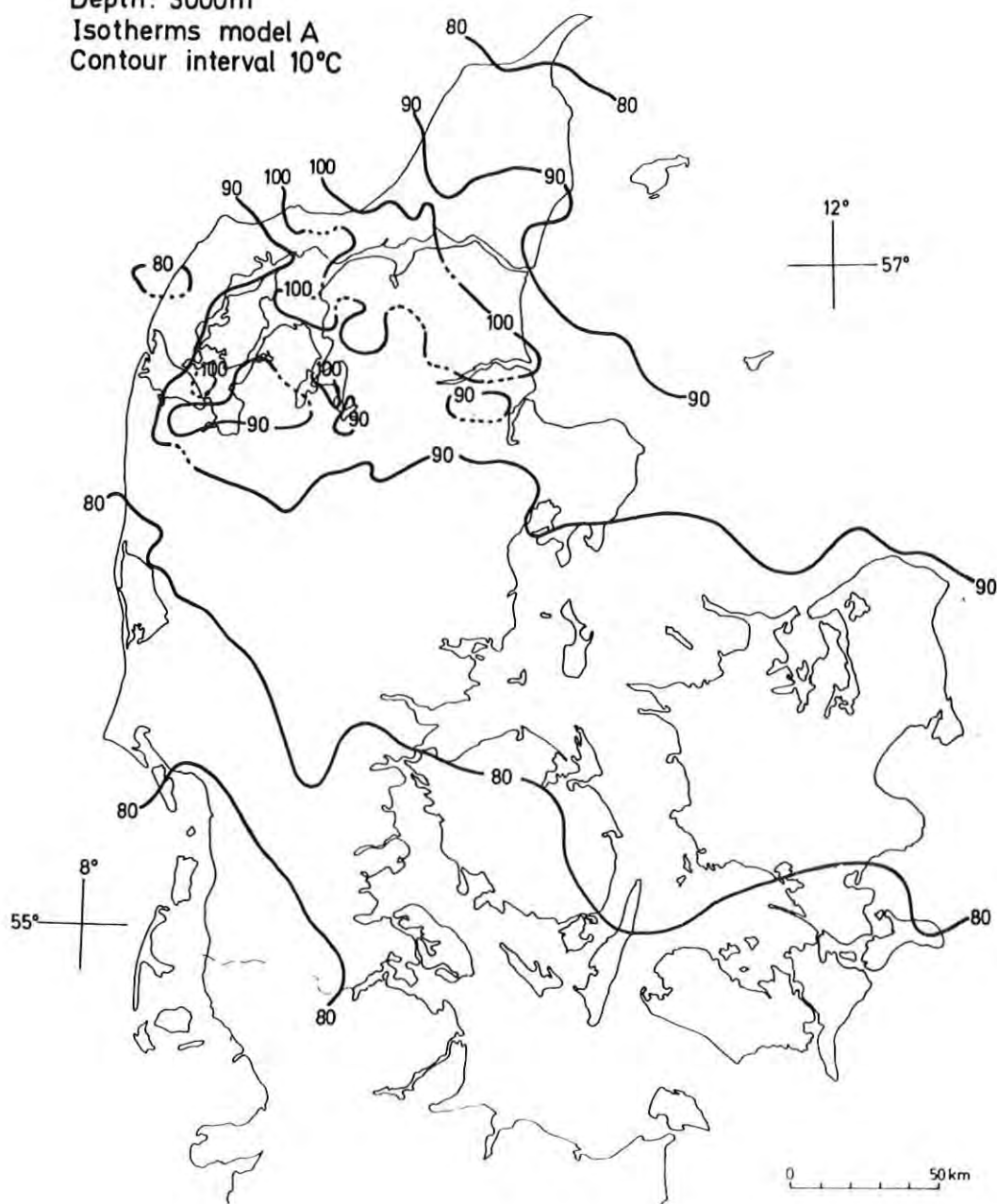


Fig. 58. Model A isothermal map for a depth of 3000 m.

System	Series	Stage	Formation	Member
CRETACEOUS	Lower	Albian	U. Cretaceous limestone	ITM
		Aptian Barremian Hauterivian Valanginian	Rødby	
		Berriasian	Vedsted	
		Portlandian	Bream	PGR
	Upper	Kimmeridgian		Børglum
		Oxfordian		Flyvbjerg
		Callovian Bathonian Bajocian	Haldager	PGR
		Aalenian		Haldager Sand
	Middle	Toarcian	Fjerritslev	ITM
		U. Pliensbachian		F - IV
		L. Pliensbachian		F - III
		U. Sinemurian		F - II
		L. Sin. Hettangian		F - I
		Rhaetian	Gassum	ITM
JURASSIC	Lower	Norian	Gassum	G <sub>0</sub> - G <sub>4</sub>
		Carnian	Vinding	PGR
		Ladinian	Oddesund	0 <sub>3</sub>
		Anisian		0 <sub>2</sub>
		Olenikian		Evaporite
	Upper	Jakutian		0 <sub>2</sub>
		Brahmanian		Evaporite
		Tønder		0 <sub>1</sub>
		Falster	Skagerrak	PGR
		Ørslev		PGR ?
TRIASSIC	Middle	Bunter Sandstone		PGR ?
		Bunter Shale		ITM

Fig. 59. Standard stratigraphic column of the Danish Triassic, Jurassic, and Cretaceous (Michelsen, 1978; Bertelsen, 1980). Potential geothermal reservoirs (PGR) and the levels for which isothermal maps are produced (ITM) are indicated.

The temperature modelling is concentrated on the sedimentary sequence from the base of the Upper Cretaceous limestone to the base of Triassic which contains the most of the reservoirs (Fig. 59).

Isothermal maps are presented for the following horizons: Base Upper Cretaceous limestone at the approximate level of Frederikshavn member (Figs. 60, 61, and 62); base Haldager Sand (Figs. 63, 64, and 65); near top Triassic at the approximate level of top of Gassum Formation (Figs. 66, 67, and 68); and the approximate level of base Triassic near the base of the Bunter Sandstone Formation (Fig. 69). With increasing depth models B and C temperatures probably become less relevant (Fig. 53), and for the base of the Triassic only model A values are presented.

The depths to layer boundaries are estimated to be accurate generally within  $\pm 200$  m (apart from local areas of boreholes or best seismic coverage with higher accuracies and the deepest horizons where, locally, accuracy may be less), and the associated model temperature accuracies are approximately  $\pm 5-10^{\circ}\text{C}$  (model A),  $\pm 5^{\circ}\text{C}$  (model B), and  $\pm 10-15^{\circ}\text{C}$  (model C).

The following summary of temperature evaluation is based mostly upon model A. For details we refer to the isothermal maps.

The Frederikshavn member is observed in Jylland north of the Ringkøbing-Fyn High at a maximum depth of about 2000 m. Temperatures are predicted at generally  $50-60^{\circ}\text{C}$ , locally increasing to about  $70^{\circ}\text{C}$  and decreasing to  $35-45^{\circ}\text{C}$  where the horizons are found at depths of some 1000 m.

The Haldager Sand is restricted to North Jylland (Fig. 63) and observed centrally in the Danish Subbasin at depths of 2000-3000 m and at temperatures generally of  $60-80^{\circ}\text{C}$ , increasing locally to about  $100^{\circ}\text{C}$  (predicted), and decreasing to  $30-50^{\circ}\text{C}$  at the northern margin.

The Gassum Formation occurs throughout most of Denmark with the exception of the central and western part of the Ringkøbing High. Centrally in the Subbasin depths of 2500-3000 m are normal, locally increasing to 3000-4000 m. Marginally, along the Feno-

Base Upper Cretaceous Limestone  
Isotherms model A  
Contour interval 10°C

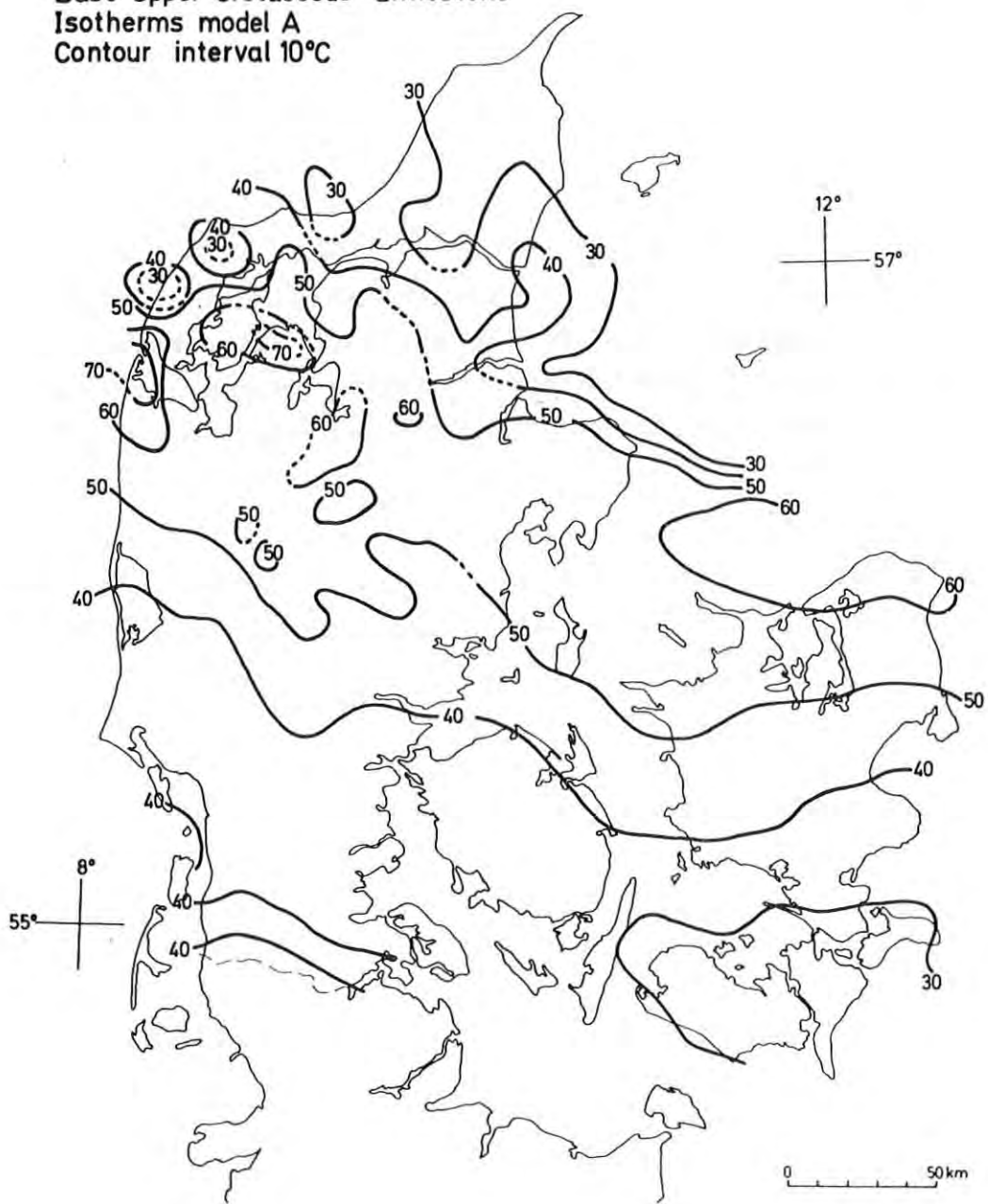


Fig. 60. Model A isothermal map of the base of the Upper Cretaceous limestone

Base Upper Cretaceous Limestone  
Isotherms model B  
Contour interval 10°C

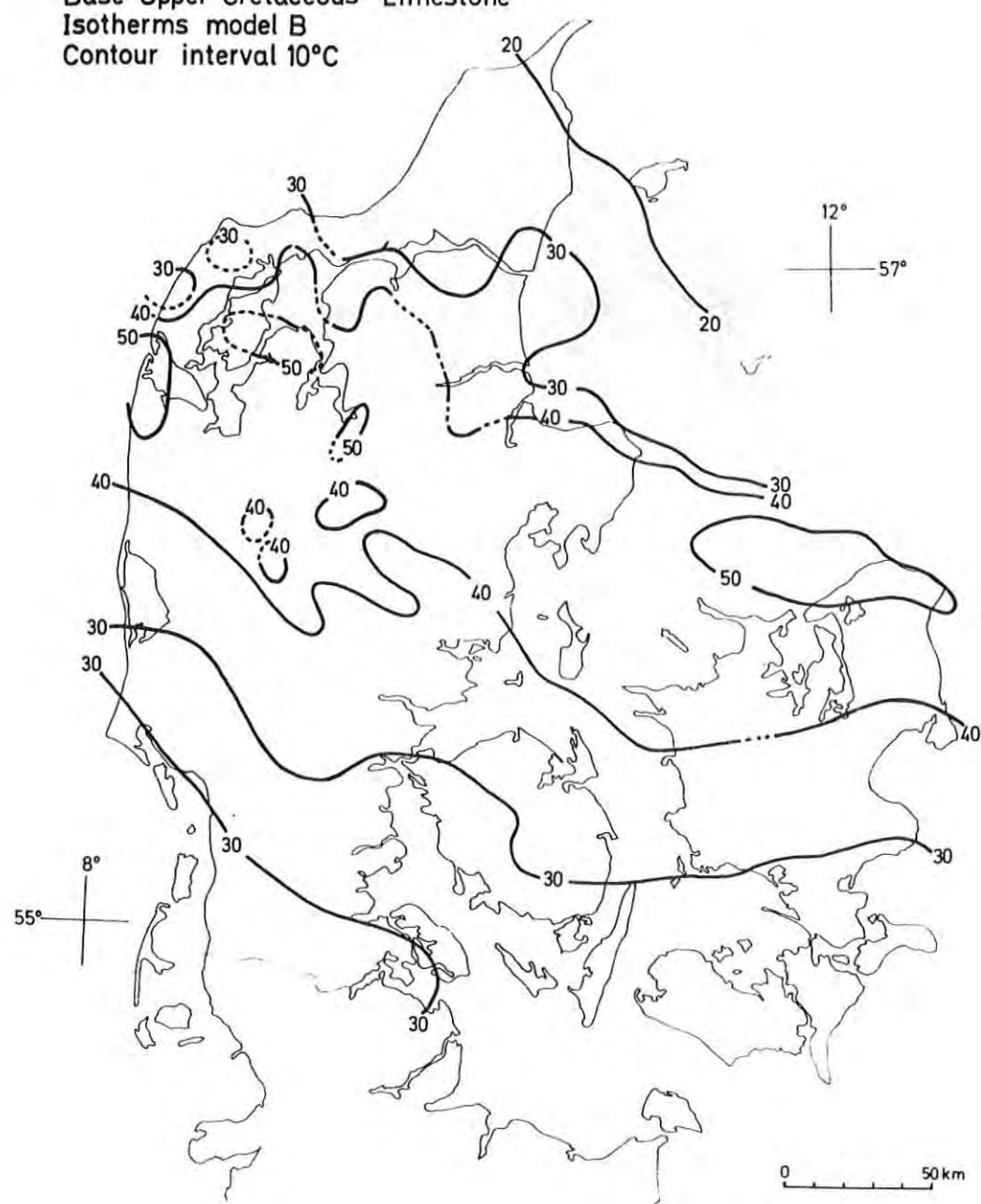


Fig. 61. Model B isothermal map of the base of the Upper Cretaceous limestone.

Base Upper Cretaceous Limestone  
Isotherms model C  
Contour interval 10°C

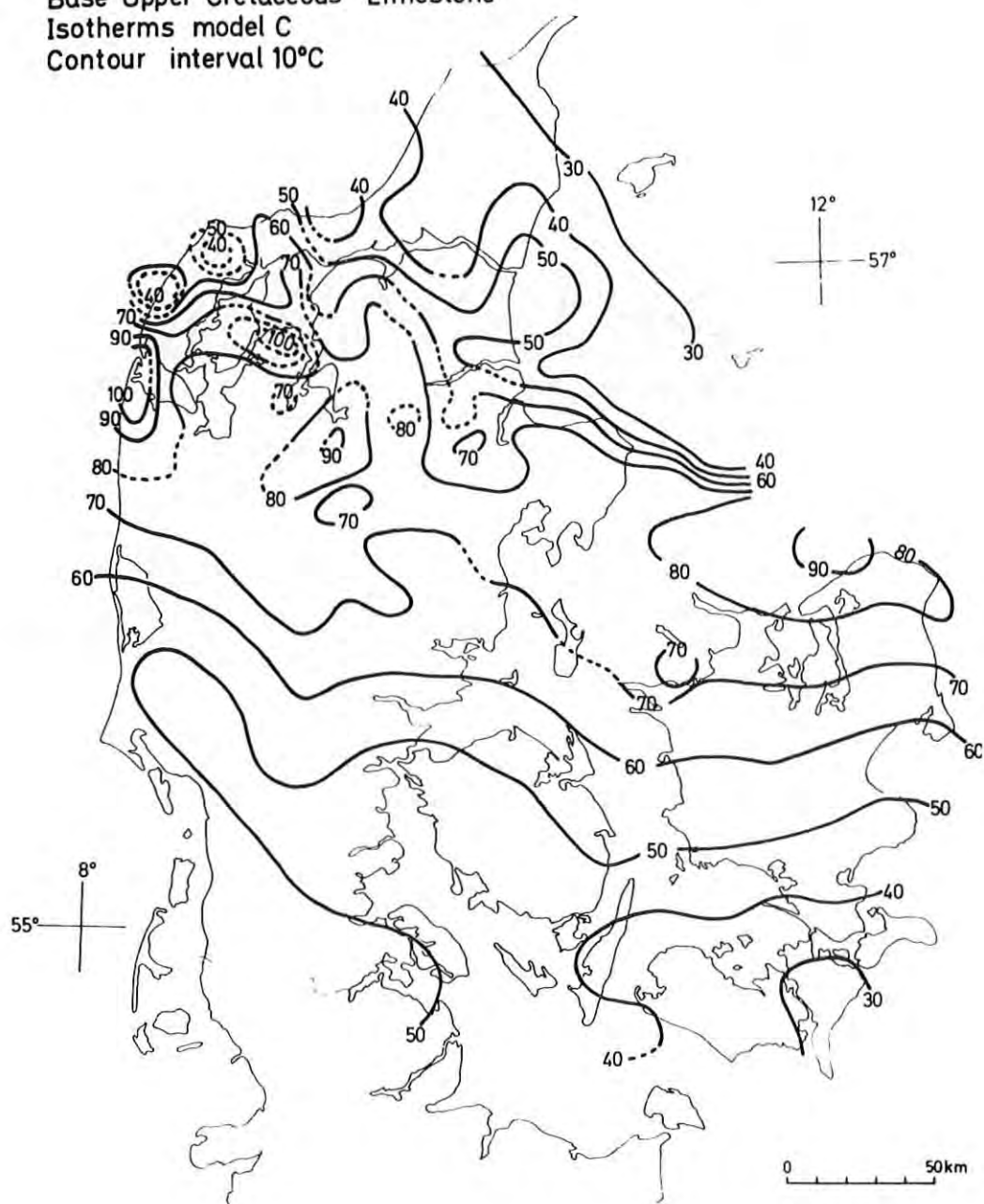


Fig. 62. Model C isothermal map of the base of the Upper Cretaceous limestone.



Fig. 63. Model A isothermal map of the base of the Haldager Sand.

Base Haldager Sand  
Isotherms model B  
Contour interval 10°C



Fig. 64. Model B isothermal map of the base of the Haldager Sand.



Fig. 65. Model C isothermal map of the base of the Haldager Sand.

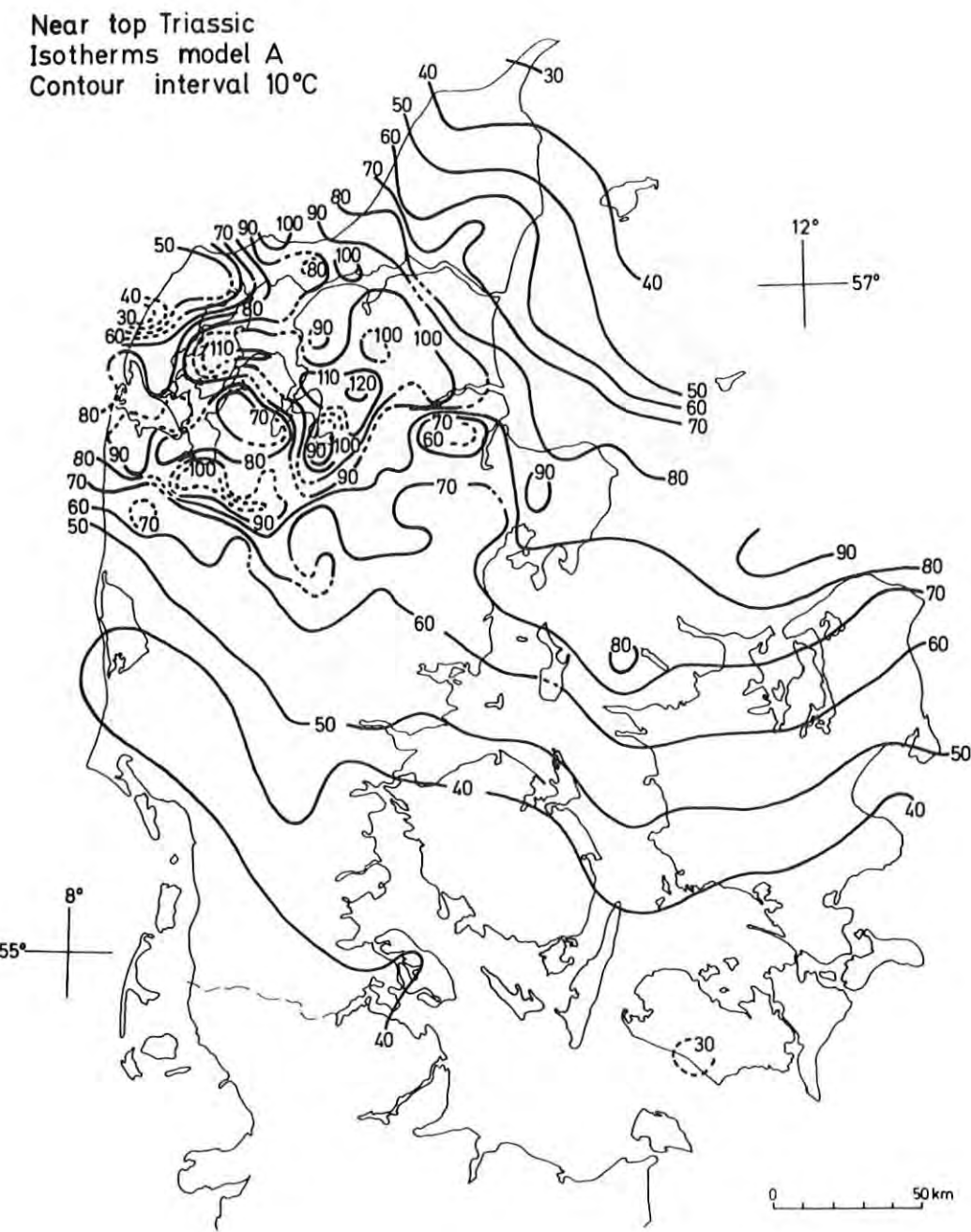


Fig. 66. Model A isothermal map of near top Triassic.

Near top Triassic  
Isotherms model B  
Contour interval 10°C

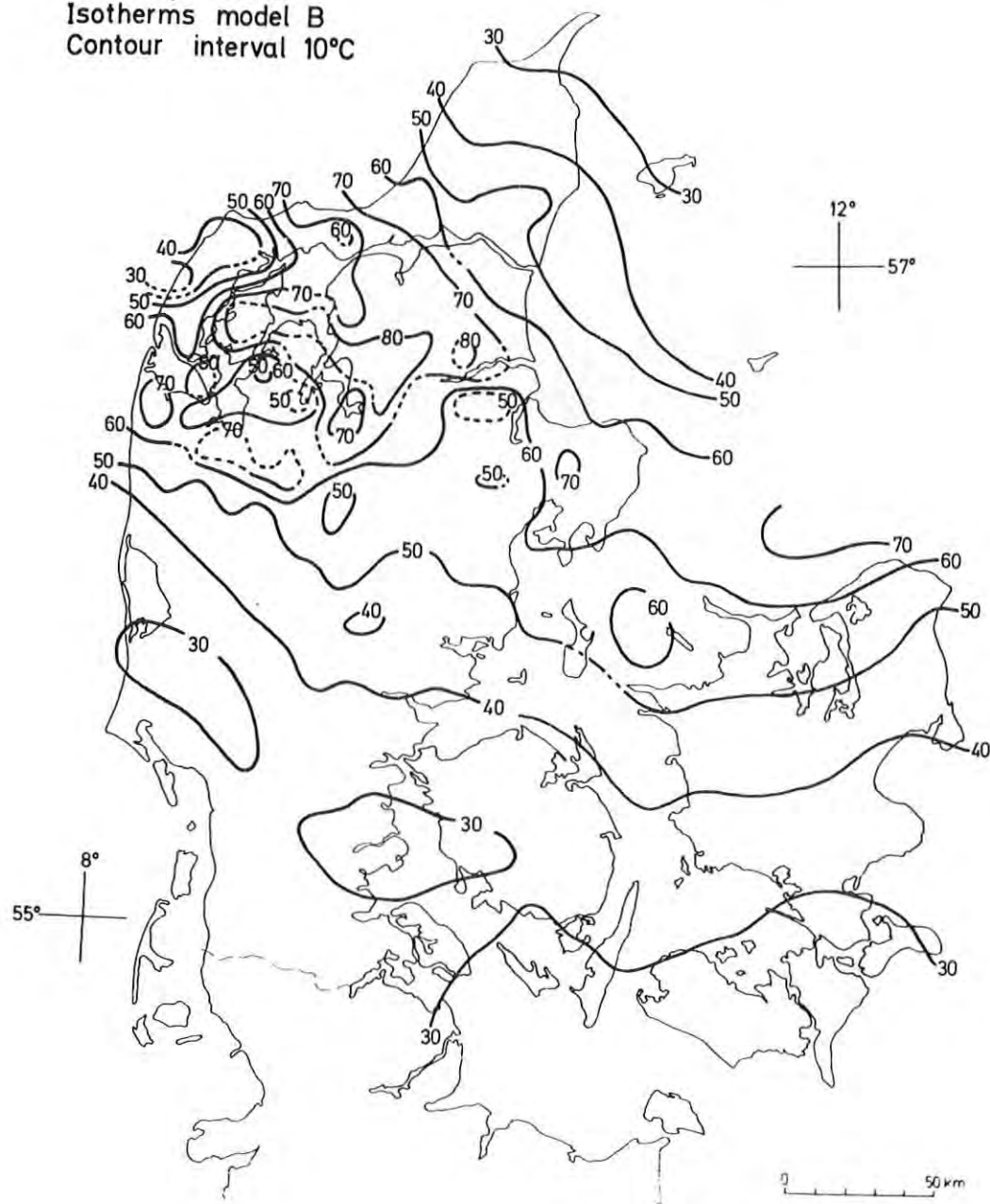


Fig. 67. Model B isothermal map of near top Triassic.

Near top Triassic  
Isotherms model C  
Contour interval 20°C

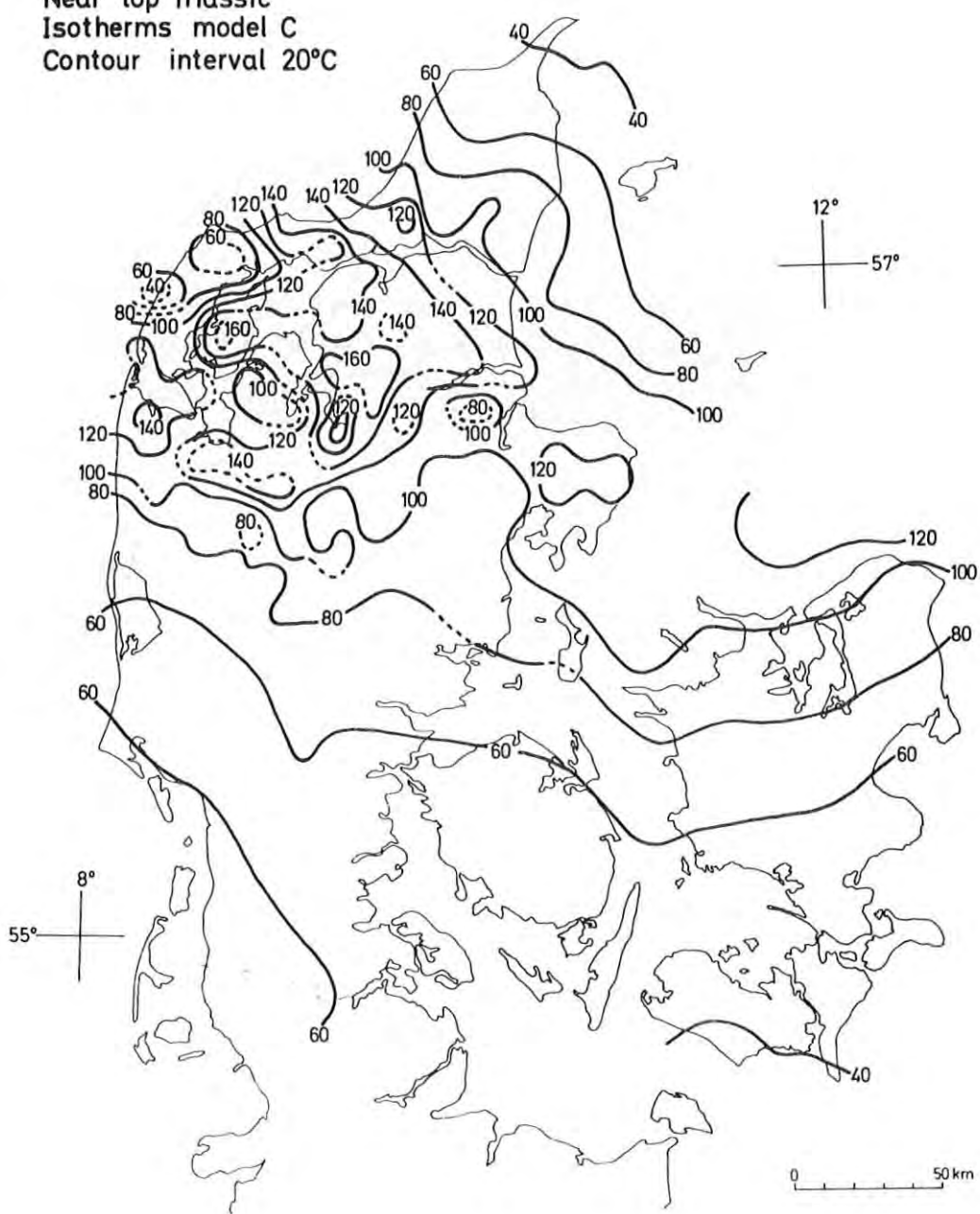


Fig. 68. Model C isothermal map of near top Triassic.

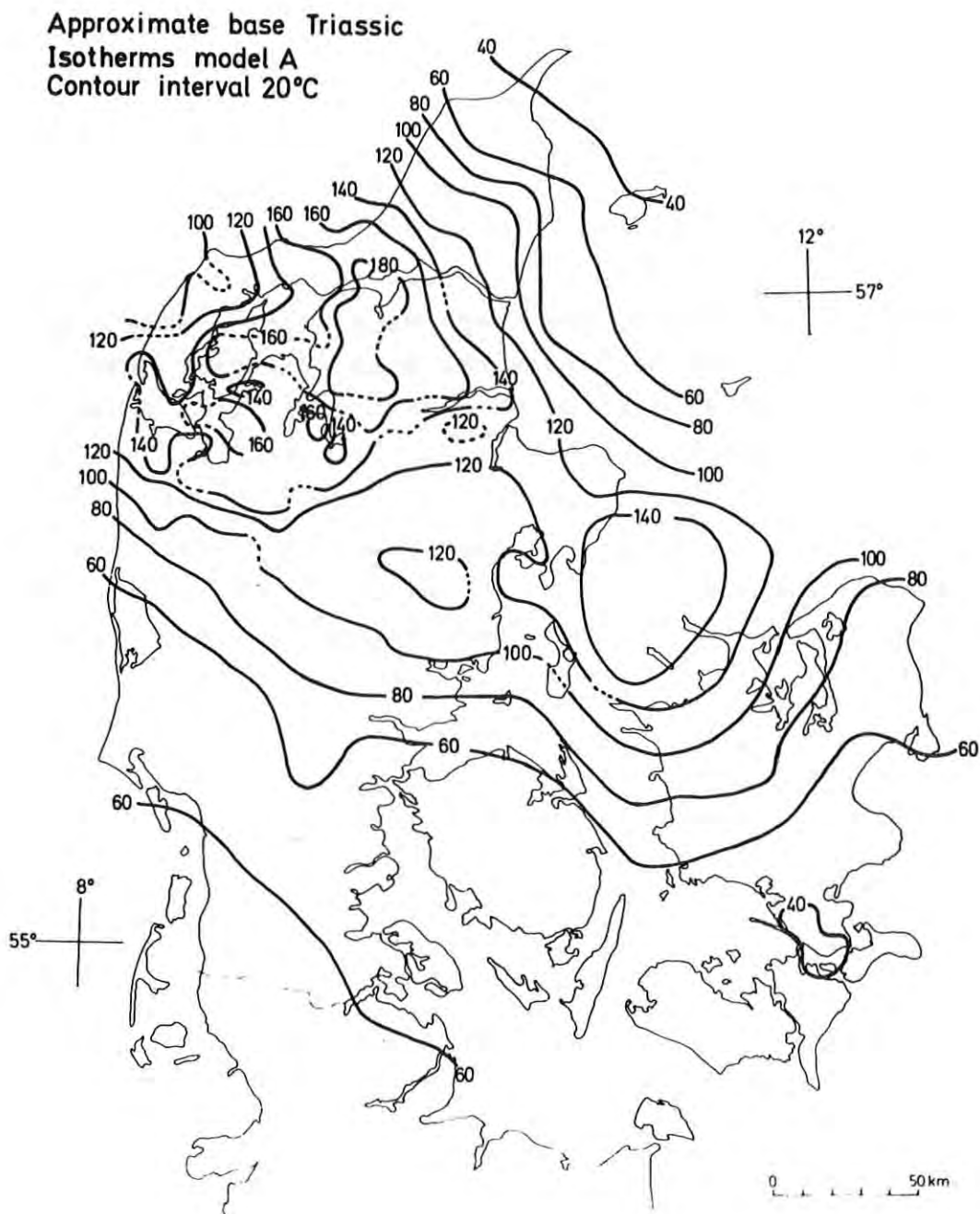


Fig. 69. Model A isothermal map of the approximate level of the base of the Triassic

scandian Border Zone and the Ringkøbing-Fyn High, depth decreases to 500-1000 m. Temperatures are (apart from local anomalies) observed and predicted at 35-45°C for the 1000 m level, 60-75°C at 2000 m, and 80-110°C at 3000 m. The highest temperatures (100-120°C) are predicted centrally in the Subbasin. Model A isotherms (Fig. 66) are expected to provide a reasonable basis for the regional evaluation. Due to lack of data the greatest uncertainty concerns areas in northernmost Jylland, along the Ringkøbing-Fyn High, and in Sjælland, where regionally model B (and C?) values are to be considered. Locally throughout the country the temperatures may reach model B and C values. At constant depth and heat flow the highest Gassum Formation temperatures are predicted for the areas where this formation is overlain by a thick sequence of the Fjerritslev Formation with predicted low thermal conductivity. In North Jylland maximum thickness of this (predicted) high temperature gradient formation is observed at ca. 900 m (Michelsen, 1978). Formation reservoir temperatures of 70-100°C are expected for most of North Jylland and lower values of 50-70°C in the southern and eastern part of the country.

Along the Fennoscandian Border Zone, Triassic sediments form the sandy series of the Skagerrak Formation. Centrally in the basin and to the south, the associated Triassic sequence is subdivided into a number of formations (Fig. 59). The Skagerrak Formation, the Bunter Sandstone, the Tønder Formation, and maybe also the Falster and Ørslev Formations, contain potential geothermal reservoirs. The approximate temperatures of the top and base of the Skagerrak Formation (where defined) are predicted by Figs. 66 and 69, respectively. The latter also predicts the approximate temperature of the base of the Bunter Sandstone Formation. The Tønder Formation is found centrally in the Subbasin at depths exceeding 3500 m, where temperatures above 100°C are expected. This also applies to the Falster and Ørslev Formations at somewhat greater depths.

The Bunter Sandstone is regionally distributed in the Subbasin at depths between 2000 and 4000 m, and locally greater than 5000 m. Here temperatures are calculated at generally 70-120°C,

increasing to above 140° at maximum depth. In the North German Basin in South Jylland temperatures at 60-80°C are observed and predicted to decrease to 30-50°C above the Ringkøbing-Fyn High.

Special geothermal interest is related to the local areas of the Danish Subbasin where a thick sequence of Triassic Formations, including the Bunter Sandstone, is elevated above deeper salt structure, to depths of 2000-3000 m. Here, in general, temperatures are obtained by combining the information of Figs. 56, 57, and 58.

If temperatures are to be predicted for specific localities with known or predicted stratigraphy, the most accurate procedure will be the direct use of the temperature gradients of Table 15, and with the possibility of adjustments according to any additional local information.

Results of the present temperature modelling study are applied in the combined geological and geophysical mapping of potential geothermal reservoirs to be published by Michelsen et al. (1981).

#### 4. CONCLUSIONS

The present study establishes the first order subsurface temperature pattern of Cenozoic and Mesozoic strata in Denmark. Depths to 7000 m are considered. The combination of Bottom Hole Temperatures reported by drilling companies, a few accurate temperature logs, and calculated regional model temperatures, enables the interpolation and extrapolation of measured temperature and temperature gradient relations. The model temperatures calculated from a one-dimensional analytical solution of the heat equation are constrained by the measured and estimated parameters of thermal conductivity, heat flow, and heat production. The first accurate measurements of parameters were carried out by newly developed thermal conductivity and temperature logging equipment. At the present state of knowledge no horizontal variations of heat flow and conductivity of layers could be modelled but the potential and probable variations are considered by presenting alternative models of constant parameters. Vertical average temperature gradient variations of typically

$10-20 \text{ mK m}^{-1}$  over intervals of hundreds of metres, are predicted and observed. Significantly higher variations are predicted locally. The main regional trends of lateral temperature variations are explained by lateral variations in thermal conductivity. Local temperature and heat flow anomalies associated with salt structures are measured and calculated. For depths down to about 3000 m measurements show regional and local temperature anomalies around  $\pm 10-20^\circ\text{C}$ . The conductivity of sediments is observed to be closely related to lithology and porosity. A distinct conductivity-porosity relation of the limestones is demonstrated. Radioactive heat production from the sediments is measured at normal low values, and the associated decrease of heat flow and temperature gradients with depth has little influence on temperatures at the depths considered here. At depths of about 2000-3000 m regional potential geothermal reservoirs normally show temperatures of  $60-100^\circ\text{C}$ . The calculated model geoisotherms form the basis of prediction of regional temperature variations at reservoir depth. Most information is available from central north Jylland and southernmost Jylland where measured and calculated temperatures agree within  $\pm 10-15^\circ\text{C}$  to depths of 3000-5000 m.

Our theoretical and experimental studies on the perturbations of terrestrial heat flow at shallow depth indicate regionally significant influence from paleoclimatic temperature variations and local major anomalies caused by ground water movements. The theoretical analyses of the possibilities of measuring heat flow in lake bottom sediments with rather high annual temperature variations indicate that accurate values may be obtained if measurements are carried out several times during the year, and results are analysed by the iterative least squares inversion method.

The technique used for the measurements of heat flow in shallow holes, based on a dense sampling of thermal conductivity on cores and high precision equilibrium temperature gradient measurements in tubes of the cemented drill holes, enables us to carry out observations of very accurate heat flow or apparent heat flow depth records. At shallow depths the impermeable Ter-

tiary formations characterized by clays are found suitable for the accurate measurement of conductive heat flow as a function of depth. The accuracies obtained permit the combined experimental and theoretical analysis of the paleoclimatic perturbations to heat flow.

So far we have measured low apparent heat flow at shallow depth ( $\leq 300$  m) compared with predictions by estimates of heat flow from greater depths ( $\geq 1000$  m). These differences may be explained by local lateral and vertical variations originating from the paleoclimatic effect and the effect of convective transfer of heat from ground water movements. More accurate observations on the lateral and vertical variations of heat flow, temperature gradients and conductivity are needed for the detailed interpretation of results. Such measurements are of general interest and will improve the basis of local Danish mapping and understanding of geothermal anomalies superimposed on the regional trends presented by the present study.

#### Acknowledgements

The authors are very grateful to the many Danish geologists who helped us with selection of cores, placing of heat flow sites, stratigraphical classifications etc., especially to O. Bjørnslev Nielsen, H. Friis and I. Madirazza, Geological Institute, Aarhus University, and O. Michelsen, S. Priisholm and L. Holm, Geological Survey of Denmark.

Thanks are due to the drilling company Foul Christiansen A/S, Højslev, for good co-operation and painstaking work; L. Løvborg at Risø National Laboratory for the measurements of radioactive heat producing elements. Søren B. Nielsen and P. Klint Jensen wrote some of the computer programs. For much practical help we are indebted to our laboratory technical staff, Erik Jensen, Vibeke Jensen, Geert Nedergaard Jensen and Otto Larsen, and to Grethe Nielsen and Mette Vels Jensen who drew the figures.

We are most grateful to E.R. Oxburgh, University of Cambridge, UK, for many fruitful discussions and suggestions, and to R. Haenel, Niedersächsisches Landesamt für Bodenforschung, Hannover, FRG, for co-operation in lake temperature measurements.

This research was financially supported by the European Economic Community (Geothermal Energy Programme - Contract No. 336-78 EG DK), Dansk Olie & Naturgas A/S (Landsdækkende geotermiske Undersøgelser), and the Danish Natural Science Research Council (Grant 511-5808).

## References

- Allis, R.G. & Garland, G.D., 1976: Geothermal measurements in five small lakes of northwest Ontario. *Can. J. Earth Sci.* 13, 987-992.
- Andersen, O.B., Kejlsø, E., and Remmer, D., 1974: Secular movements within Jutland as determined from repeated precise levellings. *Geodætisk Instituts Skrifter 3.rk.* 40, 70 pp.
- Anderson, E.M., 1934: Earth contraction and mountain building. *Beitr. Z. Geophys.* 42, 133-159.
- Balling, N., 1976a: Geothermal models of the Crust and uppermost Mantle of the Fennoscandian Shield in South Norway and the Danish Embayment. *J. Geophys.* 42, 237-256.
- Balling, N., 1976b: Rapport over geotermiske energiundersøgelser i dybdeboringen Oddesund 1. Laboratoriet for Geofysik, Aarhus Universitet, okt. 1976 (Bilag 3.1 i Handelsministeriet 1977).
- Balling, N., 1978: Geofysiske metoder til lokalisering af geotermiske energiressourcer. *Dansk geol. Foren. Årsskrift* 1977, 13-27.
- Balling, N., 1979: Subsurface temperatures and heat flow estimates in Denmark. In: Čermák & Rybach (eds.), *Terrestrial heat flow in Europe*. Springer-Verlag, Berlin, 161-171.
- Balling, N., 1980: The land uplift in Fennoscandia, gravity field anomalies and isostasy. In: Mörner, N.-A. (ed.), *Earth rheology, isostasy and eustasy*. John Wiley & Sons, New York, 297-321.
- Balling, N. & Saxov, S., 1978: Low enthalpy geothermal energy resources in Denmark. *Pageoph.* 117, 205-212.
- Balling, N., Kristiansen, J.I., Poulsen, K.D. & Saxov, S., 1980: Geothermal trends of Denmark. In: Strub, A.S. & Ungermaier, P. (eds.), *Advances in European geothermal research*. Commission of the European Communities, D. Reidel, Dordrecht, 485-495.
- Beck, A.E., 1977: Climatically perturbed temperature gradients and their effect on regional and continental heat-flow means. In: Jessop, A.M. (ed.), *Heat flow and geodynamics*. *Tectonophysics* 41, 17-39.
- Benfield, A.E., 1939: Terrestrial heat flow in Great Britain. *Proc. R. Soc. Lond. Ser. A*, 173, 428-450.
- Berger, A., 1979: Spectrum of climatic variations and their causal mechanisms. *Geophys. Surveys* 3, 351-402.
- Bertelsen, F., 1980: Lithostratigraphy and depositional history of the Danish Triassic. *Danm. geol. Unders.*, Ser.B, 4, 59 pp.
- Birch, F., 1948: The effects of Pleistocene climatic variations upon geothermal gradients. *Am. J. Sci.* 246, 729-760.

- Birch, F., 1954: Heat from radioactivity. In: Faul, H. (ed.), Nuclear geology. John Wiley and Sons, New York, 148-174.
- Birch, F. & Clark, H., 1940: The thermal conductivity of rocks and its dependence upon temperature and composition. Am. J. Sci. 238, 529-558 and 613-635.
- Bridgman, P.W., 1924: Thermal conductivity and compressibility of several rocks under high pressure. Am. J. Sci. 7, 81-102.
- Bullard, E.C., 1940: The disturbance of the temperature gradient in the earth's crust by inequalities of height. Mon. Not. R. Astr. Soc., Geophys. Suppl. 4, 360-363.
- Bullard, E.C., 1947: The time necessary for a borehole to attain temperature equilibrium. Mon. Not. R. Astr. Soc., Geophys. Suppl. 5, 125-130.
- Carslaw, H.S. & Jaeger, J.C., 1959: Conduction of heat in solids, 2nd ed., Oxford University Press, 510 pp.
- Čermák, V., 1971: Underground temperature and inferred climatic temperature of the past millennium. Palaeogeography, Palaeoclimatol., Palaeoecol. 10, 1-19.
- Conaway, J.G., 1977: Deconvolution of temperature gradient logs. Geophysics 42, 823-837.
- Conaway, J.G. & Beck, A.E., 1977: Continuous logging of temperature gradients. In: Jessop, A.M. (ed.), Heat flow and geo-dynamics. Tectonophysics 41, 1-7.
- Costain, J.K., 1970: Probe response and continuous temperature measurements. J. Geophys. Res. 75, 3969-3975.
- Dansgaard, W., Johnsen, S.J., Clausen, H.B. & Langway, C.C., 1971: Climatic record revealed by Camp Century ice core. In: Turekian, K.K. (ed.), The Late Cenozoic Glacial Ages, Yale Univ. Press, New Haven, Conn., 37-56.
- Dansgaard, W., Johnsen, S.J. Clausen, H.B. & Gundestrup, N., 1973: Stable isotope glaciology. Medd. om Grønland, C.A. Reitzel, Copenhagen, 53 pp.
- Dansk Olie & Naturgas A/S, 1980: Undersøgelse af geologi, marked, teknik og økonomi for potentielle geotermiske anlæg i Midt- og Nordjylland. Rapport af Dansk Olie & Naturgas A/S, Steensen og Varming, Forsøgsanlæg Risø og Danmarks Geologiske Undersøgelse.
- Frakes, L.A., 1979: Climates throughout geologic time. Elsevier, 310 pp.
- Gates, W.L., 1976: Modelling the ice-age climate. Science 191, 1138-1144.
- Haenel, R., 1968: Untersuchungen zur Bestimmung der terrestrischen Wärmestromdichte in Binnenseen. Diss. Univ. Clausthal-Zellerfeld, 121 pp.
- Haenel, R., Grønlie, G. & Heier, K.S., 1974: Terrestrial heat flow determinations from lakes in Southern Norway. Norsk geol. Tidsskr. 54, 423-428.

- Haenel, R., Legrand, R., Balling, N., Saxov, S., Bram, K., Gable, R., Meunier, J., Fanelli, M., Rossi, A., Salomone, M., Taffi, L., Prins, S., Burley, A.J., Edmunds, W.M., Oxburgh, E.R., Richardson, S.W. & Wheildon, J., 1979: Atlas of Subsurface Temperatures in the European Community. Commission of the European Communities, EUR 6578 EN, Brussels-Luxembourg.
- Handbook of Chemistry and Physics 1978-1979: CRC Press, Florida.
- Handelsministeriet, 1977: Udnyttelse af geotermisk energi i Danmark. Rapport fra Handelsministeriets arbejdsgruppe vedr. geotermisk energi. Febr. 1977, Ha 00-463, Statens trykningskontor.
- Horai, K., 1971: Thermal conductivity of rock-forming minerals. *J. Geoph. Res.* 76, 5, 1278-1308.
- Jackson, D.D., 1972: Interpretation of inaccurate, insufficient and inconsistent data. *Geophys. J. R. Astr. Soc.* 28, 97-109.
- Jaeger, J.C., 1965: Application of the theory of heat conduction to geothermal measurements. In: Lee, W.H.K. (ed.), Terrestrial heat flow. *Geophys. Monogr. Ser.* 8, Am. Geophys. Un., Washington, D.C., 7-23.
- Jessop, A.M., 1971: The distribution of glacial perturbation of heat flow in Canada. *Can. J. Earth Sci.* 8, 162-166.
- Jeffreys, H., 1940: The disturbance of the temperature gradient in the Earth's crust by inequalities of height. *Mon. Not. R. Astr. Soc., Geophys. Suppl.* 4, 309-312.
- Johnsen, S.J., Dansgaard, W., Clausen, H.B. & Langway, C.C., 1972: Oxygen isotope profiles through the Antarctic and Greenland ice sheets. *Nature* 235, 429-434.
- Jones, F.W. & Oxburgh, E.R., 1979: Two-dimensional thermal conductivity anomalies and vertical heat flow variations. In: Čermák, V. & Rybach, L. (eds.), Terrestrial heat flow in Europe. Springer-Verlag Berlin, 98-106.
- Kappelmeyer, O. & Haenel, R., 1974: Geothermics with special reference to application. *Geoexpl. Monogr. Ser.* 1, 4, 238 pp.
- Kristiansen, J.I., Saxov, S., Balling, N. & Poulsen, K.D., 1981: In-situ thermal conductivity measurements on Precambrian, Palaeozoic and Mesozoic rocks on the island of Bornholm, Denmark. *Geol. Fören. i Stockholm Förh.* (in press).
- Lachenbruch, A.H. & Brewer, H.C., 1959: Dissipation of the temperature effect of drilling a well in Arctic Alaska, U.S. Geol. Surv. Bull. 1083-C, 73-109.
- Lachenbruch, A.H. & Marshall, B.V., 1966: Heat flow through the Arctic Ocean floor: Canada Basin - Alpha Rise boundary. *J. Geophys. Res.* 71, 1223-1248.
- Lamb, H.H., 1972: Climate - Present, past and future. Vol. 1, Methuen & Co., London, 613 pp.
- Lamb, H.H., 1977: Climate - Present, past and future. Vol. 2, Methuen & Co., London, 835 pp.

- Lanczos, C., 1961: Linear differential operators. Van Nostrand, London, 564 pp.
- Lee, W.H.K. (ed.), 1965: Terrestrial heat flow. Geophys. Monogr. Ser. 8, Am. Geophys. Un., Washington, D.C., 276 pp.
- Lee, T.-C., 1975: Focusing and defocusing of heat flow by a buried sphere. Geophys. J. R. astr. Soc. 43, 635-641.
- Lee, T.-C. & Cohen, L.H., 1979: Onshore and offshore measurements of temperature gradients in the Salton Sea geothermal area, California. Geophysics 44, 206-215.
- Mertz, E.L., 1924: Oversigt over de sen- og postglaciale niveau-forandringer i Danmark. Danm. geol. Unders., II Rk. 41, 49 pp.
- Michelsen, O., 1978: Stratigraphy and distribution of Jurassic deposits of the Norwegian-Danish Basin. Danm. geol. Unders. Ser. B 2, 28 pp.
- Michelsen, O., Saxov, S., Leth, J.A., Andersen, C., Balling, N., Breiner, N., Holm, L., Jensen, K., Kristiansen, J.I., Laier, T., Nygaard, E., Olsen, J.C., Poulsen, K.D., Priisholm, S., Raade, T.B., Sørensen, T.R. & Würtz, J., 1981: Kortlægning af potentielle geotermiske reservoirer i Danmark. Danm. geol. Unders. Ser. B (in press).
- Oxburgh, E.R., Richardson, S.W., Turcotte, D.L. & Hsui, A., 1972: Equilibrium borehole temperatures from observations of thermal transients during drilling. Earth Planet. Sci. Lett. 14, 47-49.
- Oxburgh, E.R., Richardson, S.W., Bloomer, J.R., Martin, A. & Wright, S., 1977: Sub-surface temperatures from heat flow studies in the United Kingdom. Seminar on geothermal energy, Brussels Dec., 1977, Commission of the European Communities, EUR 5920, Brussels-Luxembourg, 155-173.
- Oxburgh, E.R., Richardson, S.W., Wright, S.M., Jones, M.Q.W., Penney, S.R., Watson, S.A. & Bloomer, J.R., 1980: Heat flow pattern of the United Kingdom. In: Strub, A.S. & Ungemach, P. (eds.), Advances in European geothermal research. Commission of the European Communities, D. Reidel, Dordrecht, 447-455.
- Pedersen, L.B., 1979: Constrained inversion of potential field data. Geophysical Prospecting 27, 726-748.
- Poulsen, K.D., Saxov, S., Balling, N. & Kristiansen, J.I., 1981: Thermal conductivity measurements on Silurian limestones from the island of Gotland, Sweden. Geol. Fören. i Stockholm Förh. (in press).
- Rasmussen, L.B., 1960: Geology of north-eastern Jylland, Denmark. Guide to excursions, part 2. Int. Geol. Congr., Copenhagen, 38 pp.
- Rasmussen, L.B., 1978: Geological aspects of the Danish North Sea sector. Danm. geol. Unders. III Rk. 44, 85 pp.
- Ratcliffe, E.H., 1959: Thermal conductivities of fused and crystalline quartz. Br. J. Appl. Phys. 10, 22-25.

- Richardson, S.W. & Oxburgh, E.R., 1979: The heat flow field in Mainland UK. *Nature* 282, 565-567.
- Roy, R.F., Blackwell, D.D. & Decker, E.R., 1968: Heat generation of plutonic rocks and continental heat flow provinces. *Earth Planet. Sci. Lett.* 5, 1-12.
- Rybäck, L., 1973: Wärmeproduktionsbestimmungen an Gesteinen der Schweizer Alpen. *Beitr. Geol. Schweiz, Geotech. Ser. Lfg.* 51, Kümmerly & Frey, Bern.
- Saxov, S., 1956: Some gravity measurements in Thy, Mors and Vendsyssel. *Geodætisk Instituts Skrifter 3. Rk.*, Bd.25, 46 pp.
- Saxov, S., 1976: Gravity measurements in Central Jylland. *Geodætisk Instituts Skrifter 3.Rk.*, Bd.42, 138 pp.
- Saxov, S. (ed.), 1979: Compilation of temperature, geological, hydrogeological and geochemical data in Denmark. - A first stage survey of the geothermal potential. Commission of the European Communities, EUR 6384 EN, Luxembourg.
- Sorgenfrei, T. & Buch, A., 1964: Deep tests in Denmark 1935-1959. *Danm. geol. Unders. III Rk.* 36, 146 pp.
- Von Herzen, R.P. & Maxwell, A.E., 1959: The measurement of thermal conductivity of deep-sea sediments by a needle probe method. *J. Geophys. Res.* 64, 1557-1563.
- Von Herzen, R.P., Hoskins, H. & Andel, T. van, 1972: Geophysical studies in the Angola diapir field. *Geol. Soc. Am. Bull.* 83, 7, 1901-1910.
- Von Herzen, R.P., Finckh, P. & Hsü, K.J., 1974: Heat-flow measurements in Swiss Lakes. *J. Geophys.* 40, 141-172.
- Woodside, W. & Messmer, J.H., 1961: Thermal conductivity of porous media. *J. Appl. Phys.* 32, 1688-1706.
- Ziegler, P.A., 1978: North-western Europe: tectonics and basin development. In: Loon, A.J. van (ed.), *Key-notes of the MEGS-II* (Amsterdam, 1978). *Geol. Mijnbouw* 57, 589-626.
- Zienkiewicz, O.C., 1971: The finite element method in engineering science. McGraw-Hill, London, 521 pp.

APPENDIX A

Geothermal Equipment

- A1 Temperature logging equipment
- A2 Divided bar apparatus
- A3 Needle probe instruments
- A4 Construction principles of needle probes
- A5 Data acquisition system

### A1 Temperature logging equipment

Temperatures in shallow holes were measured by a normal three-conductor thermistor apparatus (Fig. A-1) with resistances measured by the traditional Wheatstone bridge method.

In the following we describe the basic principles of new temperature equipment built for the accurate measurements of temperatures and temperature gradients in deep boreholes. Two methods are based on the use of a four-thermistor configuration, the Mueller bridge method and the four-point method. A third method applies the quartz thermometer principle with a long cable transmission system. The latter was developed in prototype. Furthermore, we describe a temperature probe unit.

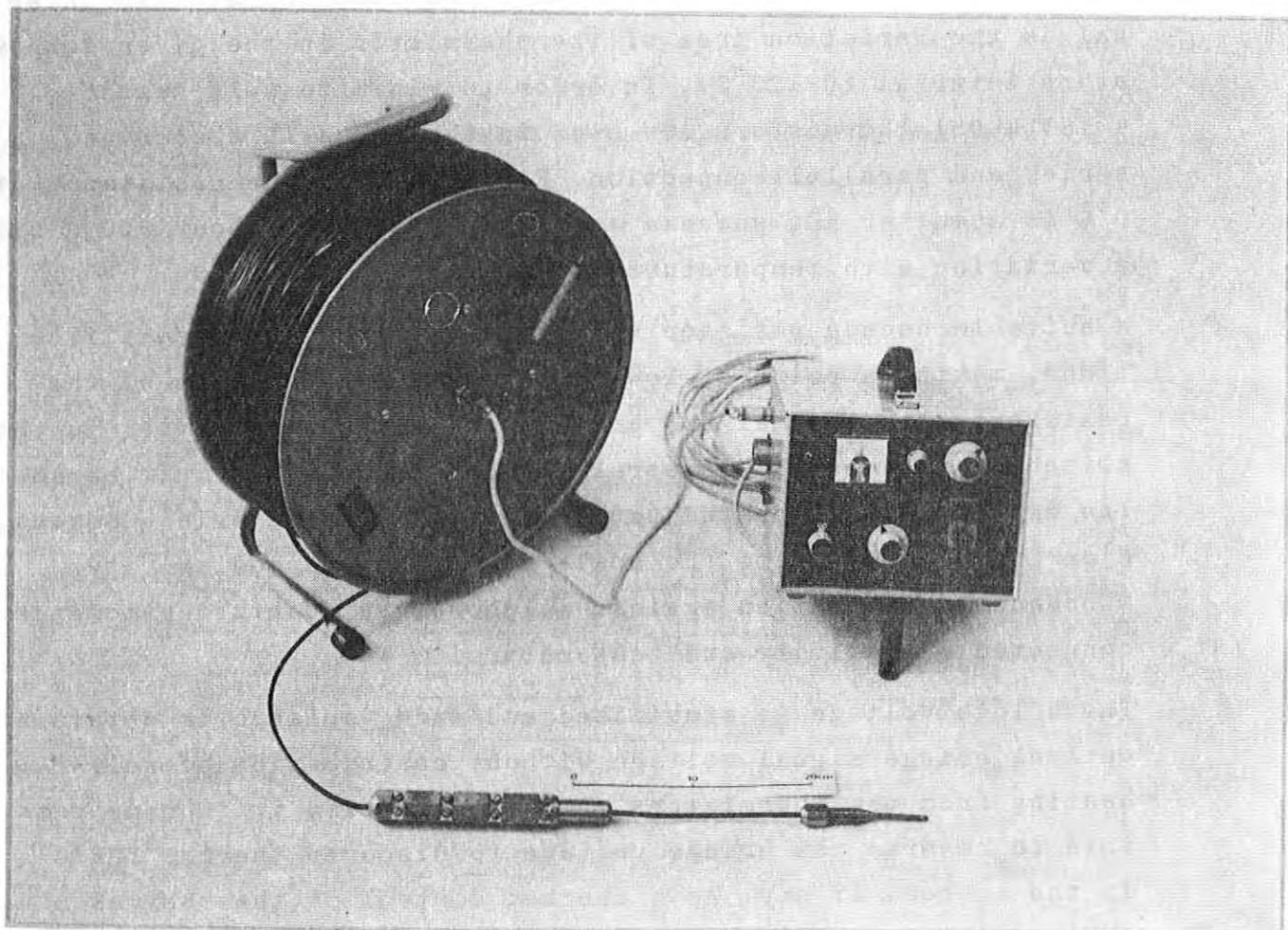


Fig. A-1. Temperature logging unit used for the measurements of shallow holes. The temperatures are measured by a traditional one-thermistor Wheatstone bridge configuration.

### The Mueller bridge method

The Mueller bridge principle is used for accurate resistivity measurements where the cable resistivity may constitute a considerable part of the value of the object measured. Two measurements are made, each with three conductors to the sensor. A suitable combination of the measurements cancels the two wire contributions provided that the wire resistances are equal. The main functions of the bridge will appear from the block diagram (Fig. A-2).

The diagram of the bridge (Fig. A-3) shows how the thermistor (RNTC) is connected to the bridge in each of the two measurements (cable switch A and B), which are the basis of one temperature determination. The location of the compensation resistor shows that it should cover the same resistivity interval as the variation area of the thermistor in the given temperature interval ( $0-120^{\circ}\text{C}$ ). In order to minimize self heating, 4 YSI 44031 thermistors are used in the probe in a combined series and parallel connection. For YSI 44031 the resistance at  $0^{\circ}\text{C}$  is about  $40 \text{ k}\Omega$ , whereas at  $120^{\circ}\text{C}$  it is only about  $800 \Omega$  with a variation with temperature of about  $0.01 \Omega/10^{-3}^{\circ}\text{C}$ .

A suitable decade resistor was built with the above specifications, making a point of low temperature coefficients of the resistors, low thermal EMF and low contact resistivities in the switches, just as the temporal change of resistors must be small. The decade was calibrated (at the Danish Army Material Command, Hjørring) to correlate the scale value and the resistivity. Subsequent calibration against a laboratory quartz thermometer connected resistivity and temperature.

The bridge voltage is stabilized and made variable to obtain an optimal bridge signal voltage without contribution of self-heating from the thermistors. At the same time it is made possible to reverse the bridge voltage to discover thermal EMF's in the system, if any. As a further control of the thermal EMF's and insulation resistances in the cable system, the probe is equipped with two small relays activated by the surface instrument unit. These relays disconnect two of the thermistor wires or short-circuit all four.

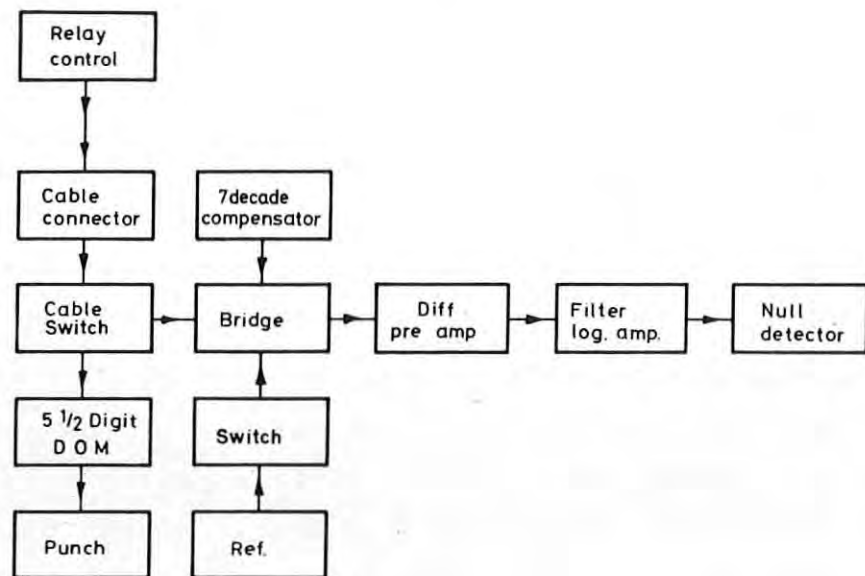


Fig. A-2. Block diagram of the four-thermistors configuration and the Mueller bridge.

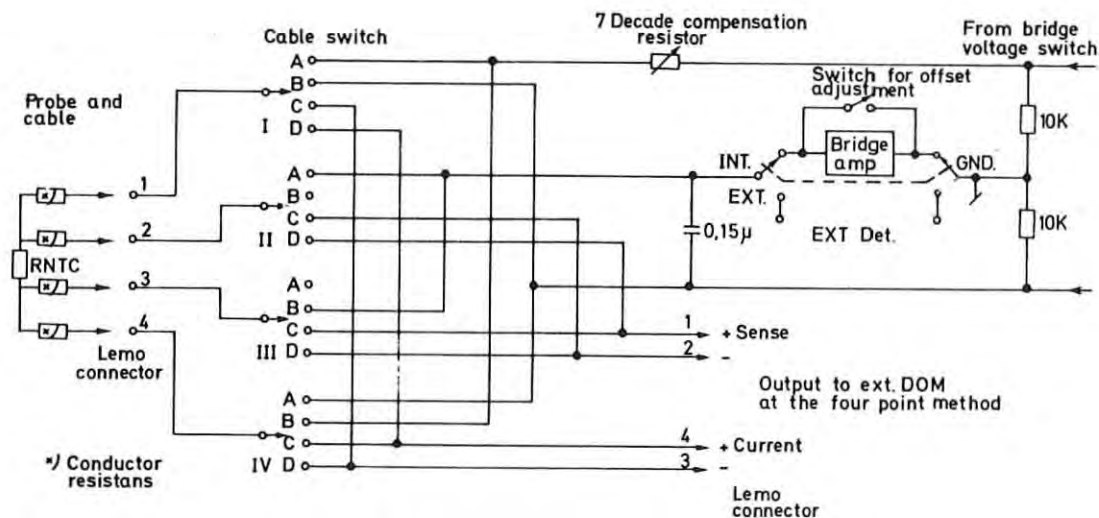


Fig. A-3. Basic measuring principles of the Mueller bridge.

To amplify the bridge signal a high performance FET amplifier is used in the first stage. Current and voltage noise and drift are kept low considering the relatively long time necessary for determination of the temperature at a point. It should be noted that the bridge voltage at 120°C is only about 1 µV per  $10^{-3}$  °C. The measuring cabin should therefore also have a reasonable temperature constancy, especially when measuring at great depths.

The bridge amplifier is equipped with a lowpass filter which cuts at about 2 Hz to avoid any influence from induced disturbance components mainly in the surface part of the cable. The postamplifier is non-linear and works around the balance point with full amplification, whereas by increasing disbalance the amplification decreases. This facilitates the bridge balancing. The non-linear amplifier drives a meter with centred zero, indicating the balance point. Alternatively, it is possible to connect an external 0-detector after the filter or via a switch at the bridge output.

The Mueller bridge method is comparatively time consuming, but if the temperature conditions around the probe are stable, it is a very accurate method with a resolution of  $10^{-3}$  K under the given conditions. The equipment is illustrated in Fig. A-4.

#### The four-point method

For the Mueller bridge four conductors are used in the measuring cable. This facilitates an alternative four-point continuous logging method (Fig. A-3). Cable switch positions C and D establish this connection. D connects the probe resistor (NTC) with reversed polarity compared with C, and it is thus again possible to discover the influence of the thermal EMF, if any.

A 5½ digit universal instrument (type DANA 5333) is used for these registrations. In this conventional four-point technique a known constant current is led to the object in question via two conductors, while the resulting voltage is sensed by the remaining conductors. The instrument displays the value of resistivity.

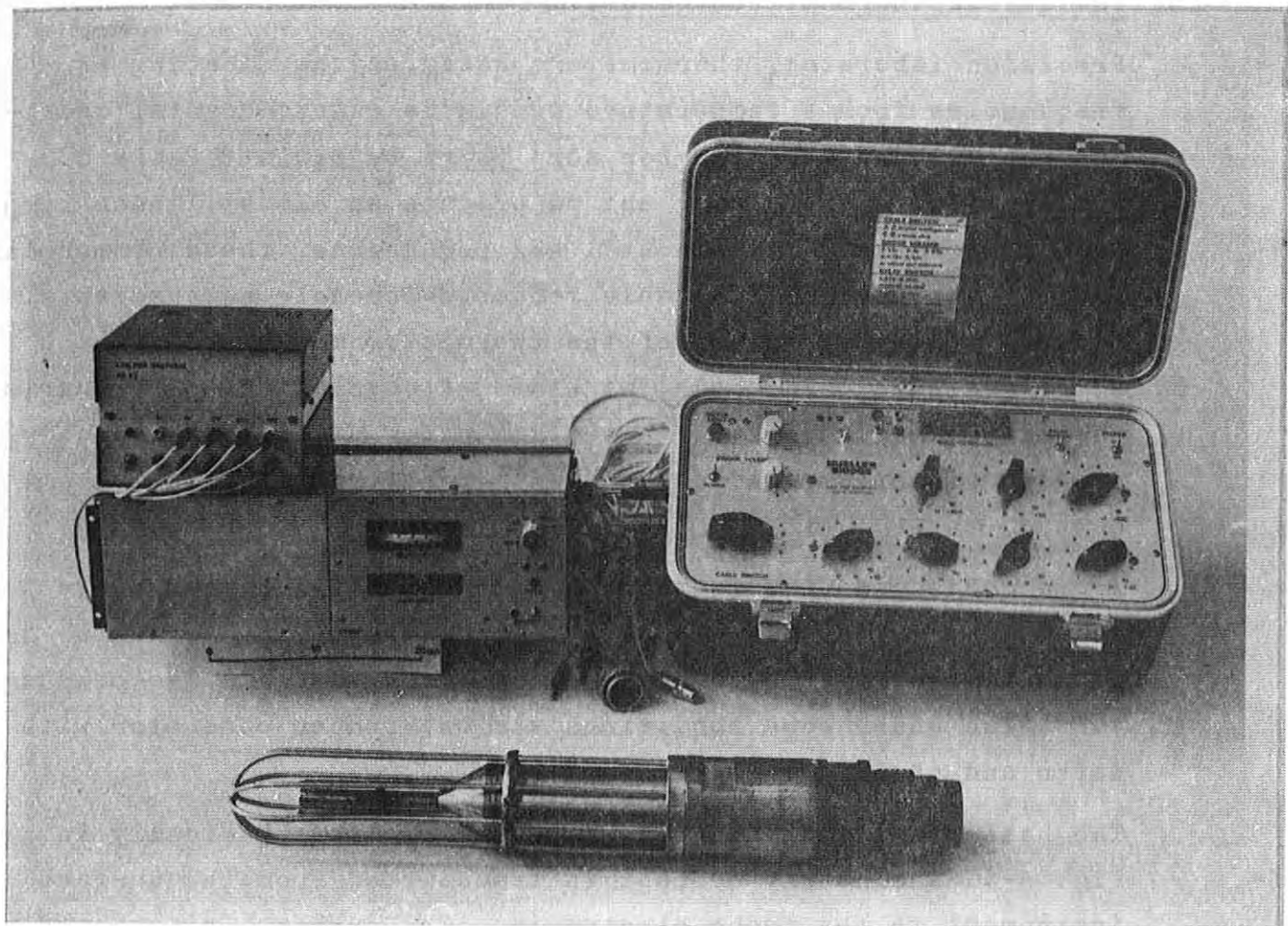


Fig. A-4. The Mueller bridge (back right) and the prototype quartz thermometer with its power supply (back left). The logging probe is shown (front) with the protection hoop covering the sensor tubes.

The immediate weaknesses of this method are that it does not compensate for thermal EMF, that the current contributes some self-heating (which, however, under known measuring conditions may be removed by calibration), and that it may be difficult to predict effects of the induced noise on long measuring cables.

Registered resistivity data with added depth signals are punched in serial BCD form on paper tape ready for computer processing.

### The quartz thermometer (QTM01)

Precision laboratory thermometers based on the counting of frequencies from a temperature sensitive quartz crystal oscillator have been marketed for some years by Hewlett Packard. The crystal is especially cut to produce an almost linear temperature coefficient of about 1 kHz per degree. These commercial thermometers are not suitable for deep borehole measurements. Because of the drawbacks of the thermistor methods, of which some were mentioned above, we aimed at developing a new quartz oscillator to be applied in two conductor cables for the comparison of methods and as a potential alternative logging method.

We succeeded in constructing a prototype based on the above quartz crystal principles. The transmission system simultaneously transfers frequency and supply current via two conductors (and under some conditions via one proper conductor with water and casing forming the other).

The basic function principles are shown diagrammatically in Fig. A-5. A constant current is transmitted from the surface instrument to the probe electronics. The current is taken from a power supply of about 60 V and serial controlled in a loop with a broadband amplifier and a low pass filter (about  $f_0 = 0.15$  Hz).

In the lower part of the probe the supply current is led via a serial transistor to a charge capacitor and then to a traditional voltage regulator, from which all probe electronics are supplied. The quartz crystal is part of the oscillator in the form of a parallel resonance circuit, and the oscillation frequency is based on the basic frequency of the crystal (about 9 MHz). Components were selected and combined to keep the temperature drift of the oscillator at a minimum and to ensure operation up to temperatures of about 115°C.

If the serial transistor of the power part is alternately opened and closed with a frequency proportional to the oscillator frequency, this signal can be detected at a surface. However, the condition is that the transmission frequency is sufficiently low to ensure that the signal amplitude is not damped beyond

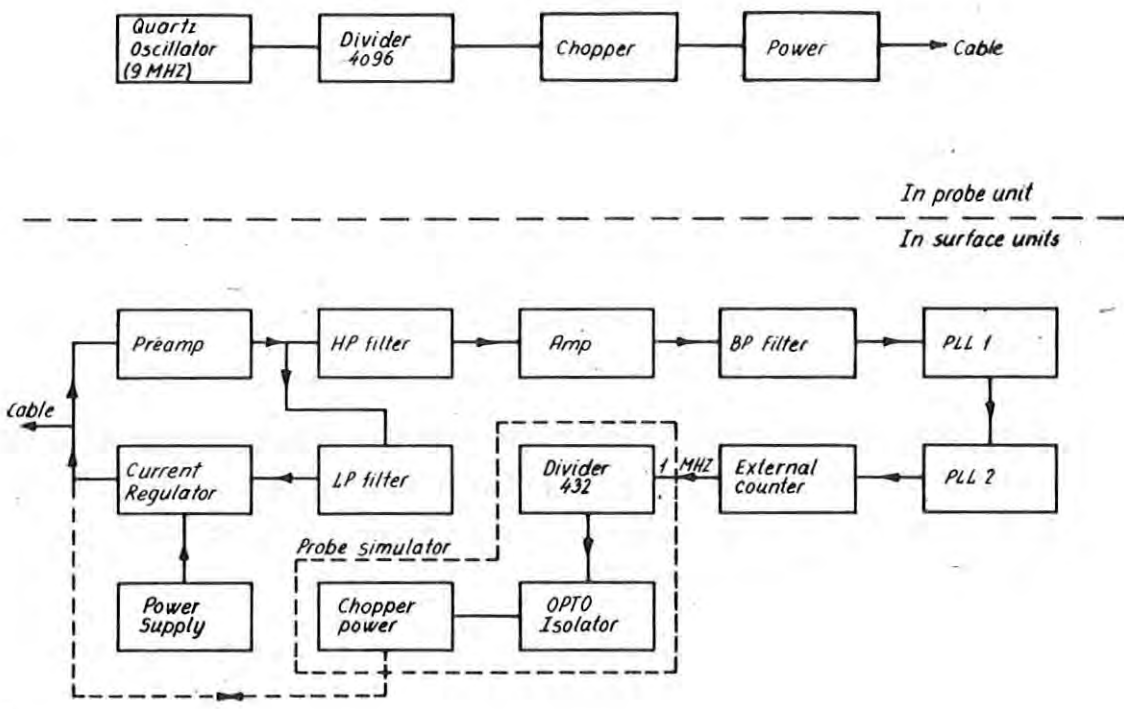


Fig. A-5. Block diagram of basic function principles of the quartz logging thermometer.

acceptance by either the parallel capacity at the two-conductor transmission or by skin effects at one proper conductor transmission. We found 2 kHz to be a good choice. The oscillator signal must then be subdivided about 4000 times. Here a CMOS divider is suitable since the oscillator frequency is chosen as the basic frequency of the crystal instead of the usual third harmonic frequency. Generally, the current consumption of the whole probe is kept below 10 mA, which enables "one-conductor transmission" even under bad resistivity conditions.

The 2 kHz temperature information is accessible on the output of the preamplifier in the current regulation loop because the cutting frequency of the low pass filter is low compared with the transmission frequency. If frequency is to be counted with a resolution corresponding to temperatures of  $10^{-3}$  K, as aimed at, the signal must be carefully filtered and further amplified. The temperature signal is separated in a high pass filter, amplified in "amp", and then passes a bandpass filter with a very narrow band ( $Q \sim 25$ ). For further filtering we apply a

phase lock loop (PLL 1) with a very low cut-off frequency in its low pass filter. PLL 1 could then be apprehended as a "tracking filter".

For practical reasons the signal frequency is multiplied about 12,000 times in a subsequent phase lock loop (PLL 2). This leads the signal back to the frequency of about 28 MHz, and here a temperature resolution of about  $10^{-3}$  K associates about 1 Hz. An external counter (Systron Donner Type 7818) yields 28 MHz in 1 sec with 1 Hz resolution read on a 7-digit display. Increasing temperature produces increasing frequency.

The counter is furnished with a BCD output from which the frequency is recorded, e.g. by the data logger system (section A5). Here the data and time of readings are registered and available for further computer processing.

Both the surface electronic unit and the cable (the transmission system) can be tested by means of a probe simulator to which the counter reference frequency of 1 MHz is connected. The reference frequency is subdivided 432 times yielding about 2 kHz, and it then passes an optic isolator to avoid problems in level differences at the output of the current generator. The insulated reference signal is supplied (as a replacement of the oscillator signal) in a circuit which is quite identical to the power and chopper part of the sensor. The reference power terminal can either be coupled to the cable point (plug) directly or to the probe end of the cable, depending on whether the instrument alone, or the cable and instrument as a whole, are to be tested. The frequency 28,444.444 MHz shown under test conditions is very stable, corresponding to the stability of the test oscillator.

The prototype is illustrated in Fig. A-4.

#### High pressure probe (HPP01)

We have designed a temperature probe satisfying the following conditions: it should fit the standard tool of a professional logging firm (Dresser-Atlas); resist a fluid pressure of at least 400 atm. at some  $120^{\circ}\text{C}$ ; and the thermal time constant for

that part of the probe in which the thermistors and the quartz crystal are located should be minimized.

The basic principles of the probe and its dimensions will appear from Fig. A-6. At its lower part it terminates in 4 thin and 1 thicker pipe (see also Fig. A-4). The 4 thermistors used in the Mueller bridge and the four-point method are placed at the point of the 4 thin tubes, while the quartz thermometer crystal is mounted in the tip of the remainder tube. This enables us to carry out simultaneous measurements with both methods. The dimensions of the internal tubes are chosen in order to obtain good thermal contact between tube and sensors. The thermistors are led down into the probe points by means of 4 thin inlet tubes which fit tightly to the tubes in which the thermistors are placed. These 4 tubes are shortened to a length slightly less than the total length of the probe. Thereby they also serve as a support for the print board on which the entire probe electronics are mounted.

The probe is shielded by a weakly elastic hoop to avoid direct transfer of mechanical stress effects during borehole measurements. The shape of the hoop is considered to allow free flow around the probe points. (Contrary to the normal logging methods, temperatures are measured during lowering).

The integrated temperature logging system was successfully tested (September and December, 1979) and applied for the measurements in the geothermal exploration well Aars 1A (section 2.1) to a maximum depth of 3260 m and a temperature of 105°C.

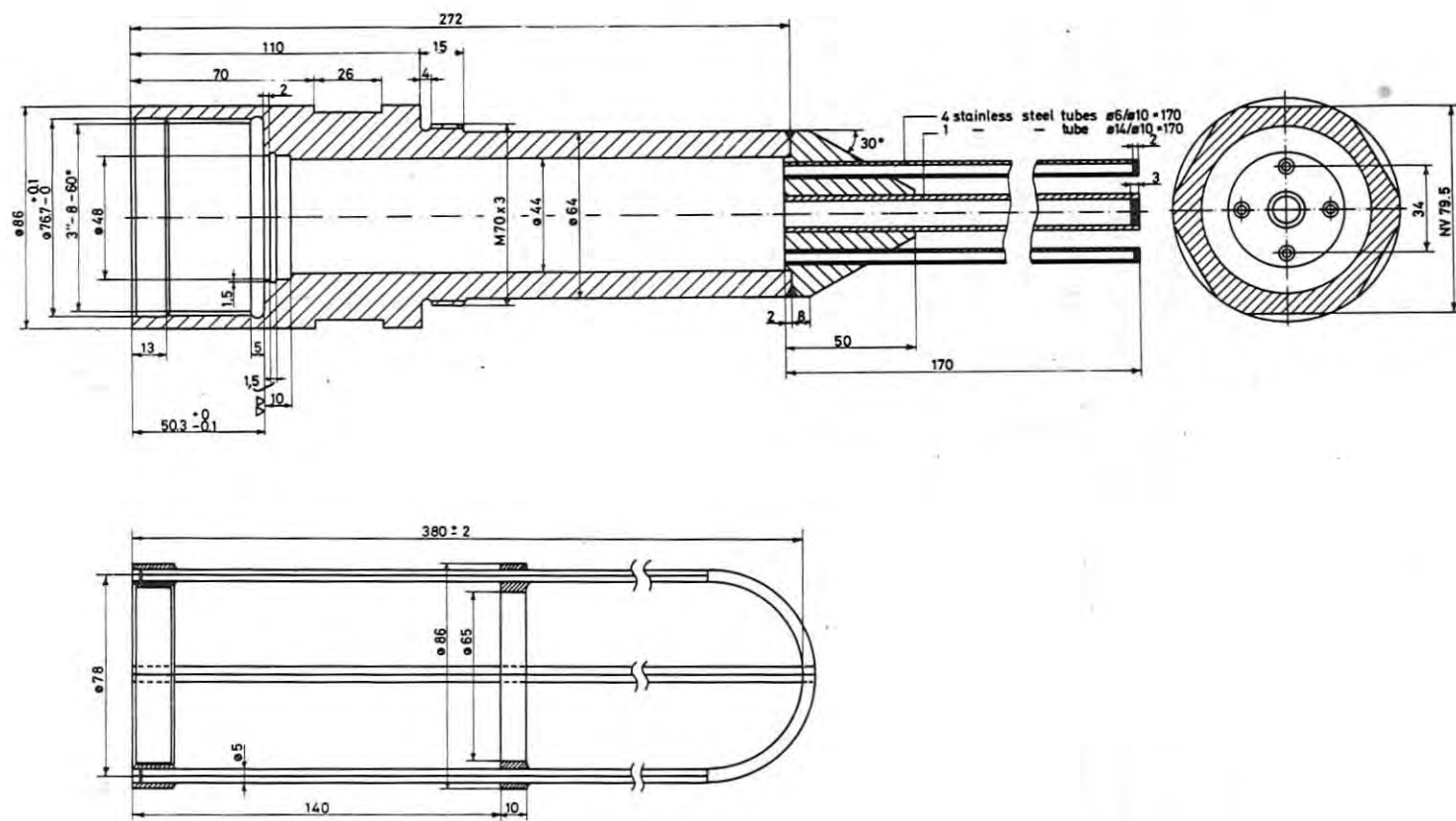


Fig. A-6. Construction principles of the probe unit with protection hoop.

## A2 Divided bar apparatus

The principles of the divided bar apparatus for thermal conductivity measurements are well known and based on the theory of one dimensional steady flow of heat through a rock sample of which the thermal conductivity is to be determined. The apparatus (Figs. A-7 and A-8) is of the comparative type and employs a conductivity standard. It operates with a constant temperature difference across a vertical pile of cylindrical discs (one or two inches in diameter) consisting of the sample with unknown thermal conductivity placed between two standards. Furthermore, two copper discs are situated between the contact surfaces. This pile is sandwiched between an upper electrically heated hot plate and a lower cold plate, the temperature of which is kept constant by circulating water that is thermally controlled by a very stable water bath. A preset stable temperature difference between hot and cold plate is achieved by electronic control of the current supply to the heating element contained in the hot plate. As sketched in Fig. A-7 two platin resistances (Pt100), supplied by a constant current from two temperature stabilized current genera-

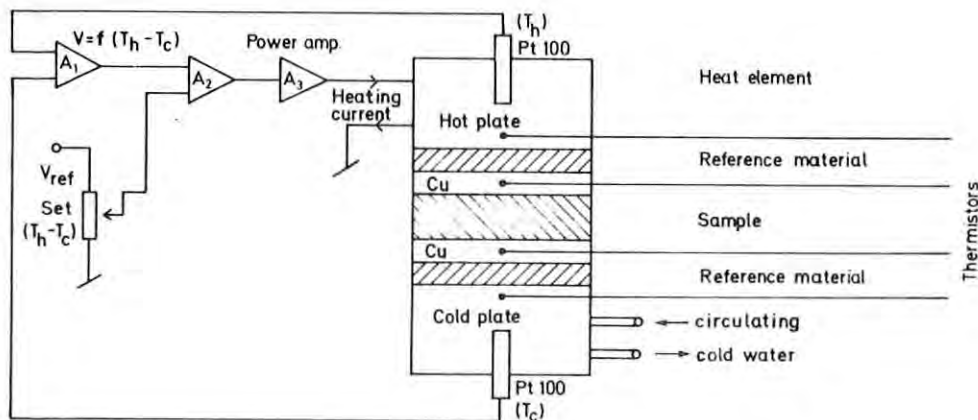


Fig. A-7. Principles of the divided bar thermal conductivity apparatus.

tors placed in an oven, are mounted in the hot and cold plate, respectively. The voltage difference between the two sensors, which is equivalent to the temperature difference, is amplified in the differential amplifier  $A_1$  to a signal level of  $200 \text{ mV}/^\circ\text{C}$  and the output is compared with a preset reference voltage  $V_{\text{ref}}$  in the differential amplifier  $A_2$ . The output of this controls the power amplifier  $A_3$  in a feed-back system, which seems to minimize the time necessary to obtain thermal steady state in the system.

To minimize contact resistance across the discs, and to investigate pressure dependence on thermal conductivity, a uniaxial pressure is suppressed on the pile by a hydraulic system. In order to minimize heat losses, which are controlled by using two references, all surfaces are insulated with polystyrene and the entire system is shielded to prevent air convection.

When the system is in a steady state condition, the temperature differences across the standards and the sample are measured with four thermistor systems with a resolution of  $0.003^\circ\text{C}$ . Knowing the lengths of the discs, the unknown thermal conductivity is calculated relative to the standard value. If contact resistances cannot be neglected, measurements over samples of different lengths are necessary.

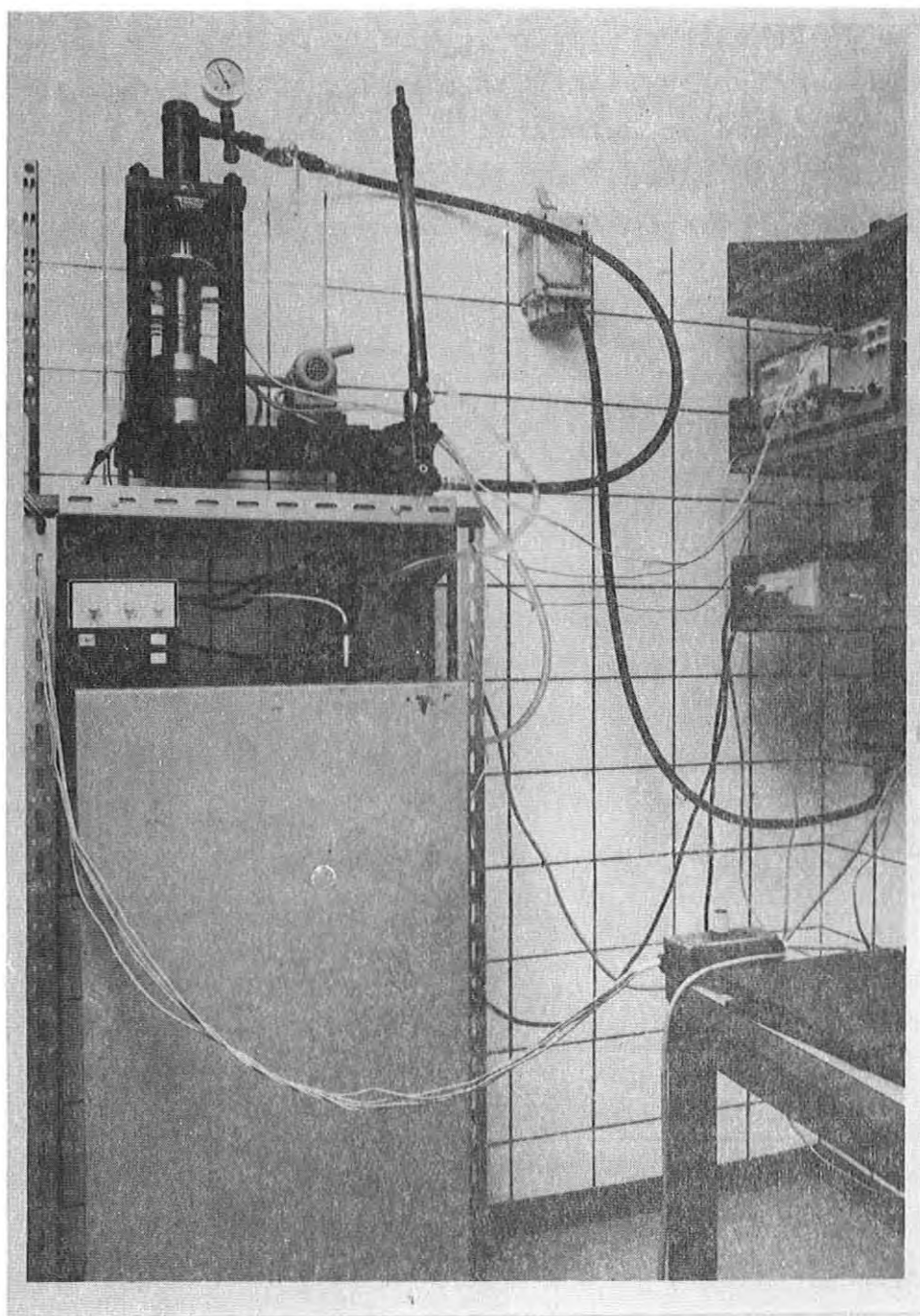


Fig. A-8. The divided bar apparatus with open bar.

### A3 Needle probe instruments

Two needle probe thermal conductivity instruments (NTC) were built, one rather simple system to be used as a handy field and laboratory system with manual readings of temperature rise (NTC-01), and an automatic system developed mainly for rapid and accurate laboratory measurements of large sample numbers (NTC-02). The apparatuses are shown in Figs. A-9, A-10, and A-11.

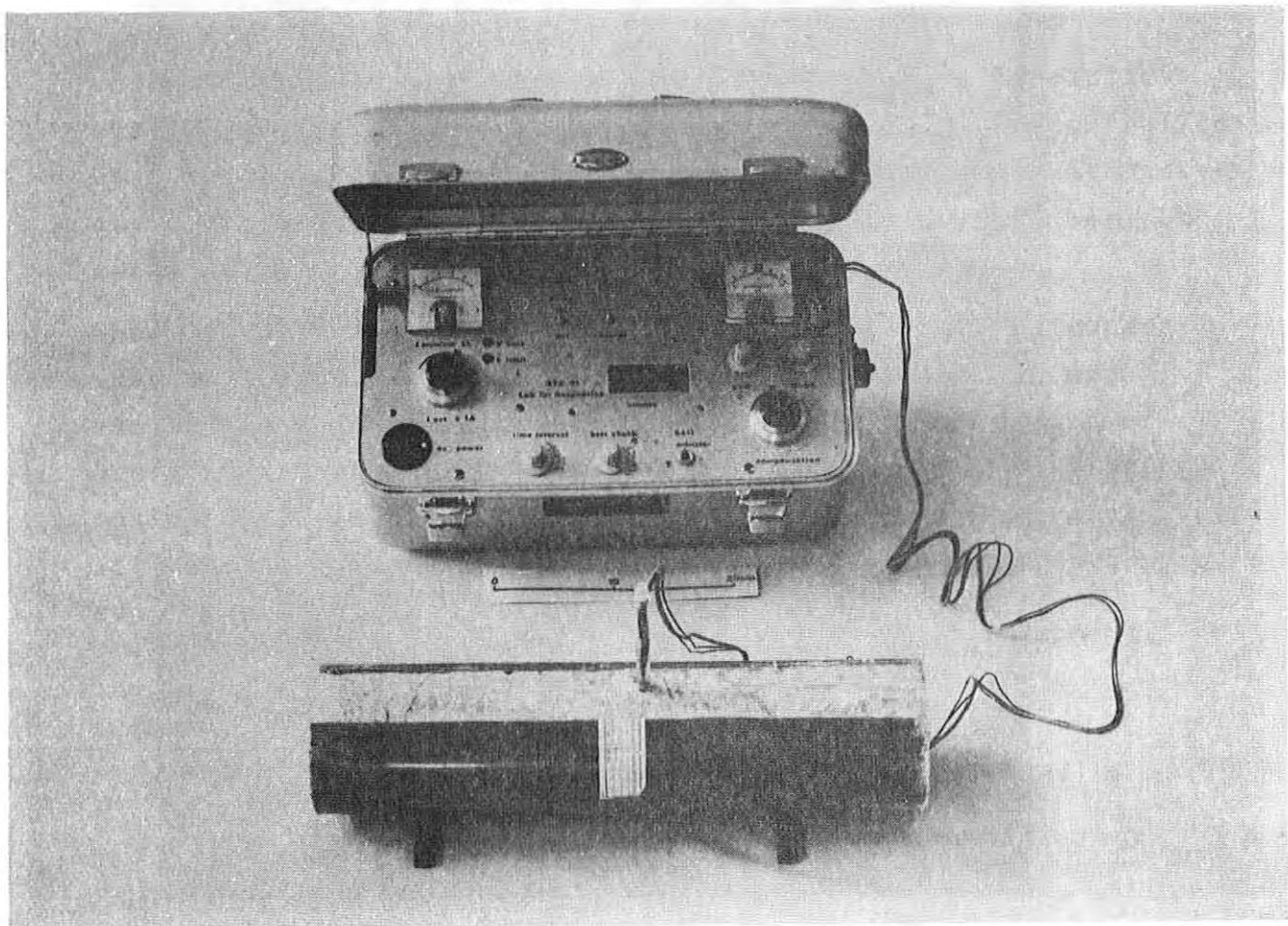


Fig. A-9. The NTC-01 equipment.

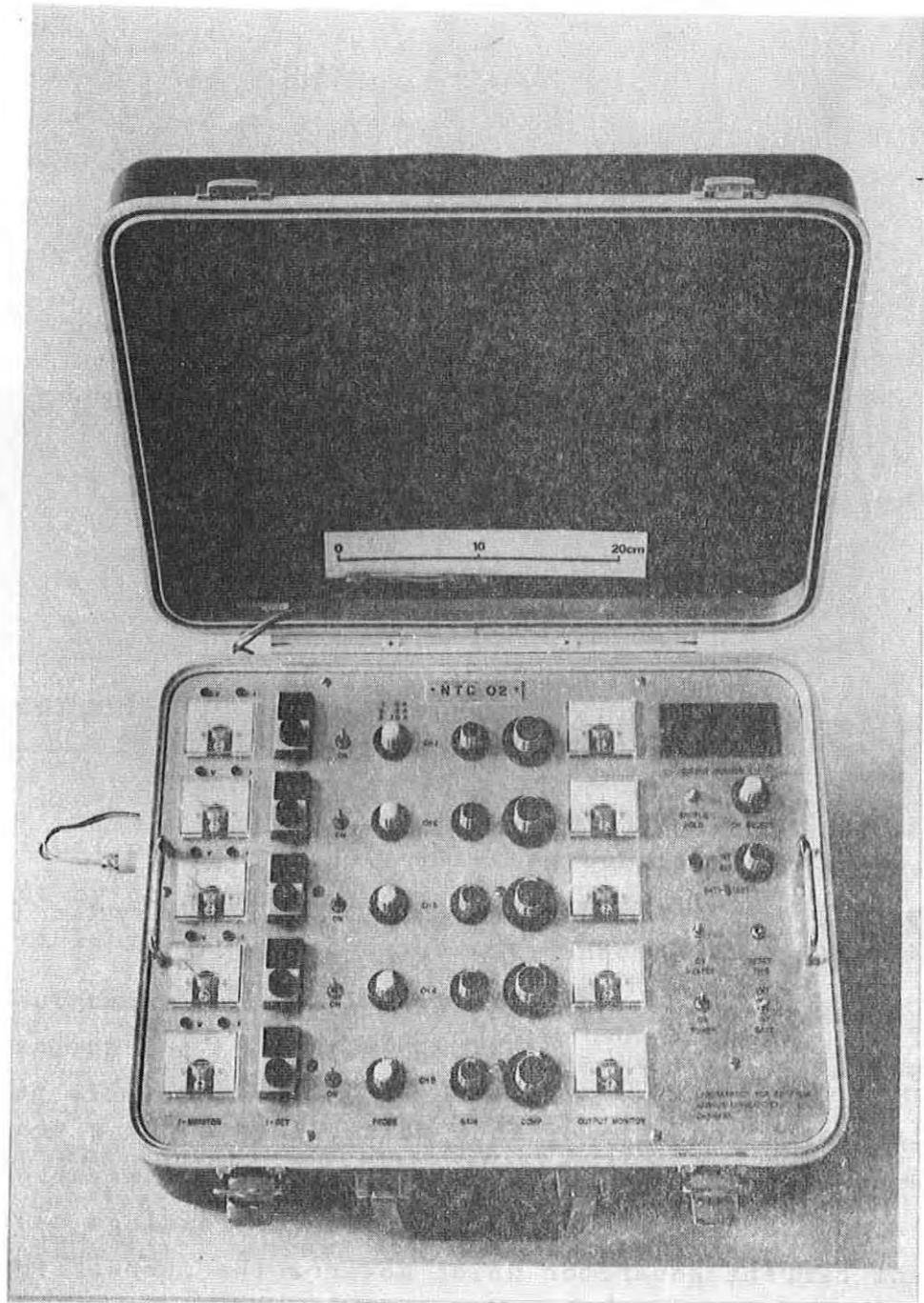


Fig. A-10. The NTC-02 equipment.

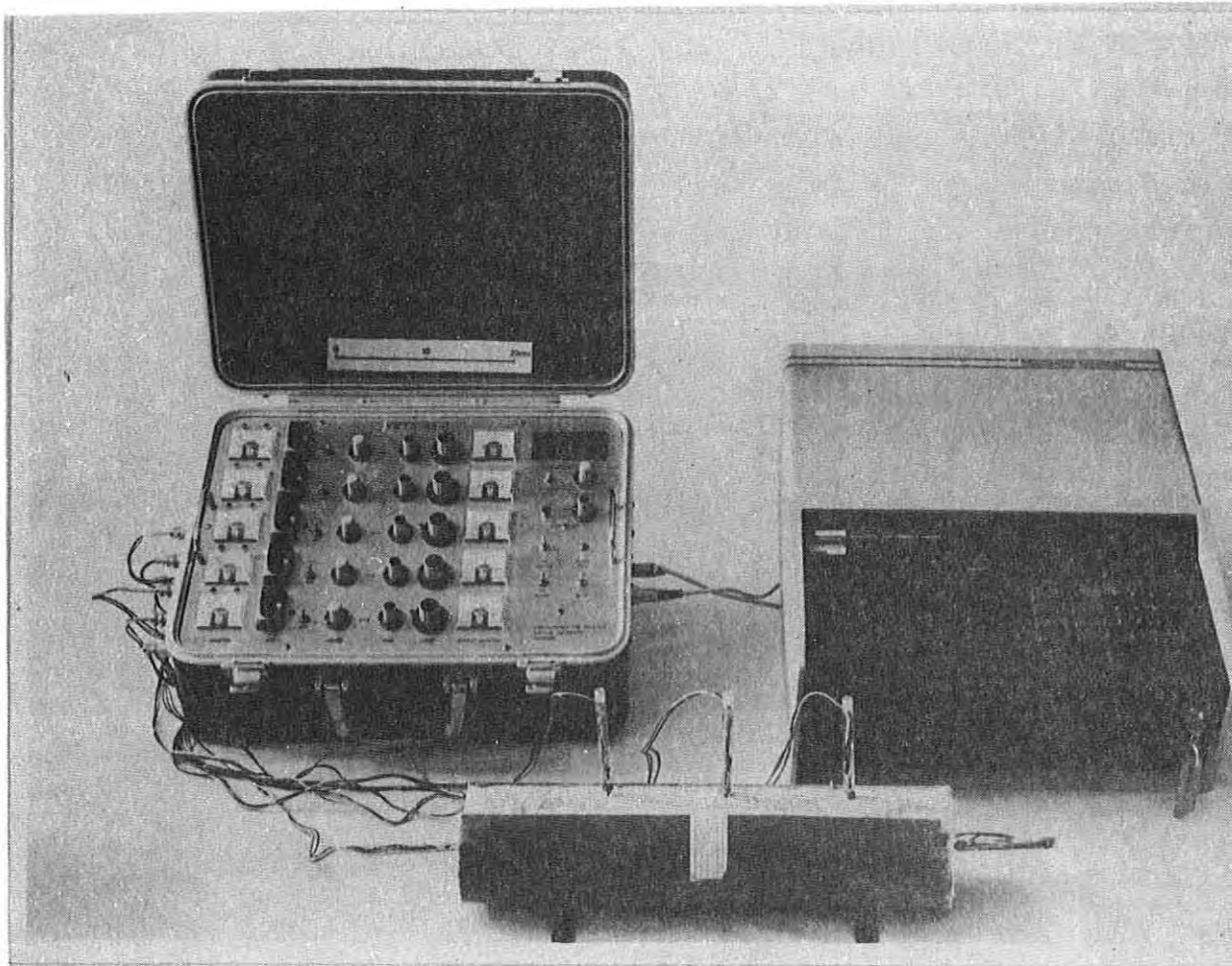


Fig. A-11. The NTC-02 equipment and the data logger system. Five probes are connected.

#### NTC-01

This system consists of four main elements 1) a traditional thermometer 2) a timer marking the times of measurements 3) a counter which counts the number of readings 4) a constant current generator which governs the current for the heating element.

The thermometer principle is based on the traditional Wheatstone bridge. One half is placed in the probe and consists of a precision thermistor and a fixed high-stable resistor. The other half is placed in the instrument and consists of a 10-turn potentiometer and a number of fixed resistors which can be connected by a switch. It is thus possible to obtain several measuring ranges from  $0^{\circ}\text{C}$  to about  $40^{\circ}\text{C}$  with about  $\pm 10^{-3}$  K resolu-

tion. The balance point is found by means of an amplifier with a variable gain and a 0-detector.

A clock is installed to mark prescribed thermometer reading times. At 5 sec. periods it gives sound and light indications in the 0-detector of the thermometer. The distance between the end of the periods (trailing edge) may be varied in steps of 10, 20, 40, 60, 120, 240, and 480 secs. The stability of the clock is better than 1 o/oo.

The number of marking impulses is counted on a 2-digit display and controls the number of measuring values registered.

The heating element in the needle probe has been made of manganin wire with a very low temperature coefficient (<50 ppm/K). By leading a constant current through the heating element, a constant effect in the heating element is achieved in cases of small temperature variations. The instrument has a built-in constant current generator which may be varied from 0 to 1 A on a 10 turn potentiometer. The stability and accuracy are better than 10 o/oo. The current generator is furnished with a "fold back" current limit which is coded in the plugs for the individual probes, thereby avoiding burning off the heating element by accident. Two indicators show limits in current or voltage if the prescribed current cannot be obtained.

The instrument has an internal current supply of the electronics and option of either internal or external supply of the heating element of the probe.

The current control and time-counter systems are schematically shown in Figs. A-12 and A-13.

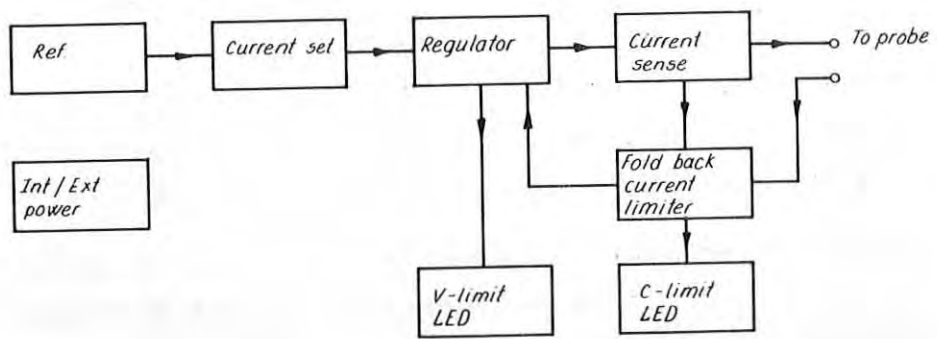


Fig. A-12. Block diagram of the NTC-01 current control system

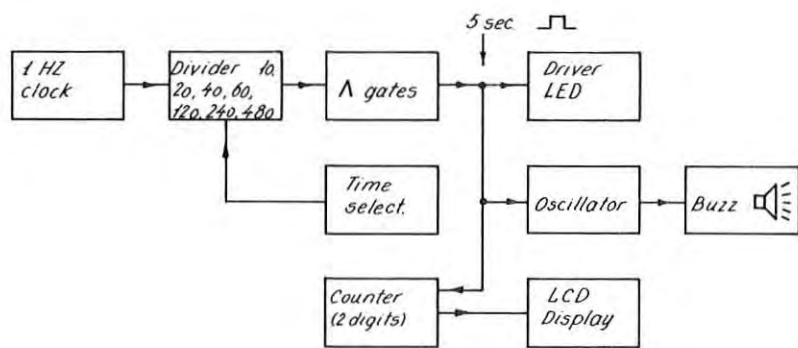


Fig. A-13. Block diagram of the NTC-01 timer-counter function.

NTC-02

This is an automatic equipment where data are collected by a data logger (section A5) and transferred to cassette or paper tape for automatic processing. The system as described here is able to measure up to five probes simultaneously (Fig. A-11).

The instrument shown diagrammatically in Fig. A-14 contains two main elements. One controls the power in the heating wire and the other performs the necessary temperature measurements. Fig. A-15 shows how the temperature is determined by letting the thermistor be part of a Wheatstone bridge which is compensated in steps. The voltage registered on the bridge output terminals when the thermistor is heated is amplified in the bridge amplifier and frozen in a sample and hold circuit (S/H) with equidistant measuring intervals. The frozen analogue value of the S/H circuit is digitized in the data logger and recorded on a cassette or paper tape. The bridge amplifier is constructed to obtain a low bias current, low temperature drift, and a temperature resolution of  $10^{-3}$  K.

To suppress outer noise components of higher frequencies a second order low pass filter with a cutting frequency of about 5 Hz is introduced. The influence of drift in the bridge supply voltage is prevented by supplying each of the five channels from a low drift amplifier. These bridge supply amplifiers have a reference in a mutual ultra-stable voltage source. The equidistant sampling signal to the S/H circuit is controlled by the data logger. When measurements start, a prescribed number of readings are made to determine the stability of the initial temperature. The counting takes place in a 4-bit counter which switches on the current for the heating wires when the required number of samples (readings) are obtained.

As the heating wire is of manganin, which has a small temperature coefficient, the power control is reduced to a current control (Fig. A-16). The actual current in the heating wire is registered as a fall in voltage over a  $1 \Omega$  precision resistor and compared with a variable reference voltage taken from the potentiometer "I set". The difference signal from this

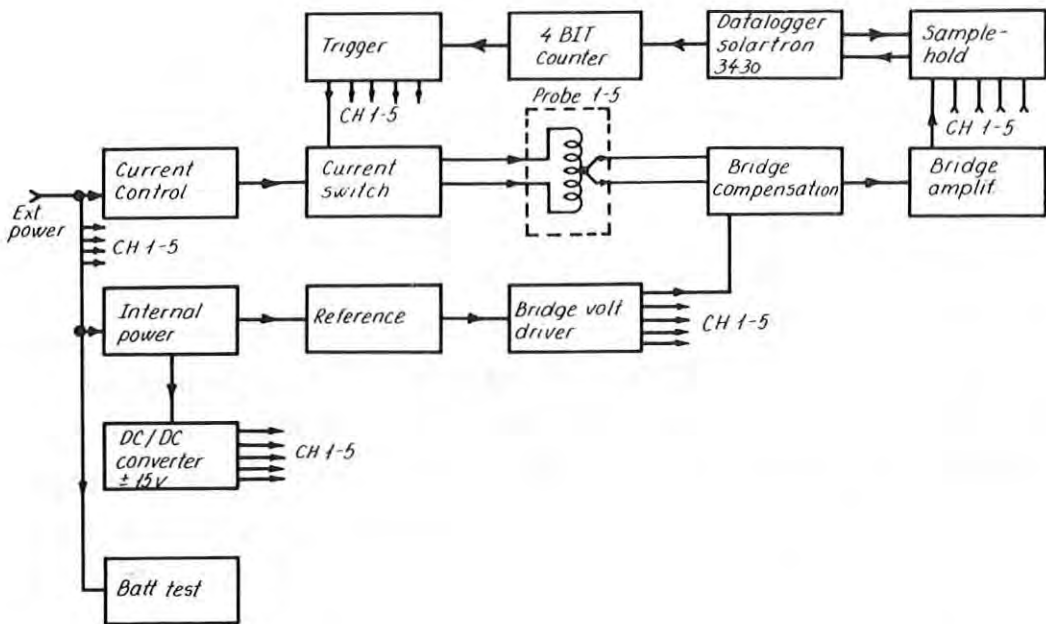


Fig. A-14. Block diagram of basic principles of the NTC-02 equipment.

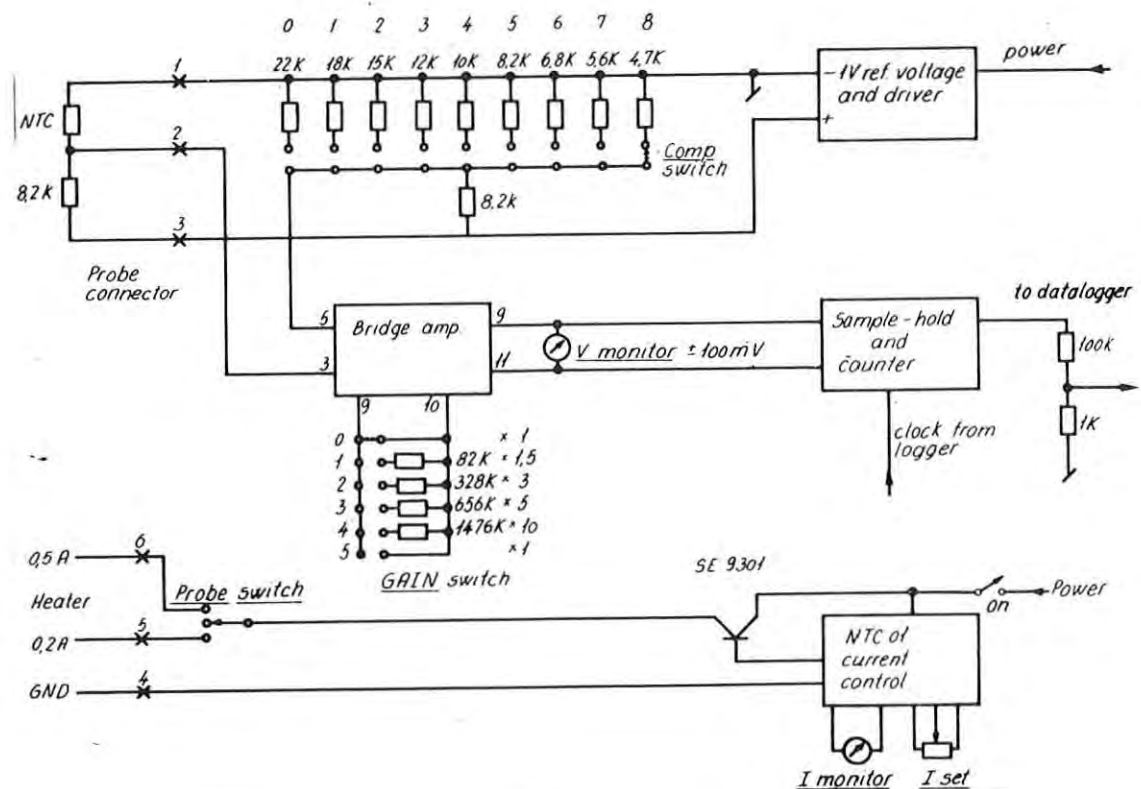


Fig. A-15. Construction and function principles of the NTC-02 system.

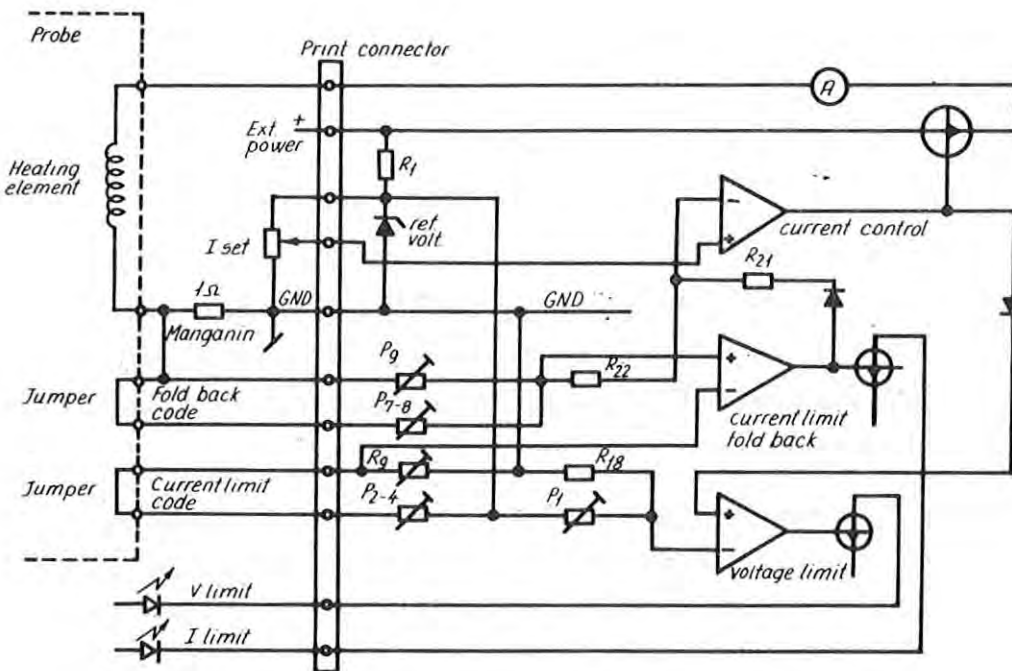


Fig. A-16. Construction and function principles of the NTC-02 current control system.

is used in the usual way to control the current in a series control. The current is chosen on the potentiometer "I set", which has a high resolution and reproduction can be obtained better than 1% of full scale. The aim is to obtain maximum current stability during temperature variations as well as battery variations.

Overloading of the heating element in probes is prevented by putting a code in the probe plug. The current generator then assesses the maximum current that may enter the individual probe types. If the maximum limit is exceeded, the current is forced back to 0 and an error indication is given. Furthermore, error is indicated if a current is emitted to a heating wire with a too low battery voltage. The instrument is power supplied by internal or external batteries, and in the latter case the internal ones are charged simultaneously.

#### A4 Construction principles of needle probes

Since the construction of needle probes suitable for accurate and stable readings is not a simple process, we describe below a needle and details of construction which, from our experience, satisfy the requirements of heat flow studies.

As is well known, the needle probe basically consists of a metal tube heated by a heating wire, and with a thermistor placed in the middle of the tube. For interpretation reasons needle length and diameter is maximized and minimized within practical limits. This facilitates accurate thermal conductivity measurements.

To obtain homogeneous heating of the metal tube it is necessary to provide good thermal contact between the wire and the metal tube along the full length of the probe. Usable thermistors available on the market are all furnished with non-insulated wires. It is therefore most appropriate to use an insulation tube inside the outer metal tube which has a diameter which just leaves space for an insulated wire. At the same time it must be possible to lead the thermistor wires, mutually insulated, through the insulation tube.

##### Insulation tube

A suitable insulation tube is the Degussit AL 23 (ceramics) with an outer diameter  $D_o = 0.9 \text{ mm}^\varnothing$ , and with two holes along its length with diameters  $D_h = 0.2 \text{ mm}^\varnothing$ . These tubes are available in lengths of 400 mm.

##### Heating

For practical reasons the heating power is controlled by controlling the current, assuming the resistance to be constant. This only necessitates a two-wire connection of the heating wire. The insulation consists of a thin silk cover which meets the temperature requirements.

##### Outer metal tube

With a heating wire of diameter  $0.05 \text{ mm}^\varnothing$  and a Degussit insulation tube of  $D_o = 0.9 \text{ mm}^\varnothing$  it is possible to obtain good

thermal contact between wire and a standard hypodermic needle with inner and outer diameters of 1.4 and 1.5 mm, respectively. This allows sufficient space for the components of the probe to be assembled without damaging the silk insulation. These needles consist of surface-coated brass tubes available in lengths of 1 m.

#### Thermistors

Considering the limited space, the diameter of the thermistor should be the same as that of the outer diameter of the insulation tube. Furthermore, the inlet wires should be long enough to connect the thermistor wires outside the hypodermic needle.

"Fenwall standard small bead thermistors" with  $R(25^{\circ}\text{C}) = 8,000 \Omega$  meet these special requirements. The unusual length of the inlet wires can be produced if the manufacturer is willing to lengthen them by welding an extra piece as specified by the customer. When placing the order it is advisable to stress that the welding is to be done with the wires overlapping, and not crossing, each other. Crossing wires give a shorter welding point with subsequent inferior mechanical strength, and even with short, projecting end pieces from the welding it may be difficult to lead the connection up through the insulation tube. The thermistor, Type GB38J1P3, is furnished with non-insulated  $0.025 \text{ mm}^{\phi}$  wires made of an alloy of platinum and iridium, and has a max. diameter of  $0.36 \text{ mm}^{\phi}$ , considerably less than the diameter of the insulation tube.

#### Manufacture

The hypodermic needle is shortened to the desired length (~90 mm) plus about 2-5 mm for the connection of a brass head (Fig. A-17). The hypodermic needle and the brass head are silver-soldered to ensure waterproofing and sturdiness (Fig. A-18).

A hollow acrylic (plexiglass) tube is shortened to form a suitable handle (about 100 mm long) and furnished with a 5 mm side hole for the outlet of wires, about 7-10 mm from the top end of the pipe (Fig. A-17). In order to reduce stress on the cable, an internal thread is made in the plexiglass tube adjacent to the cable outlet, and a standard plastic screw supports

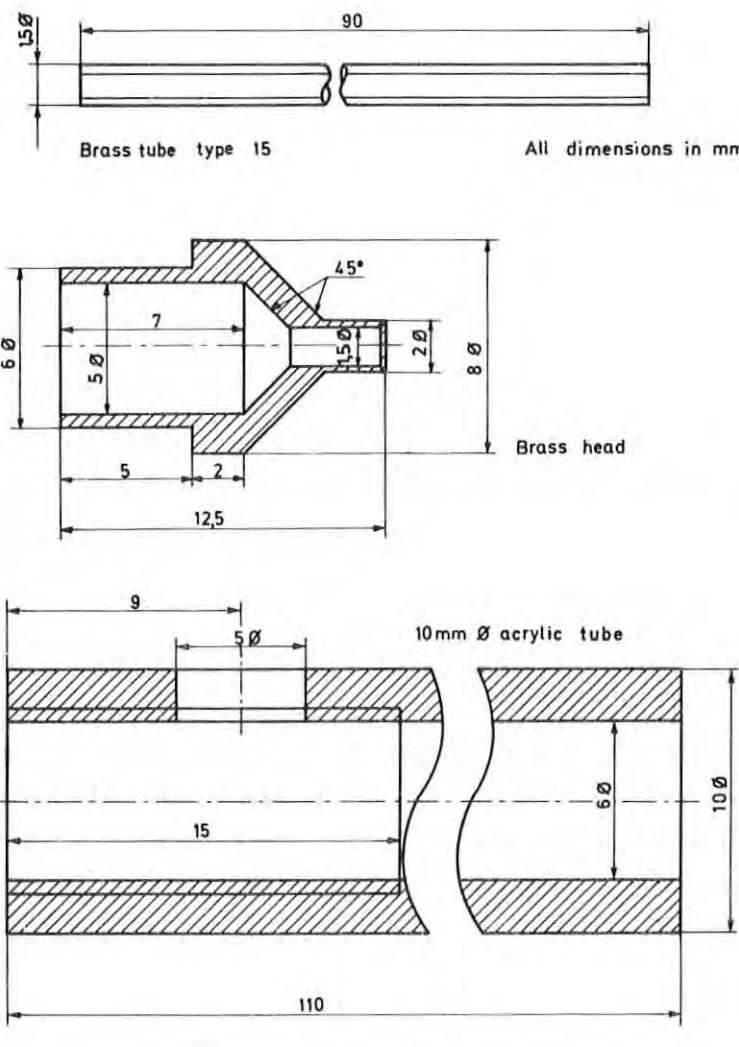


Fig. A-17. Details and dimensions of the needle probe.

the cable. A piece of Degussit insulation tube is cut to half the probe length minus 3 mm and used to establish a uniform thermal contact between the heating wire and the outer tube in its lowest part, and furthermore to secure symmetry. A similar length + about 10 mm is cut for the upper half of the probe in which the thermistor connection wires are located. As it is difficult to insulate the soldering between the thermistor and the cable separately, half the insulation tube is cut away from the side about 5-6 mm from one end. This terminates one of the holes of the insulation tube sufficiently far away from the other, and the two connection wires are soldered without danger of short circuiting.

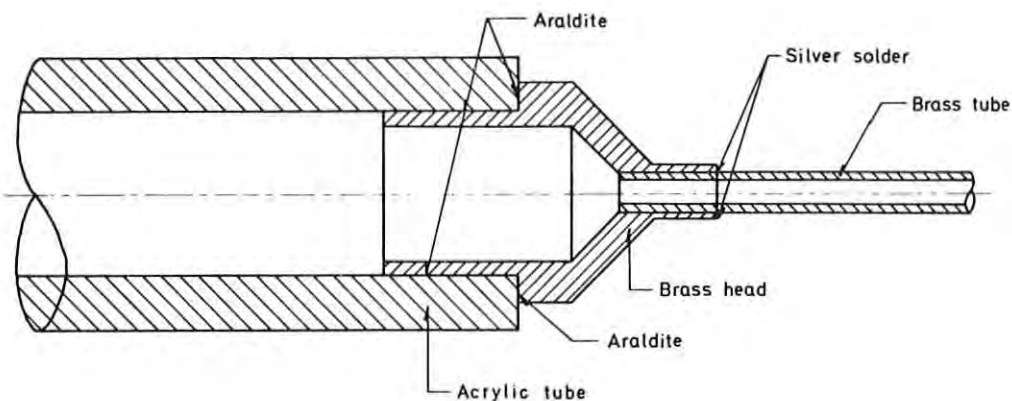


Fig. A-18. Details of the brass tube and acrylic tube assembly.

A binocular microscope with sufficient magnification is used to lead the two uninsulated thermistor wires through the insulation tube. The thermistor is first glued to the end surface of the insulation tube with silicone glue, then with araldite. (Glue must not be allowed to exceed the outer diameter of the tube). During hardening the glue may penetrate parts of the holes and pore space of the ceramics, which demands another layer. The glue serves as protection in the assembling phase. A thin  $\sim(<0.15 \text{ mm}^2)$  double shielded cable is cut and deinsulated to ensure free and displaced ends in accordance with the outlet of the wire ends from the insulation tube (Fig. A-19). The free wire ends of the thermistor are wound round the respective deinsulated cable ends and tightened, allowing for temperature expansion and small displacements. Tin solder is placed very carefully on each connection, and it is constantly controlled (with an ohmmeter) that stable electrical connections to the thermistor exist.

A  $2 \text{ mm}^\phi$  crimpflex is cut to fit the length between the end of the outer insulation of the screen cable and up to 1 mm past the cutting of the insulation tube. The flex is shrunk and both ends are smeared with glue (normal araldite).

The next step is to cut the heating wire to double the length of the probe minus 2 mm to give room for glueing of the probe tip,

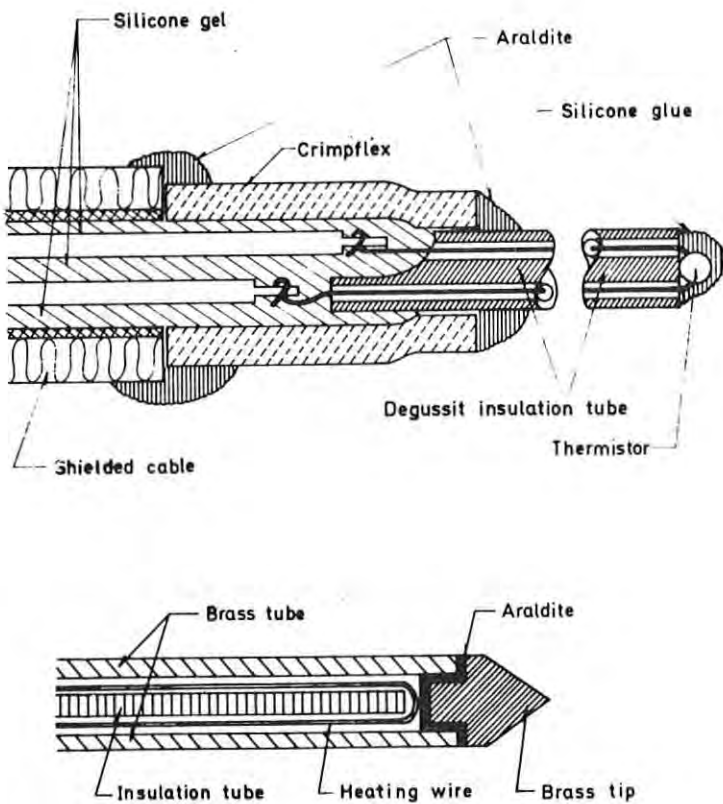


Fig. A-19. Details of the thermistor assembly and the probe point.

and plus 5-6 mm for soldering of connection wires. To avoid soldering directly between a heavy wire and the thin heating wire, a soft connecting wire, about 30 mm long (e.g. "hearing aid wires") is soldered. The insulation of the wires are prolonged beyond the soldering point. Finally, two  $0.15 \text{ mm}^2$  wires are soldered and shortened to fit the length of the screen cable. The two soldering points are insulated and kept together with crimpflex. The heating wire resistance can either be measured from the "free ends" or from the inlet wires, the resistance of the latter being taken into consideration.

A thin wire (e.g. of the heating wire type) is passed through the existing heating wire loop and further through the brass head and hypodermic needle. Hereby the heating wire can be stretched. First the insulation tube for the lower part of the probe is kept between the two heating wire branches, and the hypodermic needle is pulled on the lower insides with small forward and backward movements. The insulation tube is then placed in position. The insulation tube with the thermistor is

led in, pushing the first insulation tube with the end surface on which the thermistor has been glued. The quality of the glueing is decisive for the protection of the thermistor. The emplacement is made in steps until the entire insides are correctly positioned in the needle. The acrylic handle is cleaned in alcohol and pulled on the wires, and finally glued to the cleaned brass head. The glueing must fill the entire space between the two parts to prevent water penetration.

A brass tip with a 1 mm long dowel and with the external diameter fitting the needle (see Fig. A-19) is glued with araldite. After the glue has hardened (about 12 hours) the acrylic handle is filled with silicone gel (type RS 3025 GEL). The relief screw is mounted and the external wires are laid parallel and held together every 10 cm by crimpflex. When used with NTC-01 the external thermistor wires are connected to the thermometer via a 6-pole Lemo plug (size 2 type F) as shown in Fig. A-20. An 8.2 K $\Omega$  metal film resistance is placed between pins 2 and 3, and combined with the thermistor it constitutes half the Wheatstone bridge of the thermometer. Fig. A-20 shows the connection to heating wires, with different power ratings.

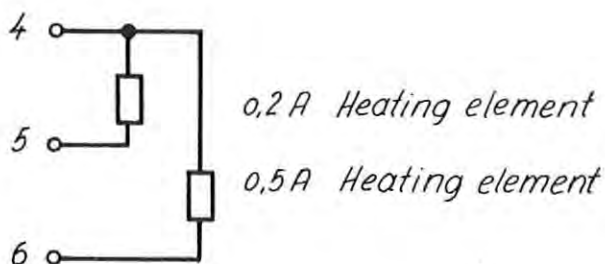
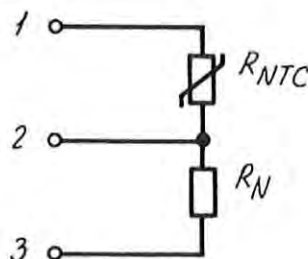
Lemo

Fig. A-20. Pin connection to the needle probe.

### A5 Data acquisition system

Since the market already provided data logger systems which could be modified to comply with our demands for a general acquisition of data produced by both the temperature logging equipment and the thermal conductivity apparatus, we did not construct these systems in our laboratory.

The system used is the Solartron Compact Logger 3430 (from Schlumberger Farnborough, England) which is described in the Instrument Technical Manual. This logger measures resolution to four significant digits and signs. The data logger scans from 1 to 30 analogue channels with a resolution of  $\pm 29999$  and transfers the data in ASCII code to cassette or paper tape. Each scan is initiated by registering time from a built-in clock, and the subsequent data are channel numbered. The system is suitable for field work and operates on either batteries or the main electricity supply.

Minimum scan-interval was changed from the original 60 seconds to 1 second. Transfer to magnetic or paper tape requires a minimum scan-interval of 3 seconds when reading from 1 channel, and 5 seconds for 5 channels. In addition, the signal which activates a new scan is made accessible for the trigger circuit in NTC-02 via an optic insulation, and a 7 sec. delay at the start of each new scan is put out of function.

The instrument is illustrated in Fig. A-11.

APPENDIX B

Bottom Hole Temperatures

Bottom Hole Temperatures

Temperatures reported from Danish boreholes drilled on land before 1977 and to depths greater than 500 m (locations are shown in Fig. 2).

$T_1$ : uncorrected temperatures reported;  $T_2$ : estimated equilibrium temperatures obtained after corrections by the procedure of Lachenbruch and Brewer (1959) or by empirical curves.

Serial No.	Name	Depth (m)	Time Since Circulation (h)	$T_1$ ( $^{\circ}$ C)	$T_2$ ( $^{\circ}$ C)
1	Grøndals Eng	100	> 42	10.5	10.5
		301	> 136	14.8	14.8
		250	> 158	13.8	13.8
		351	> 110	15.8	15.8
		150	> 86	11.3	11.3
		200	> 86	12.8	12.8
		400	> 66	17.0	17.0
		450	> 147	18.2	18.2
		505	> 71	19.2	19.2
		550	> 98	20.0	20.0
		599	> 68	21.1	21.1
		650	> 40	22.1	22.1
		700	> 41	23.5	23.5
		750	> 21	24.2	24.2
		800	> 20	25.5	25.5
		850	> 42	26.8	26.8
		861	> 23	27.0	27.0
2	Gassum 1	3027		116	
3	Haldager 1	1517	6	71 ?	78 ?
4	Risby 2	507		10	
5	Batum 1A	762		26	
6	Ringe 1	904		55 (?)	
	-	1435		41	
7	Ullerslev 1	1057	12	34	36
8	Tønder 1	1037		33	
	-	1517		44	
	-	2078		50	
	-	3084	168 ?	71	
9	Tostrup 1	759		23	
10	Glamsbjerg 1	905		28	
11	Børglum 1	1516		37	

12	Mønsted 1	762		27	
13	Uglev 1	945		38	
	-	1239		54	
14	Rødby 1	1530		41	
15	Batum 13	557	4	21	26
16	Frederikshavn 2	1026		32	
17	Frederikshavn 3	1003		32	
18	Tønder 2	1832		49	
	-	2356		60	
	-	2383	24 ?	62	63 ?
	-	2968	18 ?	82	84 ?
	-	3196	15	93	95
19	Arnum 1	1511		38	
	-	1829		54	
20	Aabenraa	971		38	
	-	1853		54	
	-	2343		66	
21	Rødby 2	1658	11.5	58	62
	-	1658	34.5	57	
	-	2720	34	74	75
22	Fjerritslev 1	907		30	
23	Fjerritslev 2	2059		55	
24	Vedsted 1	1641		46	
	-	2065		53	
25	Flyvbjerg 1	1695		40	
26	Horsens 1	1726		44	
27	Hønning 1	1922		44	
	-	2485		54	
28	Grindsted 1	1647		67	
29	Rødekro 1	1645		39	
30	Lavø 1	2438		51	
31	Slagelse 1	2972		87	
32	Suldrup 4A	1144		32	
33	Hvornum 2	1550		50	
34	Hvornum 1	1500		44	
35	Rønde 1	4057	5.5	96	102
	-	4055	11	97	102
	-	4057	16	100	102
	-	4057	5.5	96	102

35	Rønde 1	4032	16.5	98	102
	-	4056	2.5	98	102
	-	4875	6	112	
	-	4891	9	112	
	-	4893	12.5	112	?
	-	4875	17	112	
	-	5030	7	124	
	-	5029	10	124	
	-	5031	15	124	
	-	5031	?	124	?
	-	5031	> 19	124	
	-	5031	> 19	124	
	-	4899	> 19	124	
	-	5293	8	135	140
	-	5291	10.5	137	140
	-	5293	15	137	140
	-	5293	17.5	138	140
	-	5293	25.5	138	140
	-	5293	29	138	140
36	Nøvling 1	3526	8	83	96
	-	3527	11	85	96
	-	3528	22	88	96
	-	3526	32	91	96
	-	3527	37	93	96
	-	3753	8.5	94	96
	-	3751	11.5	94	96
	-	3754	13.5	94	96
	-	3752	20	95	96
37	Mors 1	2046		49	
	-	2047	8.5	48	52
	-	2047	12.5	49	52
	-	4575	5	99	108
	-	4577	13.5	103	108
	-	4576	18.5	105	108
	-	4981	96	129	129
	-	5214	4.5	129	140
	-	5213	> 4.5	132	140
	-	5216	> 10	133	140
38	Thisted 1	936	5	38	40

38	Thisted 1	937	8.5	38	40
	-	937	13.5	39	40
	-	746		38	
	-	605		26	
39	Ørslev 1	1822	6.5	56	60
	-	1820	8.5	57	60
	-	1823	14.5	58	60
	-	1822	29.5	59	60
	-	1823	25	59	60
	-	2353	4	58	72
	-	2354	8	61	72
	-	2356	10	63	72
	-	2356	13 ?	65	72 ?
	-	2354	17 ?	66	72 ?
	-	2566	3	72	78
	-	2567	7	74	78
40	Hvornum 4	1620	11	46	49
	-	1606	16	47	49
41	Vejrum 7	238		30	
	-	999	6	37	39
	-	999	12	36	39
42	Vejrum 9	999		37	39
	-	996		38	39
	-	999		39	39
43	Vejrum 8	1000	12	37	39
44	Voldum 1	1273	4	46	50
	-	1272	6	47	50
	-	1274	8	46	50
	-	1969	3	58	63
	-	2085	3	56	65
	-	2085	5	56	65
	-	2084	9	61	65
	-	2235	6	64	69
	-	2235	9	64	69
45	Hobro 1	1513	4	50	
	-	1514	6	50	
	-	1515	> 6	50	
	-	2437	4	62 }?	
	-	2438	8	62 }	

45	Hobro 1	2590	4	65	?
	-	2589	8	65	
46	Hyllebjerg	1059	5	32	38
	-	1055	7.5	32	38
	-	2875	7	67	95
	-	2872	11	77	95
	-	2875	19	80	95
	-	2873	25	88	95
47	Rødding 1	1061	4	32	38
	-	1059	6.5	34	38
	-	2186	6	60	69
	-	2183	10.5	60	69
	-	2188	27	66	69
48	Kvols 1	1051	4	38	44
	-	1048	7	40	44
	-	2533	6	71	79
	-	2635	5.5	71	79
	-	2632	8.5	71	79
	-	2635	22	78	79
	-	2635	?	78	79
	-	2425	6	60	
	-	2426	9	60	
49	Skive 1	1059	3	38	43
	-	1054	6	40	43
	-	2297	4.5	63	74
	-	2303	8.5	64	74
	-	2305	20	67	74
	-	2306	30	73	74
50	Oddesund 1	621	1.5	37	46
	-	618	3	40	46
	-	2178	3.5	60	
	-	2175	9.5	60	?
	-	2178	16	60	
	-	2178	24	60	
	-	2429	5	67	
	-	2423	6	67	?
	-	2428	9	67	
	-	2425	10	67	
	-	3026	9	90	92

---

50	Oddesund 1	3030	14	91	92
	-	3026	20	91	92
	-	3126	5	90	95
	-	3537	5	95	100
	-	3537	9	97	100
	-	3537	18	98	100
	-	1957	DST	77	77

APPENDIX C

Thermal Conductivity and Porosity

Thermal conductivity (water-saturated) and porosity measured on rocks from the Danish sedimentary sequence, most samples of post-Permian age. The locations of boreholes appear in Fig. C-1, page 169.

System	Formation	Member or series	Borehole	Material	Depth (m.b.KB)	Porosity (per cent)	Thermal conductivity (W m <sup>-1</sup> K <sup>-1</sup> )
1 Tertiary		Eocene	Tinglev 1	siltstone	568	42	1.52
2 -		Paleocene	Tinglev 1	claystone	589	43	1.60
3 -		Oligocene	Viborg 5	clay	215	49	1.39
4 -		Eocene	-	-	243	50	1.40
5 -		Paleocene	-	-	302	51	1.34
6 -		Paleocene	-	-	312	47	1.40
7 -		Paleocene	Viborg 1	-	434	46	1.56
8 -		?	Vinding 1	sand	147	45	1.71
9 -		?	-	claystone (sandy shale)	171	56	1.41
10 -		Oligocene	-	sand	185	45	1.74
11 -		Oligocene	-	clay	340	53	1.48
12 -		Eocene	-	claystone	461	59	1.46
13 -		Paleocene	-	claystone (shale)	488	55	1.20
14 Cretaceous		Upper	Gassum 1	limestone (chalk)	136	36	1.70
15 -		-	-	-	265	34	1.80
16 -		-	-	-	267	33	1.86
17 -		-	-	-	267	33	1.84
18 -		-	-	-	377	32	1.78
19 -		-	-	-	445	32	1.85
20 -		-	-	-	505	31	1.90

---

21	Cretaceous	Upper	Gassum 1	limestone (chalk)	624	22	2.07
22	-	-	-	-	757	18	2.21
23	-	-	-	-	758	16	2.37
24	-	-	-	-	758	16	2.41
25	-	-	-	limestone	801	16	2.08
26	-	-	-	-	801	16	2.12
27	-	-	Horsens 1	-	1070	14	2.53
28	-	-	Lavø 1	-	1550	10	2.60
29	-	-	-	-	1791	07	2.70
30	-	-	-	-	1917	05	2.69
31	-	-	Rønnebjerg 1	limestone (chalk)	171	42	1.55
32	-	-	-	-	213	41	1.57
33	-	-	-	-	245	35	1.67
34	-	-	-	-	283	35	1.63
35	-	-	-	-	326	31	1.91
36	-	-	-	-	360	40	1.61
37	-	-	-	-	394	35	1.61
38	-	-	-	-	432	35	1.75
39	-	-	-	-	467	38	1.60
40	-	-	-	-	504	33	1.80
41	-	-	-	-	539	32	1.85
42	-	-	-	limestone	578	22	2.21
43	-	-	-	-	601	21	2.34
44	-	-	-	-	622	20	2.27
45	-	-	-	-	641	21	2.31

---

46	Cretaceous						
47	-	Upper	Rønnebjerg 1	shale (calcareous)	673	18	2.31
48	-	-	- 2	marlstone	591	33	1.76
49	-	-	Svenstrup 1	limestone (chalk)	124	46	1.45
50	-	-	-	-	198	42	1.52
51	-	-	-	limestone	408	25	2.11
52	-	-	Vemb 1	limestone (chalk)	127	43	1.57
53	-	-	Vinding 1	-	668	37	1.75
54	-	-	-	-	1112	22	2.24
55	-	-	-	-	1221	15	2.62
56	-	-	Haldager 1	marlstone	414	22	2.25
57	-	-	Uglev 1	limestone	527	17	2.22
58	-	-	-	-	539	16	2.35
59	-	Lower	Arnum 1	finegr. sandstone	952	35	2.06
60	-	-	Børglum 1	claystone	484	42	2.57
61	-	-	-	-	484	42	2.14
62	-	-	-	finegr. sand (clayey)	550	43	2.21
63	-	-	-	- -	689	34	2.47
64	-	-	Fjerritslev 2	claystone	697	48	1.37
65	-	-	Haldager 1	claystone (silty)	489	45	1.50
66	-	-	-	- -	611	47	1.42
67	-	-	Lavø 1	finegr. sandstone	739	32	1.34
					1947	07	2.73

68	Cretaceous		Lower	Lavø 1	sandstone	1987	17	3.61
69	-	-	-	-	-	2024	23	3.66
70	-	-	-	Rødby 1	clay	464	51	1.23
71	-	-	-	Rønnebjerg 1	claystone (shale)	693	35	1.67
72	-	-	-	-	claystone (sandy) shale)	723	48	1.56
73	-	-	-	Uglev 1	claystone	657	43	1.85
74	-	-	-	-	-	789	55	1.73
75	-	-	-	Vedsted 1	-	820	45	1.81
76	-	-	-	Vinding 1	clay	1301	23	2.06
77	-	-	-	-	sandstone	1360	32	2.62
78	Jurassic	Bream	Frederikshavn	Børglum 1	sandstone	764	35	3.94
79	-	-	-	-	siltstone	843	26	1.94
80	-	-	-	Fjerritslev 1	claystone	476	11	2.08
81	-	-	-	-	2 finegr. sandstone (clayey)	1038	20	2.47
82	-	-	-	Gassum 1	sandstone	1091	23	2.90
83	-	-	-	-	-	1091	40	2.32
84	-	-	-	-	-	1108	12	3.13
85	-	-	-	-	-	1138	05	4.13
86	-	-	-	-	-	1139	06	4.20
87	-	-	-	-	-	1140	28	3.12
88	-	-	-	-	-	1142	38	2.43
89	-	-	-	Haldager 1	claystone (silty)	845	33	1.87
90	-	-	-	-	-	874	35	1.55
91	-	-	-	-	finegr. sandstone (clayey)	907	18	3.36

92	Jurassic	Bream	Frederikshavn	Haldager 1	finegr. sandstone (clayey)	907	40	2.20
93	-	-	-	-	sandstone	917	26	3.54
94	-	-	-	-	sandstone	1269	42	2.08
95	-	-	?	Vinding 1	claystone (shale)	1405	44	1.71
96	-	-	Børglum	Gassum 1	claystone (shale)	1190	29	2.33
97	-	Haldager	Flyvbjerg	Haldager 1	claystone (sandy)	1092	15	2.96
98	-	-	-	Fjerritslev 2	claystone (sandy) shale	1268	43	2.07
99	-	-	-	Vedsted 1	finegr. sandstone	1145	32	2.80
100	-	-	Haldager sand	Vedsted 1	sandstone	1156	29	3.60
101	-	Fjerritslev	F III	Børglum 1	sandstone (silty)	1248	32	2.73
102	-	-	-	-	claystone	1248	25	1.82
103	-	-	F I	-	claystone (sandy) shale	1370	24	2.65
104	-	-	F III	Fjerritslev 1	- -	698	49	1.86
105	-	-	F I	- 2	finegr. sandstone	2086	14	4.40
106	-	-	?	Gassum 1	claystone (shale)	1303	60	1.14
107	-	-	Upper	-	clayironstone	1372	09	1.82
108	-	-	Lower	Gassum 1	claystone (shale)	1374	07	3.39
109	-	-	-	-	clayironstone	1418	05	1.75
110	-	-	-	-	claystone (shale)	1481	16	3.23
111	-	-	F IV	Haldager 1	- -	1316	29	1.56
112	-	-	-	-	clayironstone	1317	14	2.53
113	-	-	F I	Horsens 1	claystone (sandy) shale	1451	25	3.01
114	-	-	F IV	Vedsted 1	claystone (sandy)	1228	33	2.35
115	-	-	F III	Vedsted 1	claystone (shale)	1407	28	2.53
116	-	-	F I	-	- -	1868	18	2.78

---

117	Triassic	Gassum	Upper	Børglum 1	sandstone	1434	30	3.10
118	-	-	-	-	-	1495	31	3.31
119	-	-	-	-	-	1526	31	3.29
120	-	-	-	Fjerritslev 2	claystone ( <sup>sandy</sup> shale)	2304	07	3.44
121	-	-	G 3	Gassum 1	claystone (shale)	1534	21	1.25
122	-	-	-	-	sandstone	1535	31	2.94
123	-	-	-	-	-	1540	28	3.11
124	-	-	G 3 / G 2	-	-	1547	35	2.52
125	-	-	G 1	-	claystone (shale)	1586	30	1.76
126	-	-	G 1	-	sandstone	1601	21	2.94
127	-	-	-	-	-	1634	30	2.43
128	-	-	-	-	-	1638	29	2.61
129	-	-	-	-	-	1647	18	3.12
130	-	-	-	-	-	1642	29	2.44
131	-	-	Upper	Lavø 1	finegr. sandstone	2164	10	3.51
132	-	-	-	-	claystone (shale)	2278	06	2.78
133	-	-	-	Rødby 1	claystone/ finegr. sand	478	47	1.83
134	-	-	-	-	claystone	522	40	1.54
135	-	-	-	-	finegr. sand	648	37	3.01
136	-	-	-	Tønder 2	finegr. sandstone	1091	26	3.17
137	-	-	G 2	Vedsted 1	sandstone	2011	27	3.84
138	-	-	Upper	Gassum 1	claystone (shale)	1674	06	2.32
139	-	-	-	-	- (calcareous)	1684	13	1.89
140	-	-	-	-	-	1685	13	1.65
141	-	-	-	-	limestone	1699	10	2.48

---

142	Triassic	Vinding	Upper	Tønder 2	limestone	1152	10	2.77
143	-	-	-	Vinding 1	claystone (shale)	1693	24	1.61
144	-	-	-	-	-	1695	16	2.11
145	-	Oddesund	-	Rødby 1	claystone	733	26	1.71
146	-	-	-	Tønder 2	-	1211	25	2.16
147	-	-	-	Ullerslev 1	-	986	21	2.49
148	-	-	-	-	-	1018	26	1.90
149	-	-	-	Vinding 1	sandstone (clayey)	1754	17	2.33
150	-	Tønder	Middle Tr.	Gassum 1	sandstone	2153	12	3.55
151	-	Falster	-	Arnum 1	finegr. sandstone (calcareous)	1153	19	2.23
152	-	-	-	Glamsbjerg 1	sandstone	860	31	2.49
153	-	-	-	Ringø 1	claystone	960	24	1.80
154	-	-	-	Rødby 1	-	799	21	2.60
155	-	-	-	Rødby 1	claystone (shale) (calcareous)	869	14	2.53
156	-	-	-	Tønder 1	claystone	1360	20	1.46
157	-	Ørslev	-	Arnum 1	claystone	1304	41	1.65
158	-	-	-	Gassum 1	siltstone	2617	17	2.86
159	-	-	-	Rødby 1	dolomite/anhydrite	1124	02	5.15
160	-	Bunter sandst.	-	Arnum 1	sandstone	1442	34	2.33
161	-	-	-	Gassum 1	-	2846	20	3.65
162	-	-	-	Rødby 1	claystone	1200	20	2.09
163	-	-	-	Tønder 1	claystone	1747	25	2.98
164	-	-	-	Vedsted 1	sandstone	2063	25	3.82

---

165	Triassic	Bunter shale	Arnum 1	claystone	1700	35	1.68
166	Permian	Zechstein	Hønning 1	dolomite/anhydrite	2295	03	6.43
167	-	-	Tønder 1	rocksalt (+anh.)	2465	03	6.17
168	-	-	-	anhydrite	3108	05	6.20
169	-	-	Tønder 2	-	2523	03	6.09
170	-	-	Uglev 1	-	949	03	5.57
171	-	-	-	rocksalt	1000	03	5.48
172	-	-	Erslev 1	-	2009	03	5.93
173	-	-	-	-	2009	03	6.13
174	-	Rotliegendes	Rødby 2	claystone (sandy)	2743	06	3.71
175	-	?	Ringe 1	sandstone	1369	06	3.48
176	Pre Upper Permian		Hønning 1	claystone (shale)	2488	11	1.86
177	Ordovician/ Silurian		Slagelse 1	dolomite	2595	01	4.49
178	-		-	sandstone	2647	02	3.48



Fig. C-1. Location of boreholes from which the core samples used to measure the listed conductivities were taken.

APPENDIX D

Radioactive Heat Production

Radioactive heat production of Danish sedimentary rocks.

Measured concentrations of natural uranium ( $c_U$ ), thorium-232 ( $c_{Th}$ ), natural potassium ( $c_K$ ), the sample (dry) density and associated heat production.

Formation or series	Material	Borehole	Depth (m.b.KB)	$c_U$ (ppm)	$c_{Th}$ (ppm)	$c_K$ (per cent)	Density ( $10^3 \text{kg m}^{-3}$ )	Heat production ( $\mu\text{Wm}^{-3}$ )
1 Eocene	clay	Viborg 5	242	0.8	8.5	1.58	1.40	0.51
2 Eocene	clay	Viborg 5	253	1.6	3.6	0.61	1.40	0.38
3 U.Cretaceous	limestone (chalk)	Gassum 1	265	0.4	0.9	0.18	1.78	0.12
4 U.Cretaceous	limestone (chalk)	Uglev 1	533	0.2	0.6	0.01	2.27	0.08
5 L.Cretaceous	claystone	Uglev 1	711	2.8	12.9	2.00	1.54	1.07
6 Vedsted	claystone (shale)	x)		3.1	12.0	1.87	2.10	1.45
7 Frederikshavn	claystone (shale)	x)		3.1	7.9	1.78	2.24	1.29
8 Frederikshavn	claystone (shale)	x)		3.1	7.9	1.60	2.24	1.28
9 Børglum	claystone	Gassum 1	1193	3.5	16.9	1.72	1.99	1.71
10 Flyvbjerg	claystone (shale)	x)		4.2	10.9	1.23	2.38	1.78
11 Haldager Sand	sandstone	x)		1.0	3.1	0.23	2.12	0.40
12 Fjerritslev	claystone (shale)	Gassum 1	1374	2.5	14.5	2.20	2.58	1.84
13 Fjerritslev	claystone (shale)	Lavø 1	2080	2.1	14.8	2.88	2.38	1.68
14 Gassum	sandstone	x)		2.6	3.3	0.27	2.33	0.82
15 Gassum	sandstone	Gassum 1	1638	0.8	2.4	1.95	1.88	0.40
16 Vinding	claystone (shale)	Gassum 1	1651	2.7	15.2	2.65	2.52	1.93
17 Oddesund	claystone (shale)	Gassum 1	1904	3.6	9.6	3.14	2.38	1.72
18 Oddesund	claystone	Tønder 2	1213	2.3	9.2	2.39	2.10	1.17
19 Tønder	claystone (shale)	Gassum 1	2271	4.1	16.8	3.36	2.38	2.31
20 Falster	claystone	Tønder 1	1361	2.2	7.1	1.78	2.24	1.05
21 Ørslev	claystone	Gassum 1	2559	3.4	11.1	3.46	2.32	1.75

---

22	Bunter sandstone	sandstone	Gassum 1	2995	0.8	2.3	0.88	2.12	0.36
23	Bunter shale	claystone	Tønder 1	1829	3.3	10.9	2.38	2.24	1.57
24	Zechstein	rocksalt	Uglev 1	1053	0.1	0.4	0.02	2.11	0.04
25	Zechstein	dolomite	Tønder 2	3018	3.0	0.8	0.12	2.79	0.88
26	Zechstein	anhydrite	Tønder 2	3048	0.9	0.3	0.01	2.94	0.28
27	Rotliegendes	claystone	Rødby 2	2751	2.6	11.1	2.36	2.63	1.67
28	Ord./Silurian	claystone (shale)	Slagelse 1	2644	3.0	15.2	2.92	2.74	2.21

---

x) Classified	Mean	2.3	8.2	1.6	2.22	1.13
	Standard deviation	1.2	5.6	1.1	0.38	0.69
	Standard error	0.2	1.0	0.2	0.07	0.13

SKRIFTER I FYSISK GEOGRAFI, (ISSN 0100-2415)

- x) 1. 1970 THEAKSTONE, W.H., STILZNER, K.S., AND KNUDSEN, H.T.: GLACIER STUDIES IN NORDLAND, NORWAY, 1970. PART I (TEXT) 96 PP. PART II (FIGURES).
2. 1970 THEAKSTONE, W.H.: SEDIMENTS, STRUCTURES AND PROCESSES. STUDIES AT THE ØSTERDALSISEN GLACIER-DAMMED LAKE. 1970. 19 PP.
3. 1970 DALSGAARD, K.: DESCRIPTION OF SOME HIGHLY POROUS SOIL PROFILES ON THE ISLAND OF BELLONA, AN EMERGED ATOLL IN THE SOLOMON ISLANDS. REPRINT FROM GEOGRAFISK TIDSSKRIFT 69, PP. 93-114.
- x) 4. 1973 THEAKSTONE, W.H., HAMBREY, M. AND KNUDSEN, H.T.: GLACIER STUDIES IN NORDLAND, NORWAY, 1971. 60 PP. & 26 FIGS.
5. 1973 CHRISTIANSEN, C.: MARIAGER FJORD. FYSISK-GEOGRAFISKE UNDERSØGELSER AF ET ØSTJYSK FJORDOMRÅDE MED SÆRLIGT HENBLIK PÅ HYDROGRAFEN. 79 PP. & MAPS. ENG. ABSTR. ISBN 87 7536 075 6.
6. 1973 TUXEN-PETERSEN, F. & HOLM, T.F.: FORURLNINGSUNDERSØGELSE I SØBYGAARD SØ. GJERN Å. MED SÆRLIGT HENBLIK PÅ MATERIALETRANSPORT OG SEDIMENTATION. 39 PP. ENG. SUMMARY. ISBN 87 7536 077 2.
7. 1974 HANSEN, FLEMMING: PROBLEMER VED ANVENDELSE  $\sqrt{2}$ -SKALAEN PÅ BAGNOLD DIAGRAM. 25 PP. 4 PP. ENG. SUMMARY. ISBN 87 87529 01 7.
8. 1974 BIRD, E.C.F.: COASTAL CHANGES IN DENMARK DURING THE PAST TWO CENTURIES. 21 PP. & FIGS. ISBN 87 87529 02 5.

X) OUT OF PRINT

NEW SERIES TITLE: **GEO**SKRIFTER (ISSN 0105-824X)

9. 1978 Rasmussen, Søren: Differences in precipitation at Svinkløv and Aggersund (Northern Jutland) During the Period 1971-1977. 29 pp. ISBN 87 87529 17 3.
10. 1978 Proceedings of the Symposium on the Role of Density, Aarhus, 1978, editor: Svend Saxov. 217 pp. ISBN 87 87529 21 1.
11. 1978 Rasmussen, Keld Rømer: The Tinning Skov Project. A Micro-Meteorological Project in a Forest. Design and Instruments. 42 pp. ISBN 87 87529 23 8.
12. 1979 Christensen, Niels Bøie: Fast Hankel Transforms. 68 pp. ISBN 87 87529 24 6.
13. 1980 Møller, Jens Tyge: Terrestrial Photogrammetry. Field Work. 58 pp. ISBN 87 87529 27 0.
14. 1981 Knudsen, N. Tvis and Weidick, Anker: Glacier Inventory, West Greenland  $63^{\circ}$ - $64^{\circ}$ N. 36 pp. ISBN 87 87529 29 7.
15. 1981 Jepsen, Jens Bach and Pedersen, Laust Børsting: Evaluation of a Tensor AMT Measurement System. 97 pp. ISBN 87 87529 31 9.
16. 1981 Balling, Niels, Kristiansen, Jan I., Breiner, Niels, Poulsen, Kurt D., Rasmussen, Rasmus, and Saxov, Svend: Geothermal Measurements and Subsurface Temperature Modelling in Denmark. 172 pp. ISBN 87 87529 35 1.